UNIVERSITY OF OKLAHOMA

GRADUATE COLLEGE

IMPLEMENTATION AND ASSESSMENT OF ADCIRC'S WETTING AND DRYING ALGORITHM

A THESIS

SUBMITTED TO THE GRADUATE FACULTY

in partial fulfillment of the requirements for the

degree of

MASTER OF SCIENCE

By

JOEL CASEY DIETRICH
Norman, Oklahoma
2005

IMPLEMENTATION AND ASSESSMENT
OF ADCIRC'S WETTING AND DRYING ALGORITHM

A THESIS APPROVED FOR THE
SCHOOL OF CIVIL ENGINEERING AND ENVIRONMENTAL SCIENCE

BY

Chair: ____________________________
Dr. Randall Kolar

Member: ____________________________
Dr. Robert Knox

Member: ____________________________
Dr. K.K. Muraleetharan

Acknowledgments

Thank you ...

... to Dr. Randall Kolar, for taking a chance on an incoming freshman. I have tried to justify that faith by working as hard and being as productive as I can. However, I would not be half the engineer I am without your help, for which I will be eternally grateful.

... to Dr. Robert Knox and Dr. K.K. Muraleetharan, for serving on my committee. Your comments and suggestions will expose the parts of this work that I could understand better, and this thesis will be better because of them.

... to Dr. Kendra Dresback, for always being willing to stop what you are doing and answer my questions, no matter how dumb or repetitive they may be. Also, thank you for deriving the truncation error terms shown in Appendix A, which are the foundation on which the study in Chapter 2 was built.

... to Dr. Rick Luettich and Dr. Joannes Westerink, for their help in understanding and implementing the wetting and drying algorithm.

... and to my parents, Joel and Virginia Dietrich, for their love and support.

Table of Contents

List of Tables

List of Figures

Abstract

Hydrodynamic models are used for a variety of purposes, such as the modeling of hurricane storm surges, the study of tidal circulation patterns, and the planning of naval fleet operations. One such hydrodynamic model is ADCIRC (ADvanced CIRCulation), which was developed more than 20 years ago and has been refined continuously by researchers across North America. ADCIRC is based on the shallow water equations and includes many of the features necessary to model complex hydrodynamic systems. However, some of these features were implemented in an attempt to solve specific problems, and their behaviors were never rigorously assessed. For instance, the model uses a wetting and drying algorithm to simulate the ebb and flow of tides in coastal regions. This behavior is important in many applications, and it must be modeled correctly. This research thesis will: (1) refute an attack on the usefulness of the finite volume method for computing mass balance errors, (2) lay the groundwork for a future study that will automate the placement of grid points based on a minimization of local mass balance error, (3) implement and assess the wetting and drying algorithm in one-, two-, and three-dimensional versions of the ADCIRC model, (4) identify a set of optimal parameters for wetting and drying simulations, (5) prove that recent updates to the wetting and drying algorithm were beneficial, and (6) show that smaller mass balance errors are obtained when they are computed for each vertical element in the water column.

1. Introduction

Shallow water equations are used by researchers and engineers to model the hydrodynamic behavior of oceans, coastal areas, estuaries, lakes and impoundments [12]. The finite element solutions of these equations have been improved by two related equations: the wave continuity equation (WCE), introduced by Lynch and Gray [19] to suppress the spurious oscillations inherent to the primitive equations without having to dampen the solution either numerically or artificially; and the generalized wave continuity equation (GWCE), introduced by Kinnmark [11] to allow a balance between the primitive and pure wave forms of the shallow water equations by using a weighting parameter G. The finite element model used in this paper, ADCIRC, was developed from the GWCE [16, 26].

One area where ADCIRC and other hydrodynamic models may have problems (such as accuracy and mass balance) is wetting and drying. Large-scale water behavior is often driven by wind and tides; for the latter, the most notable is the M_2 tide caused by the gravitational effects of the moon. Where the tides meet a sloping shoreline, the water should move up and down the beach, causing areas to alternate between being wet and dry. Simply ignoring this behavior and treating the shoreline as a firm boundary, as was done in early versions of ADCIRC, allows the water to build up on boundary nodes as if against a vertical wall. Not only is this method qualitatively incorrect, it also affects the manner in which waves reflect.

To simulate wetting and drying in a numerical model, researchers have employed several methods. Some models allow the wet/dry interface to advance and recede naturally, so that the grid is not fixed in space [14]. However, this approach requires extensive knowledge of the bathymetry along the coastline, and it is not consistent with ADCIRC's fixed grid approach. Some models allow elements to wet and dry gradually, so that an element could be half-wet and half-dry [2]. This approach does allow for a fixed grid, but it requires extensive changes to the current computational algorithm. Finally, some models add a layer of porous medium at the bottom of the water column, so that dry elements can drain naturally [9]. However, this approach is inconsistent with the underlying physics assumed by the hydrodynamic ADCIRC model.

The ADCIRC wetting and drying algorithm turns on and off elements as they are wetted and dried. The algorithm was developed by Luettich and Westerink [17, 18] and is based on simplified physics and some empirical rules. In general terms, the algorithm uses a minimum depth to dry nodes and a simple momentum balance to wet nodes. As nodes are wetted and dried, they are included and excluded from the calculations, respectively, so that the problem size can change during each time step. This algorithm was implemented in the two-dimensional version of ADCIRC and proved adequate in many problems.

The primary concern of this thesis is the implementation of the wetting and drying algorithm in the three-dimensional version of ADCIRC. Three-dimensional simulations have become increasingly practical as computer architectures become faster and more efficient. And, in most applications of the model (such as storm surges for southern Louisiana or tidal forecasts for the U.S. Navy), the near-shore behavior is most important.

Thus, a three-dimensional version of ADCIRC with wetting and drying would be beneficial.

Before its implementation in the three-dimensional version of ADCIRC, the algorithm must be rigorously assessed. One method of assessment is to compare model results with an analytical solution. Some researchers [25, 23] have presented analytical solutions for oscillations in a parabolic basin, but these solutions make for poor comparisons with a numerical model that incorporates bottom friction and thus dampens the oscillations over time. Other analytical solutions are for special atmospheric conditions, such as tsunamis [15]. The classic analytical solution for wave run-up on a sloping beach was first expressed by Carrier and Greenspan [3] and later revisited by Johns [10] and Siden and Lynch [24]. The solution is quite restrictive; it describes the behavior of a frictionless wave on a linearly-sloped beach. On the other hand, ADCIRC must be run with bottom friction to obtain stable results, and we would like to use it on complex geometries. However, because this analytical solution is forced at the ocean boundary, its qualitative behavior does not change dramatically when a relatively small bottom friction is introduced, unlike the parabolic basin solution. Thus, the analytical solution can be a useful tool for one-dimensional problems, and it can be extended to two- and three-dimensional problems.

Another method of assessment is computing mass balance error. Mass balance is especially important in wetting and drying applications because large areas of water are added and subtracted from the computational domain. However, there has been some recent discussion in the literature about how best to compute mass balance. A few papers [1, 8] have advocated computing mass balance from finite element residuals in order to be consistent with the numerical discretization. However, it has been shown [13] that the finite volume approach can be a good surrogate variable for accuracy and phasing errors; that is, small mass balance errors (as computed using a finite volume approach) correlate with small constituent errors. This thesis will continue that argument by conducting a truncation error analysis, in an attempt to show that areas with significant truncation errors also have significant mass balance errors.

Chapter 2 contains this truncation error analysis. Using four test domains, we compare the mass balance errors computed by both the finite volume and finite element methods with the truncation errors from the governing equations. We find that the correlation between finite volume mass balance errors and truncation errors depends on node spacing, but it is particularly strong for grids that have constant spacing. Thus, because most of our test domains have constant spacing, the wetting and drying studies will calculate mass balance errors using a finite volume approach, where we compute the difference between the global accumulation and the global mass flux on an element-by-element basis, as represented by the primitive continuity equation.

Chapter 3 presents the results from our analysis of the one-dimensional wetting and drying algorithm. Using four test domains and two error measures, we subjected the algorithm to a variety of tests including heuristic stability, numerical sensitivity, and convergence. We find that the current algorithm works very well, but it imposes stability constraints and it requires careful selection of input parameters. Note that this work was completed during the 2003-2004 academic year as part of my Honors' senior thesis; we include it herein for completeness.

Chapter 4 presents the results from our implementation and analysis of the two-dimensional (*x*-*z*) wetting and drying algorithm. We chose to analyze the algorithm in two dimensions before moving into three dimensions because: (1) by adding only one extra dimension at a time, we were able to control the number of new model parameters and assess the model's behavior in stages; and (2) by utilizing the speed of the two-dimensional model, we could better analyze updates to the wetting and drying algorithm that were added after the one-dimensional studies in Chapter 3 were completed. We will show that these updates improve the behavior of the algorithm, to where it produces results that are similar to those in Chapter 3.

Chapter 5 presents the results of our implementation and analysis of the three-dimensional wetting and drying algorithm. We will discuss how the wetting and drying algorithm was implemented in the three-dimensional ADCIRC model, and we will discuss the results of a series of numerical experiments conducted on it. We will show that it is possible to simulate three-dimensional wetting and drying. We will also show that the same optimal set of model parameters applies in three dimensions as did in lower dimensions.

Chapter 6 presents our conclusions, including a detailed description of a set of optimal parameters for wetting and drying simulations. Chapter 7 lists the references cited in this thesis. And Appendix A presents the truncation error terms that formed the basis of the study in Chapter 2.

2. Truncation Errors and Mass Balance

Before we begin our studies of the wetting and drying algorithm, it is important to develop error measures with which we can assess it. One such measure is mass balance error, which becomes important in wetting and drying applications where regions of the computational domain are added and subtracted as the tide inundates and recedes, respectively. Traditionally, mass balance error can be computed by using what can be called the finite volume method, but a few recent papers have suggested that another method is more appropriate for finite element models, such as ADCIRC [1, 8]. We will show that the finite volume method is more realistic and more descriptive of the overall behavior of the model, by comparing the two methods to compute mass balance with each other and with the truncation errors produced through the discretization of the governing equations.

2.1. Introduction

The mass balance properties of hydrodynamic models have been examined traditionally by using the finite volume approach, where the difference between the global accumulation and the global mass flux is computed on an element-by-element basis, as represented by the primitive continuity equation. For many applications, this difference is insignificant, but some finite element models can show significant local mass balance errors in complex applications, such as regions with rapidly converging/diverging flow or regions where large areas of water are added and subtracted from the computational domain during wetting and drying [13]. The existence of these errors is sometimes used as proof that finite element models are inferior to staggered finite difference methods, which naturally conserve mass at the element level.

Recent literature has questioned the validity of the finite volume approach for computing mass balance, instead advocating an algorithm based on the computation of mass balance from finite element residuals in order to be consistent with the numerical discretization [1,8]. We will show that the finite element approach produces insignificant mass balance errors for all simulations, even in applications that are obviously incorrect. In other words, the finite element approach is not a good indicator of other problems with the model. On the other hand, it has been demonstrated through applications that the finite volume approach produces mass balance errors that can be good surrogates for accuracy and phasing errors; that is, small mass balance errors correlate with small constituent errors and vice versa [13]. In fact, Berger et al. [1] mentioned this hypothesis, by noting that an error measure, such as the finite volume approach, could be useful as an "error indicator," even if it is not a good measure of the mass balance errors generated from the finite element residuals.

The notion of using errors to discern the behavior of a the model is not new. Gresho and Lee [5] argued that oscillatory solutions are "good" in that they provide motivation for re-examination of boundary conditions, geometry, and problem formulation. In fact, the work herein continues and builds upon that argument. The existence of these mass balance errors is not ideal, but they can provide information about the behavior of the model and about how to cut the error via techniques such as grid refinement, as discussed below. Thus, although disagreement exists over the validity of the finite volume approach, it may be useful in other ways. For example, if mass balance errors are correlated to truncation errors, then mass balance errors can be used as a diagnostic tool [4].

We will test this correlation by conducting a one-dimensional truncation error analysis, in which the truncation error associated with each term in the shallow water equations will be computed. If the areas that have significant truncation errors coincide with the areas that have significant mass balance errors, then the finite volume approach to compute local mass balance error can be used as an indicator of the spatial distribution of truncation errors. Because mass balance is relatively easy to compute, it could be used as an error estimator of sorts, identifying which areas of the grid may need more refinement. This analysis will be conducted using the ADvanced CIRCulation (ADCIRC) family of models [16].

In the next subsection, we will discuss how we developed the truncation error terms (which are presented in Appendix A), and we will establish four model problems in which we will compare the truncation errors and the mass balance errors. Then, in four subsections, we will present and discuss the results from the four model problems. Using those results, we will walk through the development of a computational mesh based on the minimization of mass balance error. Finally, we will share conclusions and recommendations based on this study.

2.2. Methods

In this subsection, we discuss the two methods to compute mass balance errors, the methods used to develop and compute the truncation error terms, and the model problems that we will use to conduct the truncation error analysis.

2.2.1. Mass Balance

To compute mass errors, we examine a simple balance between flux and accumulation within each element. Accumulation is relatively easy to compute, but there has been some recent disagreement about how best to compute flux. In this study, we compare two methods: finite volume and finite element.

The first method to compute mass balance is the traditional finite volume approach, where fluxes are obtained through an integration of the primitive continuity equation. Integrating over space and time gives:

$$\int_{t_0}^{t}\int_{\Omega}\left[\frac{\partial\zeta}{\partial t} + \nabla \cdot (H\boldsymbol{u})\right]d\Omega dt = 0, \tag{2.1}$$

where ζ is water surface elevation from the mean, H is total water depth, $\boldsymbol{u}$ is velocity, Ω is a 2D element for a local mass computation, and t is time. We integrate the first term over time and apply the divergence theorem to the second term to get:

$$\int_{\Omega}(\zeta_t - \zeta_{t_0})d\Omega + \int_{t_0}^{t}\left[\int_{\partial\Omega}(H\boldsymbol{u} \cdot \boldsymbol{n})d(\partial\Omega)\right]dt = 0, \tag{2.2}$$

where the first term represents accumulation and the second term represents net flux. Linear interpolation of the accumulation term and integration of the flux term allow us to simplify this equation to:

$$(\bar{\zeta}^{k} - \bar{\zeta}^{k_0})A + \frac{1}{2}(q_{net}^{k} + q_{net}^{k_0})(\Delta t) = 0, \tag{2.3}$$

where $\bar{\zeta}$ is the arithmetic average of the nodal values of ζ over the element, A is the area of the element, q_{net} is the net flux, and k is the time index. In higher dimensions, the flux calculation is a boundary integral, and the net flux is the sum of the fluxes on the faces of the element. For the one-dimensional ADCIRC used in this chapter, the flux at any node j boils down to:

$$q_j = H_j u_j, \tag{2.4}$$

where q is the flux, H is the total water depth, and u is the velocity. Thus, at any node in the domain, the flux becomes the product of the total water depth and the velocity. The mass balance over a one-dimensional element, then, uses an interior accumulation and the fluxes from the two nodes that define it.

The second method to compute mass balance will be referred to as the finite element approach, and it involves solving for fluxes that are consistent with the finite element formulation. According to Hughes et al. [8] and Berger and Howington [1], this method yields fluxes that are locally mass-conservative, provided the equations are solved correctly. Because the formulation is applied on an element-by-element basis, each one-dimensional element will have two fluxes: one for the left element boundary, and one for the right element boundary. Thus, there are two distinct fluxes associated with each node,

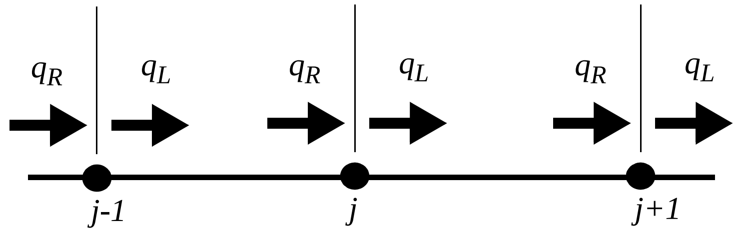

Figure 2.1. A schematic of the fluxes produced by the finite element method of computing mass balance. Each element has fluxes at the left and right boundaries; thus, each node is associated with two distinct fluxes, giving rise to the possibility of flux discontinuities.

as shown in Figure 2.1. The fluxes do not have to be the same across a node; in fact, the flux discontinuities are what allow the finite element method to be locally conservative. This behavior could be used as an error indicator in one dimension, but not in higher dimensions because then finite volume fluxes are defined over contiguous faces, making it difficult to extract nodal values.

For the one-dimensional ADCIRC model, the finite element approach can be applied to two equations: the primitive continuity equation, and the generalized wave continuity (GWC) equation. We applied the approach (similar to Massey [20]) to both equations and compared their mass balance properties. Except for a few rare cases, the two equations produced finite element residuals that were nearly identical. In this thesis, we will present only the results from the finite element approach applied to the GWC equation, so that our equations are consistent with the ADCIRC model. Thus, the flux on the left boundary of any element is given by:

$$q_L^{k+1} = e^{-G\Delta t}\left(\frac{\Delta t}{2}\right)\left\{e^{G\Delta t}\left[\left(\frac{2\zeta_L^{k+1} - 5\zeta_L^{k} + 4\zeta_L^{k-1} - \zeta_L^{k-2}}{\Delta t^2}\right)\left(\frac{1}{3}\Delta x\right)\right.\right. \tag{2.5}$$

$$+\left(\frac{2\zeta_R^{k+1}-5\zeta_R^{k}+4\zeta_R^{k-1}-\zeta_R^{k-2}}{\Delta t^2}\right)\left(\frac{1}{6}\Delta x\right)+G\left(\frac{3\zeta_L^{k+1}-4\zeta_L^{k}+\zeta_L^{k-1}}{2\Delta t}\right)\left(\frac{1}{3}\Delta x\right)$$

$$+G\left(\frac{3\zeta_R^{k+1}-4\zeta_R^{k}+\zeta_R^{k-1}}{2\Delta t}\right)\left(\frac{1}{6}\Delta x\right)+\left(\frac{1}{\Delta x}\right)((Huu)_L^{k+1}-(Huu)_R^{k+1})$$

$$+\left(g\frac{\bar{h}}{\Delta x}\right)(\zeta_L^{k+1}-\zeta_R^{k+1})+\left(\frac{g}{2\Delta x}\right)((\zeta_L^{k+1})^2-(\zeta_R^{k+1})^2)$$

$$+\varepsilon\left(\frac{1}{\Delta x}\right)\left(\left(\frac{3\zeta_L^{k+1}-4\zeta_L^{k}+\zeta_L^{k-1}}{2\Delta t}\right)-\left(\frac{3\zeta_R^{k+1}-4\zeta_R^{k}+\zeta_R^{k-1}}{2\Delta t}\right)\right)$$

$$\left.-\frac{1}{2}(Hu)_L^{k+1}\left(\frac{2\tau_L}{3}+\frac{\tau_R}{3}\right)-\frac{1}{2}(Hu)_R^{k+1}\left(\frac{\tau_L}{3}+\frac{2\tau_R}{3}\right)+\left(\frac{G}{2}\right)[(Hu)_L^{k+1}+(Hu)_R^{k+1}]\right]$$

$$+\left[\left(\frac{\zeta_L^{k+1}-2\zeta_L^{k}+\zeta_L^{k-1}}{(\Delta t)^2}\right)\left(\frac{1}{3}\Delta x\right)+\left(\frac{\zeta_R^{k+1}-2\zeta_R^{k}+\zeta_R^{k-1}}{(\Delta t)^2}\right)\left(\frac{1}{6}\Delta x\right)\right.$$

$$+G\left(\frac{\zeta_L^{k+1}-\zeta_L^{k-1}}{2\Delta t}\right)\left(\frac{1}{3}\Delta x\right)+G\left(\frac{\zeta_R^{k+1}-\zeta_R^{k-1}}{2\Delta t}\right)\left(\frac{1}{6}\Delta x\right)+\left(\frac{1}{\Delta x}\right)((Huu)_L^{k}-(Huu)_R^{k})$$

$$+\left(g\frac{\bar{h}}{\Delta x}\right)(\zeta_L^{k}-\zeta_R^{k})+\left(\frac{g}{2\Delta x}\right)((\zeta_L^{k})^2-(\zeta_R^{k})^2)$$

$$+\varepsilon\left(\frac{1}{\Delta x}\right)\left(\left(\frac{\zeta_L^{k+1}-\zeta_L^{k-1}}{2\Delta t}\right)-\left(\frac{\zeta_R^{k+1}-\zeta_R^{k-1}}{2\Delta t}\right)\right)$$

$$\left.\left.-\frac{1}{2}(Hu)_L^{k}\left(\frac{2\tau_L}{3}+\frac{\tau_R}{3}\right)-\frac{1}{2}(Hu)_R^{k}\left(\frac{\tau_L}{3}+\frac{2\tau_R}{3}\right)+\left(\frac{G}{2}\right)[(Hu)_L^{k}+(Hu)_R^{k}]\right]\right\}+e^{-G\Delta t}q_L^k\,,$$

and the flux on the right boundary of any element is given by:

$$q_R^{k+1} = e^{-G\Delta t}\left(\frac{\Delta t}{2}\right)\left\{e^{G\Delta t}\left[-\left(\frac{2\zeta_L^{k+1}-5\zeta_L^{k}+4\zeta_L^{k-1}-\zeta_L^{k-2}}{\Delta t^2}\right)\left(\frac{1}{6}\Delta x\right)\right.\right. \qquad (2.6)$$

$$-\left(\frac{2\zeta_R^{k+1}-5\zeta_R^{k}+4\zeta_R^{k-1}-\zeta_R^{k-2}}{\Delta t^2}\right)\left(\frac{1}{3}\Delta x\right)-G\left(\frac{3\zeta_L^{k+1}-4\zeta_L^{k}+\zeta_L^{k-1}}{2\Delta t}\right)\left(\frac{1}{6}\Delta x\right)$$

$$-G\left(\frac{3\zeta_R^{k+1}-4\zeta_R^{k}+\zeta_R^{k-1}}{2\Delta t}\right)\left(\frac{1}{3}\Delta x\right)+\left(\frac{1}{\Delta x}\right)((Huu)_L^{k+1}-(Huu)_R^{k+1})$$

$$+\left(g\frac{\bar{h}}{\Delta x}\right)(\zeta_L^{k+1}-\zeta_R^{k+1})+\left(\frac{g}{2\Delta x}\right)((\zeta_L^{k+1})^2-(\zeta_R^{k+1})^2)$$

$$+\varepsilon\left(\frac{1}{\Delta x}\right)\left(\left(\frac{3\zeta_L^{k+1}-4\zeta_L^k+\zeta_L^{k-1}}{2\Delta t}\right)-\left(\frac{3\zeta_R^{k+1}-4\zeta_R^k+\zeta_R^{k-1}}{2\Delta t}\right)\right)$$

$$\left.-\frac{1}{2}(Hu)_L^{k+1}\left(\frac{2\tau_L}{3}+\frac{\tau_R}{3}\right)-\frac{1}{2}(Hu)_R^{k+1}\left(\frac{\tau_L}{3}+\frac{2\tau_R}{3}\right)+\left(\frac{G}{2}\right)((Hu)_L^{k+1}+(Hu)_R^{k+1})\right]$$

$$+\left[-\left(\frac{\zeta_L^{k+1}-2\zeta_L^k+\zeta_L^{k-1}}{(\Delta t)^2}\right)\left(\frac{1}{6}\Delta x\right)-\left(\frac{\zeta_R^{k+1}-2\zeta_R^k+\zeta_R^{k-1}}{(\Delta t)^2}\right)\left(\frac{1}{3}\Delta x\right)\right.$$

$$-G\left(\frac{\zeta_L^{k+1}-\zeta_L^{k-1}}{2\Delta t}\right)\left(\frac{1}{6}\Delta x\right)-G\left(\frac{\zeta_R^{k+1}-\zeta_R^{k-1}}{2\Delta t}\right)\left(\frac{1}{3}\Delta x\right)+\left(\frac{1}{\Delta x}\right)((Huu)_L^k-(Huu)_R^k)$$

$$+\left(g\frac{\bar{h}}{\Delta x}\right)(\zeta_L^k-\zeta_R^k)+\left(\frac{g}{2\Delta x}\right)((\zeta_L^k)^2-(\zeta_R^k)^2)$$

$$+\varepsilon\left(\frac{1}{\Delta x}\right)\left(\left(\frac{\zeta_L^{k+1}-\zeta_L^{k-1}}{2\Delta t}\right)-\left(\frac{\zeta_R^{k+1}-\zeta_R^{k-1}}{2\Delta t}\right)\right)$$

$$\left.\left.-\frac{1}{2}(Hu)_L^k\left(\frac{2\tau_L}{3}+\frac{\tau_R}{3}\right)-\frac{1}{2}(Hu)_R^k\left(\frac{\tau_L}{3}+\frac{2\tau_R}{3}\right)+\left(\frac{G}{2}\right)((Hu)_L^k+(Hu)_R^k)\right]\right\}+e^{-G\Delta t}q_R^k,$$

where: q is flux; ζ is the water surface elevation from the mean; H is the total water depth; $\bar{h}$ is the average bathymetry in the element; u is the velocity; k is the time index; L and R denote the left and right boundaries of the element, respectively; Δt is the time step; Δx is the length of the element; G is a numerical parameter; ε is eddy viscosity; and g is acceleration due to gravity.

Notice the difference between the finite volume flux given in Equation 2.4 and the finite element fluxes given in Equation 2.5 and Equation 2.6. Not only is the finite volume flux significantly less complex, it also makes physical sense. The same cannot be said for the finite element fluxes. Thus, although the finite element fluxes may be a good indicator of whether the finite element formulation is being solved correctly, it is not obvious how they relate to the physical domain.

2.2.2. Development of Truncation Error Terms

ADCIRC is based on two governing equations: the GWC equation, and either the nonconservative form (NCM) or the conservative form (CM) of the momentum equation [16]. In one dimension, the GWC equation is given by:

$$\frac{\partial^2\zeta}{\partial t^2} + G\frac{\partial\zeta}{\partial t} - q\frac{\partial G}{\partial x} - \frac{\partial}{\partial x}\left[\frac{\partial}{\partial x}(qu) + (G-\tau)q + gH\frac{\partial\zeta}{\partial x} - \varepsilon\frac{\partial^2 q}{\partial x^2}\right] = 0\,, \tag{2.7}$$

the NCM equation is given by:

$$\frac{\partial u}{\partial t} + u\frac{\partial u}{\partial x} + \tau u + g\frac{\partial\zeta}{\partial x} - \frac{\varepsilon}{H}\frac{\partial^2 q}{\partial x^2} = 0\,, \tag{2.8}$$

and the CM equation is given by:

$$\frac{\partial q}{\partial t} + \frac{\partial}{\partial x}(qu) + \tau q + gH\frac{\partial\zeta}{\partial x} - \varepsilon\frac{\partial^2 q}{\partial x^2} = 0\,, \tag{2.9}$$

where the variables are defined above. The discrete forms of the equations are generated by using linear finite elements for the spatial discretization and a Crank-Nicholson scheme on the linear terms for the temporal discretization. The nonlinear terms in the equations employ an explicit formulation. We utilize exact quadrature rules and an L2 interpolation for the advective terms.

To evaluate the truncation error for each term in these three governing equations, we utilize Taylor series expansions. After the dependent variables are expanded about a common node point, j, the results are subtracted from the continuous equations in order to obtain the truncation error. In the evaluation of the truncation errors, we employ Mathematica to expand the Taylor Series to the seventh order terms; however, we report errors herein only to second order. Also, the truncation errors were computed at interior nodes only; we used centered difference approximations, which cannot be formulated at boundary nodes.

The truncation errors are presented in Appendix A. Using these truncation errors, it can be shown that the GWC equation is first-order accurate in time if the advective terms are in non-conservative form, and that it is second-order accurate in time if the advective terms are in conservative form. In space, the GWC equation is first-order accurate for variable spacing, and it is second-order accurate for constant spacing. The NCM and CM equations are first-order accurate in time and space if we use variable spacing, and they are second-order accurate in space if we use constant spacing. Also, both momentum equations become second-order accurate in time if the equations are linearized. These findings are described in detail in Dresback et al. [4].

2.2.3. Evaluation of Truncation Error Terms

Evaluation of the truncation error terms requires information from both fine and coarse grid solutions. The derivatives in each of the truncation error terms were evaluated using information from a fine grid solution. For instance, the first term in the GWC equation is the time derivative term, $\partial^2\zeta/\partial t^2$, and the second term in its truncation error expression is:

$$\underbrace{\frac{1}{36}(\Delta x_j - \Delta x_{j+1})(\Delta t)^2}_{coarse}\ \underbrace{\left(\frac{\partial^5\zeta_{j,k}}{\partial x\partial t^4}\right)}_{fine}, \tag{2.10}$$

where ζ is the water surface elevation from the mean, j is the space index, and k is the time index.

To approximate all derivatives, we use second-order central difference schemes on the fine grid solution. For example, for the derivative in Equation 2.10, we used a two-level centered difference scheme in space and a five-level centered difference scheme in time:

$$\frac{\partial^5\zeta_{j,k}}{\partial x\partial t^4} = \frac{\begin{array}{c}[(\zeta_{j+1}^{k+2} - 4\zeta_{j+1}^{k+1} + 6\zeta_{j+1}^{k} - 4\zeta_{j+1}^{k-1} + \zeta_{j+1}^{k-2}) \\ -(\zeta_{j-1}^{k+2} - 4\zeta_{j-1}^{k+1} + 6\zeta_{j-1}^{k} - 4\zeta_{j-1}^{k-1} + \zeta_{j-1}^{k-2})]\end{array}}{2\Delta x(\Delta t)^4}, \tag{2.11}$$

where the water surface elevations, grid spacing, and time step in Equation 2.11 come from a fine grid ("true") solution, which was obtained by refining the grid until the solution converged to the sixth decimal place. We use similar centered finite difference approximations to evaluate all of the derivatives in the truncation error terms. Thus, because the highest derivative in either space or time is fourth order, we need to save output from five consecutive time steps.

The rest of the truncation error term part shown in Equation 2.10 is evaluated using information from a coarse grid solution, namely, a coarse grid spacing and a coarse time step. Note that we do not need to save output for any of the dependent variables in a coarse grid simulation to compute the truncation error; all we need are the values of the independent variable increments: time step and grid spacing. Thus, the truncation errors were computed using the following procedure:

- A fine grid simulation was developed, in order to obtain a true solution. The parameters of these simulations are described in Section 2.2.4.
- Each truncation error term was evaluated independently, using the fine grid data to evaluate the derivatives, and the coarse grid data to evaluate the increments of time step and grid spacing.
- The behavior of each truncation error term was examined. Additionally, the truncation error terms for each equation were summed to produce overall truncation errors.
- The truncation errors were compared with the mass balance errors, from both the finite volume and the finite element approaches, as computed from the coarse grid simulation.

Note the distinction between "*coarse*" and "*fine*" in Equation 2.10. For all of the truncation error terms, the fine component is the derivative part of the term. It is independent of discretization, and thus fixed for any grid. And, it is evaluated by using a true solution, which in our case is a fine grid solution that remains the same for all coarse discretizations. Figure 2.2 shows only the fine components of the truncation errors for one equation in one domain. Note that the value of the fine component varies throughout the domain; it is at its maximum in the area of interest, as we will discuss below. Regardless

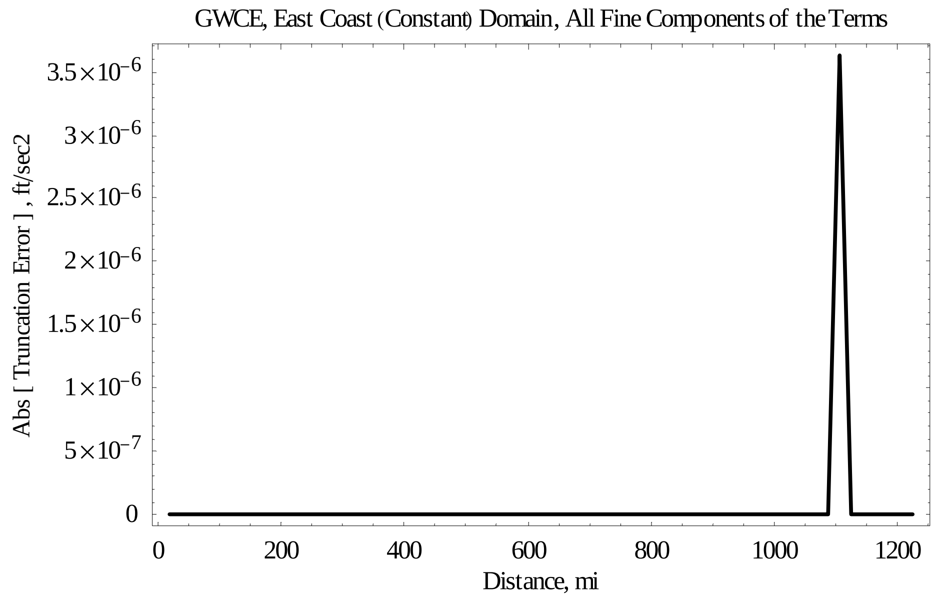

Figure 2.2. The fine components of the truncation error terms for one of our governing equations and one of our

of the coarse grid that is used in this domain, these values from the fine components will persist.

On the other hand, the coarse component of each truncation error term is dependent on the discretization and other user-selected parameters. This component can be manipulated. In fact, as we will discuss later, some grids are designed to minimize the coarse component in regions where the fine component is large (and vice versa), so that the overall truncation error is uniform throughout the computational domain.

The behavior of the truncation errors and their comparison with the mass balance errors are discussed in Section 2.3 through Section 2.6. Before that discussion, though, we will present the model problems on which these analyses were performed.

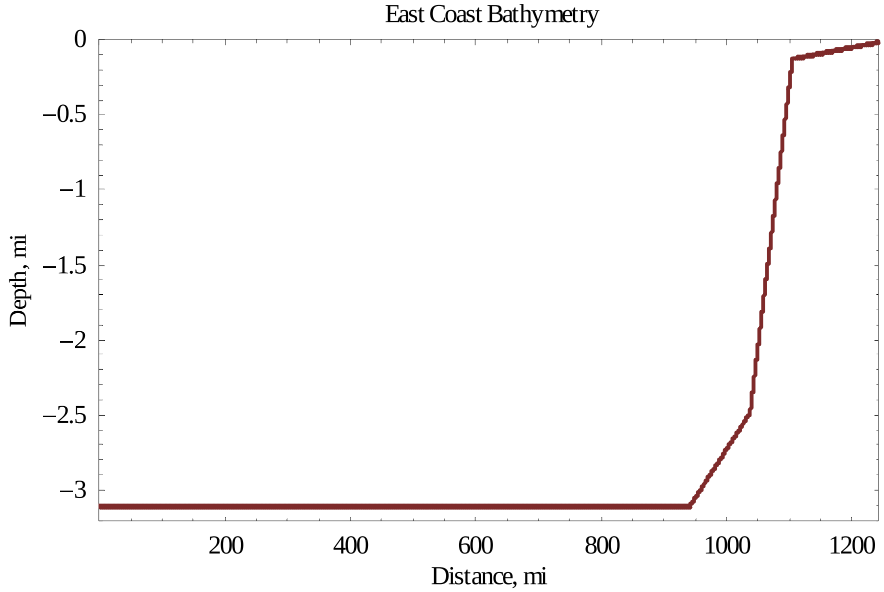

Figure 2.3. Bathymetry for the first three model problems. Note that the bathymetry is about 3 miles at the open ocean boundary, and it rises steeply toward a plateau as it approaches the

2.2.4. Model Problems

The first three model problems are based on a one-dimensional slice of the Western North Atlantic grid; we will refer to this as the East Coast domain. The slice is shown in Figure 2.3. Note that the bathymetry is deep throughout much of the domain, but it rises steeply and forms a plateau near the closed land boundary. Historically, mass balance errors manifest themselves in areas with rapidly changing bathymetry where the flow converges or diverges [13]. Thus, this domain should be a good test of the model's mass balance and truncation error properties.

The fine grid solution for this domain has a grid spacing of about 800 feet, which corresponds to 8,193 nodes. Other simulation parameters include: a time step of 1 second, a simulation time of 3.24 M2 tidal cycles (or 40.24 hours), a constant bottom friction of

0.0001, and a G value of 0.001 sec^{-1}. The elevation and velocity outputs were saved for the last five time steps and used to compute the truncation error terms. (Recall that the truncation errors depend on the fine grid solution; the only input from the coarse grid solution is the coarse grid and time step.)

The first model problem has a constant grid spacing. To compute the truncation errors, we used a coarse grid spacing of 103,526 feet, which corresponds to 65 nodes and a $\lambda / \Delta x$ ratio of about 40 in the shallowest waters. (The $\lambda / \Delta x$ ratio relates the wave celerity, forcing period, and grid resolution; larger ratios correspond to better resolution.)

The second model problem uses the same East Coast bathymetry, but with a variable spacing based on a $\lambda / \Delta x$ ratio of about 125. This coarse grid has 46 nodes, and its grid spacing ranges from about 250,000 feet in the deep water to about 26,000 feet on the shelf. The fine grid remains the same, and so do the rest of the parameters listed above.

The third model problem also uses the East Coast bathymetry, but with a variable spacing developed with a localized truncation error analysis (LTEA) [6,7]. The LTEA method places node points based on the truncation errors associated with the discrete equations, and it has been show to improve both accuracy and efficiency. This coarse grid also has 46 nodes, although they are placed differently than for the East Coast ($\lambda / \Delta x$) domain, and its grid spacing ranges from about 370,000 feet in the deep water to less than 5,000 feet on the shelf. Again, the fine grid remains the same, and so do the rest of the parameters listed above. Figure 2.4 shows how the nodes are placed for the three East Coast domains. Note how the LTEA method clusters nodes along the shelf break at the distance of about 1,100 miles.

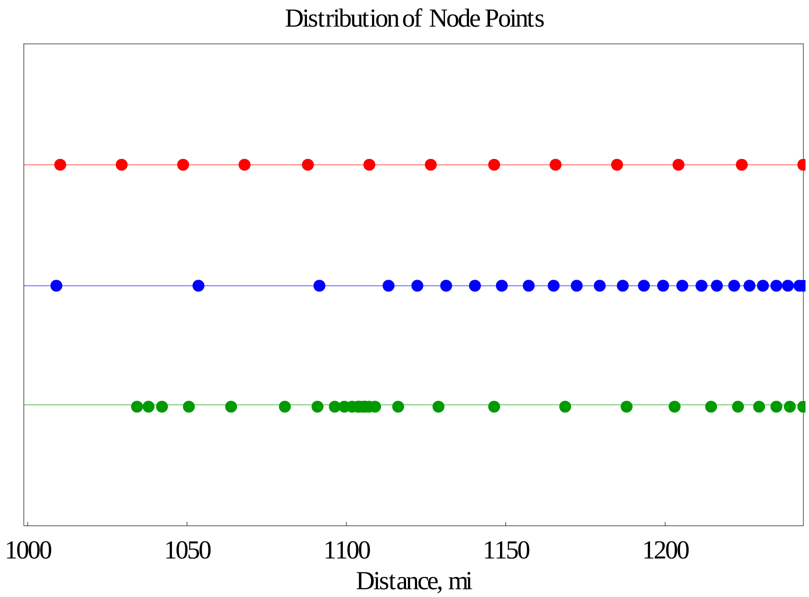

Figure 2.4. Distribution of node points
in the last 250 miles of the East Coast domain for the three discretizations. The red line is the constant grid spacing, the blue line is the variable ($\lambda/\Delta x$) spacing, and the green line is the variable (LTEA) spacing. Note how the LTEA method clusters nodes along the shelf break at the distance of about

The fourth model problem is a one-dimensional wetting and drying simulation; we will refer to this as the Linear Sloping Beach domain. This domain is shown in Figure 2.5. For the fine grid solution, we used a grid spacing of 50 meters, which corresponds to 481 nodes; for the coarse grid solution, we used a grid spacing of 500 meters, which corresponds to 49 nodes. Other simulation parameters include: a time step of 1 second, a simulation time of 4 M2 tidal cycles (or 48 hours), a constant bottom friction of 0.0001, and a G value of 0.01 sec^{-1}. To calculate the truncation errors, we saved the elevation and velocity outputs for the last five time steps. Note that, at this time in the simulation, the interface between wetting and drying is at a distance of about 18 kilometers.

We will present the results from these four model domains over the next four subsections. For each domain, we tested two forms of the one-dimensional ADCIRC

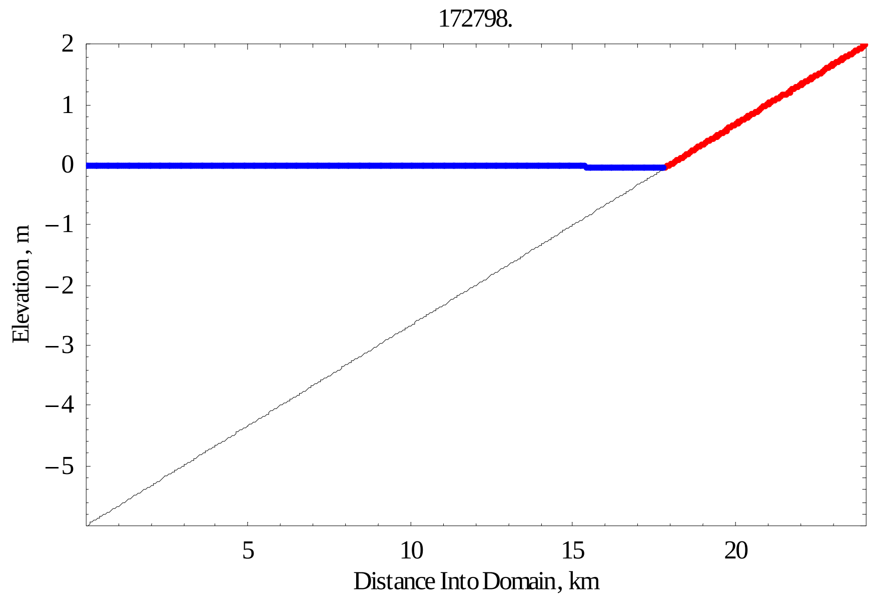

Figure 2.5. Bathymetry for the Linear Sloping Beach domain. The solid black line is the bathymetry, and the solid blue and red lines are the wet and dry regions, respectively, of the grid at the point in time when we calculate the truncation errors. Note that the wet/dry interface is at a distance of about 18 kilometers.

model: the non-conservative form and the conservative form. The former uses the non-conservative form of the advective term in the GWCE, which is used to solve for water surface elevations, and the non-conservative form of the momentum equation, which is used to solve for velocities. The latter uses the conservative form of the advective term in the GWCE, which is used to solve for water surface elevations, and the conservative form of the momentum equation, which is used to solve for fluxes. Note the difference in dependent variables between the two forms of the momentum equation; the non-conservative form solves for velocities, while the conservative form solves for fluxes. To compare truncation errors in this paper, we will divide the truncation errors from the conservative form of the momentum equation by the water depth, so that the units are consistent. Thus, for each of the four domains, we will show mass balance and truncation

Table 2.1: Summary of test domains, error measures, and where their results are reported. Thus, within each section, we will present six sets of results: three for the non-conservative forms of the governing equations, and three for the conservative forms. Note that "T.E." stands for truncation error.

		Error Measure					
		Non-Conservative			Conservative		
		Mass Balance	GWCE T.E.	NCM T.E.	Mass Balance	GWCE T.E.	CM T.E.
Domain	East Coast (Constant)	Section 2.3.1			Section 2.3.2		
	East Coast ($\lambda/\Delta x$)	Section 2.4.1			Section 2.4.2		
	East Coast (LTEA)	Section 2.5.1			Section 2.5.2		
	Linear Sloping Beach	Section 2.6.1			Section 2.6.2		

error results for both forms. Table 2.1 presents a summary of the model domains, error measures, and their corresponding sections.

2.3. East Coast (Constant) Domain

The East Coast bathymetry was selected because its shelf break is a robust test of both mass balance errors and truncation errors. In this subsection, we focus on a version of this domain that has constant node spacing, and we present the results for both the non-conservative and conservative forms of the governing equations. For both forms, the results indicate that finite volume mass balance errors are a good indicator of truncation errors.

2.3.1. Non-Conservative Form

Herein, we present the mass balance errors, truncation errors for the non-conservative form of the GWCE, and truncation errors for the non-conservative momentum equation. These errors will be shown in graphical form in the following subsections; however, it is important to remember the big picture when making these comparisons. Thus, Table 2.2 presents a summary of the truncation errors for every term in the equation and their relationships with the finite volume mass balance errors. (The governing equations are presented in Section 2.2.2 and Appendix A.) As will be shown, the finite volume method of computing mass balance errors is a good indicator of truncation errors, and we have tried to summarize that idea in the last column of Table 2.2. We will discuss this behavior in more detail when we present the truncation errors in Section 2.3.1.2 and Section 2.3.1.3, but first we will present the mass balance errors computed by the finite volume and finite element methods.

2.3.1.1. Mass Balance Errors

Figure 2.6 shows the mass balance errors for the coarse grid simulation, and Figure 2.7 shows an expanded view in the vertical scale to highlight the finite element mass balance errors. The units of mass balance error are square feet. Note that, in both figures, the finite volume method shows significant non-zero errors where the flow accelerates up the continental slope. It is only when the vertical scale is exaggerated in Figure 2.7 that significant finite volume residuals become evident in other parts of the domain. The finite element method shows residuals that are six to eight times smaller in magnitude, and these

Table 2.2: Summary of truncation errors for the non-conservative form of the ADCIRC model, for the East Coast (Constant) domain. In the first column, the names refer to terms in Appendix A. In the second column, the units of truncation error are feet/sec^2. The last column refers to whether the behavior of the truncation errors matches that of the mass balance errors, as computed by using the finite volume method.

Term	Maximum Truncation Error	Follows Mass Balance?
GWCE (Figure 2.10)	**7.0E-02**	**Yes**
First (Figure 2.8)	1.2E-05	No
Second	1.5E-08	No
Finite Amplitude, Part 1 (Figure 2.9)	5.0E-02	Yes
Finite Amplitude, Part 2	1.2E-04	Yes
Advective, Part 1	1.7E-06	Yes
Advective, Part 2	2.5E-02	Yes
Flux	5.0E-04	Yes
Viscous	0.0E+00	
NCM (Figure 2.12)	**4.0E-03**	**Yes**
Accumulation	4.5E-05	Yes
Advective (Figure 2.11)	1.2E-03	Yes
Bottom Friction	1.0E-03	Yes
Finite Amplitude	2.0E-03	Yes
Viscous	0.0E+00	

residuals do not change as dramatically in the shelf break region. Thus, the residuals from the finite volume method are much more sensitive to bathymetry changes.

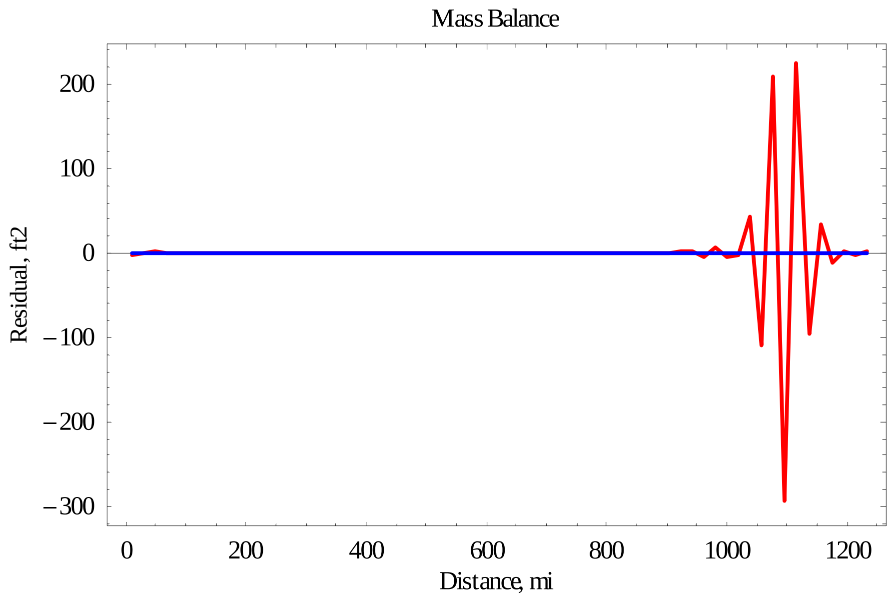

Figure 2.6. Mass balance residuals for the
coarse grid simulation, for the East Coast (Constant) domain and the non-conservative form of ADCIRC. The red line shows the residuals from the finite volume method, and the blue line shows the residuals from the finite

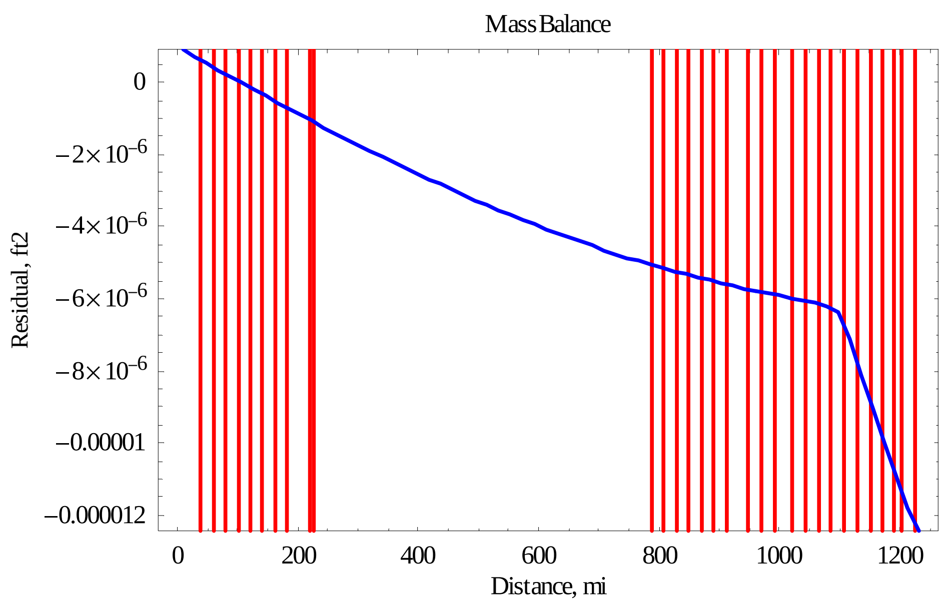

Figure 2.7. An expanded view of the mass balance residuals for the coarse grid simulation, for the East Coast (Constant) domain and the non-conservative form of ADCIRC. The red line shows the residuals from the finite volume method, and the blue line shows the residuals from the finite element method.

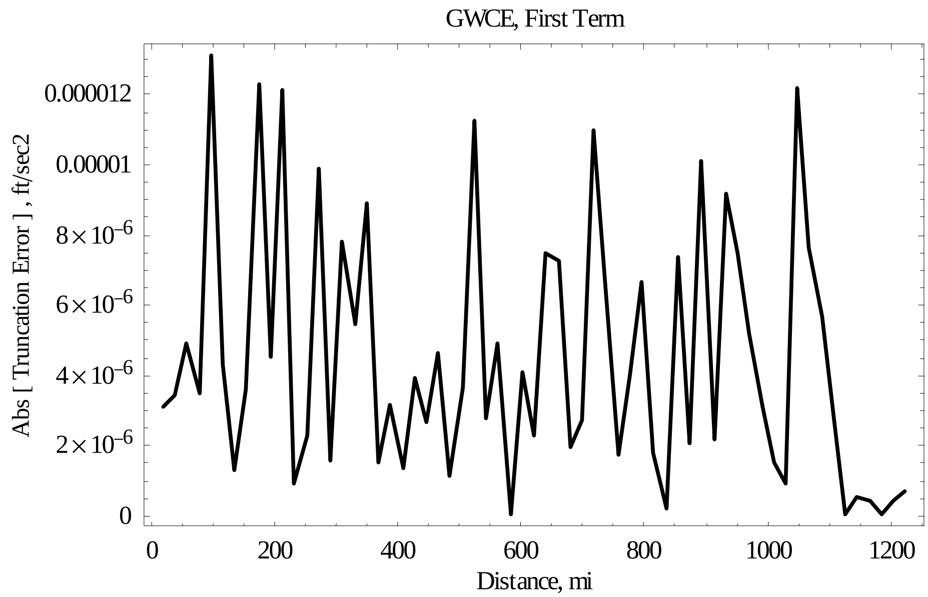

Figure 2.8. Absolute values of the truncation errors for the first term in the GWC equation, for the East Coast (Constant) domain. Note that the units of truncation error are feet/sec^2.

2.3.1.2. Truncation Errors for the GWC Equation

We evaluated each truncation error term for every interior node in the model domain. However, instead of showing a graph for all nine of the GWC truncation error terms (and all five of the non-conservative momentum terms), we will present graphs that are representative of all of the terms. Then, we will present a graph with the combined truncation errors.

Figure 2.8 shows the truncation errors for the first term, $\partial^2\zeta/\partial t^2$, in the GWC equation. Note the vertical scale, which ranges from a minimum of about zero to a maximum of about 0.000012 feet/sec^2. As shown in Table 2.2, this term and the second GWCE truncation error term are the only ones that show random noise over the domain; most of the rest of the terms show truncation errors that are larger in magnitude, and all of

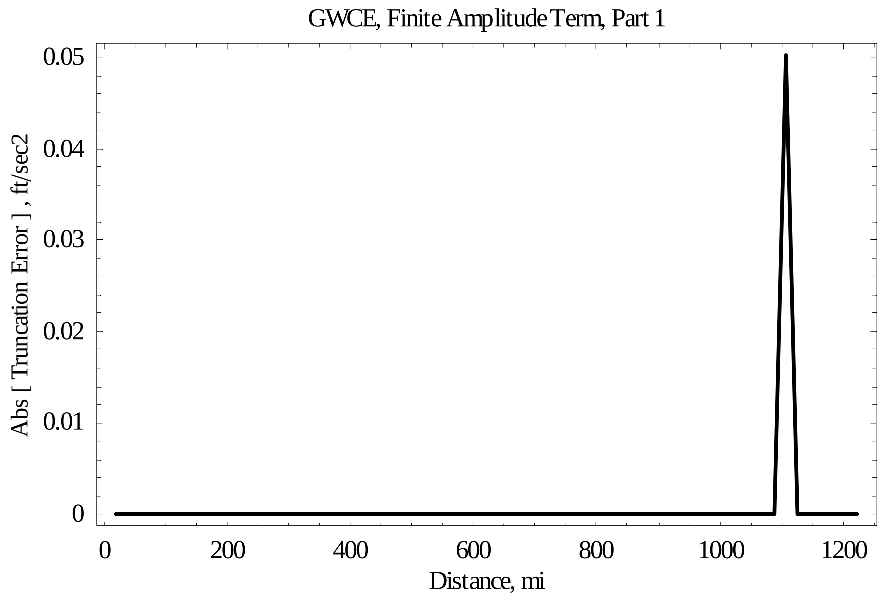

Figure 2.9. Absolute values of the truncation errors for the first part of the finite amplitude term in the GWC equation, for the East Coast (Constant) domain. Note that the units of

the other terms show significant truncation errors in the region where the steep slope occurs. For instance, Figure 2.9 shows the truncation errors for the first part of the finite amplitude term, $gh(\partial^2\zeta/\partial x^2)$, in the GWC equation. The truncation errors are insignificant everywhere except in the steep slope region. Also, the maximum truncation errors in Figure 2.9 are more than three orders of magnitude larger than those in Figure 2.8. Most of the rest of the truncation error terms produce graphs similar to Figure 2.9, with a significant maximum in the region with the steepest slope.

The truncation errors can be combined to produce a single graph, as in Figure 2.10. The total truncation error shown is computed as a sum of the absolute values of the truncation errors for each of the terms in the non-conservative GWC equation. Note the significant maximum at a distance of about 1,100 miles, which corresponds to the region in Figure 2.6 where the finite volume mass balance errors are significant. In this case, the

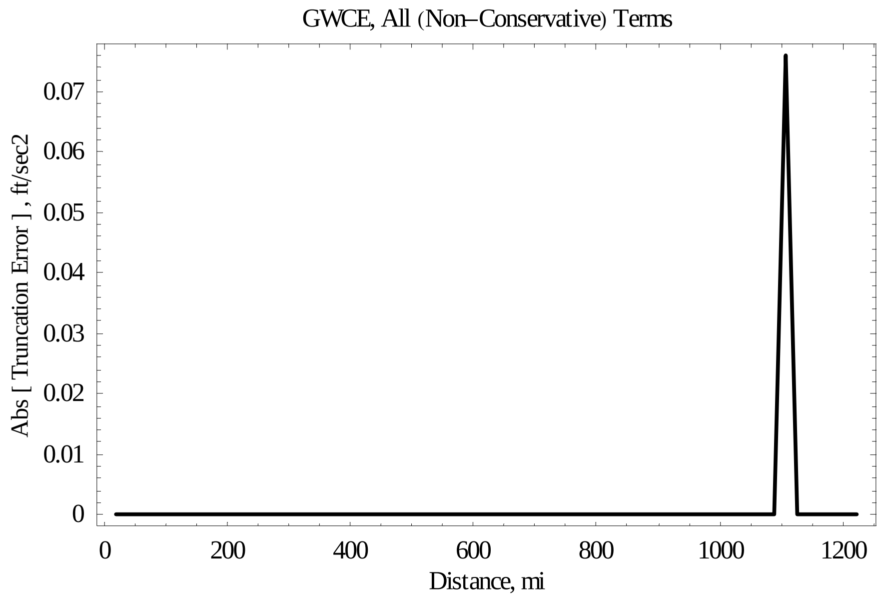

Figure 2.10. Absolute values of the truncation errors for all of the terms in the non-conservative GWC equation, for the East Coast (Constant) domain. Note that the units of truncation error are feet/sec^2. Also note that the significant maximum at a distance of 1,100 miles corresponds to the region with the steepest slope.

finite volume mass balance errors are a good predictor of truncation errors. For the GWC equation in the other test domains, we will show only these cumulative graphs, for both the conservative and non-conservative terms.

In summary, many of the individual truncation error terms and the sum of the truncation errors all show significant errors in the region where the finite volume mass balance errors were greatest, as indicated in Table 2.2.

2.3.1.3. Truncation Errors for the NCM Equation

Again, instead of showing the individual truncation error graphs for all five of the terms in the NCM equation, we will show a representative graph before moving forward to the cumulative graphs. Figure 2.11 shows the truncation errors for the advective term,

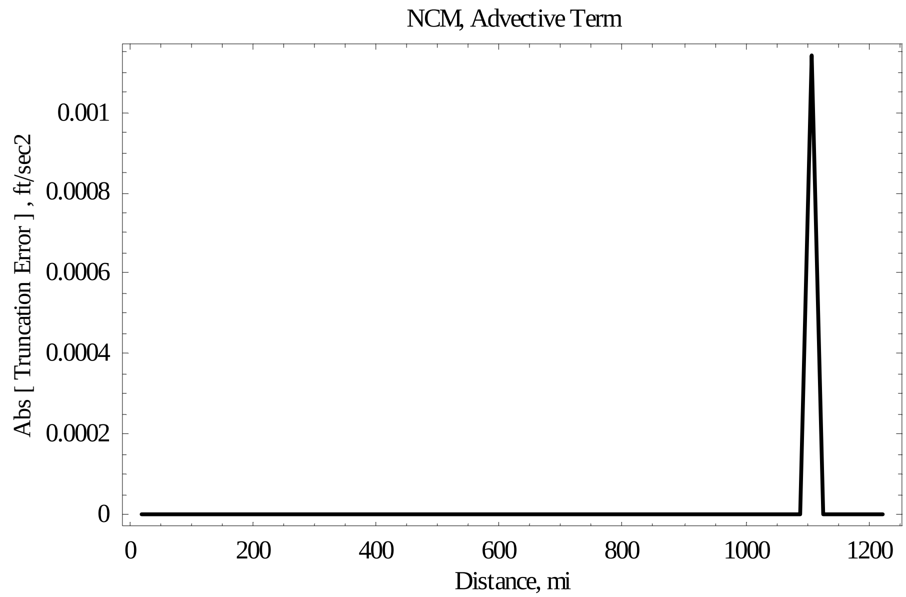

Figure 2.11. Absolute values of the truncation errors for the advective term in the NCM equation, for the East Coast (Constant) domain. Note that the units of truncation error are feet/sec^2. Also note that the significant maximum at a distance of 1,100 miles corresponds to the region with the steepest slope.

$u(\partial u/\partial x)$, in the NCM equation. As in Figure 2.9, this graph shows significant truncation errors only near the boundaries and in the region with the steepest slope. This trend is repeated for almost all of the other terms in the NCM equation, with the lone exception being the viscous term, because it was not used in this simulation.. The largest truncation errors occur in the region with rapid bathymetry changes. Figure 2.12 shows the sum of the absolute values of the truncation errors for the five terms. Again, the largest truncation errors occur in the region with rapid bathymetry changes.

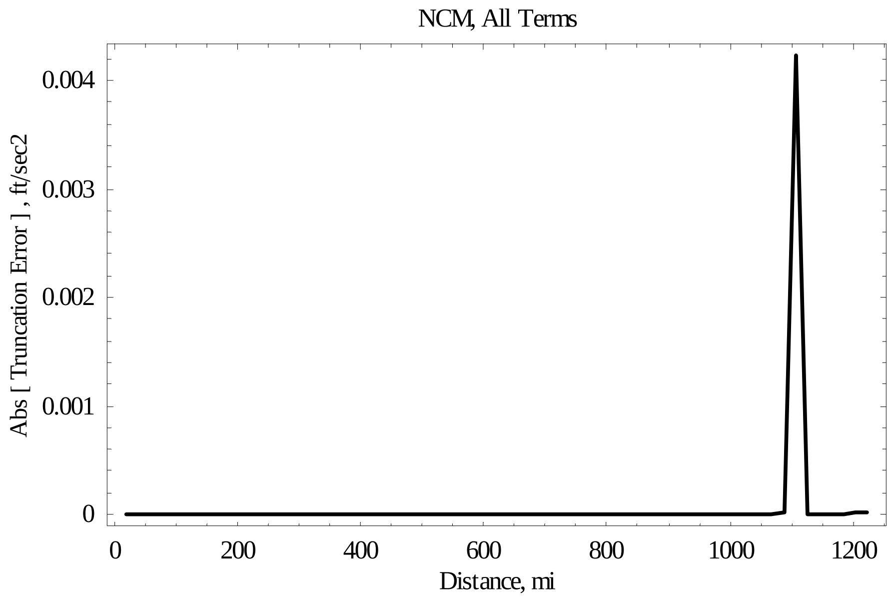

Figure 2.12. Absolute values of the truncation errors for all terms in the NCM equation, for the East Coast (Constant) domain. Note that the units of truncation error are feet/sec^2. Also note that the significant maximum at a distance of 1,100 miles corresponds

2.3.2. Conservative Form

In this subsection, we will present and discuss the results for the conservative form of the ADCIRC model. Table 2.3 summarizes these results. Once again, the finite volume mass balance errors are a good indicator of truncation errors.

2.3.2.1. Mass Balance Errors

Figure 2.13 shows the mass balance errors for the conservative form of the one-dimensional ADCIRC model, and Figure 2.14 shows a close-up of those same mass balance errors. Note that the conservative forms of the GWC equation and the momentum equation greatly reduce the mass balance errors, as computed by the finite volume method, in the region of rapid bathymetry changes. The maximum finite volume mass

Table 2.3: Summary of truncation errors for the conservative form of the ADCIRC model, for the East Coast (Constant) domain. In the first column, the names refer to terms in Appendix A. In the second column, the units of truncation error are feet/sec^2. The last column refers to whether the behavior of the truncation errors matches that of the mass balance errors, as computed by using the finite volume method.

Term	Maximum Truncation Error	Follows Mass Balance?
GWCE (Figure 2.15)	**1.0E-01**	**Yes**
First	1.2E-05	No
Second	1.5E-08	No
Finite Amplitude, Part 1	5.0E-02	Yes
Finite Amplitude, Part 2	1.2E-04	Yes
Advective	5.0E-02	Yes
Flux	5.0E-04	Yes
Viscous	0.0E+00	
CM (Figure 2.17)	**2.0E-04**	**Yes**
Accumulation	1.4E-06	No
Advective (Figure 2.16)	9.0E-05	Yes
Bottom Friction	4.0E-05	Yes
Finite Amplitude, Part 1	8.0E-05	Yes
Finite Amplitude, Part 2	2.0E-07	Yes
Viscous	0.0E+00	

balance error for the non-conservative forms in Figure 2.6 was about 200 ft^2, but the conservative forms reduce the error in that region to about 0.2 ft^2. Nevertheless, these finite volume mass balance errors are several orders of magnitude greater than the finite element mass balance errors shown in Figure 2.14. Also note that, although the finite

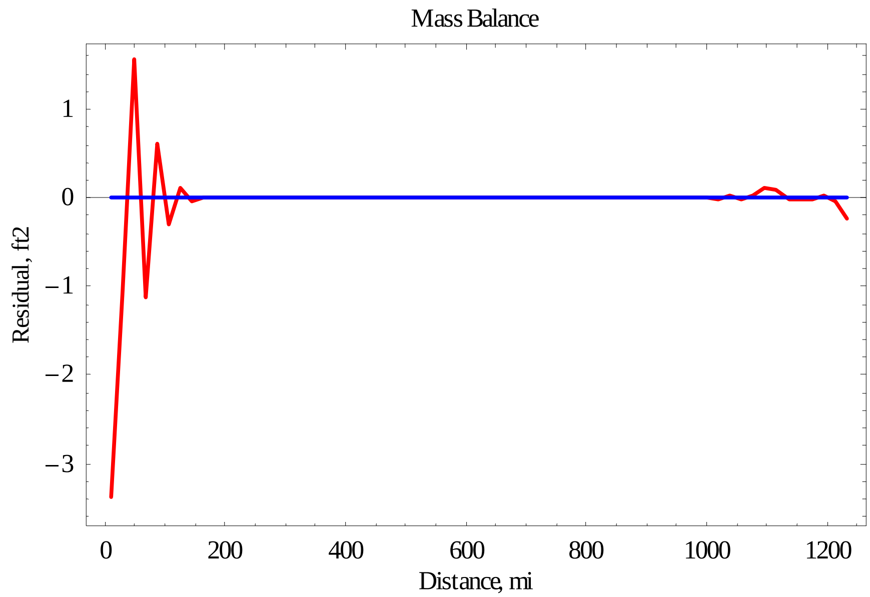

Figure 2.13. Mass balance residuals for
the coarse grid simulation, for the East Coast (Constant) domain and the conservative form of ADCIRC. The red line shows the residuals from the finite volume method, and the blue line shows the residuals from the finite

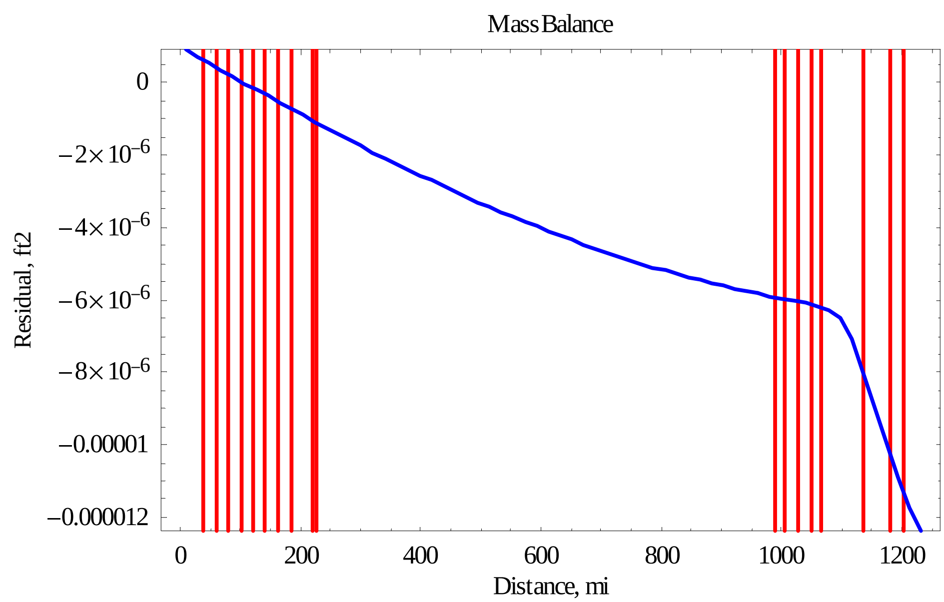

Figure 2.14. An expanded view of the mass balance residuals for the coarse grid simulation, for the East Coast (Constant) domain and the conservative form of ADCIRC. The red line shows the residuals from the finite volume method, and the blue line shows the residuals from the finite element method.

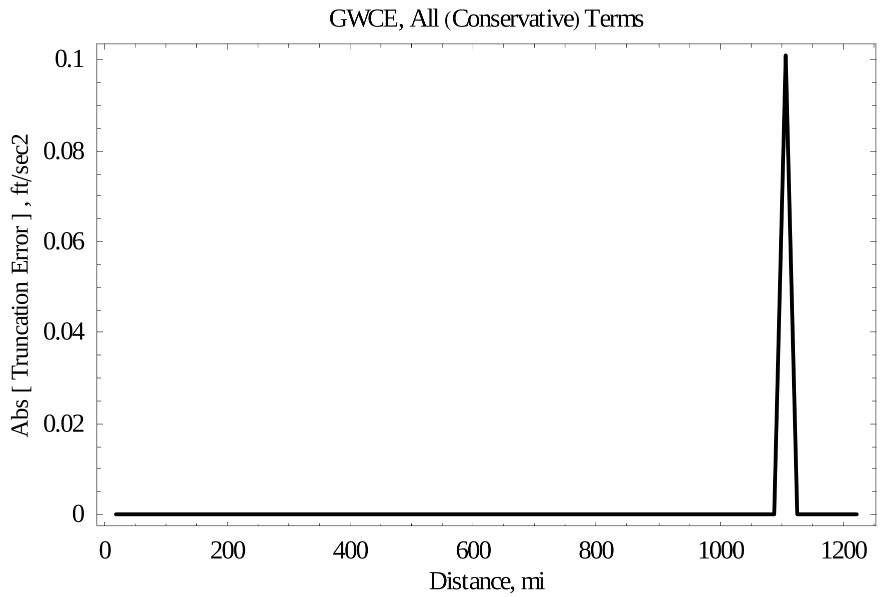

Figure 2.15. Absolute values of the truncation errors for all of the terms in the conservative GWC equation, for the East Coast (Constant) domain. Note that the units of truncation error are feet/sec^2. Also note that the significant maximum at a distance of 1,100 miles corresponds to the region with the steepest slope.

volume mass balance errors near the left boundary in Figure 2.13 appear large, they are of the same magnitude as the errors near the ocean boundary in Figure 2.6. The conservative forms of the equations only affect the finite volume mass balance errors in the region with rapid bathymetry changes.

2.3.2.2. Truncation Errors for the GWC Equation

Figure 2.15 shows the absolute values of the truncation errors for all of the terms in the conservative GWC equation. This figure has a similar shape to that of Figure 2.10, in that the significant truncation errors occur in the same region of the domain. However, the conservative form of the equations increases the magnitude of the maximum GWCE truncation error by about 40 percent, from about 0.07 feet/sec^2 to about 0.1 feet/sec^2.

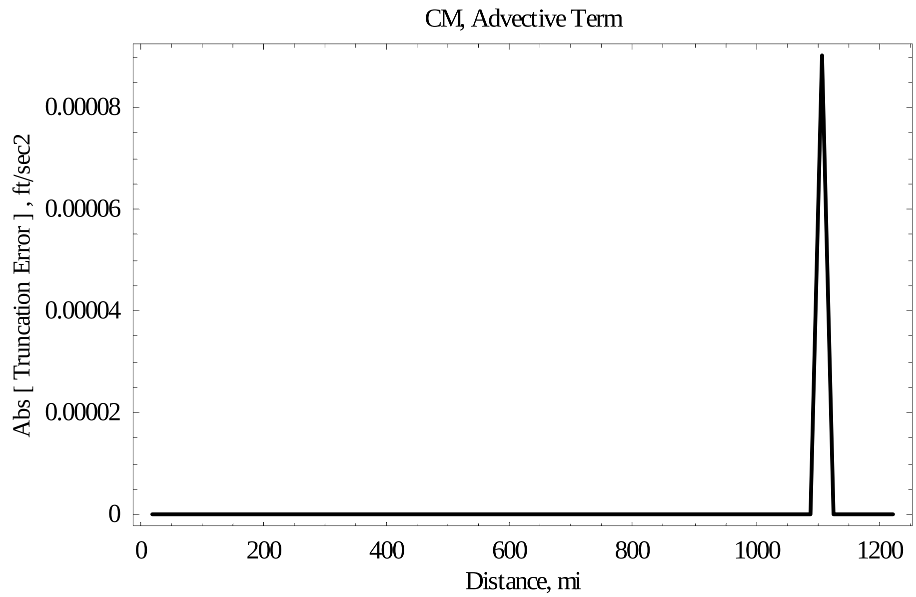

Figure 2.16. Truncation errors for the advective term in the CM equation, for the East Coast (Constant) domain. Note that the units of truncation error are feet/sec^2. Also note that the significant maximum at a distance of 1,100 miles corresponds to the region

(This difference can also be seen by comparing the "GWCE" rows in Table 2.2 and Table 2.3.) The finite volume mass balance errors and truncation errors still occur in the same place, but their magnitudes are going in different directions, i.e., the finite volume mass balance errors are decreasing, while the truncation errors are increasing.

2.3.2.3. Truncation Errors for the CM Equation

As with the NCM equation in Section 2.3.1.3, the only individual term we will show is the truncation error graph for the advective term, which in this case is $\partial(qu)/\partial x$. Figure 2.16 shows those truncation errors. Note that this term shows similar error behavior to most of the truncation error terms described above, in that there exists a clear maximum at the shelf break. Also note the difference in magnitude between the truncation errors associated with the CM advective term in Figure 2.16 and those

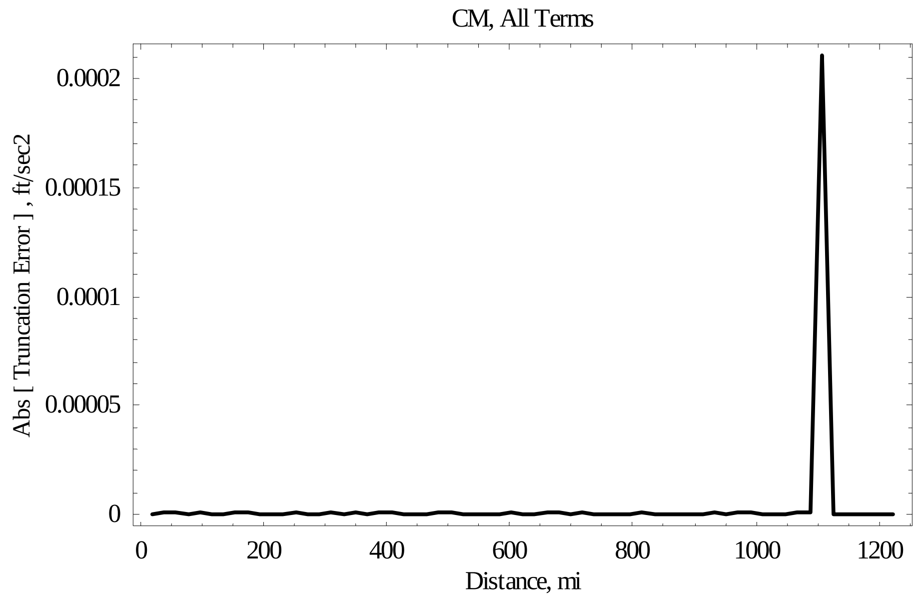

Figure 2.17. Absolute values of the truncation errors for all terms in the CM equation, for the East Coast (Constant) domain. Note that the units of truncation error are feet/sec^2. Also note that the significant maximum at a distance of 1,100 miles corresponds to the region with the steepest slope.

associated with the NCM advective term in Figure 2.11; the conservative formulation decreases the magnitude by about a factor of ten. This behavior is consistent with other studies involving the form of the momentum equation [4]. Most of the rest of the terms in the CM equation show similar truncation error behavior to that of the advective term; the lone exception is the viscous term.

Figure 2.17 shows the sum of the absolute values of all terms in the CM equation. Note that the magnitude of the truncation errors shown in Figure 2.17 (about 9.0E-05 feet/sec^2) is smaller than those in the corresponding Figure 2.12 (about 4.0E-03 feet/sec^2) for the NCM equation. The conservative formulation does decrease the truncation errors, but the maximum still occurs along the shelf break.

2.4. East Coast ($\lambda/\Delta x$) Domain

The second version of the East Coast Domain used a variable spacing based on a $\lambda/\Delta x$ ratio of 125, as described above in Section 2.2.4 and Figure 2.4. As with the constant spacing version in Section 2.3, we will present and discuss the mass balance and truncation error results for both the non-conservative and conservative versions of the one-dimensional nonlinear ADCIRC model.

2.4.1. Non-Conservative Form

In this subsection, we will present and discuss the mass balance results, the truncation errors for the non-conservative form of the GWC equation, and the truncation errors for the non-conservative momentum equation. Table 2.4 summarizes these results. Note that the variable node spacing causes many of the terms in the non-conservative GWCE to not follow the finite volume mass balance errors; however, the NCM equation continues to produce truncation errors that support our hypothesis. We will discuss these results when we present the qualitative behavior of the truncation errors, but first we present the mass balance errors.

2.4.1.1. Mass Balance Errors

Again, we present two figures for mass balance: Figure 2.18 shows the mass balance residuals for the coarse grid simulation, and Figure 2.19 shows the same graph with a refined vertical scale. The red line shows the residuals for the finite volume

Table 2.4: Summary of truncation errors for the non-conservative form of the ADCIRC model, for the East Coast $(\lambda/\Delta x)$ domain. In the first column, the names refer to terms in Appendix A. In the second column, the units of truncation error are feet/sec^2. The last column refers to whether the behavior of the truncation errors matches that of the mass balance errors, as computed by using the finite volume method.

Term	Maximum Truncation Error	Follows Mass Balance?
GWCE (Figure 2.20)	**9.0E-05**	**No**
First	6.0E-05	No
Second	6.0E-08	No
Finite Amplitude, Part 1	3.0E-05	No
Finite Amplitude, Part 2	6.5E-09	No
Advective, Part 1	1.2E-08	No
Advective, Part 2	2.0E-06	Yes
Flux	1.0E-06	Yes
Viscous	0.0E+00	
NCM (Figure 2.21)	**6.0E-05**	**Yes**
Accumulation	6.0E-06	No
Advective	3.0E-06	Yes
Bottom Friction	2.0E-05	Yes
Finite Amplitude	3.0E-05	Yes
Viscous	0.0E+00	

method, and the blue line shows the residuals for the finite element method. The variable node space produces slightly different results from the corresponding Figure 2.6 and Figure 2.7 for the constant-spacing East Coast domain, but the overall behavior is similar. The magnitudes of both the finite volume residuals and the finite element residuals are similar for both grids, and the horizontal positions of the maximum residuals is similar as

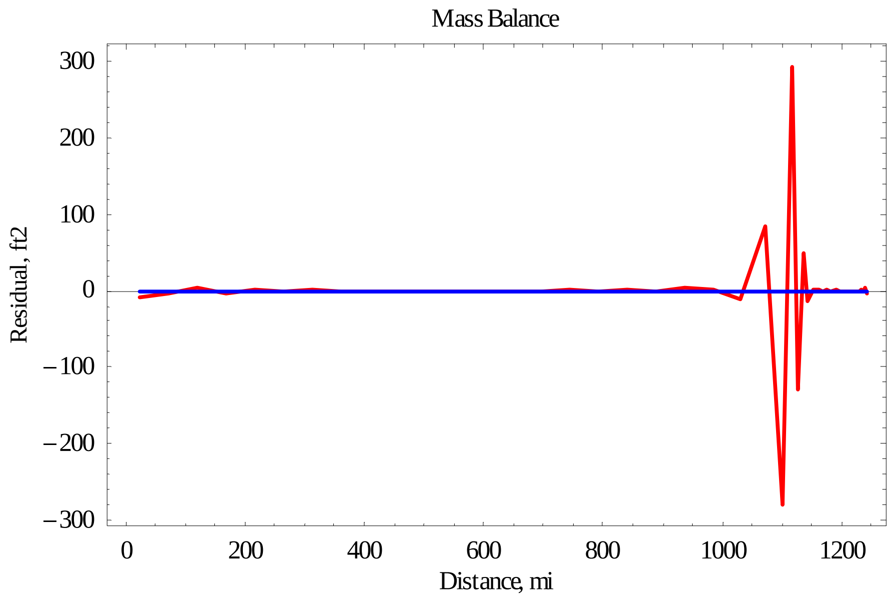

Figure 2.18. Mass balance residuals for the coarse grid simulation, for the East Coast ($\lambda/\Delta x$) domain. The red line shows the residuals from the finite volume method, and the blue line shows the residuals from the finite element method.

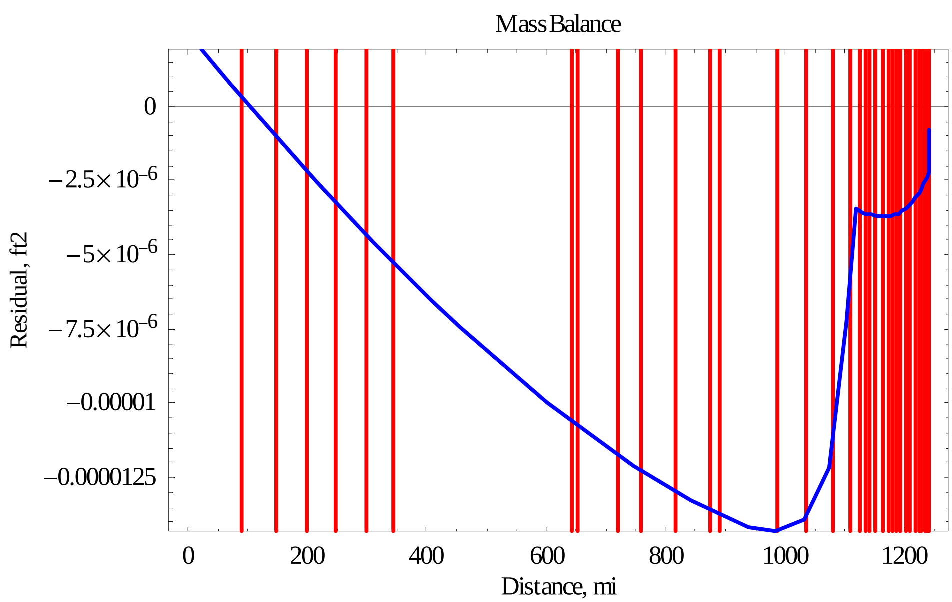

Figure 2.19. An expanded view of the mass balance residuals for the coarse grid simulation, for the East Coast ($\lambda/\Delta x$) domain. The red line shows the residuals from the finite volume method, and the blue line shows the residuals from the finite element method.

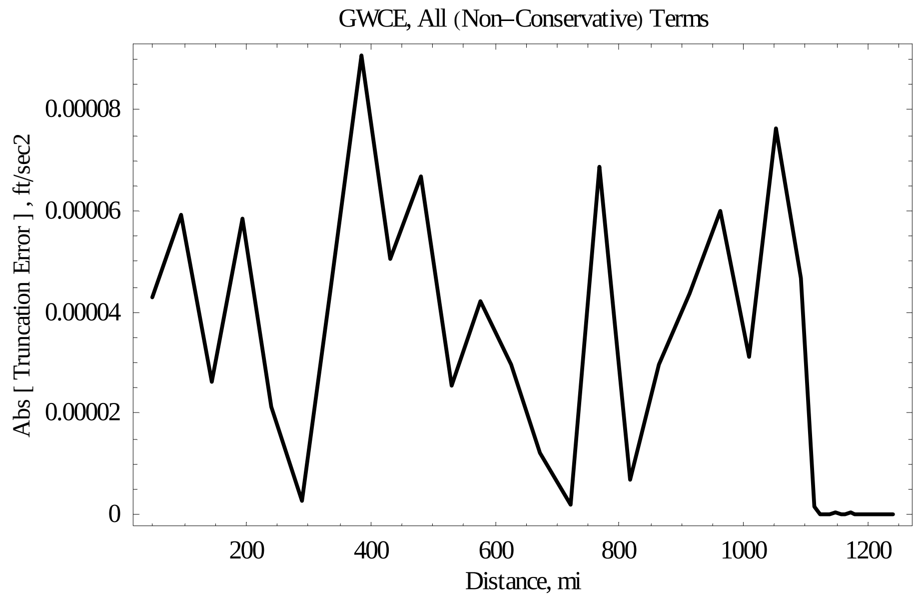

Figure 2.20. Absolute values of the truncation errors for all of the terms in the non-conservative GWC equation, for the East Coast ($\lambda / \Delta x$) domain. Note that the units of truncation error are feet/sec^2.

well. Again, the finite volume method produces residuals that are much more sensitive to changes in bathymetry.

2.4.1.2. Truncation Errors for the GWC Equation

Figure 2.20 shows the absolute values of the truncation errors for the non-conservative form of the GWC equation. Although a peak still exists at a distance of about 1,100 miles, several similar peaks occur in the deep-water region of the domain. To explain this behavior, we refer again to Table 2.4 and the breakdown of the truncation error behavior for all eight terms in the non-conservative form of the GWC equation. Only two terms (the second part of the advective term and the flux term) show behavior similar to that of the finite volume mass balance errors in Figure 2.18. The rest of the terms show significant truncation errors in all parts of the domain. As we discussed above

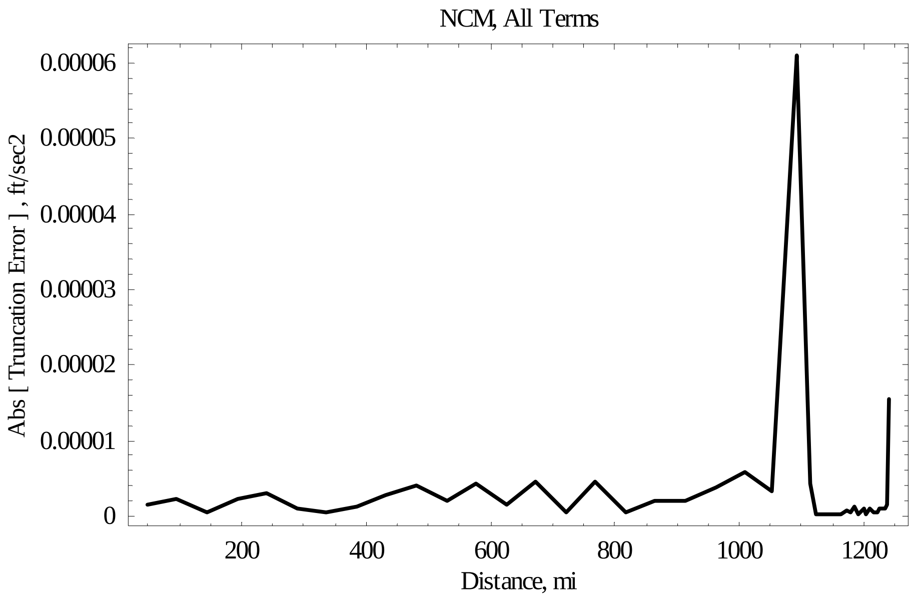

Figure 2.21. Absolute values of the truncation errors for all of the non-conservative terms in the NCM equation, for the East Coast ($\lambda/\Delta x$) domain. Note that the units of truncation error are feet/sec^2. Note that there is a clear maximum at a distance of about 1,100 miles, where the steep slope begins.

in Section 2.2.3, parameters (such as grid spacing) can be adjusted so that the truncation errors are relatively constant throughout the computational domain. It is this behavior that dominates the cumulative truncation errors shown in Figure 2.20.

2.4.1.3. Truncation Errors for the NCM Equation

Figure 2.21 shows the sum of the absolute values of the truncation errors for all of the terms in the NCM equation. Unlike the GWC equation, the NCM equation produces a significant maximum in the region where the steep slope begins. And, again in contrast to the GWC equation, this behavior is repeated for all of the individual terms in the NCM equation to varying degrees, with the exception of the viscous term, which was not used in the simulation. Even the accumulation term, although it registers as a “No” in Table 2.4

because it shows truncation errors in other parts of the domain, shows a maximum truncation error at the shelf break that is at least twice as large as those other errors. Thus, every term shows a significant maximum at a distance of about 1,100 miles, where the bathymetry changes rapidly. The overall behavior of the NCM truncation errors repeats this maximum, which again is similar to that for the finite volume mass balance errors.

2.4.2. Conservative Form

In this subsection, we will present and discuss the mass balance results, the truncation errors for the conservative form of the GWC equation, and the truncation errors for the conservative momentum equation. These results are summarized in Table 2.5. With the exception of the advective terms, the same terms are used in both the non-conservative and conservative forms of the GWCE; thus, the behavior of its truncation errors does not change dramatically for the East Coast $(\lambda / \Delta x)$ domain. However, the behavior of the truncation errors from the CM equation does change. For the NCM equation in Table 2.4, the bottom friction and finite amplitude terms dominated, and thus the overall behavior of the truncation error terms followed that of the finite volume mass balance errors. Now for the CM equation in Table 2.5, the dominant term is the first part of the finite amplitude term, whose behavior does not follow. Thus, for the CM equation and variable node spacing, the finite volume mass balance errors are not good indicators of truncation errors.

Table 2.5: Summary of truncation errors for the conservative form of the ADCIRC model, for the East Coast ($\lambda / \Delta x$) domain. In the first column, the names refer to terms in Appendix A. In the second column, the units of truncation error are feet/sec^2. The last column refers to whether the behavior of the truncation errors matches that of the mass balance errors, as computed by using the finite volume method.

Term	Maximum Truncation Error	Follows Mass Balance?
GWCE (Figure 2.24)	**8.0E-05**	**No**
First	6.0E-05	No
Second	6.0E-08	No
Finite Amplitude, Part 1	3.0E-05	No
Finite Amplitude, Part 2	6.0E-09	No
Advective	1.2E-06	Yes
Flux	1.0E-06	Yes
Viscous	0.0E+00	
CM (Figure 2.25)	**5.0E-06**	**No**
Accumulation	3.0E-06	No
Advective	4.0E-07	Yes
Bottom Friction	1.2E-07	Yes
Finite Amplitude, Part 1	3.5E-06	No
Finite Amplitude, Part 2	2.5E-09	Yes
Viscous	0.0E+00	

2.4.2.1. Mass Balance Errors

The conservative form of ADCIRC causes a reduction in the mass balance errors. Figure 2.22 shows the mass balance errors for the conservative form of the one-

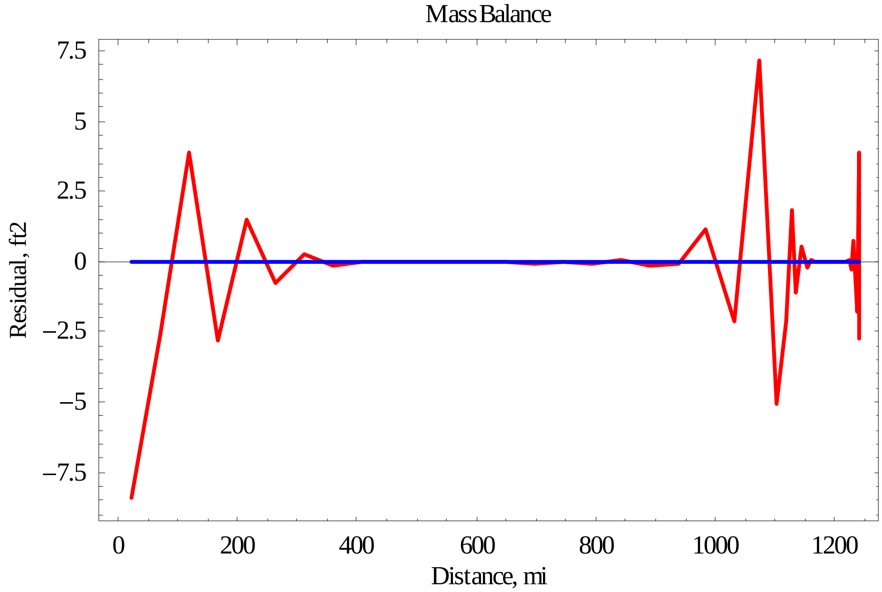

Figure 2.22. Mass balance residuals for the coarse grid simulation, for the East Coast ($\lambda/\Delta x$) domain. The red line shows the residuals from the finite volume method, and the blue line shows the residuals from the finite element method.

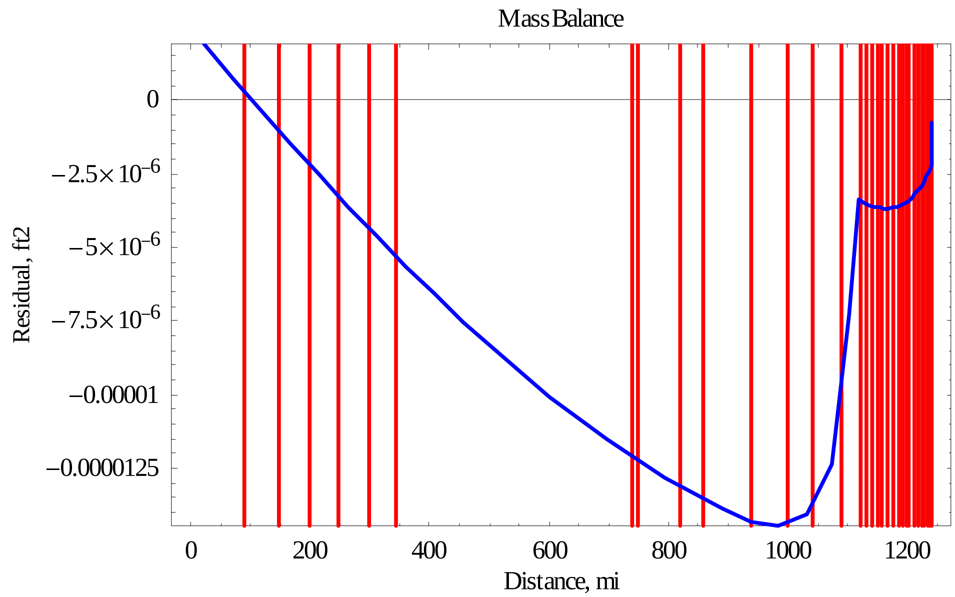

Figure 2.23. An expanded view of the mass balance residuals for the coarse grid simulation, for the East Coast ($\lambda/\Delta x$) domain. The red line shows the residuals from the finite volume method, and the blue line shows the residuals from the finite element method.

dimensional ADCIRC model, and Figure 2.23 shows an expanded view of those same errors. As with the East Coast (Constant) domain results in Section 2.3.1.1 and Section 2.3.2.1, the conservative forms of the equations cause the finite volume mass balance errors to decrease. For the East Coast ($\lambda/\Delta x$) domain, these errors are decreased from a maximum of about 300 ft^2 in Figure 2.18 to a maximum of about 7.5 ft^2 in Figure 2.22. However, the trends remain the same. The finite volume method produces mass balance errors near the boundaries and in the region with the steep bathymetry change; while the finite element method produces trivial mass balance errors throughout the domain.

2.4.2.2. Truncation Errors for the GWC Equation

Figure 2.24 shows the absolute values of the truncation errors for the conservative form of the GWC equation. Note that the same terms that dominate the non-conservative

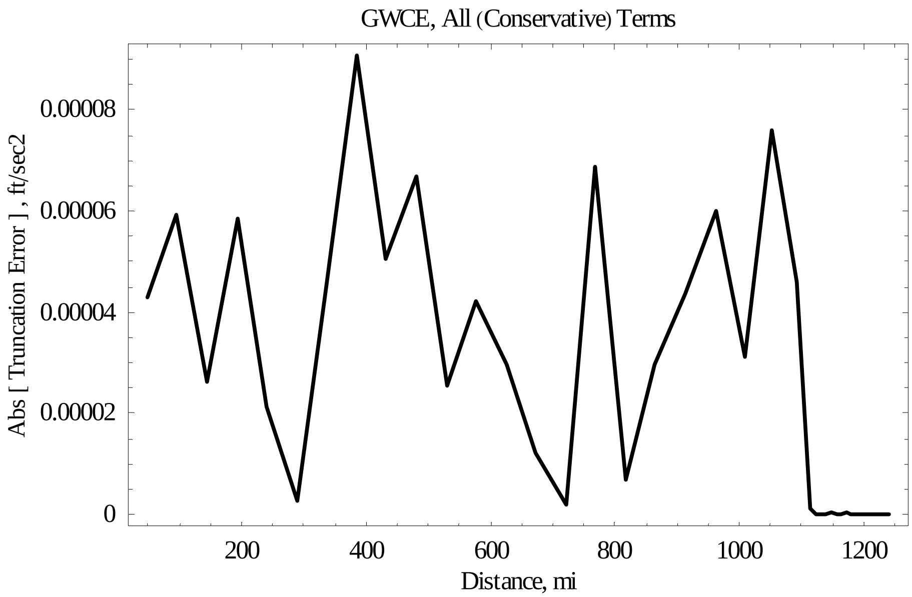

Figure 2.24. Absolute values of the truncation errors for all of the terms in the conservative GWC equation, for the East Coast ($\lambda/\Delta x$) domain. Note that the units of truncation error are feet/sec^2.

form in Figure 2.20 also dominate the conservative form in Figure 2.24 (see Table 2.4 and Table 2.5), so the overall behavior is almost identical.

2.4.2.3. Truncation Errors for the CM Equation

Figure 2.25 shows the absolute values of the truncation errors for all of the terms in the CM equation. Note the differences between the truncation errors from the non-conservative form in Figure 2.21 and those from the conservative form in Figure 2.25; the conservative form has decreased the maximum truncation errors at the shelf break so that they are the same magnitude as the truncation errors in the rest of the domain. Thus, when a variable node spacing ($\lambda/\Delta x$) is used, the finite volume mass balance errors are not nearly as good of a predictor of truncation errors from the CM equation.

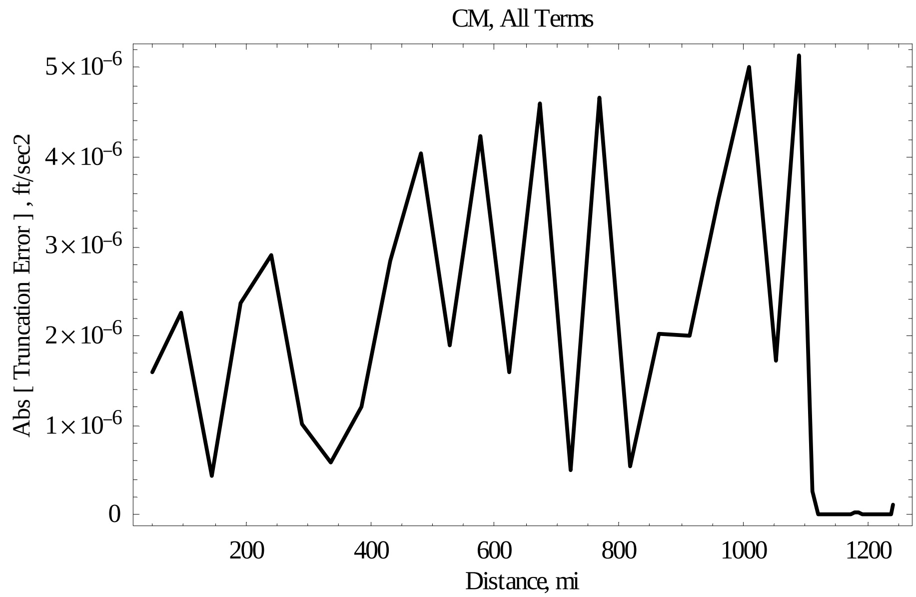

Figure 2.25. Absolute values of the truncation errors for all of the terms in the CM equation, for the East Coast ($\lambda/\Delta x$) domain. Note that the units of truncation error are feet/sec^2.

2.5. East Coast (LTEA) Domain

As described in Section 2.2.4, the third model domain is a version of the East Coast slice that uses a variable node spacing based on a localized truncation error analysis. As shown in Figure 2.4, this method clusters nodes near the shelf break, where, as shown in Section 2.3, the truncation errors are significant when a constant spacing is used. Thus, the East Coast (LTEA) domain should be a good test of the hypothesis; it should cut the truncation errors, and hopefully the mass balance errors will follow.

2.5.1. Non-Conservative Form

The results of the truncation error studies are shown in Table 2.6. Note that, if anything, the qualitative results in the third column are more closely aligned with the

Table 2.6: Summary of truncation errors for the non-conservative form of the ADCIRC model, for the East Coast (LTEA) domain. In the first column, the names refer to terms in Appendix A. In the second column, the units of truncation error are feet/sec^2. The last column refers to whether the behavior of the truncation errors matches that of the mass balance errors, as computed by using the finite volume method.

Term	Maximum Truncation Error	Follows Mass Balance?
GWCE (Figure 2.28)	**2.5E-04**	**No**
First	1.7E-04	No
Second	1.5E-07	No
Finite Amplitude, Part 1	1.1E-04	No
Finite Amplitude, Part 2	2.5E-07	Yes
Advective, Part 1	4.0E-07	Yes
Advective, Part 2	5.0E-05	Yes
Flux	1.5E-05	Yes
Viscous	0.0E+00	
NCM (Figure 2.29)	**5.0E-04**	**Yes**
Accumulation	6.0E-06	No
Advective	2.4E-04	Yes
Bottom Friction	7.0E-06	Yes
Finite Amplitude	3.0E-04	Yes
Viscous	0.0E+00	

constant node spacing results in Table 2.2 than the variable node spacing ($\lambda/\Delta x$) results in Table 2.4. If the first term, $\partial^2\zeta/\partial t^2$, did not cause large truncation errors in the deep water part of the domain, then the overall truncation errors for the GWCE would show good agreement with the finite volume mass balance errors. The LTEA method of

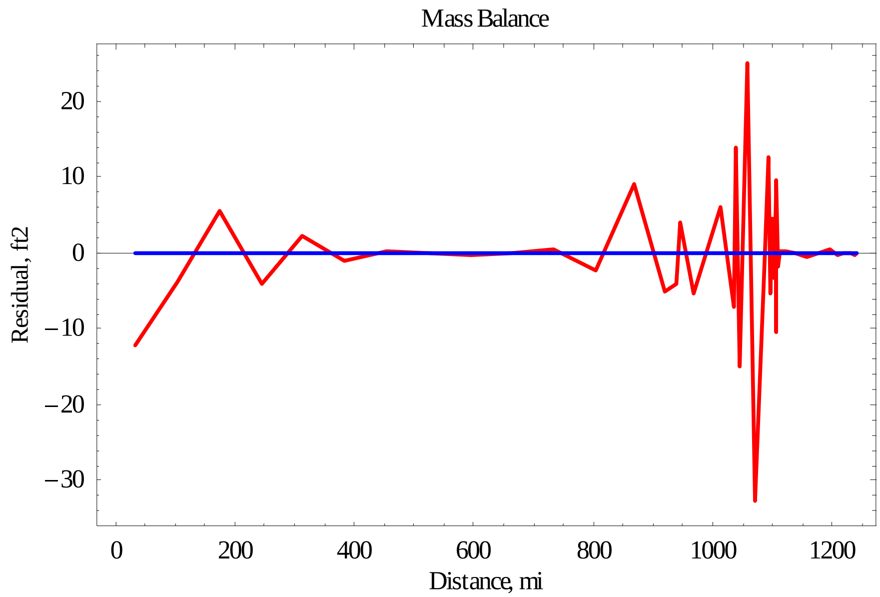

Figure 2.26. Mass balance residuals for the coarse grid simulation, for the East Coast (LTEA) domain. The red line shows the residuals from the finite volume method, and the blue line shows the residuals from the finite element method.

variable node spacing decreases the truncation errors, but it does not change their behavior.

2.5.1.1. Mass Balance Errors

Figure 2.26 shows the mass balance errors for the non-conservative version of the ADCIRC model, and Figure 2.27 shows an expanded view of those same mass balance errors. Note that the errors computed from the finite element method are still small, to where the axis has to be refined to the order of 10^{-5} ft^2 before they become evident. Also note that the errors computed from the finite volume method follow a similar pattern: the significant errors occur near the boundaries and near the shelf break. The LTEA method of placing node points has a positive effect on the finite volume mass balance errors, which decrease from a maximum magnitude of 200-300 ft^2 for the East Coast (Constant)

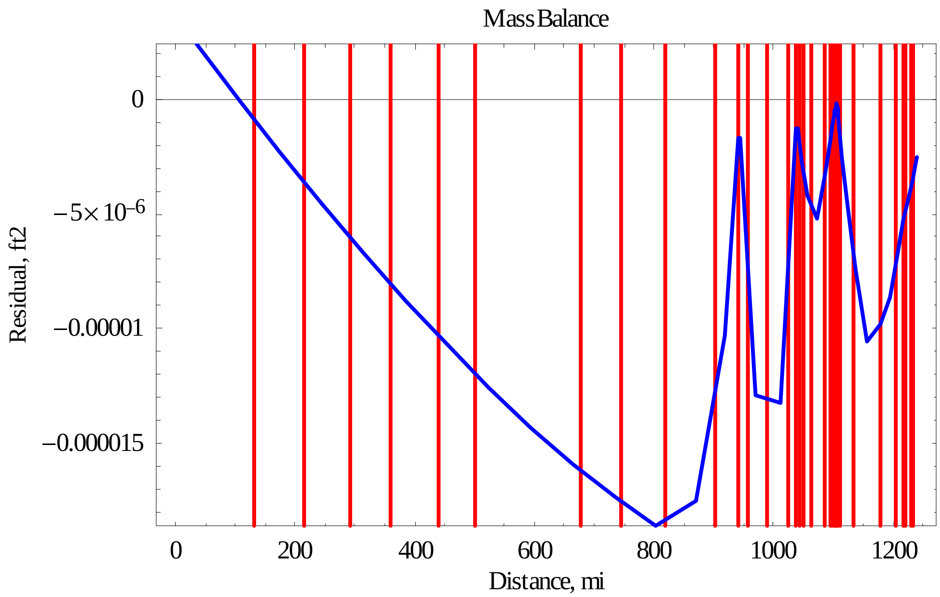

Figure 2.27. An expanded view of the mass balance residuals for the coarse grid simulation, for the East Coast (LTEA) domain. The red line shows the residuals from the finite volume method, and the blue line shows the residuals from the finite element method.

results in Figure 2.6 and the East Coast ($\lambda / \Delta x$) results in Figure 2.18 to a maximum magnitude of 30 ft^2 for the East Coast (LTEA) results in Figure 2.26. The lower mass balance errors from the finite volume method reflect the extra LTEA resolution in the region of interest.

2.5.1.2. Truncation Errors for the GWC Equation

Figure 2.28 shows the absolute values of the truncation errors for all of the non-conservative terms in the GWC equation. Note that, as with the East Coast ($\lambda / \Delta x$) domain in Figure 2.20, the variable spacing of the East Coast (LTEA) domain causes a decrease in the maximum truncation error from the GWC equation. Instead of showing a clear peak of 0.07 feet/sec^2 at the shelf break, like for the East Coast (Constant) domain in Figure 2.10, the truncation errors show several peaks of about 0.0002 feet/sec^2. Once

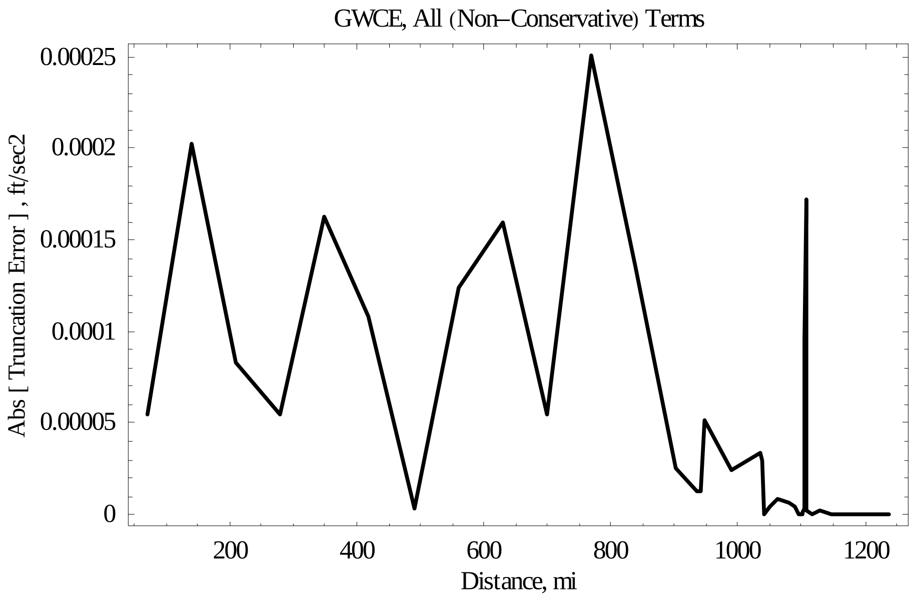

Figure 2.28. Absolute values of the truncation errors for all of the terms in the non-conservative GWC equation, for the East Coast (LTEA) domain. Note that the units of truncation error are

again, the error behavior varies for each of the terms in the GWC equation. All of the terms show skinny spikes at a distance of about 1,100 miles, in the very-refined steep slope region. The truncation errors in the deep water are the result of three terms: the first term, $\partial^2\zeta/\partial t^2$; the second term, $G(\partial\zeta/\partial t)$; and the first part of the finite amplitude term, $gh(\partial^2\zeta/\partial x^2)$.

2.5.1.3. Truncation Errors for the NCM Equation

Figure 2.29 shows the truncation errors for the NCM equation. The LTEA method of placing node points causes a decrease of about an order of magnitude from the constant spacing results in Figure 2.12, but it is about an order of magnitude larger than the NCM results from the East Coast ($\lambda/\Delta x$) domain shown in Figure 2.21. (We would propose that this difference in magnitude is caused by the greater variation in grid spacing for the

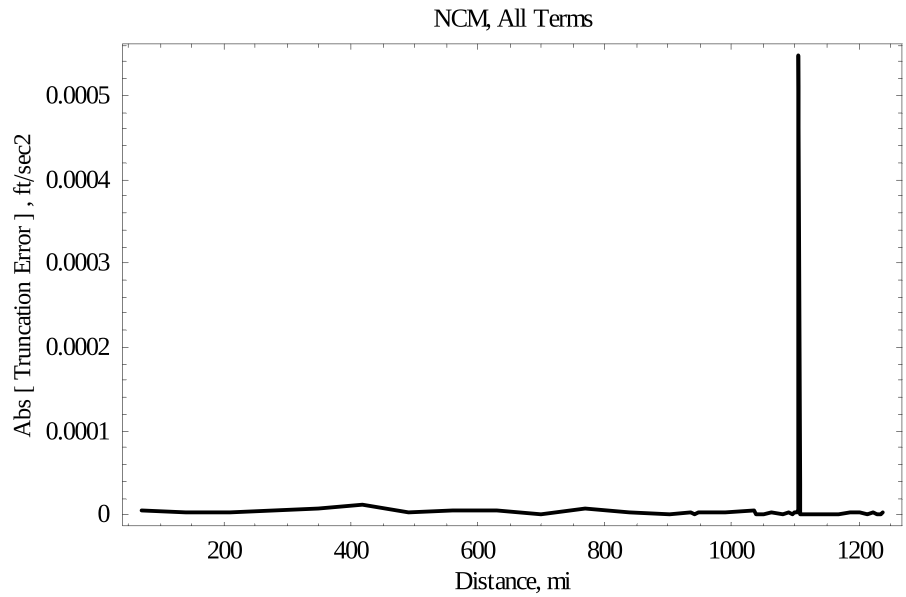

Figure 2.29. Absolute values of the truncation errors for all of the non-conservative terms in the NCM equation, for the East Coast (LTEA) domain. Note that the units of truncation error are feet/sec^2. Also note that there is a clear maximum at a distance of about 1,100 miles, where the steep slope begins.

East Coast (LTEA) domain; a greater variation would cause some of the coefficients of the derivatives in the truncation error terms to become more dominant.) More importantly, the only significant truncation errors occur near the shelf break, and the overall behavior of the truncation errors is similar to that of the finite volume mass balance errors.

2.5.2. Conservative Form

Table 2.7 summarizes the truncation errors results for the East Coast (LTEA) domain and the conservative form of the ADCIRC model. The same terms dominate the conservative GWCE as did the non-conservative GWCE earlier, so that equation also produces overall truncation errors that do not follow the finite volume mass balance errors. However, the CM equation does produce results that correlate well.

Table 2.7: Summary of truncation errors for the conservative form of the ADCIRC model, for the East Coast (LTEA) domain. In the first column, the names refer to terms in Appendix A. In the second column, the units of truncation error are feet/sec^2. The last column refers to whether the behavior of the truncation errors matches that of the mass balance errors, as computed by using the finite volume method.

Term	Maximum Truncation Error	Follows Mass Balance?
GWCE (Figure 2.32)	**2.5E-04**	**No**
First	1.7E-04	No
Second	1.5E-07	No
Finite Amplitude, Part 1	1.0E-04	No
Finite Amplitude, Part 2	2.5E-07	Yes
Advective	1.0E-04	Yes
Flux	1.5E-05	Yes
Viscous	0.0E+00	
CM (Figure 2.33)	**2.0E-05**	**Yes**
Accumulation	6.0E-06	No
Advective	1.1E-05	Yes
Bottom Friction	3.0E-07	Yes
Finite Amplitude, Part 1	1.0E-05	Yes
Finite Amplitude, Part 2	2.5E-08	Yes
Viscous	0.0E+00	

2.5.2.1. Mass Balance Errors

Figure 2.30 shows the mass balance residuals for the conservative version of the one-dimensional ADCIRC model, and Figure 2.31 shows an expanded view of those same

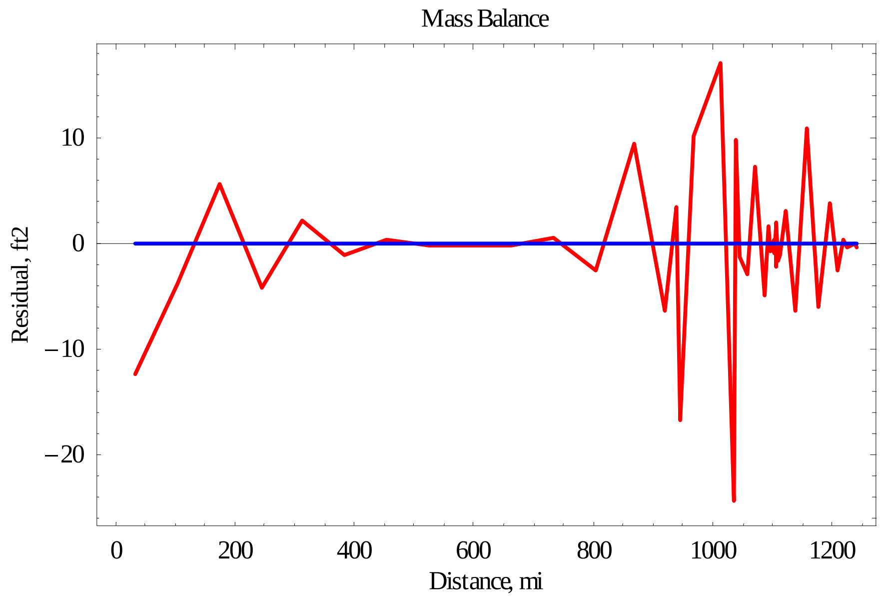

Figure 2.30. Mass balance residuals for the coarse grid simulation, for the East Coast (LTEA) domain. The red line shows the residuals from the finite volume method, and the blue line shows the residuals from the finite element method.

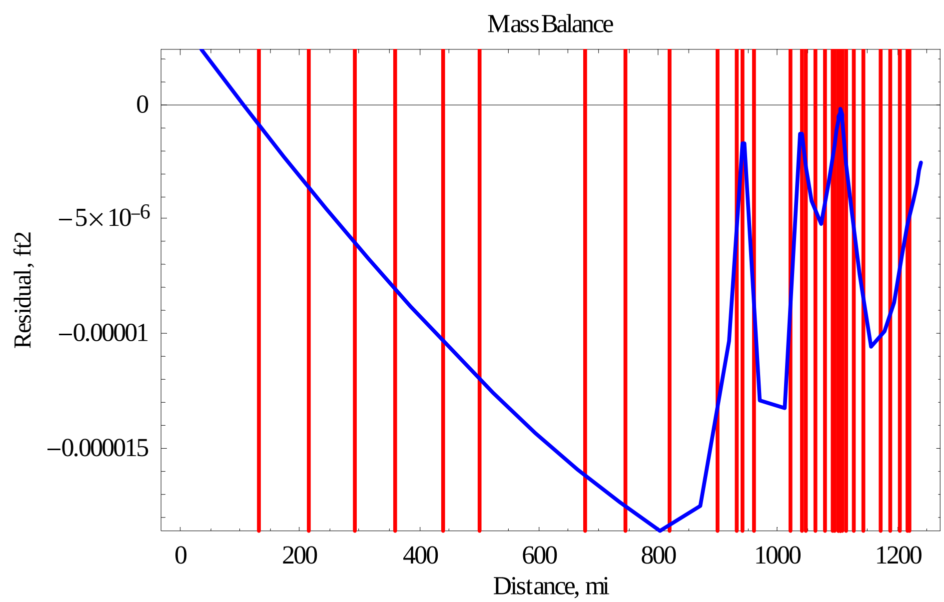

Figure 2.31. An expanded view of the mass balance residuals for the coarse grid simulation, for the East Coast (LTEA) domain. The red line shows the residuals from the finite volume method, and the blue line shows the residuals from the finite element method.

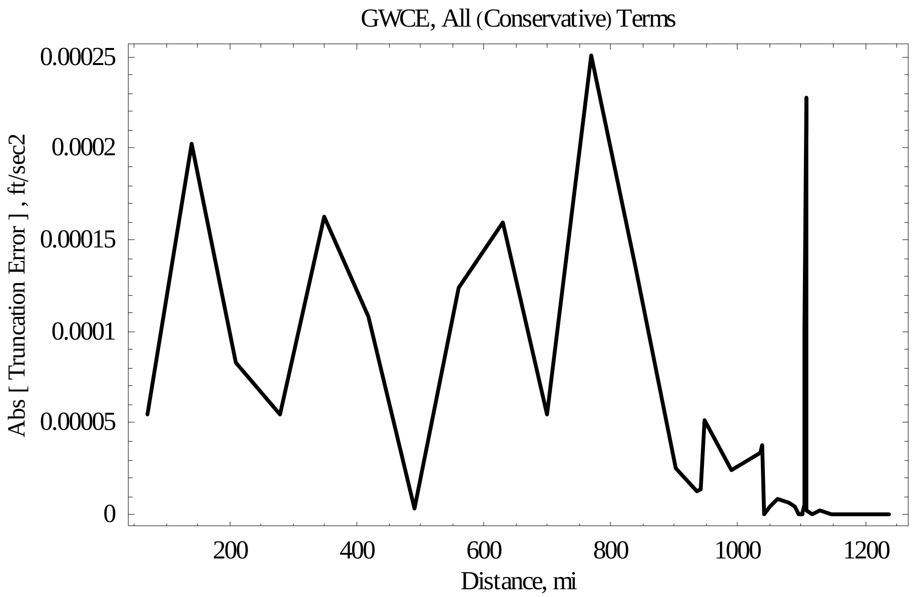

Figure 2.32. Absolute values of the truncation errors for all of the terms in the conservative GWC equation, for the East Coast (LTEA) domain. Note that the units of truncation error are feet/

residuals. The conservative version again decreases the maximum mass balance error, which is about 40 percent less than the maximum error from the non-conservative version in Figure 2.26, but the difference is not as significant as it was for the East Coast (Constant) domain. Significant errors occur over a larger region than they did for the non-conservative version, but the maximum errors still occur near the shelf break.

2.5.2.2. Truncation Errors for the GWC Equation

Figure 2.32 shows the absolute value of the truncation errors for the GWC equation. These errors are almost identical to those shown in Figure 2.28 from the non-conservative form of the GWC equation, because the dominant terms are the same in both forms. Thus, the peak at the shelf break is the same order of magnitude as the peaks in the deeper regions of the domain.

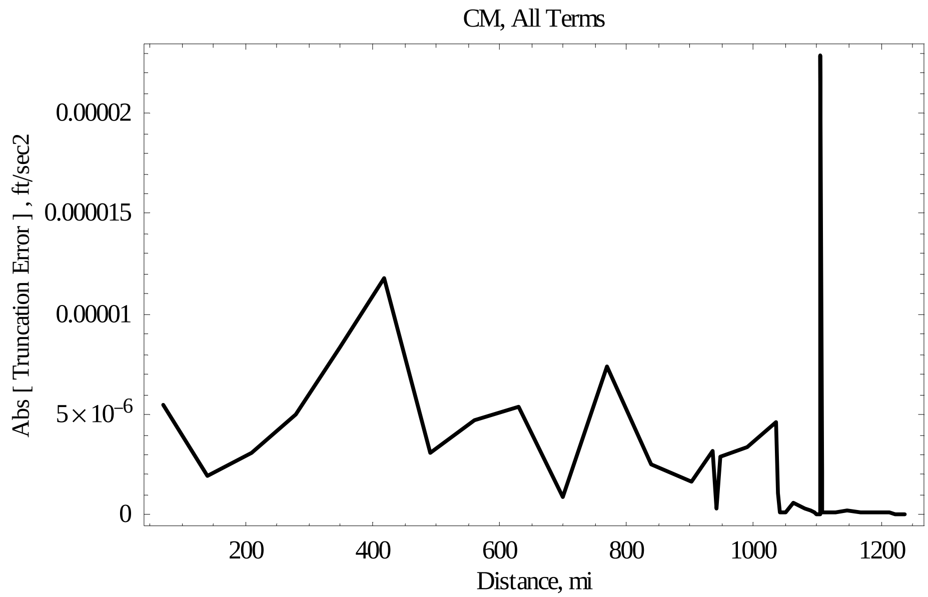

Figure 2.33. Absolute values of the truncation errors for all of the terms in the CM equation, for the East Coast (LTEA) domain. Note that the units of truncation error are feet/sec^2.

2.5.2.3. Truncation Errors for the CM Equation

Figure 2.33 shows the absolute values of the truncation errors for the CM equation. As with the results from the NCM equation in Figure 2.29, the significant truncation errors occur at the shelf break. However, the conservative form decreases the magnitude of those errors by about 96 percent, so that the errors in the rest of the domain become more pronounced at this scale. Nevertheless, the overall behavior of these truncation errors follows that of the finite volume mass balance errors in Figure 2.30.

2.6. Linear Sloping Beach Domain

The first three test domains were based on the East Coast bathymetry with a fixed land boundary, but with different node spacings. Those domains are good tests for mass balance because they contain converging flow over a shelf break, which has historically caused problems for the ADCIRC model. Another good test case for mass balance is any problem that contains wetting and drying, because, as will be discussed in later chapters, the ADCIRC wetting and drying algorithm adds and subtracts elements from the computational domain as regions are wetted and dried. Thus, our fourth test domain is the Linear Sloping Beach domain, which was described in Section 2.2.4. We chose this domain because it has an analytical solution, which proved useful in the wetting and drying studies. In this subsection, we will present the mass balance and truncation errors for the non-conservative and conservative versions of the one-dimensional ADCIRC model.

2.6.1. Non-Conservative Form

Table 2.8 summarizes the truncation error results for the non-conservative form of the ADCIRC model. Like the constant node spacing results for the East Coast (Constant) domain in Section 2.3, the constant node spacing results for the Linear Sloping Beach domain produce truncation errors that are consistent with the finite volume mass balance errors. In fact, they are uniformly consistent, in that the truncation errors for every term follow the finite volume mass balance errors.

2.6.1.1. Mass Balance Errors

Figure 2.34 shows the mass balance errors for the non-conservative version of the one-dimensional ADCIRC model, and Figure 2.35 shows an expanded view of the same errors. At the point in time when we calculate these errors, the wet/dry interface is at a

Table 2.8: Summary of truncation errors for the non-conservative form of the ADCIRC model, for the Linear Sloping Beach domain. In the first column, the names refer to terms in Appendix A. In the second column, the units of truncation error are meters/sec^2. The last column refers to whether the behavior of the truncation errors matches that of the mass balance errors, as computed by using the finite volume method.

Term	Maximum Truncation Error	Follows Mass Balance?
GWCE (Figure 2.36)	**7.0E-05**	**Yes**
First	4.0E-05	Yes
Second	1.7E-05	Yes
Finite Amplitude, Part 1	2.0E-05	Yes
Finite Amplitude, Part 2	2.0E-06	Yes
Advective, Part 1	6.0E-06	Yes
Advective, Part 2	1.2E-05	Yes
Flux	2.5E-06	Yes
Viscous	0.0E+00	
NCM (Figure 2.37)	**1.5E-02**	**Yes**
Accumulation	6.0E-03	Yes
Advective	1.5E-03	Yes
Bottom Friction	3.5E-05	Yes
Finite Amplitude	8.0E-03	Yes
Viscous	0.0E+00	

distance of about 18 kilometers, as shown in Figure 2.5, and moving toward the right (land-ward side of the domain). Thus, the significant finite volume mass balance errors in Figure 2.34 occur in the region where wetting and drying is taking place. This trend continues throughout the rest of the simulation; i.e., significant finite volume mass balance errors follow the wet/dry interface as it inundates and recedes. Note that the finite element

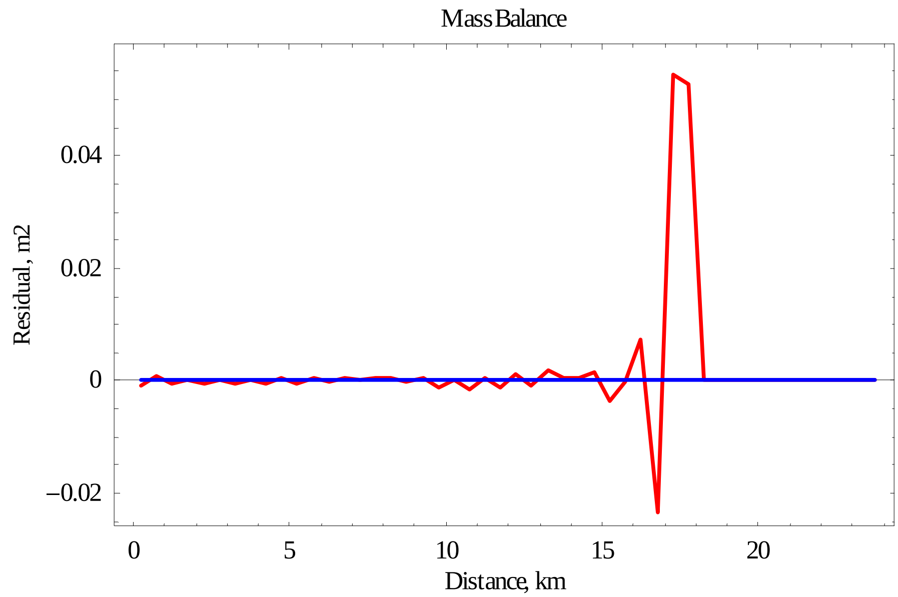

Figure 2.34. Mass balance residuals for the coarse grid simulation, for the Linear Sloping Beach domain. The red line shows the residuals from the finite volume method, and the blue line shows the residuals from the finite element method.

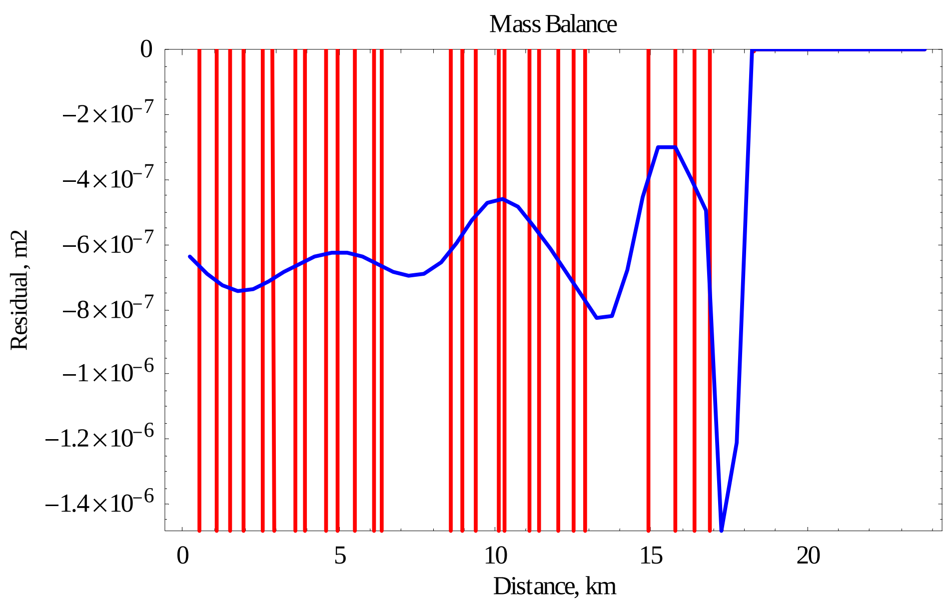

Figure 2.35. Close-up of the mass balance residuals for the coarse grid simulation, for the Linear Sloping Beach domain. The red line shows the residuals from the finite volume method, and the blue line shows the residuals from the finite element method.

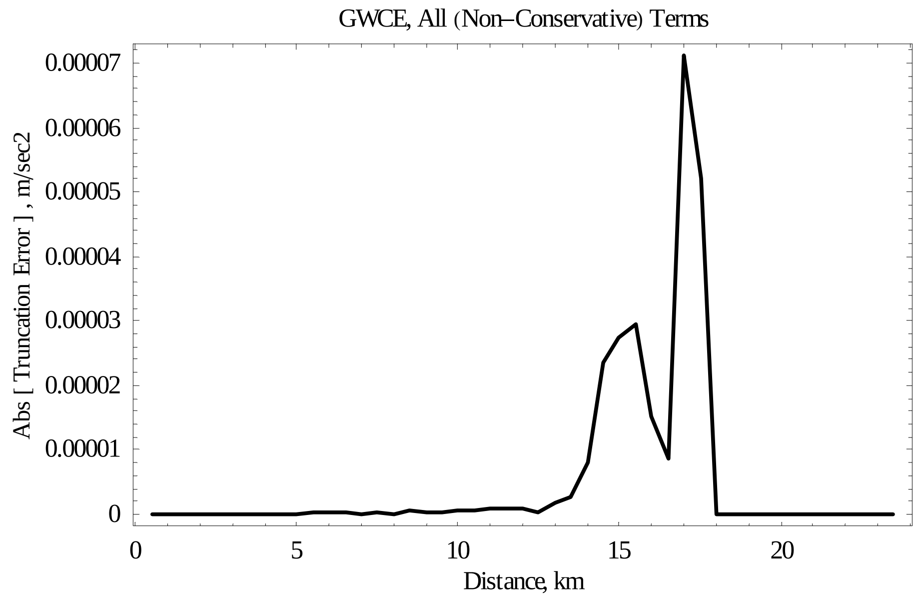

Figure 2.36. Absolute values of the truncation errors for all of the terms in the non-conservative GWC equation, for the Linear Sloping Beach domain. Note that the units of truncation error

mass balance errors, shown in Figure 2.35, show a similar oscillatory pattern and have their largest magnitude near the wet/dry interface. However, the errors oscillate around a non-zero value in the deeper region of the domain, and the scale must be refined by four orders of magnitude before they become apparent.

2.6.1.2. Truncation Errors for the GWC Equation

Figure 2.36 shows the absolute values of the truncation errors for the non-conservative form of the GWC equation. Note the similarities in behavior between the truncation errors and the finite volume mass balance errors; both show trivial errors in the deeper region of the domain, and both have significant peaks in the wetting and drying region. The finite volume mass balance errors follow the truncation errors.

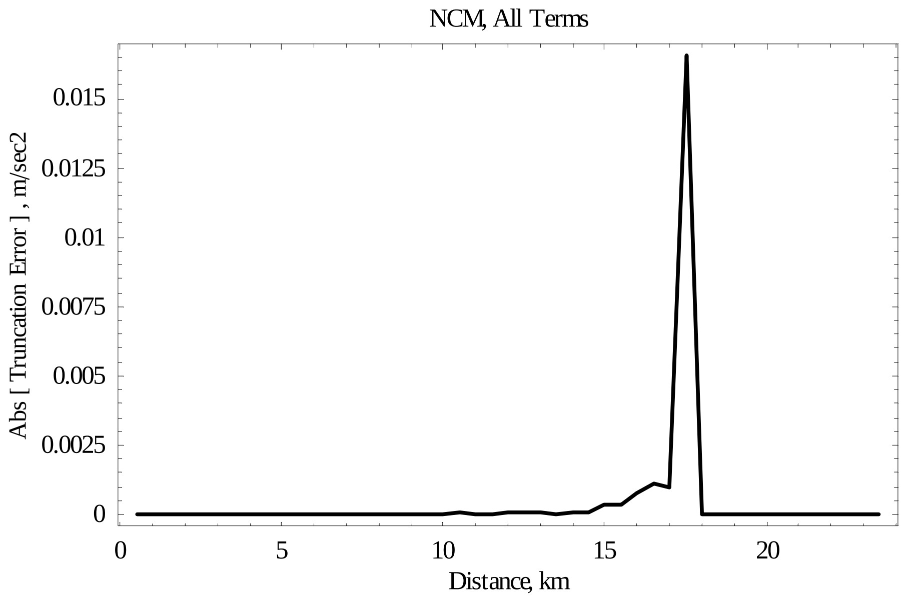

Figure 2.37. Absolute values of the truncation errors for all of the terms in the NCM equation, for the Linear Sloping Beach domain. Note that the units of truncation error are meters/sec^2.

2.6.1.3. Truncation Errors for the NCM Equation

Figure 2.37 shows the absolute values of the truncation errors for the NCM equation. Again, the truncation errors show a behavior similar to the finite volume mass balance errors. The maximum truncation error occurs near the wet/dry interface, and the rest of the truncation errors are approximately zero.

2.6.2. Conservative Form

Table 2.9 summarizes the truncation error results for the conservative form of the ADCIRC model, for the Linear Sloping Beach domain. Like the non-conservative results in Table 2.8, the conservative results all show good agreement between the finite volume mass balance errors and the truncation errors. Note that the conservative form of the

Table 2.9: Summary of truncation errors for the conservative form of the ADCIRC model, for the Linear Sloping Beach domain. In the first column, the names refer to terms in Appendix A. In the second column, the units of truncation error are meters/sec^2. The last column refers to whether the behavior of the truncation errors matches that of the mass balance errors, as computed by using the finite volume method.

Term	Maximum Truncation Error	Follows Mass Balance?
GWCE (Figure 2.40)	**7.0E-05**	**Yes**
First	4.0E-05	Yes
Second	1.7E-05	Yes
Finite Amplitude, Part 1	2.0E-05	Yes
Finite Amplitude, Part 2	2.0E-06	Yes
Advective	2.5E-06	Yes
Flux	2.5E-06	Yes
Viscous	0.0E+00	
CM (Figure 2.41)	**3.5E-04**	**Yes**
Accumulation	5.0E-05	Yes
Advective	2.0E-05	Yes
Bottom Friction	6.0E-07	Yes
Finite Amplitude, Part 1	2.5E-04	Yes
Finite Amplitude, Part 2	6.0E-05	Yes
Viscous	0.0E+00	

momentum equation again decreases the truncation errors, this time by about two orders of magnitude. However, the maximum truncation errors continue to appear in the region near the wet/dry interface.

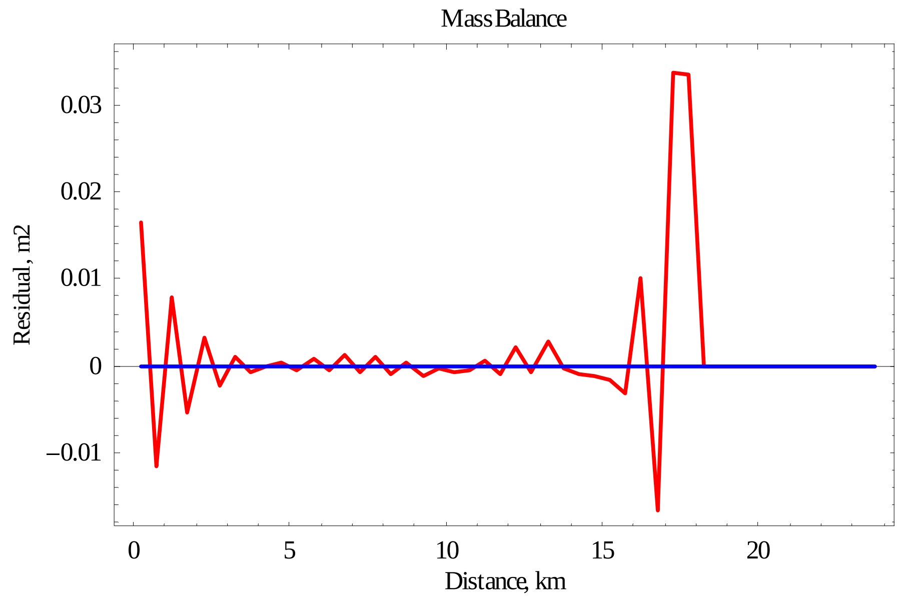

Figure 2.38. Mass balance residuals for the coarse grid simulation, for the Linear Sloping Beach domain. The red line shows the residuals from the finite volume method, and the blue line shows the residuals from the finite element method.

2.6.2.1. Mass Balance Errors

Figure 2.38 shows the mass balance errors for the conservative version of the one-dimensional ADCIRC model, and Figure 2.39 shows an expanded view of those same errors. The conservative version produces slightly smaller finite volume mass balance errors; the non-conservative version had a maximum of about 0.05 m^2 in Figure 2.34, whereas the conservative version has a maximum of about 0.03 m^2 in Figure 2.38. The conservative version also produces larger finite volume mass balance errors near the left boundary. Note that the behavior of the finite element mass balance errors does not change, but their magnitudes are decreased slightly.

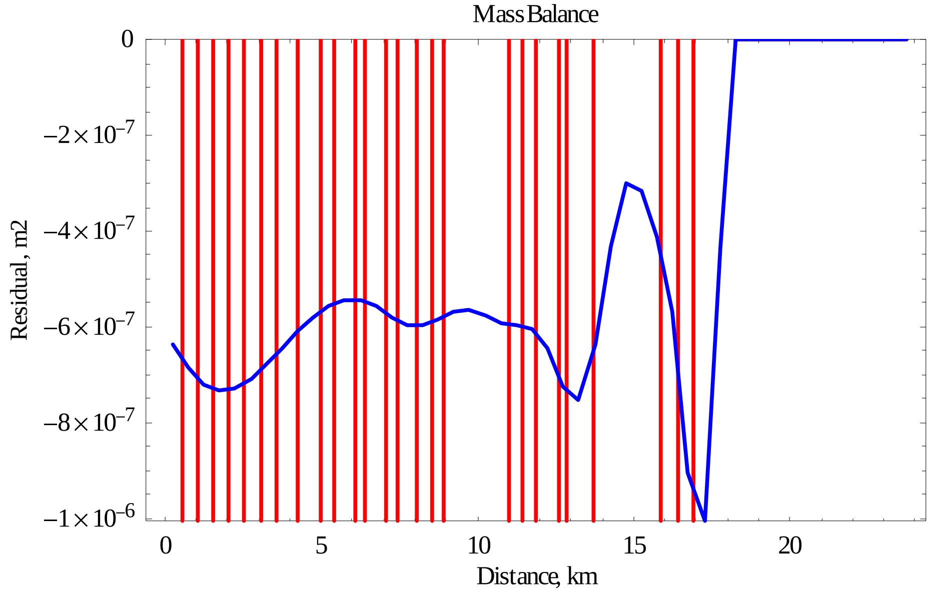

Figure 2.39. An expanded view of the mass balance residuals for the coarse grid simulation, for the Linear Sloping Beach domain. The red line shows the residuals from the finite volume method, and the blue line shows the residuals from the finite element

2.6.2.2. Truncation Errors for the GWC Equation

Figure 2.40 shows the absolute values of the truncation errors for the conservative form of the GWC equation. Once again, the behavior of the truncation errors matches the behavior of the finite volume mass balance errors. And, as shown in Table 2.8 and Table 2.9, the form of the GWC equation does not affect the magnitude of the truncation errors, at least for this grid.

2.6.2.3. Truncation Errors for the CM Equation

Figure 2.41 shows the absolute values of the truncation errors for the CM equation. The conservative form again causes a decrease in the magnitude of the truncation errors, this time by about two orders of magnitude from the non-conservative results in Section

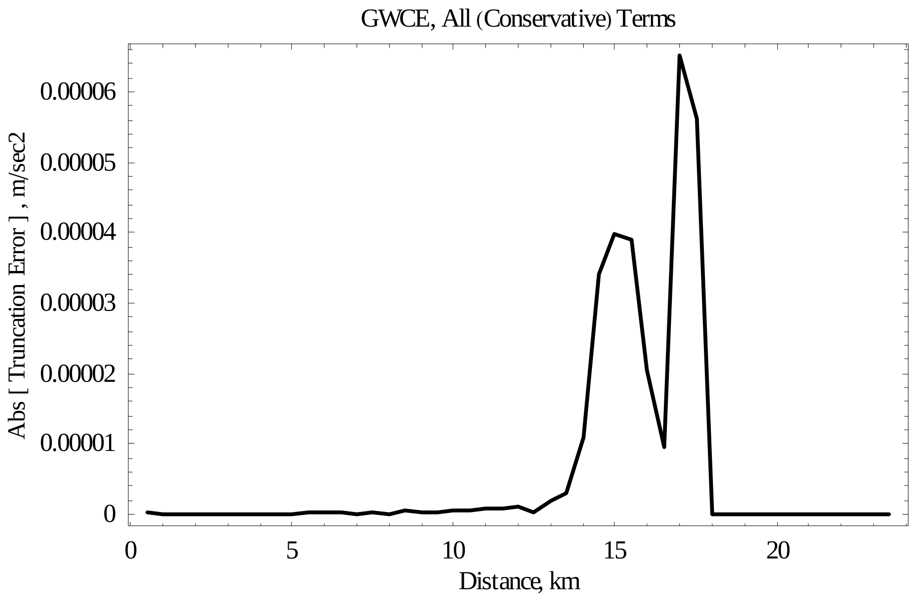

Figure 2.40. Absolute values of the truncation errors for all of the terms in the conservative GWC equation, for the Linear Sloping Beach domain. Note that the units of truncation error are

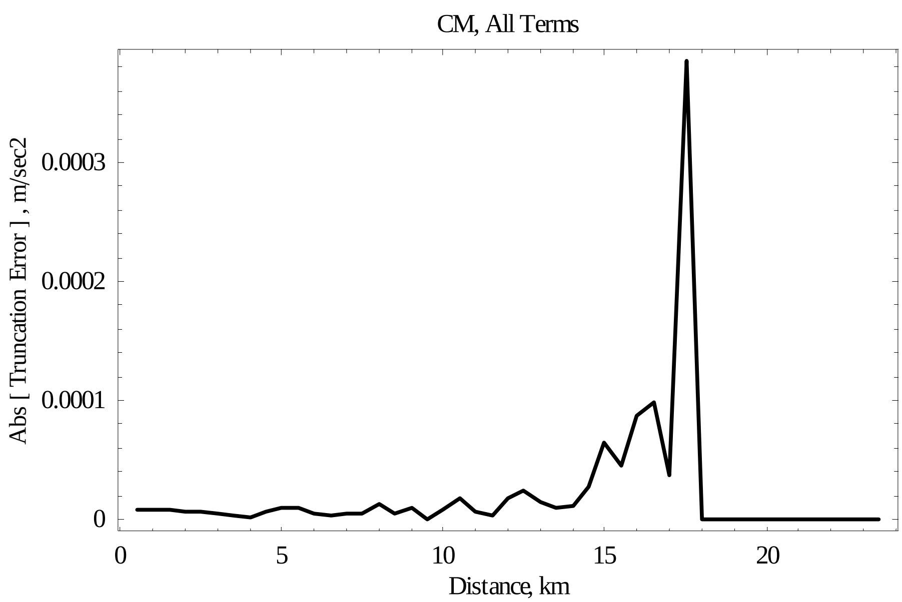

Figure 2.41. Absolute values of the truncation errors for all of the terms in the CM equation, for the Linear Sloping Beach domain. Note that the units of truncation error are meters/sec^2.

2.6.1.3, but it does not change the overall shape. Significant truncation errors occur in the wetting and drying region, and they follow the finite volume mass balance errors.

2.7. Grid Generation using Finite Volume Mass Balance Errors

The results in the previous four subsections indicate that finite volume mass balance error can be used as an indicator of truncation error, especially for grids with constant node spacing. This trend can be exploited. When grids (such as the East Coast (LTEA) domain in Section 2.5) are developed by minimizing truncation errors, they exhibit better behavior overall [6, 7]. However, it is costly to develop these grids because they require computation of the truncation errors, which require knowledge of the true or "fine" solution. It would be much more efficient if mass balance error could be used as the criterion for grid development. In fact, it would lead to dynamic (run-time) meshing.

In this section, we will "pilot" the idea by walking through the development of a grid that uses mass balance error as the criterion for node placement. We will begin with the East Coast (Constant) domain described in Section 2.2.4 and Section 2.3 and use the following assumptions:

- The study should use the non-conservative form of the ADCIRC model.
- The criterion should be mass balance error computed by the finite volume method, because we have shown that the finite volume method is a better indicator of truncation errors than is the finite element method.
- The total number of nodes should remain constant. In other words, in order to place a node in a region with high mass balance errors, a node must first be removed from a region with low mass balance errors. The East Coast (Constant) domain has 65 nodes, so our concept domain will have more nodes than either of the variable-spaced East Coast domains described previously, which both had 46 nodes.

- The removal of a node in a region with low mass balance errors should not affect the neighboring nodes. Thus, when a node is removed, its neighbors should not be moved to compensate. In effect, the grid spacing in that region is doubled, and it can be increased further after successive iterations.
- When a node is added to a region with high mass balance errors, it should be placed at the midpoint of an existing element. In effect, the grid spacing in that region is halved.
- When a node is added, its bathymetry should be computed from a linear interpolation of the surrounding bathymetries. In an automated grid-generation scheme, a background grid and higher-order interpolation could be used to compute bathymetries.

These assumptions were made as much for convenience as for scientific correctness. However, they allow for a grid development scenario that illustrates how mass balance error can be used to generate a grid that minimizes truncation errors.

We begin with the finite volume mass balance errors shown in Figure 2.6. The largest magnitude error is -293 ft^2, and it occurs at a distance of about 1,097 miles, which is about where the continental shelf begins its steep descent, as shown in Figure 2.3. All of the significant finite volume mass balance errors occur in this region. Thus, to minimize these mass balance errors, we removed nodes from the deeper parts of the domain and added them to the shelf-break region. After several iterations, in which we moved four or eight nodes at a time and re-computed mass balance, we obtained the node placement depicted in Figure 2.42.

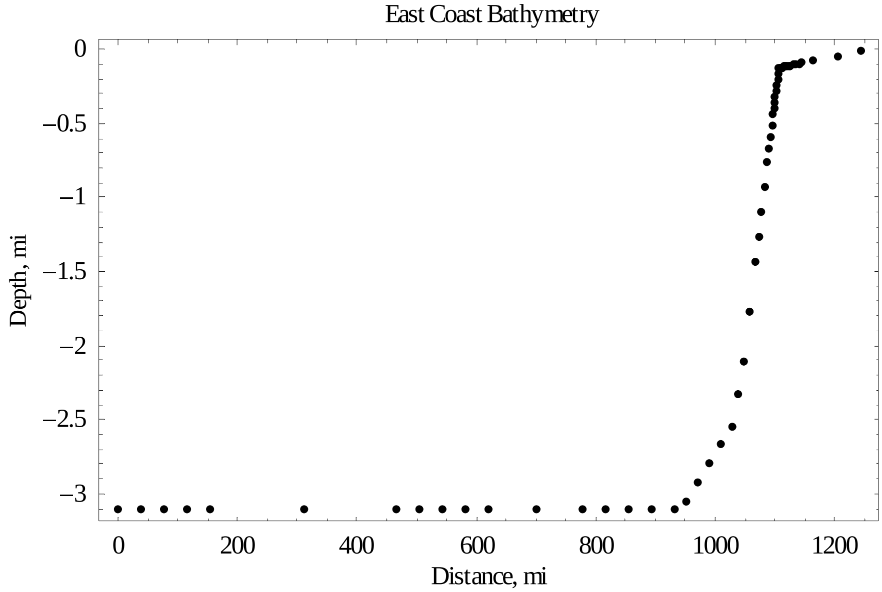

Figure 2.42. Distribution of nodes for the concept East Coast domain. Note how nodes are clustered at the shelf break. The grid spacing ranges from about 820,000 feet in the deep water to about 6,400 feet near the shelf break.

We can make several observations based solely on the node distribution. First, in order to minimize the finite volume mass balance errors, the majority of the nodes were placed in the region where the shelf begins its steep descent. The grid spacing in this region is about 6,400 feet, or 16 times smaller than the original node spacing. Second, the deep water portion of this domain can be modeled with relatively few nodes. We were able to increase the grid spacing in this region as high as 820,000 feet, or eight times larger than the original grid spacing. Third, after six iterations, a total of 34 nodes were moved during the grid development.

The effects of this grid on simulation results are dramatic. Mass balance results are shown in Figure 2.43. Adding nodes at the shelf break decreases the finite volume mass balance errors in that region, and removing nodes from the deep water increases the errors in that region. The end result is a domain that shows similar errors in all regions.

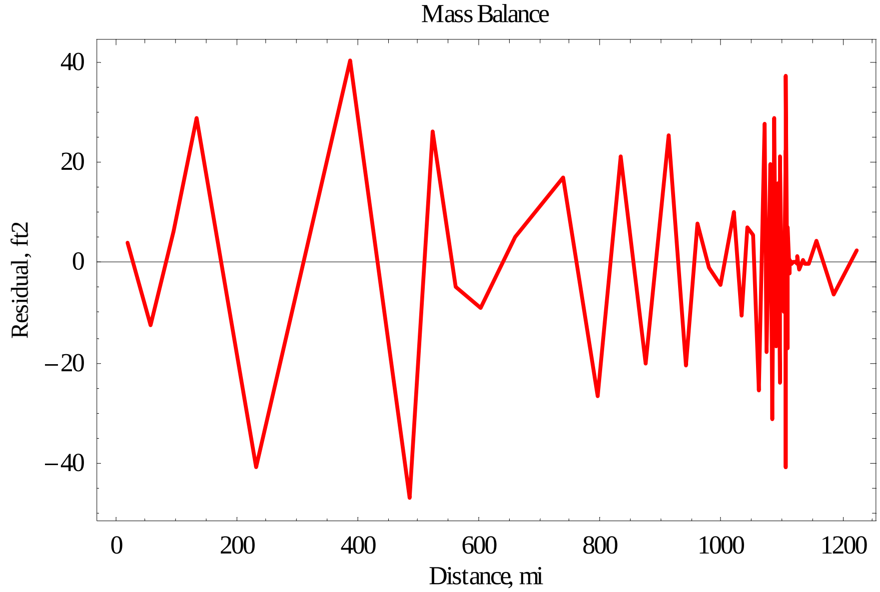

Figure 2.43. Mass balance residuals for
the concept East Coast domain. The red line shows the residuals from the
finite volume method.

Note that the largest magnitude error is -46.9 feet^2, which is a decrease of about 84 percent from the original, constant-spacing grid. Further iteration on node placement, specifically by moving more nodes from the shelf and continental rise to the deep water and shelf break regions, would further decrease these mass balance errors.

Similar behavior is observed with respect to truncation errors. Table 2.12 summarizes the truncation errors for the concept East Coast domain, for the non-conservative form of the ADCIRC model. Note that, although many of the individual terms do not produce truncation errors that are qualitatively similar to the finite volume mass balance errors, the overall equations do. Figure 2.44 shows the cumulative truncation errors for the non-conservative form of the GWC equation, and Figure 2.45 shows the cumulative truncation errors for the NCM equation. Note that, although both figures have peaks at the shelf break, there are significant truncation errors in the deep

Table 2.10: Summary of truncation errors for the non-conservative form of the ADCIRC model, for the concept East Coast domain. In the first column, the names refer to terms in Appendix A. In the second column, the units of truncation error are feet/sec^2. The last column refers to whether the behavior of the truncation errors matches that of the mass balance errors, as computed by using the finite volume method.

Term	Maximum Truncation Error	Follows Mass Balance?
GWCE (Figure 2.44)	**1.0E-03**	**Yes**
First	5.0E-04	No
Second	5.0E-07	No
Finite Amplitude, Part 1	4.6E-04	No
Finite Amplitude, Part 2	1.2E-06	No
Advective, Part 1	1.9E-07	No
Advective, Part 2	5.0E-04	No
Flux	1.0E-05	No
Viscous	0.0E+00	
NCM (Figure 2.45)	**1.0E-04**	**Yes**
Accumulation	1.5E-05	Yes
Advective	4.7E-05	No
Bottom Friction	4.0E-05	No
Finite Amplitude	3.5E-05	Yes
Viscous	0.0E+00	

water region of the domain. Qualitatively, the truncation errors match well with the finite volume mass balance errors; they are distributed throughout the domain.

It is also important to examine the effect of this grid development in comparison to the original East Coast (Constant) domain and to the East Coast (LTEA) domain, which

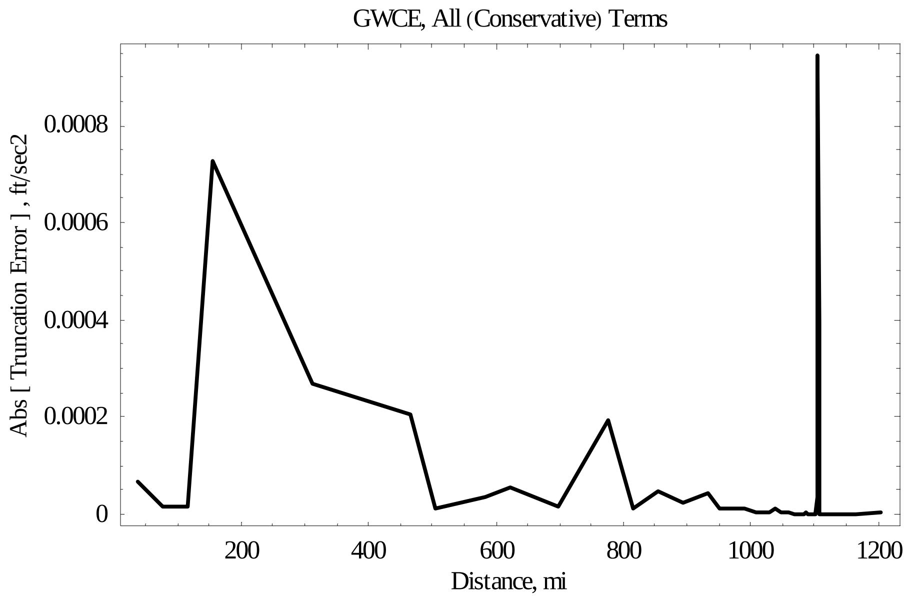

Figure 2.44. Absolute values of the truncation errors for all of terms in the non-conservative GWC equation, for the concept East Coast domain. Note that the units of truncation error are feet/

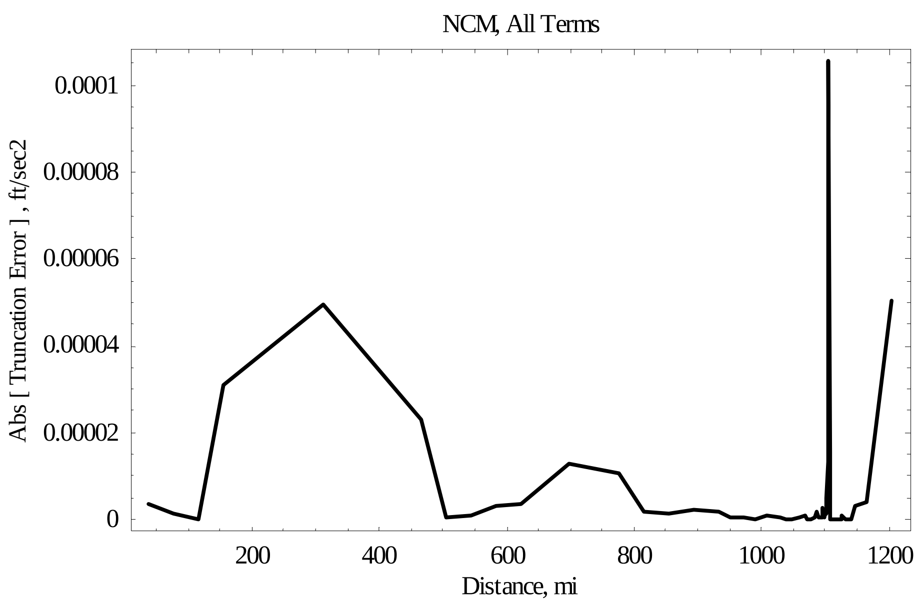

Figure 2.45. Absolute values of the truncation errors for all of the terms in the NCM equation, for the concept East Coast domain. Note that the units of truncation error are feet/sec^2.

was developed by minimizing truncation error. Table 2.12 compares the truncation errors for all three domains. Note that the truncation errors from the concept domain are

Table 2.11: Comparison of truncation error results for the East Coast (Constant) domain, the East Coast (LTEA) domain, and the concept East Coast domain. In the second column, the units of truncation error are feet/sec^2. The last column refers to whether the behavior of the truncation errors matches that of the mass balance errors as computed by using the finite volume method.

Equation	Domain	Maximum Truncation Error	Follows Mass Balance?
GWCE	East Coast (Constant)	7.0E-02	Yes
	East Coast (LTEA)	2.5E-04	No
	Concept	**1.0E-03**	**Yes**
NCM	East Coast (Constant)	4.0E-03	Yes
	East Coast (LTEA)	5.0E-04	Yes
	Concept	**1.0E-04**	**Yes**

considerably less than those from the East Coast (Constant) domain. An 84 percent decrease in finite volume mass balance errors created a 98 percent decrease in GWC truncation errors and a 97 percent decrease in NCM truncation errors. Also note that the truncation errors from the concept domain are comparable to those from the East Coast (LTEA) domain; in fact, the NCM truncation errors are smaller. This behavior could be due to the fact that Hagen [6, 7] only used the linear, harmonic form of the NCM equation to develop the East Coast (LTEA) domain; this study uses the full, nonlinear, transient form of the NCM equation. Thus, not only does this method of grid development decrease the truncation errors, it also mirrors the results from a grid that was developed by minimizing truncation errors.

The final test is heuristic stability, in which we find the maximum time step (within the nearest five seconds) where the model is still stable. Except for the time step, though, every run-time parameter stays the same. The maximum stable time step for the East Coast (Constant) domain is 195 seconds, and the maximum stable time step for the East Coast (LTEA) domain is 175 seconds. The concept East Coast domain causes a decrease in the maximum stable time step to 130 seconds, which is a decrease of about 33 percent from the domain with constant node spacing. There are two possible reasons why the East Coast (LTEA) domain is more stable than the concept East Coast domain. First, the East Coast (LTEA) domain was developed using a technique in which heuristic stability was a consideration. If the LTEA method called for a small grid spacing to be followed immediately by a large grid spacing, then extra nodes were added to smooth the transition. This relaxation criterion improves stability for that domain. Second, the East Coast (LTEA) domain has 46 nodes, while the concept East Coast domain has 65 nodes. In any event, for some simulations, the extra cost of using a smaller time step might be outweighed by the time saved while generating the grid by using mass balance errors instead of truncation errors. In other simulations, the grid development should be conducted using an automated method, in which the optimization of heuristic stability should be a secondary goal.

2.8. Conclusions

In this chapter, we examined the mass balance and truncation errors for four one-dimensional test problems, in an attempt to determine whether the mass balance errors computed by the finite volume or finite element method could be used as an indicator of

Table 2.12: Summary of truncation error results for all four test problems. This table is similar to Table 2.1, except now we have indicated which combinations of test problem and error measure produce good agreement between finite volume mass balance errors and truncation errors. Note that the two test problems with constant node spacing produce good agreement for all error measures.

		Truncation Error Measure			
		Non-Conservative		Conservative	
		GWCE	NCM	GWCE	CM
Domain	East Coast (Constant)	Yes	Yes	Yes	Yes
	East Coast ($\lambda/\Delta x$)	No	Yes	No	No
	East Coast (LTEA)	No	Yes	No	Yes
	Linear Sloping Beach	Yes	Yes	Yes	Yes

truncation errors. If so, then that method would be useful as an error measure for the wetting and drying studies, among other uses. Table 2.12 summarizes how the finite volume mass balance errors compare to the truncation errors for all four test problems.

For grids with constant spacing, the finite volume mass balance errors are an excellent indicator of truncation errors. For the East Coast (Constant) domain in Section 2.3, the non-conservative version showed great agreement between the finite volume mass balance errors and the truncation errors, and the conservative version showed reasonable agreement. For the Linear Sloping Beach domain in Section 2.6, both versions showed good agreement. And for both domains, the smaller magnitudes and different behaviors of the finite element mass balance errors prevented them from matching the truncation error results.

For grids with variable spacing, the results were mixed. Once again, the finite element mass balance errors did not provide a good match with the truncation errors, for any domain or version of the model. The finite volume mass balance errors agree well with the truncation errors from both forms of the momentum equation, but they do not agree with the truncation errors from the GWCE. However, as discussed earlier, we believe the GWCE would produce better agreement for the East Coast (LTEA) domain if the LTEA method had been employed on all of the terms in the equation. Based on the information in Table 2.12, we recommend using the truncation errors for the NCM to correlate with mass balance errors.

Finally, a walk-through of a possible mesh generation algorithm shows promising results. By using mass balance errors instead of truncation errors as the meshing criteria, we were able to produce a concept East Coast domain that has behavior that is comparable to (and sometimes better than) the East Coast (LTEA) domain. An automated algorithm based on this technique could produce better domains, perhaps even in real time.

Almost all of the test domains in the wetting and drying studies herein will use constant node spacing, so we will use the finite volume method to compute mass balance errors for the remainder of this thesis. Not only is that method a good indicator of truncation errors, but it also is more physically realistic.

3. One-Dimensional Wetting and Drying

The ultimate goal of this research is to implement the wetting and drying algorithm in the three-dimensional ADCIRC model. Before doing that, however, we felt it necessary to implement and assess the algorithm in a one-dimensional version of the model, for two reasons: (1) it allows for a study of the behavior of a simplified version of the algorithm, which will assist in interpreting its behavior in two- and three-dimensional versions; and (2) it allows for the development of an optimal set of run-time parameters.

This chapter is composed of three main subsections. The Methods subsection summarizes the wetting and drying algorithm that was implemented in the one-dimensional ADCIRC model, presents the four model problems on which the algorithm was tested, and describes the two error measures used to assess the performance of the algorithm. The Numerical Experiments subsection presents the results of a suite of studies on all four model problems. Finally, the Conclusions subsection summarizes the most important results from these studies and lays the groundwork for further implementation in two- and three-dimensional versions of the model.

3.1. Methods

In this section, we will discuss the implementation of a wetting and drying algorithm in the one-dimensional ADCIRC model. We will also describe our four model problems and the methods in which we assess the errors in our numerical results.

3.1.1. Wetting and Drying Algorithm

The one-dimensional ADCIRC wetting and drying algorithm is an approach developed by Luettich and Westerink [17,18] and is based on simplified physics and some empirical rules. The algorithm is located in the middle of the time loop, after the solution of the continuity equation but before the solution of the momentum equation. The algorithm was updated in 2004 to allow for better wetting in floodplains and better mass balance properties in barely wet areas. Those updates were included in our study of the two- and three-dimensional wetting and drying algorithms and will be discussed in Section 4.1.2 and Section 5.1.2, but they were not included in the one-dimensional algorithm. Thus, the one-dimensional wetting and drying algorithm is comprised of three parts.

First, the total water depth at every node is checked against a minimum wetness height, H_{min}. If the total water depth is larger than this minimum value, then the node remains active ("wet") and is included in the rest of the calculations. However, if the total water depth has fallen below this minimum value, then the node is deemed inactive ("dry") and removed from the calculations. Note that a dry node can have a positive water depth that is smaller than H_{min}. To help control oscillations, an input parameter allows the user to control the number of time steps that a node has to remain wet before it can be turned off. Note that, for all of the results from this one-dimensional algorithm, that parameter was set to 5 time steps.

Second, the steady state velocity that would result from a balance between the water level gradient and the bottom friction between a wet and an inactive node is checked against a minimum wetting velocity, U_{min}. The balance is given by:

$$U = \frac{g(\zeta_{i-1} - \zeta_i)}{\tau_i \Delta x_i}, \tag{3.1}$$

where g is gravity; ζ_{i-1} and ζ_i are the free surface elevations at the adjacent node and the node of interest, respectively; τ_i is the equivalent linear bottom friction coefficient (see Equation 3.7); and Δx_i is the grid spacing. Note that in many situations, only the free surface elevations will change significantly from time step to time step. In this case, the U_{min} criterion almost becomes a height restriction, where a node becomes active if the adjacent node's free surface elevation is sufficiently larger than its own. Again, to help control oscillations, another input parameter allows the user to control the number of time steps that a node has to remain inactive before it can be wetted. For all of the results from the one-dimensional algorithm, that parameter was set to 5 time steps.

Third, every landlocked wet node is tagged as inactive. A landlocked wet node is not connected to any active elements, and thus does not receive contributions to either side of the equation corresponding to that node. For some bathymetries, this criterion allows a node to remain inactive even if its total water depth is larger than the minimum wetting height. This is a slight change from the original two-dimensional (*x*-*y*) wetting and drying algorithm, which allows pockets of wet nodes to be surrounded by dry nodes. This allows wind stresses and other types of forcing to continue to act on the active elements. However, because we are not modeling wind stresses in this study, there is no reason to make landlocked nodes active.

3.1.2. Model Problems

The studies in this paper utilize four model problems with sloping beaches. These problems have open ocean boundaries on the left-hand side and are forced by a tide.

The first model problem is similar to a test problem presented by Luettich and Westerink [17] in an earlier ADCIRC wetting-and-drying paper. We chose this bathymetry because: (1) it allows for a comparison with an analytical solution, as discussed in Chapter 1; and (2) it allows for a simple test case before moving forward to more complicated bathymetries. The problem has the following parameters (unless stated otherwise): a linear slope, an undisturbed length of 20 kilometers, a bathymetric depth at the open ocean boundary of 5 meters, a grid spacing of 250 meters, a time step of 10 seconds, a forcing amplitude of 0.25 meters, a tidal period of 12 hours (43,200 seconds), a duration of 4 tidal periods, a *cftau* value of 0.001 and a G value of 0.001 sec^{-1} (both defined in Section 3.2.1.3), an H_{min} value of 0.01 meters, and a U_{min} value of 0.01 meters per second. We will refer to this as Linear Problem 1.

The second model problem creates a situation where waves can wet and dry a larger number of nodes on the beach. This problem is deeper but shorter, and it allows wave run-up to cover more of the beach. This problem has the following parameters (unless stated otherwise): a linear slope, an undisturbed length of 18 kilometers, a bathymetric depth at the open ocean boundary of 6 meters, a grid spacing of 250 meters, a

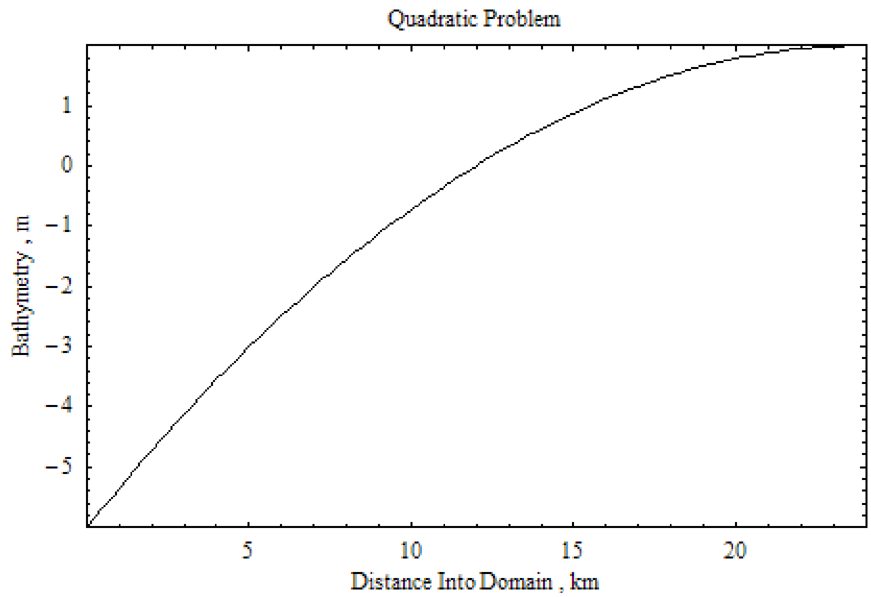

Figure 3.1. Bathymetry for the Quadratic Problem. Note that the bathymetric depth is 6 meters at the ocean boundary, the total length is 24 kilometers, and the undisturbed

time step of 10 seconds, a forcing amplitude of 1.0 meter, a tidal period of 12 hours (43,200 sec), a duration of 4 tidal periods, a *cftau* value of 0.001 and a G value of 0.001 sec^{-1} (both defined in Section 3.2.1.3), an H_{min} value of 0.01 meters, and a U_{min} value of 0.01 meters per second. We will refer to this as Linear Problem 2.

The third model problem uses a quadratic sloping beach, as shown in Figure 3.1. This problem has the following parameters (unless stated otherwise): a quadratic slope, an undisturbed length of 12 kilometers, a bathymetric depth at the open ocean boundary of 6 meters, a grid spacing of 250 meters, a time step of 10 seconds, a forcing amplitude of 1.0 meter, a tidal period of 12 hours (43,200 sec), a duration of 4 tidal periods, a *cftau* value of 0.001 and a G value of 0.001 sec^{-1} (both defined in Section 3.2.1.3), an H_{min} value of 0.01 meters, and a U_{min} value of 0.01 meters per second. We will refer to this as the Quadratic Problem.

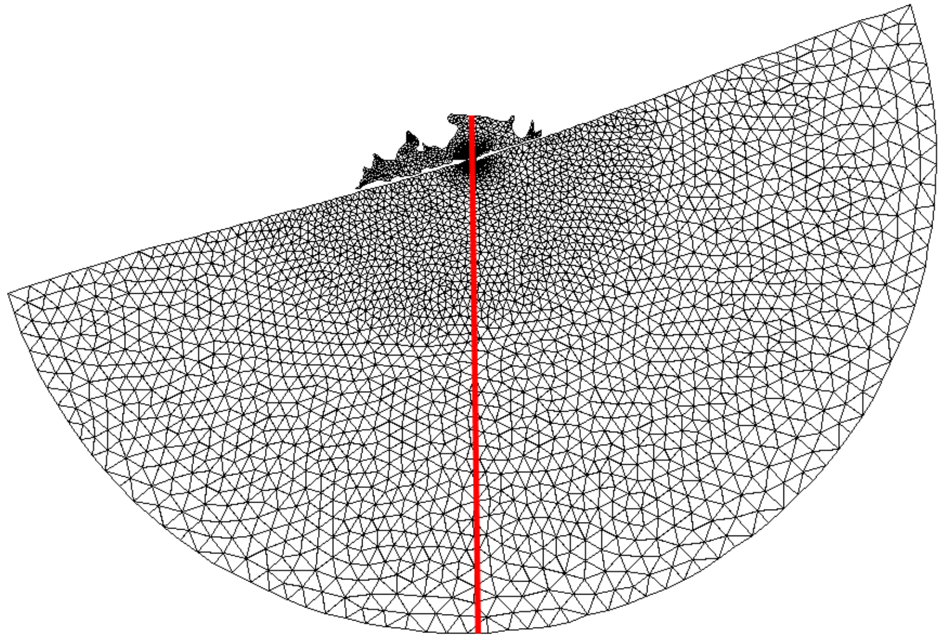

Figure 3.2. The finite element
grid for the two-dimensional Shinnecock Inlet domain. Note that the resolution is high around the inlet itself, but that it decreases near the ocean boundary. A schematic of the one-dimensional slice used in this study is shown in red. It begins inside the inlet, moves through the opening, and

The fourth model problem is a one-dimensional slice of a two-dimensional domain. The finite element grid for the Shinnecock Inlet domain is shown in Figure 3.2 [21,22,27]. Shinnecock Inlet is located on the coast of Long Island, New York, and its realistic bathymetry is an appropriate test of the wetting and drying algorithm, especially in one-dimension. We extracted a one-dimensional slice from this domain. The slice runs approximately north-to-south, beginning within the inlet and ending at the open ocean boundary, as shown in Figure 3.2. The bathymetry for this slice is shown in Figure 3.3. Note that this problem is significantly deeper than the idealistic model problems, and the bathymetry is much more varied, especially near the inlet itself. Also note that, because we followed the resolution in the two-dimensional domain, this one-dimensional domain

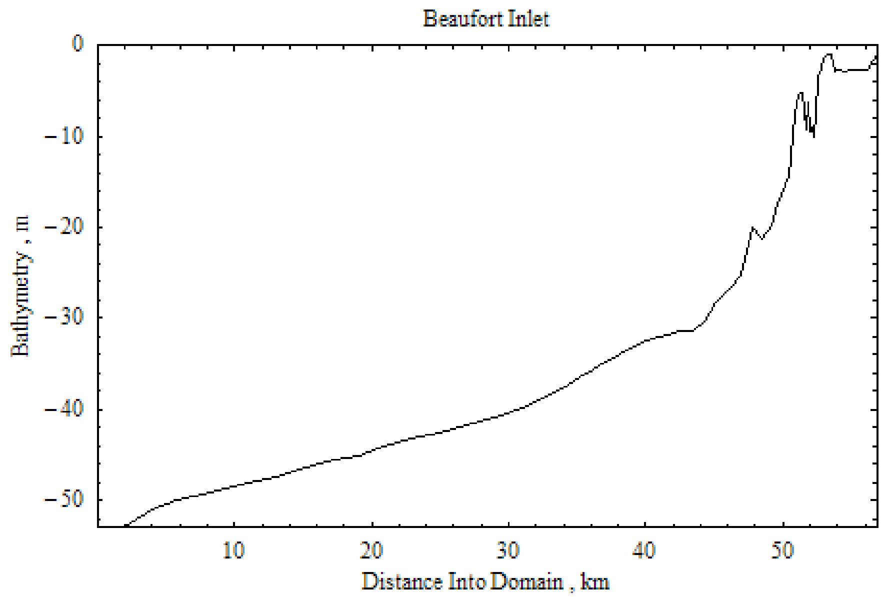

Figure 3.3. Bathymetry for the Inlet Problem. The opening between the inlet and the ocean is located about 51 kilometers into the domain, where the depth is about 10 meters. Note that the bathymetric depth ranges from a maximum of about 53 meters at the ocean boundary, to 0.94 meters at a distance of 53 kilometers into the domain. The total length of the domain is 56.8 kilometers.

utilizes a variable grid spacing. This problem has the following parameters (unless stated otherwise): an undisturbed length of 56.8 kilometers, a bathymetric depth at the open ocean boundary of about 53 meters, a variable grid spacing, a time step of 10 seconds, a forcing amplitude of 1.0 meter, a tidal period of 12 hours (43,200 sec), a duration of 4 tidal periods, a *cftau* value of 0.001 and a *G* value of 0.001 sec^{-1} (both defined in Section 3.2.1.3), an H_{min} value of 0.01 meters, and a U_{min} value of 0.01 meters per second. We will refer to this as the Inlet Problem.

3.1.3. Error Computations

The most important reason for selecting two test domains with linear sloping beaches is that this problem has an analytical solution. Thus, for Linear Problem 1 and Linear Problem 2, our sensitivity studies utilize a comparison between our numerical results and the analytical solution described in Section 3.2.1.1. This comparison is calculated through an examination of the position of the wet/dry interface over the fourth tidal period (because the model is spun up from a cold start for the first three periods). After every 10 minute interval in that fourth period, we calculate the difference between the position of the interface given by the numerical results and the position of the interface given by the analytical solution. These differences are then averaged. If the numerical results successfully approximate the analytical solution, then the average difference should be zero. However, spatial discretization often prevents a perfect match between numerical and analytical, so we are satisfied if the average difference is less than the grid spacing of 250 meters.

Our studies also utilize a computation of mass balance error. This is a cumulative mass balance error over the entire simulation. It is calculated using a finite volume approach, where we compute the difference between the global accumulation and the global mass flux, as represented by the primitive continuity equation. Recently, several papers [1, 8] have advocated computing mass balance from finite element residuals in order to be consistent with the numerical discretization. However, we have shown (Kolar et al. [13]) the finite volume approach to be a good surrogate variable for accuracy and phasing errors; that is, small mass balance errors (as computed with finite volume) correlate with small constituent errors. Additionally, in Chapter 2, we showed that the finite volume method is a good indicator of truncation errors, especially for domains that have a constant node spacing. Hence our reason for using the finite volume approach herein.

3.2. Numerical Experiments

In this section, we discuss the results of several tests involving the one-dimensional wetting and drying algorithm and our model problems. We will first examine Linear Problem 1 and Linear Problem 2, then the Quadratic Problem, and then the Inlet Problem.

3.2.1. Linear Problem 1 and Linear Problem 2

The results in this subsection are from tests on the two model problems with linear sloping beaches. First, we compare the numerical results with an analytical solution. Second, we examine the algorithm's effect on temporal stability. Third, we conduct parameter sensitivity studies for bottom friction and the G numerical parameter. Fourth, we conduct parameter sensitivity studies for the wetting and drying parameters H_{min} and U_{min}. Fifth, we examine the effect of spatial resolution on the performance of the algorithm.

3.2.1.1. Comparison with an Analytical Solution

The classic analytical solution for wave run-up on a sloping beach was first expressed by Carrier and Greenspan [3] and later revisited by Johns [10] and Siden and Lynch [24]. The solution is quite restrictive; it describes the behavior of a frictionless wave on a linearly-sloped beach. The one-dimensional wetting-and-drying ADCIRC model incorporates bottom friction and can be applied to complex bathymetries. However, it is important to verify its performance against an analytical solution in this simple test case.

The full equations for the analytic solution are given in the latter two references. We will reproduce the important ones here. The equations for the velocity, horizontal position, and elevation of the shoreline are given by:

$$u = \frac{\partial \xi}{\partial t} = -u\frac{\partial u}{\partial t} - \frac{2A\pi}{T}\left(1 + \frac{\partial u}{\partial t}\right)\sin\left(\frac{2\pi}{T}(t+u)\right), \tag{3.2}$$

$$\xi = -\frac{1}{2}u^2 + A\cos\left(\frac{2\pi}{T}(t+u)\right), \tag{3.3}$$

and

$$\zeta = \xi, \tag{3.4}$$

where u is the scaled velocity, ξ is the scaled horizontal displacement, A is the scaled amplitude, T is the scaled period, t is the scaled time, and ζ is the scaled free surface elevation from the mean. Note that Equation 3.4 holds true because the scaling changes the slope to 45 degrees. We solve for u in Equation 3.2 by using an iterative technique, a finite difference approximation on the $\partial u / \partial t$ terms, and the knowledge that the velocity of the shoreline at maximum inundation is zero. Once the shoreline information is calculated, then the velocity and elevation at interior points can be calculated using the following equations:

$$u = -\frac{4AJ_1\left(\frac{4\pi\sqrt{\zeta - x}}{T}\right)}{\alpha}\sin\left(\frac{2\pi}{T}(t+u)\right), \tag{3.5}$$

and

$$\zeta = -\frac{1}{2}u^2 + AJ_0\left(\frac{4\pi\sqrt{\zeta - x}}{T}\right)\cos\left(\frac{2\pi}{T}(t+u)\right), \tag{3.6}$$

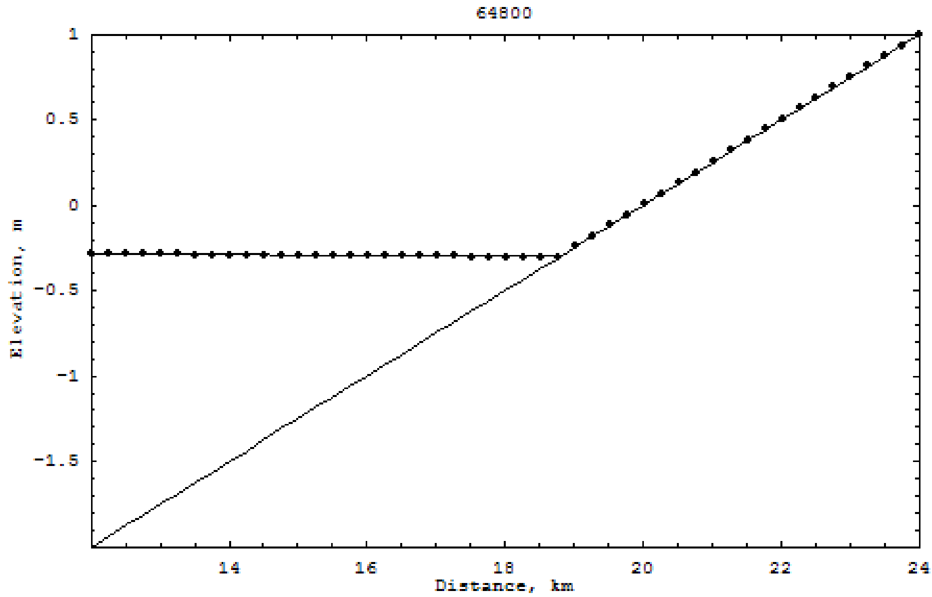

Figure 3.4. The numerical results
(black dots) and the analytical solution (solid line) halfway through the second tidal cycle. The solid diagonal line is the bathymetry. Note that the number at the top of the figure is the time in seconds.

where J_0 and J_1 are Bessel functions and x is scaled horizontal position. Equation 3.5 and Equation 3.6 must also be solved iteratively. Note that the ADCIRC boundary forcing was adjusted to match the cosine forcing of the analytical solution.

We attempted to match our numerical results with the analytical solution by using Linear Problem 1. Figure 3.4 and Figure 3.5 show the analytical solution and numerical results at two different times in the second tidal cycle. (Without using a ramp function to smooth the transition from a cold start, the numerical solution experiences some start-up noise during the first tidal cycle.) Note that the numerical results show good agreement with the analytical solution and that there is no friction-induced lag at the shoreline. We believe the good agreement is due to our relatively small value of *cftau*, so that the bottom friction does not dominate the momentum balance. Note that the one-dimensional ADCIRC model is not stable with a bottom friction coefficient of zero, so an exact

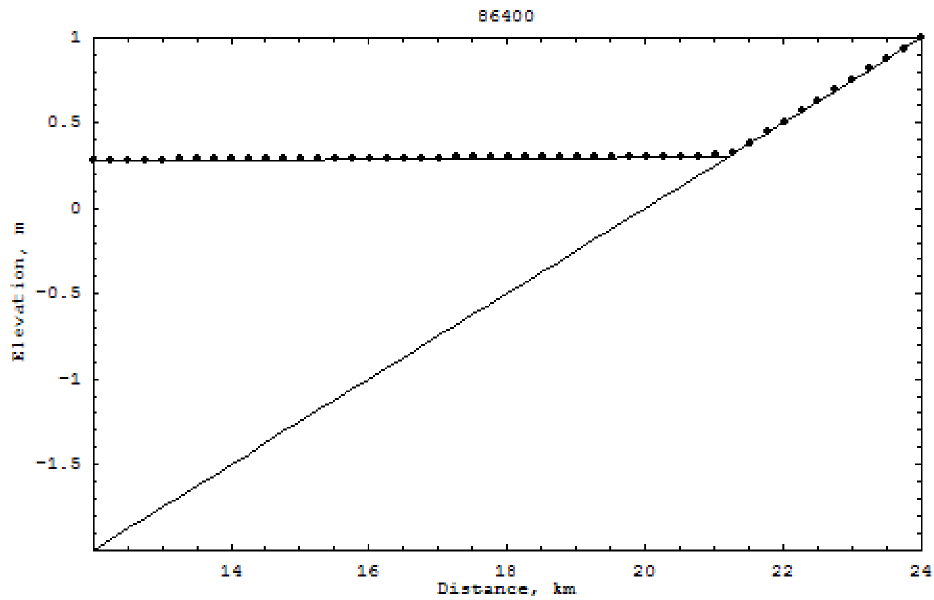

Figure 3.5. The numerical results
(black dots) and the analytical solution (solid line) at the end of the second tidal cycle. The solid diagonal line is the bathymetry. Note that the number at the top of the figure is the time in seconds.

comparison to the analytical solution is impossible. However, we are forcing our problem at the boundary, so bottom friction does not damp out the response.

Figure 3.6 shows the position of the shoreline over the first three tidal periods. (This is similar to Figures 2 and 3 in Johns [10].) After the numerical results fight through the noise of the first tidal period, they show very good agreement with the analytical solution. There is some visible lag during the wetting phase, which raises the question of whether we need to relax our wetting criterion. That question will be addressed in a parameter study in Section 3.2.1.4; for now, we believe the information in these figures shows that the ADCIRC model can provide accurate results for this simple test case.

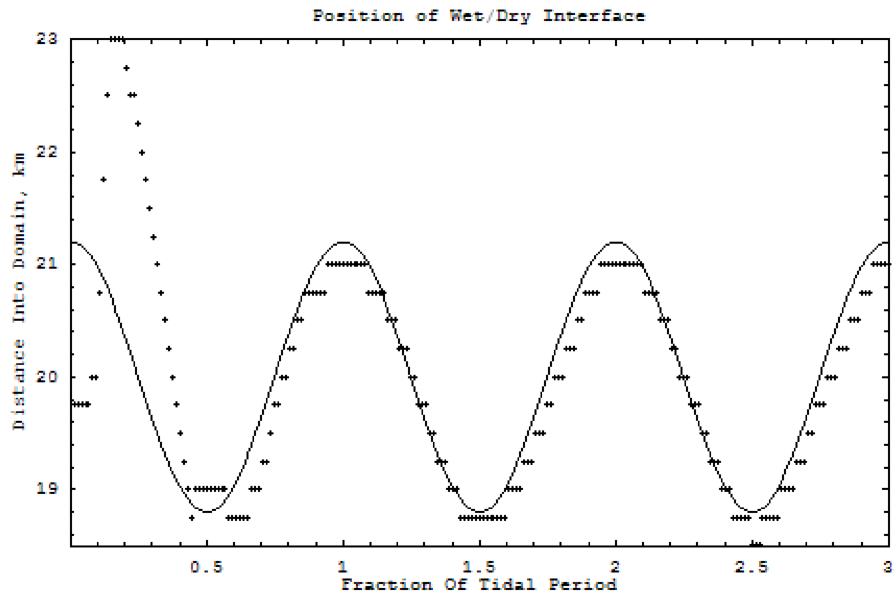

Figure 3.6. The position of
the shoreline, as given by the numerical results (black dots) and the analytical solution (solid line) for the first three tidal periods.

3.2.1.2. Hueristic Stability

Stability was measured by determining the maximum time step (within 5 seconds) at which the model still provided valid results. However, it is difficult to measure the impact of the wetting and drying algorithm on stability because our model problems cannot be run with the original fixed-boundary ADCIRC model. In order to prevent instabilities during the ebb phase when nodes should dry but cannot, we altered our model problems so that they could be run with the original model.

For Linear Problem 1, we shortened the domain to 16 kilometers so that there is a bathymetry of 1 meter at the land boundary. This prevents the 0.25 meter forcing amplitude from trying to dry out nodes on the beach. All of the other parameters, including the slope, remained the same. Under these conditions, the original ADCIRC model provided a maximum stable time step of 60 seconds. The wetting and drying model, when applied to the unaltered Linear Problem 1, provided a maximum stable time step of 55 seconds. This is a decrease of 8.3 percent.

For Linear Problem 2, we shortened the domain to 12 kilometers so that there is a bathymetry of 2 meters at the land boundary. This prevents the 1 meter forcing amplitude from trying to dry out nodes on the beach. All of the other parameters, including the slope, remained the same. The original ADCIRC model provided a maximum stable time step of 50 seconds. The wetting and drying model, when applied to the unaltered Linear Problem 2, provided a maximum stable time step of 15 seconds. This is a decrease of 70 percent.

Note that, for both problems, mass balance errors were an order of magnitude greater for the wetting and drying model. These errors were concentrated on the beach where nodes are turned on and off.

3.2.1.3. Parameter Sensitivity - *cftau* and *G*

Two important parameters in the ADCIRC model are *cftau* and *G*, the former being a physical parameter and the latter being purely numerical. The parameter *cftau* controls bottom friction in the model. It is used as a coefficient in the calculation of the equivalent linear bottom friction coefficient, τ, in the momentum equation for each node *i*:

$$\tau_i = cftau\left(\frac{|u_i|}{H_i}\right). \tag{3.7}$$

Note that the magnitude of τ is directly proportional to the magnitude of *cftau*; as *cftau* goes to zero, so does *tau*. As expected, bottom friction plays a significant role in the wetting and drying process. Its relative magnitude increases in shallower, near-shore waters and hence it directly affects the speed at which waves inundate or recede.

The parameter *G* is the numerical parameter introduced by Kinnmark [11] to control the balance between the wave continuity equation and the primitive continuity equation. As *G* is decreased, the GWCE become more like a pure wave equation; as *G* is increased, the GWCE more closely approximates the primitive equation. As reported elsewhere [13], if *G* is too high, the solution develops spurious oscillations, which prevent the model from capturing the behavior of the waves.

Because these two parameters are related in their effects on the model's behavior, it is important to examine them in tandem. Kolar et al [13] determined an optimal range of G/τ to be on the order of 1 to 10. However, that study examined the effects of these parameters on barotropic tides without wetting and drying. Herein, we examine their effects on wetting and drying by varying the parameters *cftau* and *G* from 0.000001 to 0.5 (always in sec^{-1} for *G*; *cftau* is dimensionless), creating a matrix of *cftau*-*G* combinations. For each combination, we compared the behavior of the model with the analytical solution described above, and we examined the model's mass balance properties. The tests in this section use Linear Problem 2.

The comparison with the analytical solution was performed by averaging the differences between the numerical results and the analytical solution over the fourth tidal cycle, as discussed above in Section 3.1.3. By plotting these averages for each combination in the matrix, we developed a three-dimensional surface that is shown in Figure 3.7. We can share some observations from this surface. First, the model is unstable in almost one fourth of the matrix, in the region where both *cftau* and *G* approach

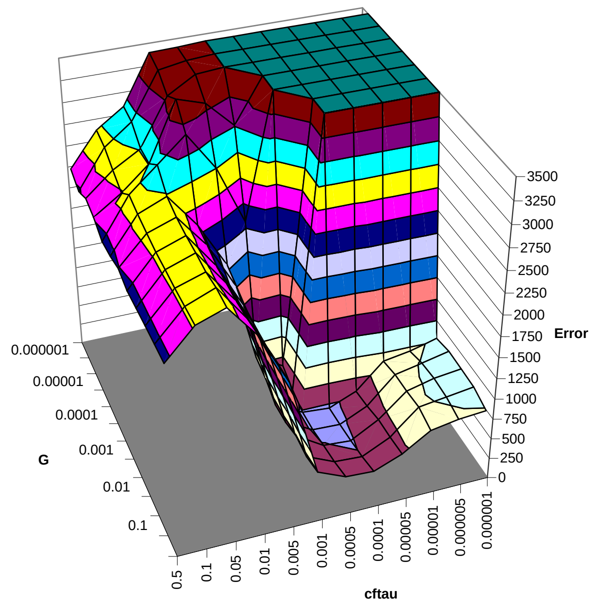

Figure 3.7. The average difference between the numerical results and the analytical solution over the fourth tidal cycle, as discussed in Section 2.3, for 144 combinations of *cftau* and *G*. The errors are shown in intervals of 250 meters, which is the grid spacing.

0.000001. It is stable, however, in the regions where only one of these parameters approaches this minimum value. Second, the model is significantly more sensitive to variations in *cftau*. If *G* is held constant at a relatively high value, then variations in *cftau* produce average differences that range over an order of magnitude. The errors that occur when *cftau* is held constant and *G* is varied are not nearly so pronounced.

Third, in general, the average differences between the numerical results and the analytical solution decrease as *cftau* is decreased. This trend is intuitive, considering the analytical solution is frictionless. A slice of the matrix where *cftau* is held constant at a value of 0.000001 and *G* is varied would show average differences on the magnitude of three times the grid spacing of 250 meters.

The best agreement between the numerical results and the analytical solution occurs with a combination such as *cftau* = 0.0001 and *G* = 0.01 sec^{-1}, which provides an

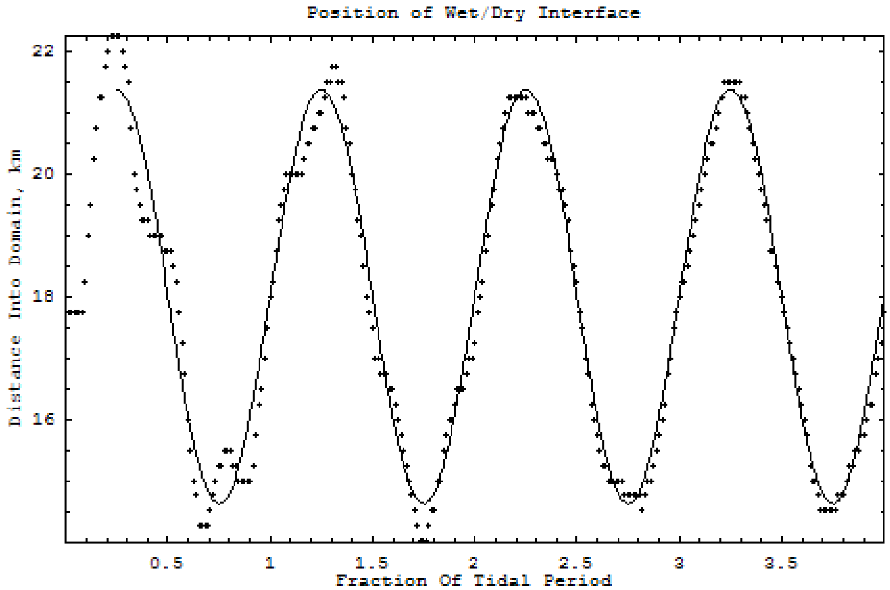

Figure 3.8. The position of
the shoreline, as given by the numerical results (black dots) and the analytical solution (solid line) for the first four tidal periods.

average difference of 211 meters, or less than one grid spacing. Figure 3.8 shows the position of the wet/dry interface over time for a simulation using this combination. The numerical results experience some start-up noise during the first two tidal cycles, but then they show very good agreement with the analytical solution during the fourth tidal cycle. We will use this combination of *cftau* and *G* in Section 3.2.1.4, where we are explicitly trying to match the analytical solution. However, it should be remembered that the analytical solution does not include bottom friction, so it will not be accurate for all situations. In general, the values of *cftau* and *G* should be determined based on the bottom friction requirements of the particular simulation.

The examination of the model's mass balance properties was performed in the same manner, by creating a matrix of *cftau*-*G* combinations. The mass balance error was calculated using the finite volume approach, described in Section 3.1.3. Using these

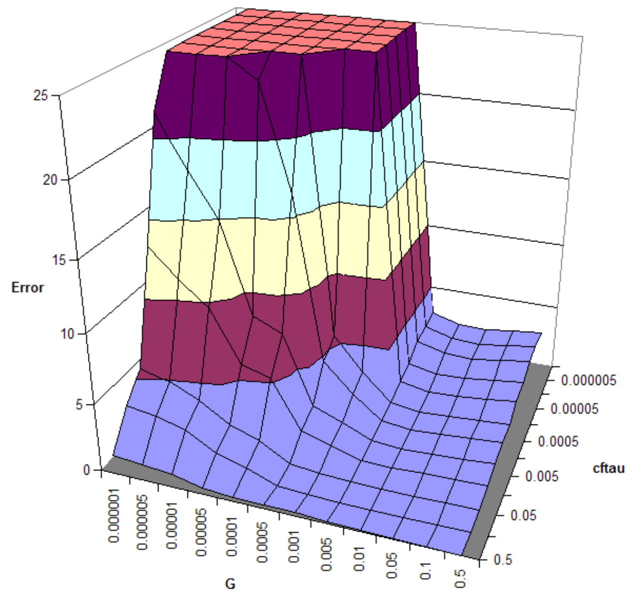

Figure 3.9. Mass balance errors for 144 combinations of *cftau* and *G*. The errors are shown in intervals of 5,000 square meters. The errors in the region at the front of the graph are on the order of 1,000 to 2,000 square meters, or 1.9 to 3.7 percent of the undisturbed water area.

average mass balance errors, we created another three-dimensional surface, this time shown in Figure 3.9. The model is unstable for the same region of combinations, where both *cftau* and *G* approach 0.000001. However, if *G* remains relatively large, then *cftau* can be decreased without significant penalty. For example, a typical range of cftau from 10^{-3} to 10^{-5} shows: (1) mass balance errors on the order of 2,000 square meters, or approximately 3.7 percent of the total undisturbed water area; and (2) when *G* is decreased to its minimum stable value, ratios of G/τ are in the range of 1 to 10 (optimum range reported by Kolar et al. [13] in their fixed-boundary barotropic studies). Note that values of cftau larger than 10^{-3} do show good mass balance, but they produce unrealistically damped simulations.

3.2.1.4. Parameter Sensitivity - H_{min} and U_{min}

Another pair of important numerical parameters is H_{min} and U_{min}, described above in Section 3.1.1. Both parameters affect the ability of the algorithm to wet or dry nodes. The parameter H_{min} controls the drying phase, and the parameter U_{min} controls the wetting phase. For example, a large value for H_{min} would allow nodes to dry while still holding a significant amount of water, causing nodes to dry much faster than they should. Similar problems would be experienced if the value for H_{min} is too small or if the value of U_{min} is at either extreme. Thus, it is important to consider the effects of the two parameters in tandem.

We performed this consideration by using the same technique as for *cftau* and *G*. We examined the effects of H_{min} and U_{min} by varying each parameter from 0.0001 to 0.5 (meters for H_{min}; meters per second for U_{min}), creating a matrix of H_{min}-U_{min} combinations. For these runs, we used *cftau* = 0.0001 and G = 0.01 sec^{-1}, which the previous study found to produce meaningful solutions. We also used Linear Problem 2. For each combination of H_{min} and U_{min}, we compared the behavior of the model with the analytical solution and we examined the model's mass balance properties.

The comparison with the analytical solution was performed by using the same technique as above, where we built a matrix of average differences between the numerical results and the analytical solution, as shown in Figure 3.10. We offer the following observations. First, the model does not go unstable anywhere in the range from 0.0001 to 0.5. In fact, we were able to successfully decrease H_{min} to 10^{-10} meters; the model behaves similarly for all values of H_{min} less than 0.01 meters. However, increasing H_{min}

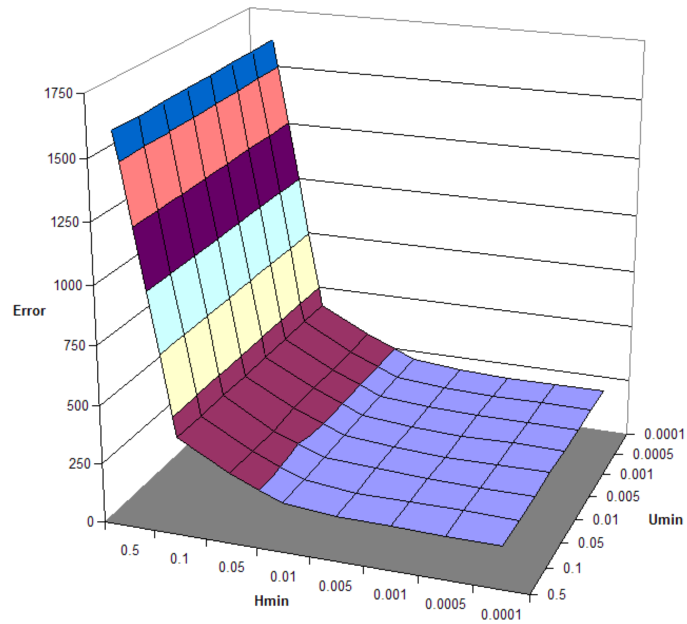

Figure 3.10. The average difference between the numerical results and the analytical solution in their calculation of the position of the shoreline over the fourth tidal cycle. (See Section 3.1.3.) The error is shown in intervals of 250 meters, which is the grid spacing.

beyond the upper limit of this range does cause instabilities, especially for unrealistic values such as 10 meters. Second, the parameter U_{min} has no significant effect on the behavior of the model for the conditions of this problem. In this graph, there is no noticeable change between the average differences for the extreme values of U_{min} = 0.0001 meters per second and U_{min} = 0.5 meters per second. Results are insensitive to the parameter U_{min} for this test problem.

The examination of the model's mass balance properties was performed in the same manner as described in Section 3.1.3. The mass balance error was calculated by computing the difference between the global accumulation and the global mass flux. A three-dimensional surface of average mass balance errors over four tidal cycles is shown in Figure 3.11, and it reveals the following. First, again, the model does not experience

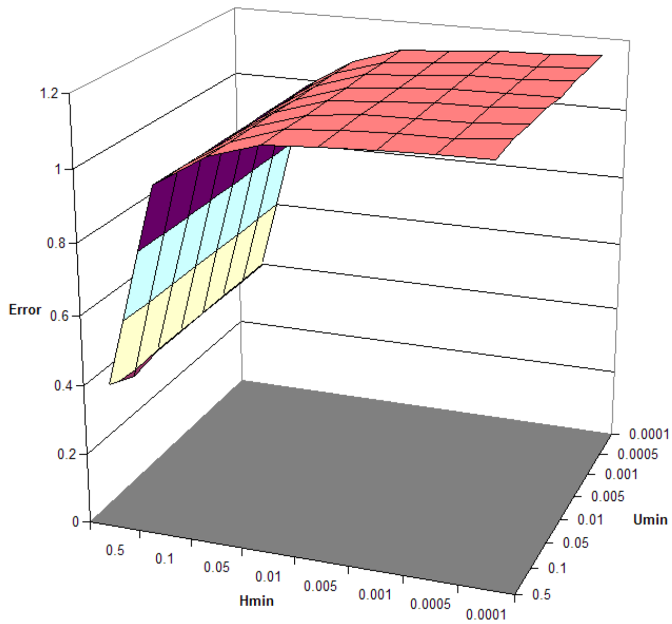

Figure 3.11. The mass balance errors for a range of H_{min} and U_{min} values. (See Section 3.1.3.) The errors are shown in intervals of 200 square meters.

instabilities for any combination of H_{min} and U_{min} within the range from 0.0001 to 0.5. Second, the wetting criterion U_{min} does not have an effect on mass balance. Third, the average mass balance errors decrease as H_{min} is increased. The errors decrease from a steady 1100 square meters when H_{min} is less than 0.01 to about 400 square meters when H_{min} = 0.5. However, this decrease is at the expense of accuracy, as discussed above and shown in Figure 3.10. For such a large value of H_{min}, the numerical results are unable to match the analytical solution.

Thus, results indicate an optimal value for these two parameters H_{min} and U_{min} is around 0.01. There does not appear to be a lower limit for either parameter; however, nothing is gained by decreasing either parameter to the limits of machine precision. We will continue to use values of 0.01 for both parameters.

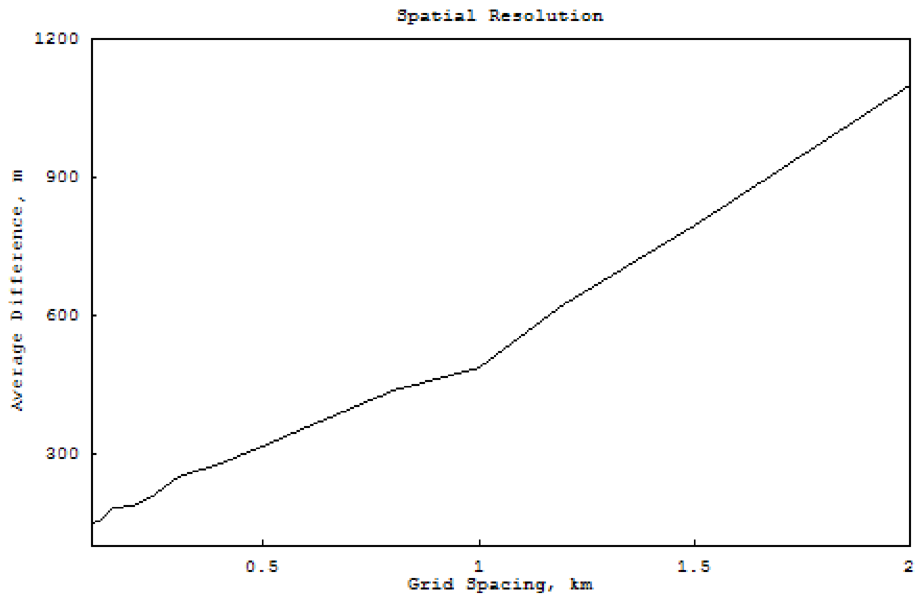

Figure 3.12. The average differ-
ence between the numerical results and the analytical solution. (See Sec-

3.2.1.5. Spatial Resolution

Spatial resolution also plays a significant role in the simulation of wetting and drying, because it controls the model's ability to follow the position of the shoreline as it inundates and recedes. Using Linear Problem 2, we varied the spatial resolution from a minimum of 100 meters to a maximum of 2000 meters. For each grid spacing, we compared the behavior of the model with the analytical solution, and we examined the model's mass balance properties.

Figure 3.12 shows the average difference between the numerical results and the analytical solution for the various spatial resolutions. Note that all of the simulations were run with a time step of 10 seconds except for those with spatial resolutions of 100 meters and 120 meters, which were run with a time step of 1 second in order to maintain stability. The graph shows a sublinear (0.64) convergence rate as the grid spacing is decreased.

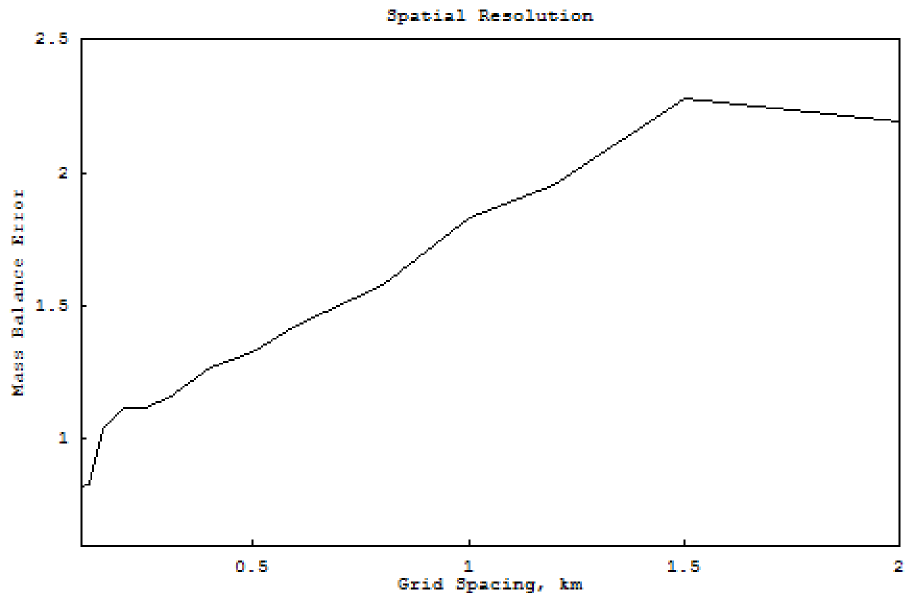

Figure 3.13. Mass balance errors (10^3 square meters) for a range of spatial resolutions. (See Section

Figure 3.13 shows the mass balance errors for the various spatial resolutions. This graph supports the use of the finite volume approach as a predictor of model behavior because, as the grid spacing is decreased, the mass balance errors also decrease (with an exception at $\Delta x = 2$ km.

3.2.2. Quadratic Problem

The results in this subsection are from tests on a model problem with a quadratic-sloping beach. First, we examine the algorithm's effect on temporal stability. Second, we conduct parameter sensitivity studies for bottom friction and the G numerical parameter. Third, we conduct parameter sensitivity studies for the wetting and drying parameters H_{min} and U_{min}. Fourth, we examine the effect of spatial resolution on the performance of the algorithm.

3.2.2.1. Hueristic Stability

Stability was measured by determining the maximum time step (within 5 seconds) at which the model still provided valid results. However, we encountered the same problem that we had with the sloping beach, viz, our wetting and drying model problems cannot be run with the original fixed-boundary ADCIRC model. In order to prevent instabilities during the ebb phase when nodes should dry but cannot, we altered our model problem so that it can be run with the original model.

For the Quadratic Problem, we shortened the domain to 7 kilometers so that there is a bathymetry of 2 meters at the land boundary. This prevents the 1 meter forcing amplitude from trying to dry out nodes on the beach. All of the other parameters, including the slope, remained the same. The original ADCIRC model provided a maximum stable time step of 45 seconds. The wetting and drying model, when applied to the unaltered Quadratic Problem, provided a maximum stable time step of 15 seconds, which is a decrease of 66 percent.

Note that, once again, the wetting and drying problem experienced larger local mass balance errors, and they were concentrated on the beach where nodes are turned on and off.

3.2.2.2. Parameter Sensitivity - *cftau* and *G*

The effects of the ADCIRC model parameters *cftau* and *G* on the wetting and drying algorithm were again examined. As described above in Section 3.2.1.3, the parameter *cftau* controls the bottom friction in the model, and the parameter *G* controls the balance between the wave continuity equation and the primitive continuity equation.

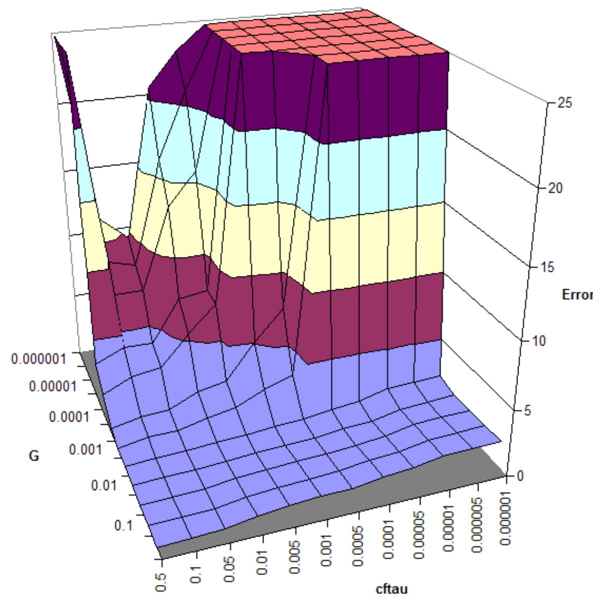

Figure 3.14. Mass balance errors for 144 combinations of *cftau* and *G*. The errors on the vertical axis are shown in intervals of 5,000 square meters. The errors in the region where *cftau* and *G* are near maximum are 500 square meters or less.

Herein, we examine their effects on wetting and drying by varying the parameters from 0.000001 to 0.5 (always in sec^{-1} for *G*; *cftau* is dimensionless), creating a matrix of *cftau*-*G* combinations. For each combination, we examined the model's mass balance properties. Note that we were unable to compare the behavior of the model with an analytical solution, because such a solution does not exist for a quadratic sloping beach. Also note that previous work has shown that mass balance errors, as computed with a finite volume approach, correlate well with truncation errors.

The average mass balance error for each combination is shown as a surface plot in Figure 3.14. The mass balance error was calculated using the finite volume approach, which is described in Section 3.1.3. We offer several observations. First, the model is unstable for the same region of *cftau*-*G* combinations, as it was for the linear sloping beach, namely when both parameters are decreased below 0.001. Second, the shape of the three-dimensional surface is similar to the shape of the surface for the linear sloping beach in Figure 3.9. The only exception is a spike in this graph at the combination of *cftau* = 0.5 and *G* = 0.000001. However, although the shapes of the two graphs are similar, the magnitude of the mass balance errors are slightly smaller for the quadratic sloping beach. The errors in the region where *cftau* and *G* are large are on the order of 500 square meters, or approximately 1.5 percent of the undisturbed water area. And some errors are even less; the minimum occurs at the combination of *cftau* = 0.5 and *G* = 0.05, where the average mass balance error is 16.3 square meters, or approximately 0.05 percent of the undisturbed water area. The corresponding error for the linear sloping beach was 41.1 square meters, or 0.07 percent of the undisturbed water area. Overall, as the values of *cftau* and *G* increase, the model's mass balance properties improve.

We were unable to quantitatively assess (a la Figure 3.7) the algorithm's impact on accuracy because we do not have an analytical solution for a quadratic sloping beach. However, we believe the behavior is similar to that observed for the linear sloping beach; large values for *cftau* prevent the wetting and drying algorithm from capturing the behavior of the shoreline. Figures 3.15 and 3.16 show the position of the shoreline for different resolutions and combinations of *cftau* and *G*. In Figure 3.15, we show the combination of *cftau* = 0.0001 and *G* = 0.01, which was in the region of optimal accuracy for the linear sloping beach. Note that the normal coarse grid solution (blue line) of Δx = 250 meters and Δt = 10 seconds provides a reasonably close match to the fine grid solution (red line) of Δx = 100 meters and Δt = 1 second. However, if we increase the value of *cftau*, as in Figure 3.16, we do not achieve nearly as good of a match. The coarse

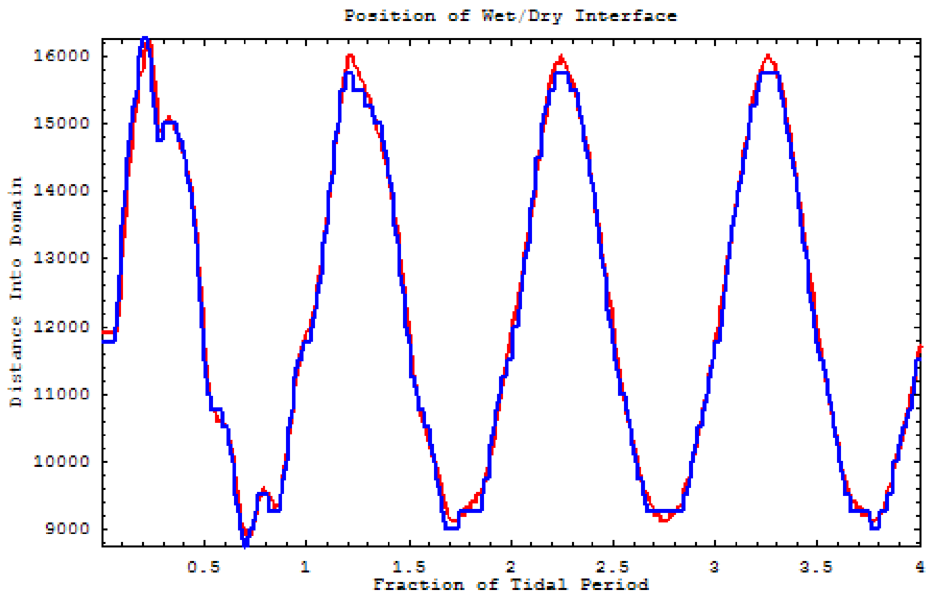

Figure 3.15. The position of the shoreline for the combination of *cftau* = 0.0001 and *G* = 0.01. The blue line is a coarse solution (Δx = 250 meters, Δt = 10 seconds), and the red line is a fine solution (Δx = 100 meters, Δt = 1 second).

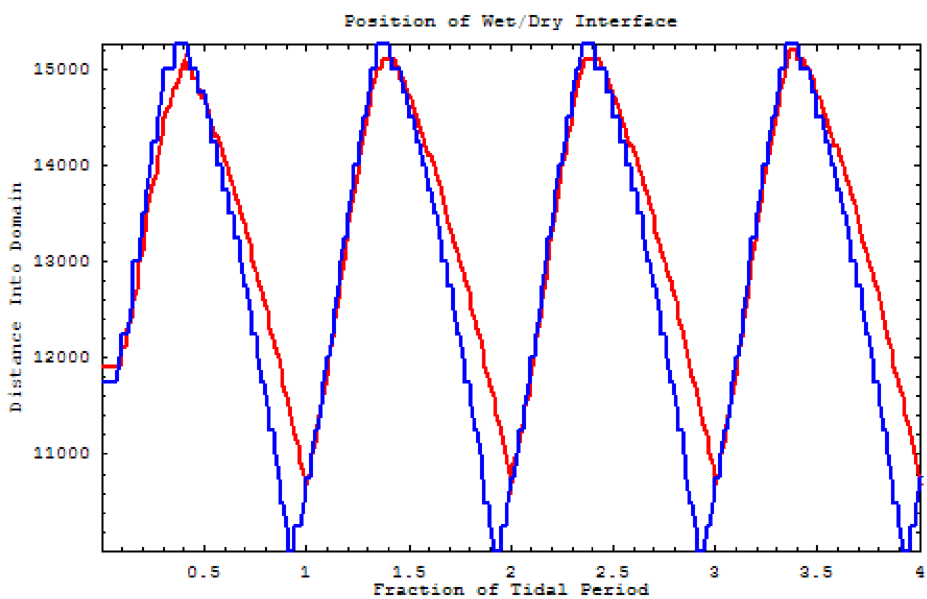

Figure 3.16. The position of the shoreline for the combination of *cftau* = 0.01 and *G* = 0.01. The blue line is a coarse solution (Δx = 250 meters, Δt = 10 seconds), and the red line is a fine solution (Δx = 100 meters, Δt = 1 second).

solution recedes 700 meters farther down the shoreline than does the fine solution, and there is a lag in the drying phase. In addition, when compared with Figure 3.15, the range of inundation and recession is considerably smaller. The maximum inundation is down from 16.2 kilometers to 15.2 kilometers, and the maximum recession is up from 8.75 kilometers to 10.0 kilometers. The larger value of *cftau* prevents the algorithm from wetting and drying as much of the beach, because, as *cftau* increases, so does the bottom friction. Thus, although we cannot quantitatively assess the impact of these parameters on the accuracy of the algorithm, our qualitative analysis suggests that they behave similarly for quadratic sloping and linear sloping beaches.

3.2.2.3. Parameter Sensitivity - H_{min} and U_{min}

Another pair of numerical parameters is H_{min} and U_{min}, described above in Section 3.1.1 and Section 3.2.1.4. Both parameters affect the ability of the algorithm to wet or dry nodes, so it is important to consider the effects of the two parameters in tandem.

We accomplished this by varying each parameter from 0.0001 to 0.5 (meters for H_{min}; meters per second for U_{min}), creating a matrix of combinations. For these runs, we again used *cftau* = 0.0001 and G = 0.01 sec^{-1}, partially to match the study on Linear Problem 2 in Section 3.2.1.4 and partially because we believe this is an accurate combination, based on the parameter sensitivity results in Section 3.2.1.3 and Section 3.2.2.2. For each combination of H_{min} and U_{min}, we examined the model's mass balance properties.

The examination of the model's mass balance properties was performed in the same manner as described in Section 3.1.3. The mass balance error was calculated by

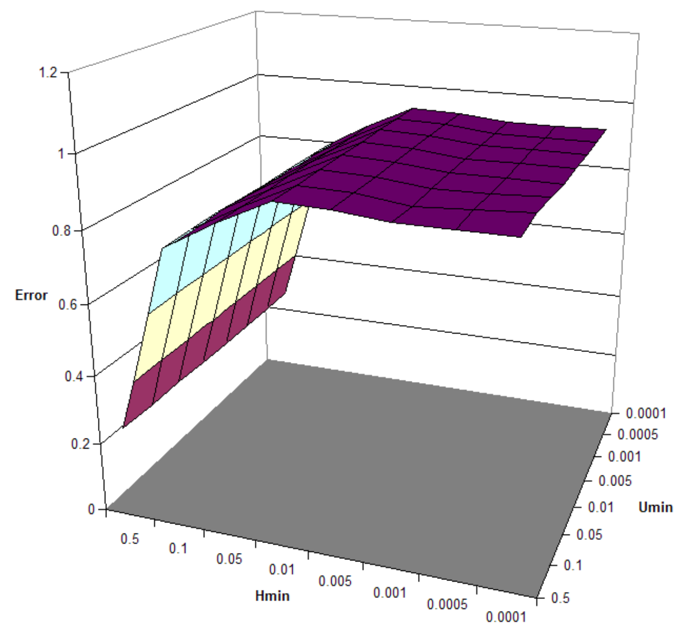

Figure 3.17. Mass balance errors for a range of H_{min} and U_{min} values. (See Section 3.1.3.) The errors on the vertical axis are shown in intervals of 200 square meters.

computing the difference between the global accumulation and the global mass flux. A three-dimensional surface of average mass balance error over four tidal cycles is shown in Figure 3.17, and it reveals the following. First, the model does not experience instabilities for any combination of H_{min} and U_{min} within the range from 0.0001 to 0.5. Second, as with the linear sloping problem, the wetting criterion U_{min} does not have an effect on mass balance for the quadratic sloping beach. There is not a significant difference between the average mass balance errors for the extreme values of U_{min} = 0.0001 meters per second and U_{min} = 0.5 meters per second. Third, the average mass balance errors decrease as H_{min} is increased. The errors decrease from a steady 900 square meters when H_{min} is less than 0.01 meters to about 250 square meters when H_{min} = 0.5 meters. Fourth, as with the *cftau-G* test, the average mass balance errors are slightly smaller for the quadratic sloping beach than they are for the linear sloping beach. The plateau of 900 square meters in

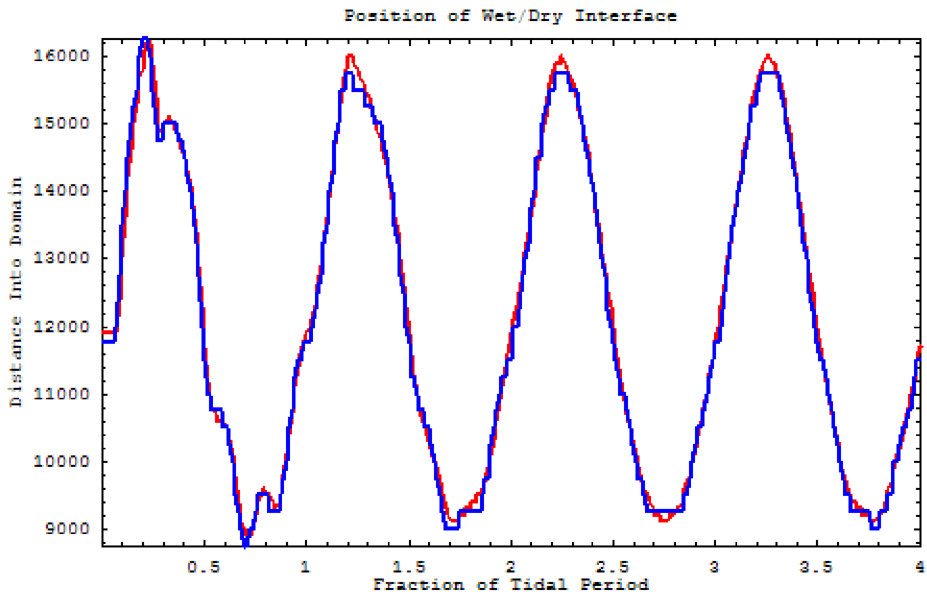

Figure 3.18. The position of the shoreline for the combination of H_{min} = 0.01 and U_{min} = 0.01. The blue line is a coarse solution (Δx = 250 meters, Δt = 10 seconds), and the red line is a fine solution (Δx = 100 meters, Δt = 1 second).

Figure 3.17 is about 2.8 percent of the undisturbed water area for the quadratic sloping beach, while the plateau of 11 square meters in Figure 3.11 is about 3.1 percent of the undisturbed water area for the linear sloping beach. We believe this behavior is a function of the geometry; the wetting and drying region is shallower on the quadratic sloping beach, and thus the algorithm has less of an effect on the global water budget. Overall, however, the mass balance results are remarkably similar.

A qualitative assessment of the effect of these two parameters reveals that it is best to keep H_{min} below a reasonable limit. Figure 3.18 and Figure 3.19 show the position of the shoreline for two different combinations of H_{min} and U_{min}, each compared to a fine solution. Figure 3.18 shows the combination of H_{min} = 0.01 and U_{min} = 0.01, which has been used for most of the studies in this paper. It shows a reasonably good match between the coarse and fine solutions, and the coarse solution ranges from a maximum inundation

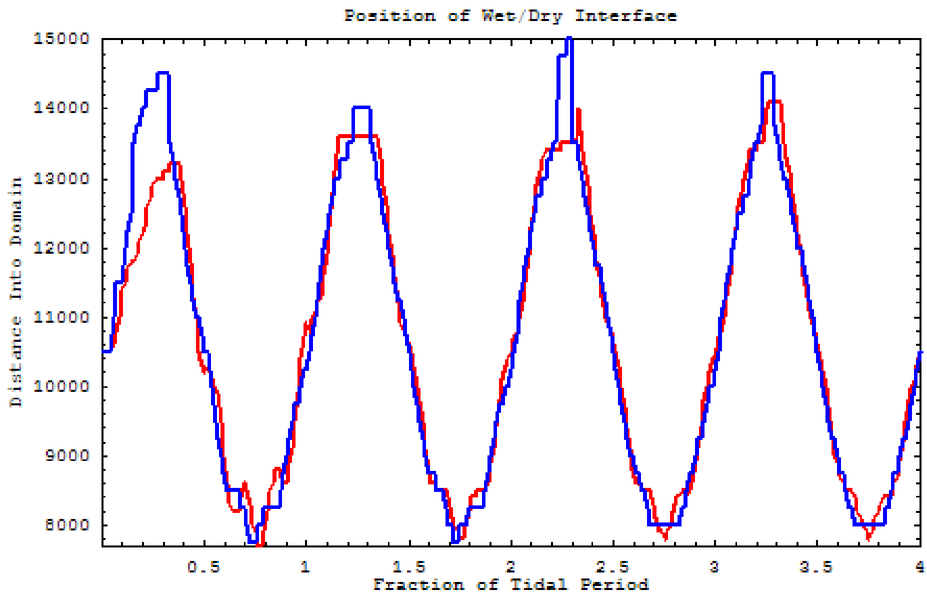

Figure 3.19. The position of the shoreline for the combination of H_{min} = 0.5 and U_{min} = 0.01. The blue line is a coarse solution (Δx = 250 meters, Δt = 10 seconds), and the red line is a fine solution (Δx = 100 meters, Δt = 1 second).

of 16.25 kilometers to a maximum recession of 8.75 kilometers. Figure 3.19 shows the combination of H_{min} = 0.5 and U_{min} = 0.01. By increasing H_{min}, we have decreased the average mass balance error from about 900 square meters to about 250 square meters. However, we have also dramatically changed the accuracy. The match between the coarse and fine resolutions is not as good, and the maximum inundation is 15 kilometers and the maximum recession is 7.7 kilometers. The unrealistically large value of H_{min} = 0.5 meters allows the algorithm to dry nodes that should be wet, and it also prevents the wetting phase to extend as far up the beach. Again, without an analytical solution, there is no way to know which representation of the shoreline is correct. However, our experience with the linear sloping beach suggests that an unrealistic value for H_{min} produces unrealistic results.

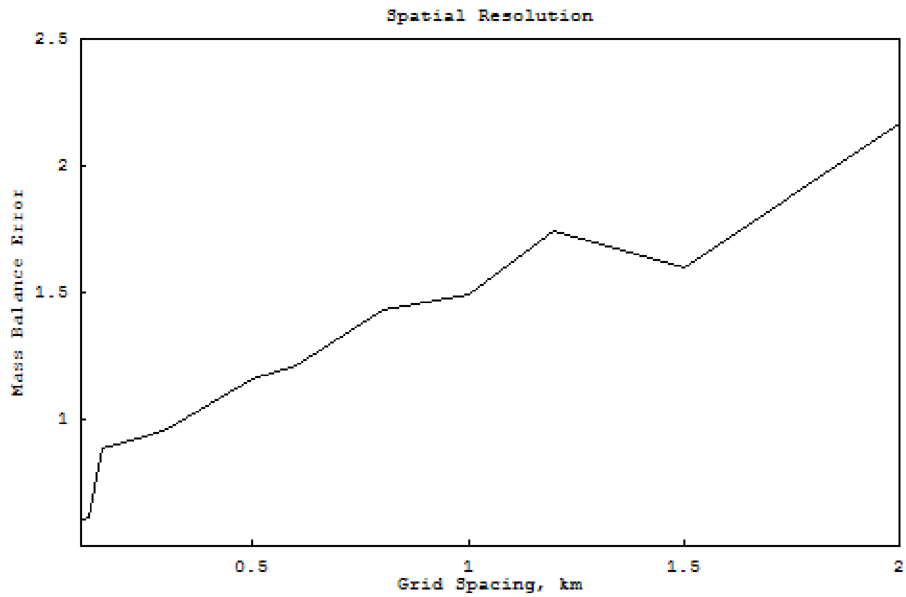

Figure 3.20. Mass balance errors (10^3 square meters) for a range of spatial resolutions. (See Section 3.1.3.)

Thus, results indicate an optimal value for these two parameters H_{min} and U_{min} is around 0.01. There does not appear to be a lower limit for either parameter; however, nothing is gained by decreasing either parameter to the limits of machine precision. We will continue to use values of 0.01 for both parameters in subsequent tests.

3.2.2.4. Spatial Resolution

Spatial resolution also plays a significant role in the simulation of wetting and drying, because it controls the model's ability to follow the position of the shoreline as it inundates and recedes. Using the Quadratic Problem, we varied the spatial resolution from a minimum of 100 meters to a maximum of 2000 meters, where each test maintained a constant Δx. For each grid spacing, we examined the model's mass balance properties.

Figure 3.20 shows the mass balance errors for the various spatial resolutions. The graph shows a sublinear (0.38) convergence rate as the grid spacing is decreased. Note that all of the simulations were run with a time step of 10 seconds except for those with spatial resolutions of 100 meters and 120 meters, which were run with a time step of 1 second in order to maintain stability. This graph supports the use of the finite volume approach as a predictor of model truncation error because, as the grid spacing is decreased, the mass balance errors also decrease.

3.2.3. Inlet Problem

The results in this subsection are from tests on a one-dimensional slice of the Shinnecock Inlet. First, we examine the algorithm's effect on temporal stability. Second, we conduct parameter sensitivity studies for bottom friction and the numerical G parameter. Third, we conduct parameter sensitivity studies for the wetting and drying parameters H_{min} and U_{min}. Fourth, we examine the effect of spatial resolution on the performance of the algorithm.

3.2.3.1. Heuristic Stability

Stability was measured by determining the maximum time step (within 5 seconds) at which the model still provided valid results. In order to prevent instabilities during the ebb phase when nodes should dry but cannot, we altered our model problem so that it can be run with the original model.

For the Inlet Problem, we shortened the domain to 52.8 kilometers so that there is a bathymetry of 2.5 meters at the land boundary. This prevents the 1 meter forcing amplitude from trying to dry out nodes within the inlet itself. All of the other parameters, including bathymetry, remained the same. The original ADCIRC model provided a maximum stable time step of 45 seconds. The wetting and drying model, when applied to the unaltered Inlet Problem, provided a maximum stable time step of 40 seconds, which is a decrease of 11 percent. In comparison to the previous model problems, the wetting and drying region for the Inlet Problem is a much smaller fraction of the overall domain, so the stability constraint is not as severe.

3.2.3.2. Parameter Sensitivity - *cftau* and *G*

The effects of the ADCIRC model parameters *cftau* and *G* on the wetting and drying algorithm were again examined. As described above in Section 3.2.1.3, the parameter *cftau* controls the bottom friction in the model, and the parameter *G* controls the balance between the wave continuity equation and the primitive continuity equation. Herein, we examine their effects on wetting and drying by varying the parameters from 0.000001 to 0.5 (always in sec^{-1} for *G*; *cftau* is dimensionless), creating a matrix of *cftau*-*G* combinations. For each combination, we examined the model's mass balance properties. Note that we were unable to compare the behavior of the model with an analytical solution, because such a solution does not exist for the Inlet Problem.

The average mass balance error for each combination is shown as a surface plot in Figure 3.21. The mass balance error was calculated using the finite volume approach, which is described in Section 3.1.3. We offer several observations. First, nearly the same region of *cftau*-*G* combinations is unstable for the Inlet Problem, as had been unstable for the Quadratic Problem and the two Linear Problems. The unstable region is slightly larger for the Inlet Problem, especially when *G* is small (such as the combination of *cftau* = 0.01 and *G* = 0.000001). Second, the shape of the three-dimensional surface is similar to the

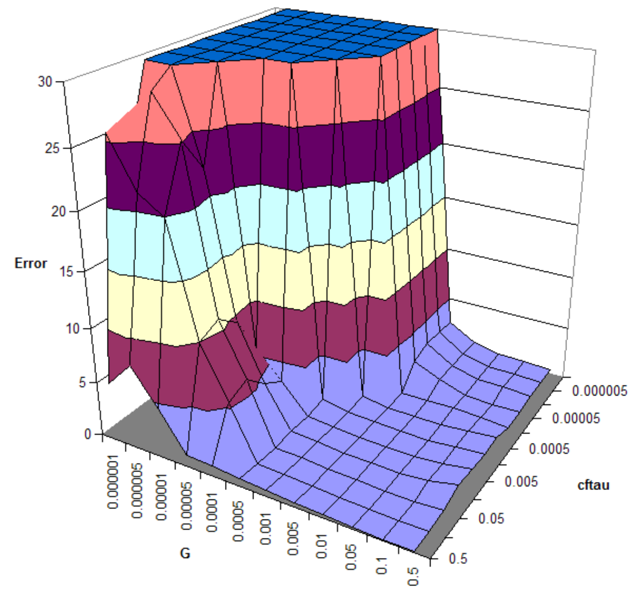

Figure 3.21. Mass balance errors for 144 combinations of *cftau* and *G*. The errors on the vertical axis are shown in intervals of 5,000 square meters. The errors in the region where *cftau* and *G* are near maximum are 300 square meters or less.

shapes of the surfaces for the other problems, as shown in Figure 3.9 and Figure 3.14. However, for this problem, even the stable combinations that have a small *G* value (such as *cftau* = 0.1 and *G* = 0.000001) experience significant mass balance errors and should not be used, which was not necessarily the case for the previous two model problems. Also, for this problem, there is not as much variation in the "good" region of combinations (i.e., where *G* is at least 0.01). In this region, a slice of the matrix with a constant *G* value shows mass balance errors that are all within one order of magnitude, whereas a similar slice for the Quadratic Problem shows errors that vary over two orders of magnitude. Also, when compared to the undisturbed water area of 2.07 million square meters, these relative mass balance errors are significantly smaller. The minimum mass balance error occurs at the corner of the matrix where *cftau* = 0.5 and *G* = 0.5 and has a value of 58.8 square meters, or 0.003 percent of the undisturbed water area. The mass balance error at the combination of *cftau* = 0.0001 and *G* = 0.01 is 386.3 square meters, or 0.02 percent of the undisturbed water area. Thus, although the magnitude of mass balance errors for the Inlet Problem are similar in magnitude than the errors for the previous model problems, the larger size of the Inlet Problem diminishes their significance.

This problem is an interesting test of the wetting and drying algorithm because the minimum bathymetry occurs about three kilometers from the land boundary. In fact, this minimum bathymetry of 0.94 meters is the only place where the bathymetric depth is less than the 1.0 meter forcing amplitude. This node is located just inside the inlet opening, and, when it dries, the rest of the inlet is forced to dry as well, as described in Section 3.1.2. Thus, the wetting and drying processes do not occur gradually, as for the previous model problems. As the node near the inlet opening is dried, so is the rest of the inlet; and as that node is wetted, so is the rest of the inlet. Thus, the mass balance errors in the "good" region of the matrix (where $G > 0.01$) may be smaller for the Inlet Problem because the wetting and drying processes happen less often overall.

A quantitative assessment of the effect of *cftau* and *G* on accuracy could not be performed, because there is no analytical solution for the Inlet Problem. However, a review of the position of the wetting and drying interface for each combination suggests that accuracy may be significantly hindered when *cftau* is larger than 0.005. For smaller values of *cftau*, the wetting and drying processes occur four times, once for each tidal period. As *cftau* is increased above that value, the wetting and drying processes may occur only one or two times or not at all, depending on the value of *G*. This makes sense physically; as *cftau* is increased, so is the bottom friction, which would work to dampen the 1.0 meter forcing amplitude to where it would not have as much of an effect on a node that is more than 50 kilometers into the domain. Thus, users who wish to allow near-shore wetting and drying should select an appropriately small value of the bottom friction coefficient.

3.2.3.3. Parameter Sensitivity - H_{min} and U_{min}

The numerical parameters H_{min} and U_{min} are described above in Section 3.1.1. Both parameters affect the ability of the algorithm to wet or dry nodes, so it is important to consider the effects of the two parameters in tandem. Each parameter was varied from 0.0001 to 0.5 (meters for H_{min}; meters per second for U_{min}), creating a matrix of combinations. For these runs, we again used *cftau* = 0.0001 and G = 0.01 sec^{-1}, to match the studies in Section 3.1.4 and Section 3.2.3. For each combination of H_{min} and U_{min}, we examined the model's mass balance properties.

The examination of the model's mass balance properties was performed in the same manner as described in Section 3.1.3. The mass balance error was calculated by computing the difference between the global accumulation and the global mass flux. A three-dimensional surface of average mass balance error over four tidal cycles is shown in Figure 3.22, and it reveals the following. First, the model does not experience instabilities for any combination of H_{min} and U_{min} within the range from 0.0001 to 0.5. Second, as with the previous two model problems, the wetting criterion U_{min} does not have an effect on mass balance. There is not a significant difference between the average mass balance errors for the extreme values of U_{min} = 0.0001 meters per second and U_{min} = 0.5 meters per second.

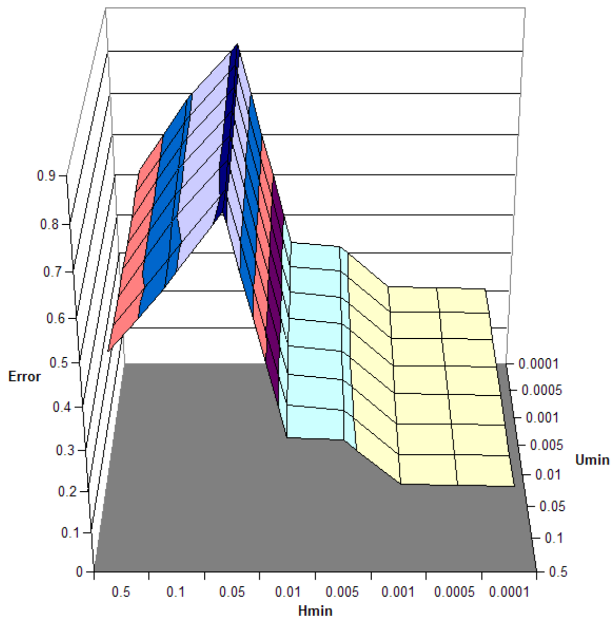

Figure 3.22. Mass balance errors for a range of H_{min} and U_{min} values. (See Section 3.1.3.) The errors are shown in intervals of 100 square meters.

Third, and most importantly, the shape of the surface is different from that of the previous two model problems. For both the Linear Problems and the Quadratic Problem, the average mass balance errors increased until about H_{min} = 0.01, and then they leveled off. For the Inlet Problem, the errors follow the same pattern until H_{min} = 0.05, but then they decrease to new minimums as H_{min} is decreased further. The unrealistically large values of H_{min} cause premature and excessive drying of the inlet region. Figure 3.23 and Figure 3.24 show the position of the wet/dry interface for two different values of H_{min}. In Figure 3.23, where H_{min} = 0.5 meters, the drying process occurs earlier in each tidal period than it does in Figure 3.24, where H_{min} = 0.0001 meters. This causes problems, especially in the first tidal period where the inlet is fully dried and wetted twice. The average mass balance errors are noticeably larger for the case when H_{min} is larger.

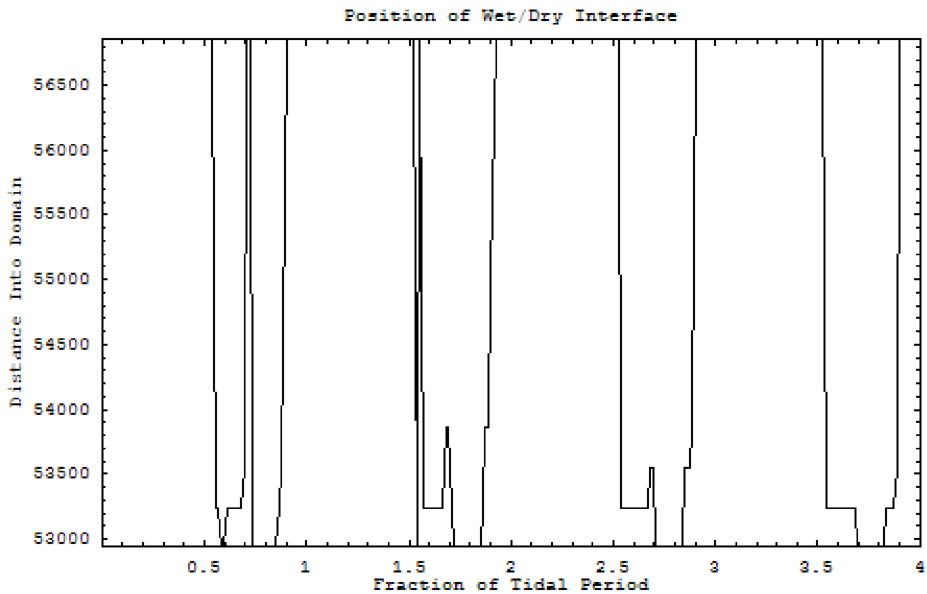

Figure 3.23. Position of the shoreline for the Inlet Problem. Note that H_{min} = 0.5 meters and U_{min} = 0.01 meters per second.

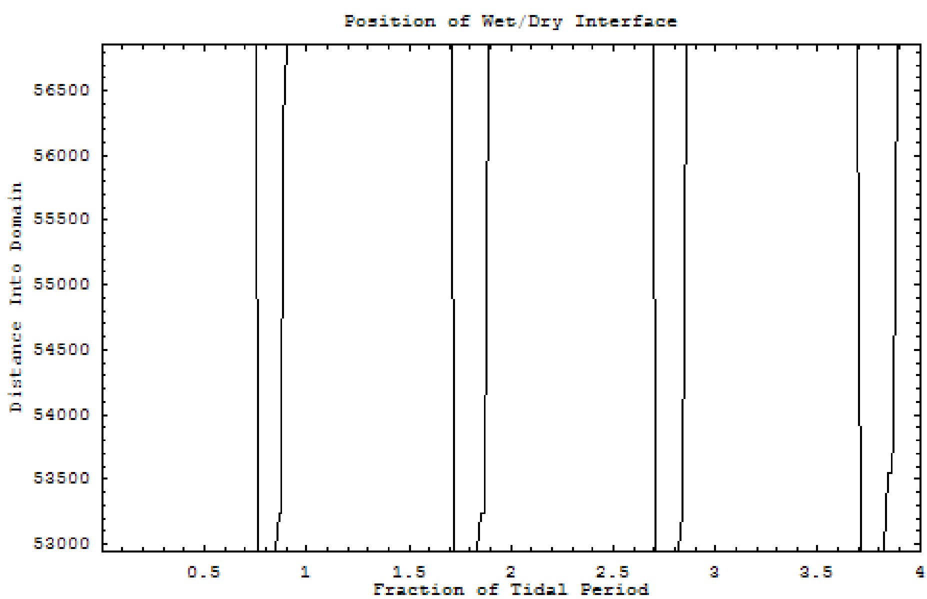

Figure 3.24. Position of the shoreline for the Inlet Problem. Note that H_{min} = 0.0001 meters and U_{min} = 0.01 meters per second.

Thus, both the quantitative mass balance results and the qualitative accuracy results indicate that H_{min} should be kept at or below 0.01 meters, at most, and there does not appear to be a penalty for decreasing it even further. Once again, the wetting criterion U_{min} does not have an effect on mass balance.

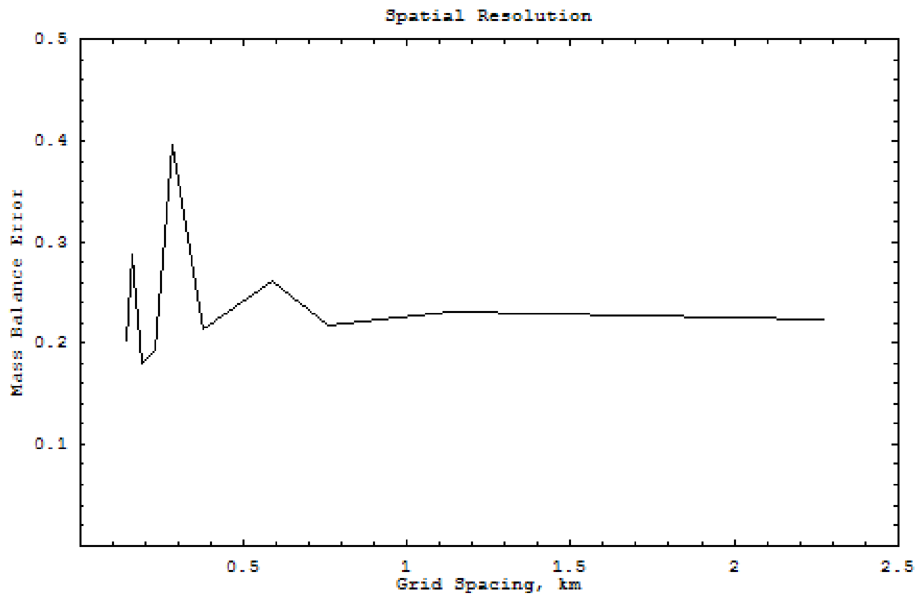

Figure 3.25. Mass balance errors (10^3 square meters) for a range of spatial resolutions. (See Section 2.3.)

3.2.3.4. Spatial Resolution

The effect of spatial resolution on mass balance was once again considered. Instead of using the variable spacing that is natural for the Inlet Problem, we used a constant grid spacing. Nodal bathymetries were interpolated by fitting a cubic spline to the data from the two-dimensional grid. The number of elements was varied from 25 to 400, and the corresponding spacings were varied from a maximum of about 2.3 kilometers to a minimum of 142 meters. We tried to hold the time step at a constant 10 seconds, but the fine resolutions (i.e., with 300 elements or more) required a smaller time step of 1 second.

Figure 3.25 shows the mass balance errors for the various spatial resolutions. Note that the mass balance errors do not converge as the grid spacing is refined. In fact, many of the smaller grid spacings produce anomalously large mass balance errors. For instance,

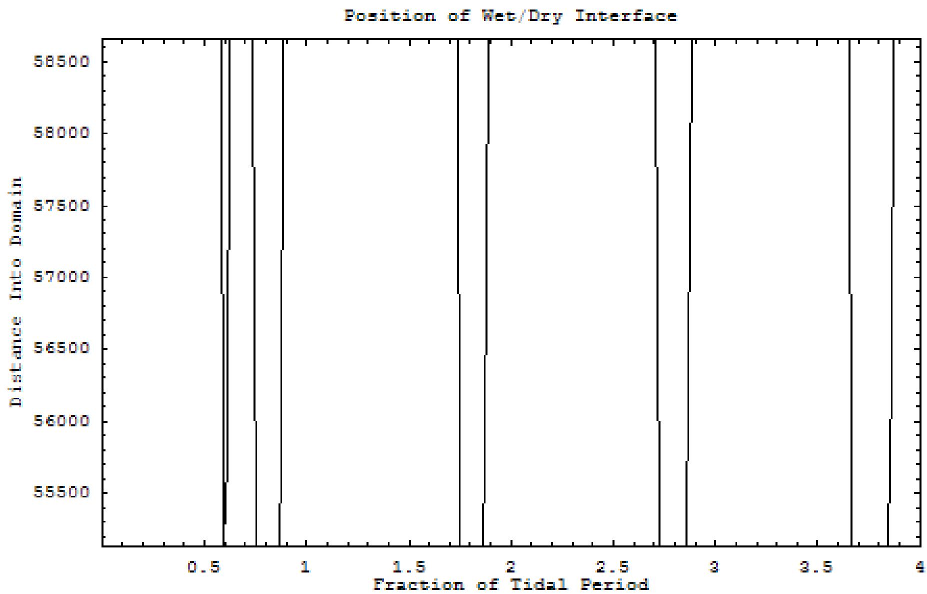

Figure 3.26. The position of the shoreline for the Inlet Problem. Note that the grid spacing is about 586 meters (100 elements).

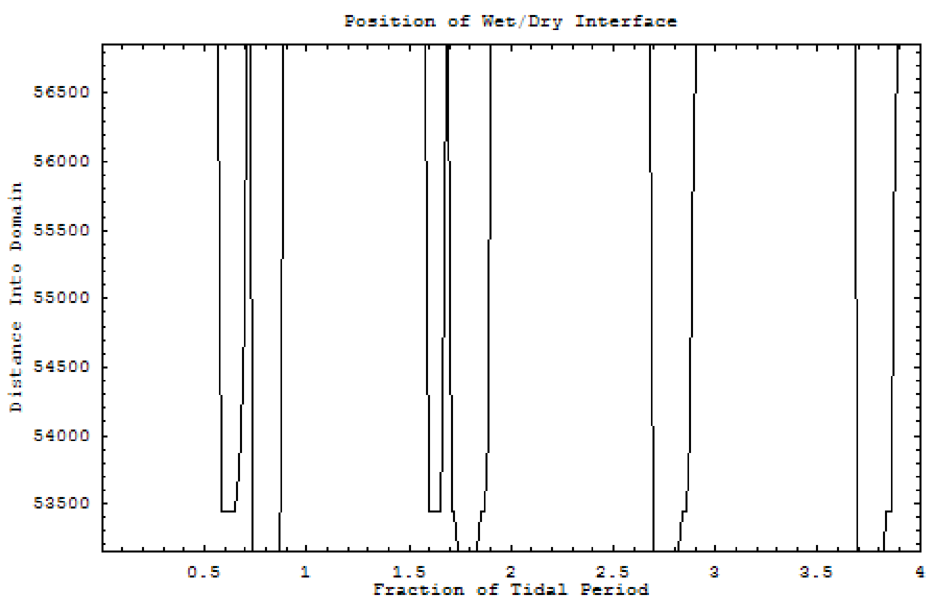

Figure 3.27. The position of the shoreline for the Inlet Problem. Note that the grid spacing is about 284 meters (200 elements).

a grid spacing of 284 meters (200 elements) produces a mass balance error of about 397 square meters. This behavior may be caused by extra wetting and drying in these simulations, as described above in Section 3.2.3.3. Figure 3.26 and Figure 3.27 show the

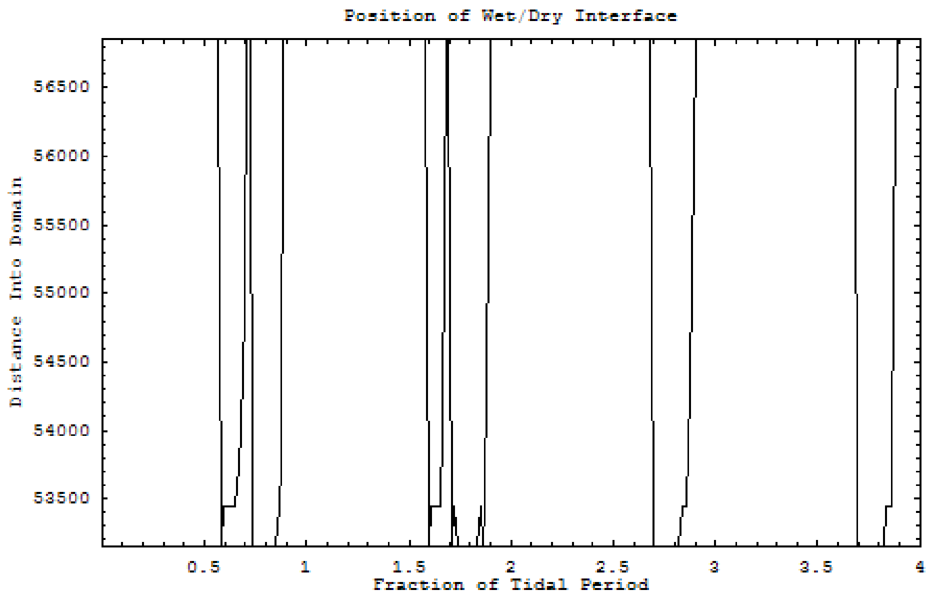

Figure 3.28. The position of the shoreline for the Inlet Problem. Note that the grid spacing is about 284 meters (200 elements), and that each node is required to remain dry or wet for 50 time steps before changing states.

position of the shoreline for two different spatial resolutions. Note that in Figure 3.27, where the grid spacing is smaller, there is extra wetting and drying during the second tidal cycle. The inlet is actually turned off and on twice during the same period, and this additional wetting and drying may cause the larger mass balance error.

As described in Section 3.1.1, the algorithm includes input parameters that can be used to prevent the rapid wetting and drying of the same node. We increased these parameters from 5 time steps to 50 time steps, but the model behavior remained the same, as shown in Figure 3.28. Thus, this behavior may just be start-up noise, and not a product of the algorithm itself. Note that both simulations (Figure 3.26 and Figure 3.27) fight through this start-up noise and provide similar results for the third and fourth tidal periods.

It should also be noted that all of the mass balance errors shown in Figure 3.25 are very small when compared to the actual size of the Inlet Problem. For instance, the maximum error of about 397 square meters is only about 0.02 percent of the undisturbed water area. Thus, although the extra wetting and drying can cause greater mass balance errors, these errors are still relatively small. Spatial resolution appears to have only a secondary effect on mass balance.

3.3. Conclusions

The results from the wetting and drying studies using the one-dimensional ADCIRC model are promising. We offer the following conclusions:

- ADCIRC's wetting and drying algorithm can simulate wave run-up on beaches, even one tidal period after a cold start. Most start-up noise is concentrated in the first two tidal periods, after which the model provides better results.
- The algorithm imposes stability restrictions, which can be severe depending on the extent of the wetting and drying. Our Linear Problem 2 experienced a 70 percent reduction in the maximum stable time step, and the Quadratic Problem experienced a 66 percent reduction. For the Inlet Problem, where the region of wetting and drying is smaller, the decrease was 11 percent.
- The numerical parameter G must remain relatively large (i.e., greater than 0.001 $\sec^{-1}$), especially for typical values of *cftau* in the range from 0.001 to 0.00001. However, combinations of *cftau* and G in that range show reasonable mass balance errors and values of G/τ in the same range as for non-wetting/drying barotropic applications.
- The minimum wetness height H_{min} shows acceptable behavior for all values less than or equal to 0.01 meters. Our results do not suggest that there is a lower bound

for this parameter. In fact, for the Inlet Problem, mass balance errors continued to decrease as H_{min} was decreased to 0.0001 meters.

- The minimum wetting velocity U_{min} has no significant effect on the behavior of the model, for any of the four model problems.
- For the idealized model problems, accuracy and mass balance improve as the spatial resolution is refined. That trend was not evident for the Inlet Problem. However, for all four problems, a stability restriction prevents simulations with small grid spacings from being run with the same time step of 10 seconds.

These results are helpful in that they: (1) benefit users who, to this point, may have relied on nothing more than personal experience when they selected run-time parameters such as time step, roughness coefficient, wetness and drying heights, etc.; and (2) prove that the existing ADCIRC wetting and drying algorithm is robust. The eventual goal of this research is to implement the algorithm in the three-dimensional ADCIRC model, but first we should test its behavior in the vertical dimension by implementing and assessing it in a two-dimensional, x-z slice ADCIRC model.

4. Two-Dimensional Wetting and Drying

One of the purposes of this research thesis is to implement and assess ADCIRC's wetting and drying algorithm in a three-dimensional version of the model. We will address that task in Chapter 5. However, before doing so, we will implement and assess the algorithm in a two-dimensional (x-z) version of the model, for two reasons.

First, by adding only one extra dimension at a time, we are able to control the number of new model parameters and assess the model's behavior in stages. The main difference between the one-dimensional and two-dimensional (x-z) models is that the two-dimensional (x-z) model does not solve for a depth-averaged velocity; instead, the velocities at a user-specified number of layers are computed. (For most of the studies in this chapter, we specified 11 vertical layers.) This treatment of velocity is similar to that in the three-dimensional model, so it is a good opportunity to test the wetting and drying algorithm. At the same time, though, the two-dimensional (x-z) ADCIRC model can be applied to problems that are very similar to the model problems used in Chapter 3. (The Linear Sloping Beach domain in this chapter is similar to Linear Problem 2 in the previous chapter.) The similarities of these model problems provide a framework with which we can judge the results in this chapter.

Second, as we will describe in Section 4.1.2, the wetting and drying algorithm was updated after the one-dimensional studies in Chapter 3 were completed. Two parameters were removed entirely, and the algorithm itself was lengthened. These updates were implemented to address specific situations where the original wetting and drying algorithm struggled. We will show that the updates were necessary and beneficial. However, we would rather test the effects of the improved algorithm by using the two-dimensional (x-z) ADCIRC model, because its run-times are understandably smaller. If we can establish the worthiness of the improved algorithm here, then our burden of proof will be more manageable in three dimensions.

Third, this study of the two-dimensional (x-z) ADCIRC model is necessary because, without it, wouldn't be able to pass 200 pages on this thesis. And that is an important goal.

The structure of this chapter is similar to that for the one-dimensional wetting and drying algorithm. We will discuss our methods, including a description of how the algorithm was implemented in the two-dimensional (x-z) model. We will present the results of our numerical experiments on our two model problems. And we will draw conclusions based on those results.

4.1. Methods

This subsection contains a discussion of how the wetting and drying algorithm was implemented in this form of the ADCIRC model, an introduction of the two major changes to the algorithm since the study of the one-dimensional model in Chapter 3, a description of the two model problems used in this chapter, and a review of the two error measures used in our numerical experiments.

4.1.1. Implementation in 2D (*x*-*z*) ADCIRC

The wetting and drying algorithm for the two-dimensional (*x*-*z*) ADCIRC model occurs in the middle of the time step, between the solution of the GWC equation (for water surface elevations) and the solution of the momentum equation (for velocities or fluxes). This algorithm did not exist previously in this form of the ADCIRC model, so we developed and implemented it based on the algorithm currently in the two-dimensional (*x*-*y*) ADCIRC model. To ensure its compatibility with the two-dimensional (*x*-*z*) version, we made two changes.

First, the algorithm was added as its own subroutine. This choice was made primarily for ease of coding; instead of having several hundred lines of wetting and drying code in the middle of another subroutine, the code exists as its own unit. If the wetting and drying algorithm is ever modified or re-designed, then it will be easier to simply swap in the new algorithm as its own subroutine.

Second, we updated the subroutines that solve for water surface elevations, horizontal velocities, and vertical velocities. As noted earlier in Section 3.1.1, dry regions are not technically dry; the water depth at a dry node can be larger than zero, so long as it is less than the user-specified H_{min}. Thus, a thin film of water can exist at dry nodes. This water should not contribute to the continuity or momentum computations at a neighboring wet node. If a wet node is connected to a dry node, then the contribution from the dry node is not included in the summation.

4.1.2. Updates to the Wetting and Drying Algorithm

In the summer of 2004, two changes were made to the wetting and drying algorithm. First, the two parameters *NODEDRYMIN* and *NODEWETMIN* were eliminated. Second, an elemental drying check was added.

The first change relates to the propagation of waves on relatively flat flood plains. The user specified the two parameters in the input file, and they were used to control how long a node had to remain either dry or wet. Thus, if *NODEDRYMIN* was set to 20, then any node had to remain dry for at least 20 time steps. These parameters were included originally to control oscillations at the wetting front, but it was discovered that they also slowed the propagation of flood waves. To prevent this, the two parameters were removed from the algorithm.

The second change relates to the flow of water down a steep incline. It was discovered that the simple momentum balance used in the node-based wetting check allowed "barely wet" nodes to remain active in areas with steep topography. Thus, a thin film of water would be allowed to remain wet if it was on an incline where water was flowing from above. Mass balance problems occurred in these regions. To prevent this, a new parameter, H_{OFF}, was hardwired into the code, and it is set to 120 percent of the H_{min} parameter. (The "120 percent" criterion was an *ad hoc* selection; nonetheless, it works.) If any of the nodes on an element has a water depth that is less than H_{OFF}, then the element itself is dried. This change allows water to build up on an incline before it is allowed to flow downhill.

We will use this study of the two-dimensional (*x-z*) model to test the relative behavior of the "original" and "improved" wetting and drying algorithms. All of our numerical experiments will be run twice, (once for each version of the wetting and drying algorithm,) so that their behavior can be quantified. We expect the improved algorithm to show significantly better results in model problems that contain the features for which it was designed.

4.1.3. Model Problems

The purpose of this study of the two-dimensional (*x*-*z*) ADCIRC model is to verify that its wetting and drying algorithm(s) behaves similarly to that of the one-dimensional ADCIRC model that was examined in Chapter 3. We will examine the three-dimensional wetting and drying algorithm in Chapter 5. Thus, in this chapter, we will examine only two model problems: the Linear Sloping Beach domain and the Plateau domain.

A schematic of the Linear Sloping Beach domain is similar to the linear beach domains used in Chapter 2 and Chapter 3. This problem has the following parameters (unless stated otherwise): a linear slope, an undisturbed length of 18 kilometers, a bathymetric depth at the open ocean boundary of 6 meters, a grid spacing of 250 meters, 11 vertical layers, a time step of 1 second, a forcing amplitude of 1.0 meter, a tidal period of 12 hours (43,200 sec), a duration of 4 tidal periods, a K_{slip} value of 0.0001 and a G value of 0.01 sec^{-1}, an H_{min} value of 0.01 meters, and a U_{min} value of 0.01 meters per second. Note that we have backed off the time step to 1 second (compared to 10 seconds in Chapter 3), and we have adopted the "optimal" conditions established in the study of the one-dimensional model. The added dimension in the *z*-direction affects the bottom friction (which is controlled by the K_{slip} parameter, as we will discuss in Section 4.2.1.2) and adds the ability to specify the number of vertical layers (which we will discuss in

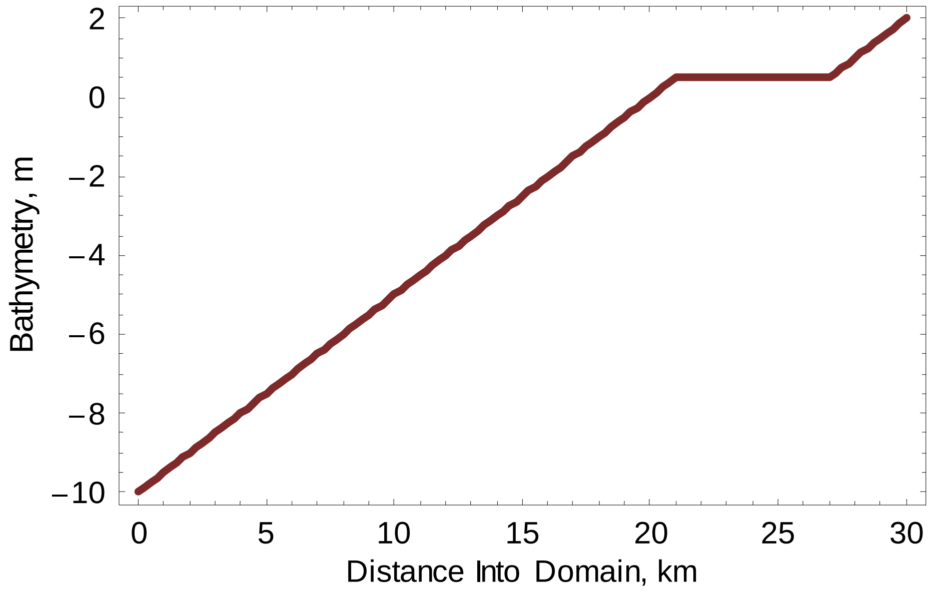

Figure 4.1. A schematic of the bathymetry for the Plateau domain. The flat region has a bathymetry of 0.5 meters (above sea level) and extends between the *x*-distances of 21 kilometers to 27 kilometers.

Section 4.2.1.5).

The Plateau domain is shown in Figure 4.1, and it was designed to test the improved wetting and drying algorithm. Specifically, there are two features that distinguish it from the Linear Sloping Beach domain. First, the Plateau domain has a 6-kilometer long region where the bathymetry is a constant 0.5 meters above sea level. This feature should test the improved algorithm's ability to simulate flood waves, which tended to be slowed down by the *NODEDRYMIN* and *NODEWETMIN* parameters in the original algorithm. The forcing amplitude is 1 meter at the open ocean boundary, so the waves should wet the sloped beach and then flow across the flat region. Second, the Plateau domain has sloped regions that are 50 percent steeper than the Linear Sloping Beach. This feature should test the improved algorithm's new elemental drying check, which was added to better simulate flow down steep inclines. As the tide recedes, water from the flat region should drain down the incline. In addition to those two features, this problem has the following parameters (unless stated otherwise): a total length of 30 kilometers, an undisturbed water length of 20 kilometers, a bathymetric depth at the open ocean boundary of 10 meters, a grid spacing of 250 meters, 11 vertical layers, a time step of 1 second, a forcing amplitude of 1.0 meter, a tidal period of 12 hours (43,200 sec), a duration of 4 tidal periods, a K_{slip} value of 0.0001 and a G value of 0.01 sec^{-1}, an H_{min} value of 0.01 meters, and a U_{min} value of 0.01 meters per second.

4.1.4. Error Computations

In this chapter, we use the same error measures as for the previous wetting and drying studies. For the Linear Sloping Beach domain, we can compare our numerical results and the analytical solution described in Section 3.2.1.1. The domain is sliced at $y = 6000$ meters to obtain results that can be compared with the one-dimensional analytical solution. Then we examine the position of the wet/dry interface over the fourth tidal period (because the model is spun up from a cold start for the first three periods). After every 10 minute interval in that fourth period, we calculate the difference between the position of the interface given by the numerical results and the position of the interface given by the analytical solution. These differences are then averaged. If the numerical results successfully approximate the analytical solution, then the average difference should be zero. However, spatial discretization often prevents a perfect match between numerical and analytical, so we are satisfied if the average difference is less than the grid spacing of 250 meters. Also, it is important to remember that the analytical solution does not include bottom friction, so optimal ADCIRC results will occur at relatively low values of that parameter.

The second error measure is an examination of mass balance. Again, we use a procedure similar to that from the one-dimensional wetting and drying study. It is calculated using a finite volume approach, where we compute the difference between the global accumulation and the global mass flux, as represented by the vertically-averaged primitive continuity equation. Recently, several papers [1, 8] have advocated computing mass balance from finite element residuals in order to be consistent with the numerical discretization. However, we have shown (Kolar et al. [13]) the finite volume approach to be a good surrogate variable for accuracy and phasing errors; that is, small mass balance errors (as computed with finite volume) correlate with small constituent errors. Additionally, in Chapter 2, we showed that the finite volume method is a good indicator of truncation errors, especially for domains that have a constant node spacing. Hence our reason for using the finite volume approach herein.

4.2. Numerical Experiments

This subsection contains the results of numerical experiments conducted using the Linear Sloping Beach domain and the Plateau domain.

4.2.1. Linear Sloping Beach Domain

This subsection contains the results of five numerical experiments: heuristic stability, parameter sensitivity with G and K_{slip}, parameter sensitivity with H_{min} and U_{min}, horizontal resolution, and vertical resolution.

Table 4.1: Summary of heuristic stability results for the two versions of the wetting and drying algorithm. The two versions do not show significant differences for the Linear Sloping Beach domain. Note that mass balance error is an average error over all four tidal cycles, while the difference between the shoreline from the numerical results and the shoreline from the analytical solution is an average over only the fourth tidal cycle.

	Original Algorithm	Improved Algorithm
Maximum stable time step	30 sec	30 sec
Mass balance error	627.232 m^2	608.442 m^2
Average difference from analytical solution	177.384 m	180.856 m

4.2.1.1. Heuristic Stability

To examine the stability of the two versions of the two-dimensional wetting and drying algorithm, we increased the time step (in increments of 5 seconds) until the model became unstable. The heuristic stability results for the two versions of the wetting and drying algorithm are shown in Table 4.1. Note that there is not a significant difference between the two versions of the algorithm. Both show maximum stable time steps of 30 seconds, and each version has a slight advantage in either mass balance error or accuracy.

4.2.1.2. Parameter Sensitivity - K_{slip} and G

As discussed in Section 3.2.1.3, two important parameters in the ADCIRC model are the bottom friction and the numerical parameter G (sometimes called τ_0). In two (x-z) dimensions, bottom friction is implemented as a term in the vertical stress calculation:

$$\frac{\tau_{bx,j}}{\rho_0} = K_{slip,j}u_j, \qquad (1)$$

where τ_{bx} is the bottom stress; ρ_0 is the reference density of water; u is the velocity; j is the node index; and K_{slip} is the bottom boundary condition. For a "no slip" bottom boundary condition:

$$K_{slip,j} \to \infty. \qquad (2)$$

For a "linear slip" bottom boundary condition:

$$K_{slip,j} = \text{constant}. \qquad (3)$$

And, for a "quadratic slip" bottom boundary condition:

$$K_{slip,j} = C_d|u_j|, \qquad (4)$$

where C_d is a quadratic drag coefficient.

The two-dimensional (x-z) ADCIRC model does not include all three types of bottom boundary condition; only the linear slip bottom boundary condition is available. The results shown in this section utilize that linear slip bottom boundary condition, where K_{slip} is a user-specified constant. We varied both K_{slip} and G from 10^{-5} to 10^{-1} (sec^{-1} for G, unitless for K_{slip}), creating a test matrix of 25 combinations of K_{slip} and G. Then we examined the effect of each combination on the model's accuracy and mass balance properties, for both the original and improved versions of the wetting and drying algorithm.

Figure 4.2 shows the average difference between the shoreline predicted by the numerical results and the shoreline predicted by the analytical solution, for the original version of the wetting and drying algorithm. Figure 4.3 shows a similar graph for the

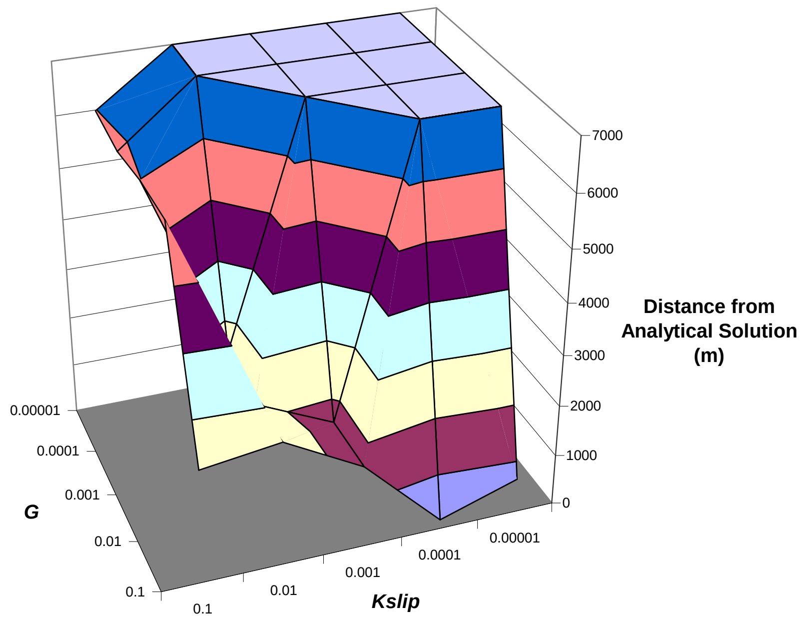

Figure 4.2. For the original wetting and drying algorithm, the average difference between the numerical results and the analytical solution over the fourth tidal cycle, as discussed in Section 4.1.4, for 25 combinations of K_{slip} and G. The errors are shown in intervals of 1000 meters; the grid spacing is 250 meters.

improved algorithm. First, note the similarity between both figures and the corresponding Figure 3.7 from the one-dimensional results. In all three studies, there exists a region where the respective models are unstable, specifically where both of the bottom friction and G parameters are relatively small. The best match with the analytical solution occurs in the region around K_{slip} = 0.0001 and G is relatively large, where the model is able to predict the correct shoreline within one grid spacing. However, the improved two-dimensional (x-z) algorithm shows much better stability and a better match to the one-dimensional results. In fact, at the optimal combination of K_{slip} = 0.0001 and G = 0.01 sec^{-1} from the one-dimensional results, the improved algorithm has an average difference from the analytical solution of about 180 meters, which is less than the grid spacing of 250 meters. The improved algorithm is stable for more combinations of K_{slip} and G, and its

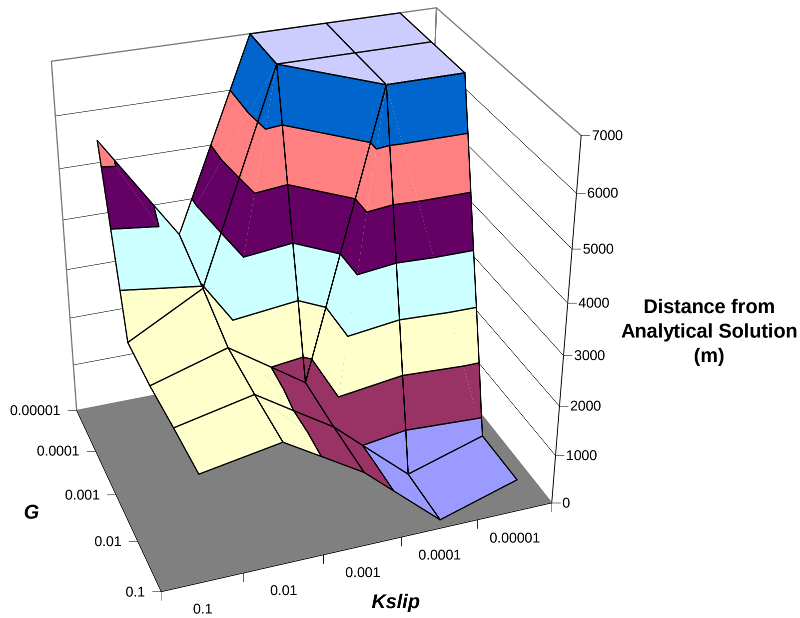

Figure 4.3. For the improved wetting and drying algorithm, the average difference between the numerical results and the analytical solution over the fourth tidal cycle, as discussed in Section 4.1.4, for 25 combinations of K_{slip} and G. The errors are shown in intervals of 1000 meters; the grid spacing is 250 meters.

results follow those from the one-dimensional study in Chapter 3.

Figure 4.4 shows the mass balance errors for the original algorithm, while Figure 4.5 shows the mass balance errors for the improved algorithm. The difference between the two versions of the algorithm becomes even more obvious. For all combinations where $G < 0.1$ sec^{-1}, the original algorithm is either unstable or shows significantly worse mass balance properties than the improved algorithm. Again, note the similarity between the mass balance results from the improved two-dimensional algorithm (Figure 4.5) and the mass balance results from the one-dimensional algorithm (Figure 3.9). Even in a model domain that does not include the features for which the improved algorithm was designed (such as a flood plain or a steep incline), it shows significant improvement.

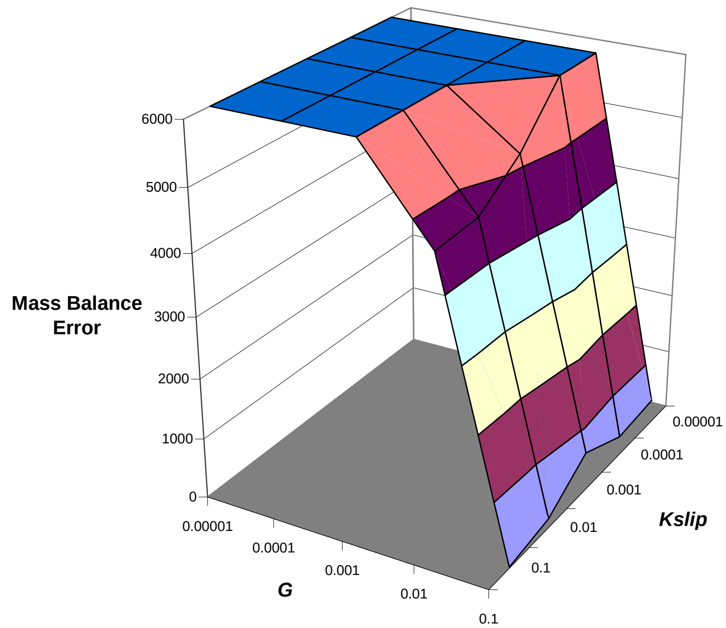

Figure 4.4. For the original wetting and drying algorithm, mass balance errors for 25 combinations of K_{slip} and G. The errors are shown in intervals of 1,000 square meters. Note that the vertical scale has been cropped to allow for a comparison with Figure 4.5; the combinations where K_{slip} is relatively large and G is relatively small show mass balance errors that range from about 40,000 square meters to 2,000,000 square meters.

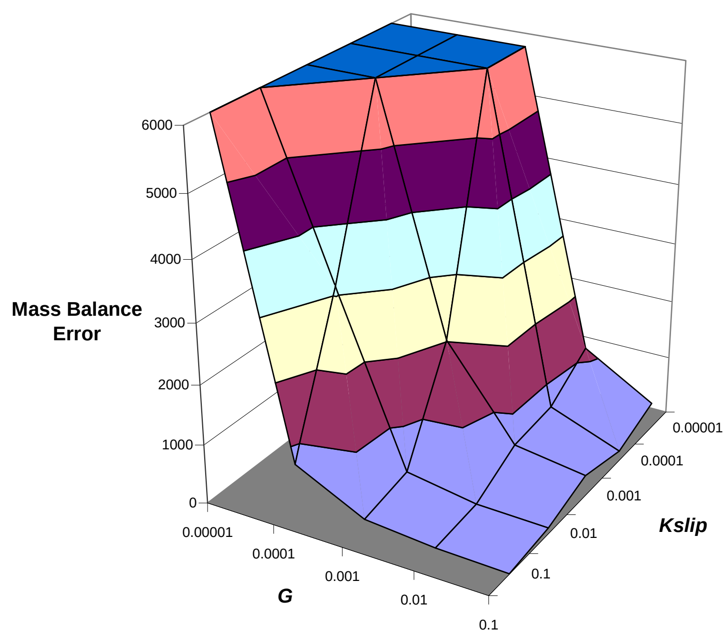

Figure 4.5. For the improved wetting and drying algorithm, mass balance errors for 25 combinations of K_{slip} and G. The errors are shown in intervals of 1,000 square meters.

It should be noted that the original version of the two-dimensional (x-z) wetting and drying algorithm has problems with the Linear Sloping Beach domain. For example, as shown in Section 4.2.1.1, the model is stable at a time step of 30 seconds and shows a mass balance error of 627 square meters. However, if the same combination of K_{slip} and G is run at a time step of 1 second, as in Figure 4.4 or Figure 4.5, then the model is unstable. This behavior, where the original version of the algorithm is unstable at both small and large time steps, is a significant problem. Not only is this behavior an inconvenience for users searching for a stable time step, it is also evidence of a bad numerical algorithm. Thus, it is good when the improved version of the algorithm is stable at all time steps below its maximum of 30 seconds.

4.2.1.3. Parameter Sensitivity - H_{min} and U_{min}

The relevance of the H_{min} and U_{min} parameters was established in Section 3.2.1.4; this section repeats that sensitivity study for the two-dimensional (x-z) version of the ADCIRC model. Specifically, we will vary both parameters from 0.00001 to 1.0 (meters for H_{min}; m/sec for U_{min}) and examine their effects on accuracy and mass balance.

Figure 4.6 shows the average distance between the shoreline from the simulation results and the shoreline from the analytical solution for the original version of the wetting and drying algorithm. Figure 4.7 shows a similar graph for the improved version. Note that, although the original version is unstable for combinations of H_{min} and U_{min} where $H_{min} > 0.01$ meters, the improved version is stable for all combinations. And, for the combinations where both versions are stable, the improved version produces slightly better matches with the analytical solution. For example, when $H_{min} = 0.0001$ meters,

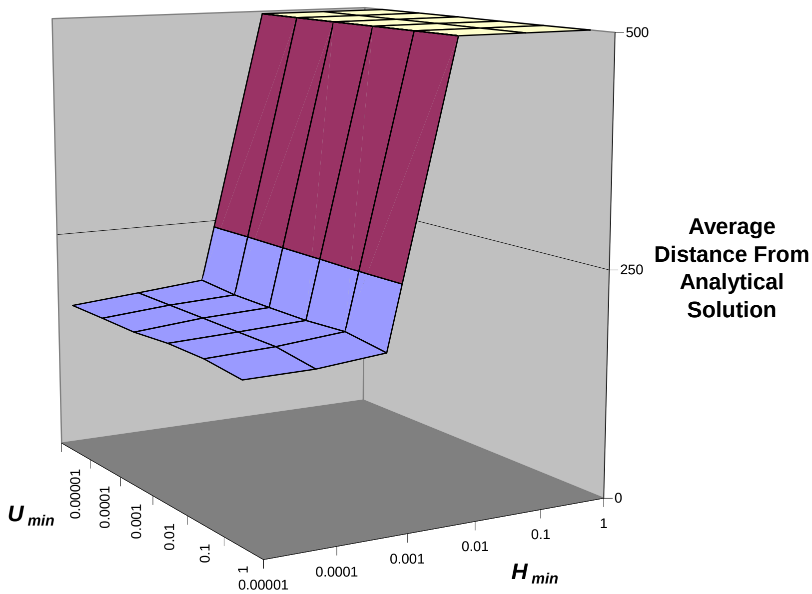

Figure 4.6. The average distance between the shoreline from the solution results and the shoreline from the analytical solution over the fourth tidal cycle, for the original version of the wetting and drying algorithm.

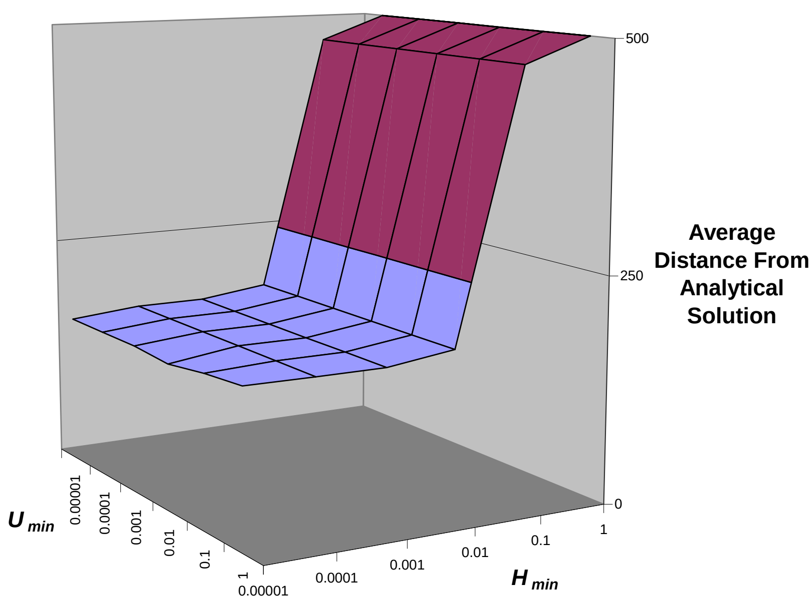

Figure 4.7. The average distance between the shoreline from the solution results and the shoreline from the analytical solution over the fourth tidal cycle, for the improved version of the wetting and drying algorithm. This version is stable for all combinations.

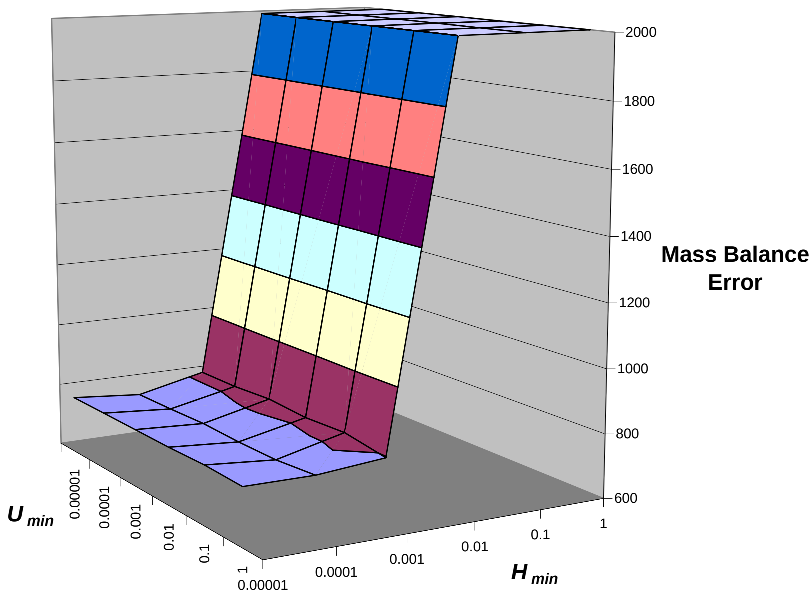

Figure 4.8. Mass balance errors over the first four tidal cycles for 36 combinations of H_{min} and U_{min}, for the original version of the wetting and drying algorithm. Note that this version is unstable for combinations when $H_{min} > 0.01$ meters.

the shoreline from the original version is an average of 185 meters from the analytical solution, while the shoreline from the improved version is only 172 meters away. The best matches occur when $H_{min} \leq 0.001$ meters for either version.

Figure 4.8 shows the mass balance errors for the original version of the wetting and drying algorithm, while Figure 4.9 shows the mass balance errors for the improved version. The versions are stable or unstable for the same combinations, as from the accuracy results in the previous paragraph. Again, for the combinations where both versions are stable, the improved version produces better mass balance errors. For example, when $H_{min} = 0.0001$ meters, the original version produces mass balance errors of about 760 m^2, while the improved version produces errors of about 700 m^2. The best results occur with the improved version of the wetting and drying algorithm with any

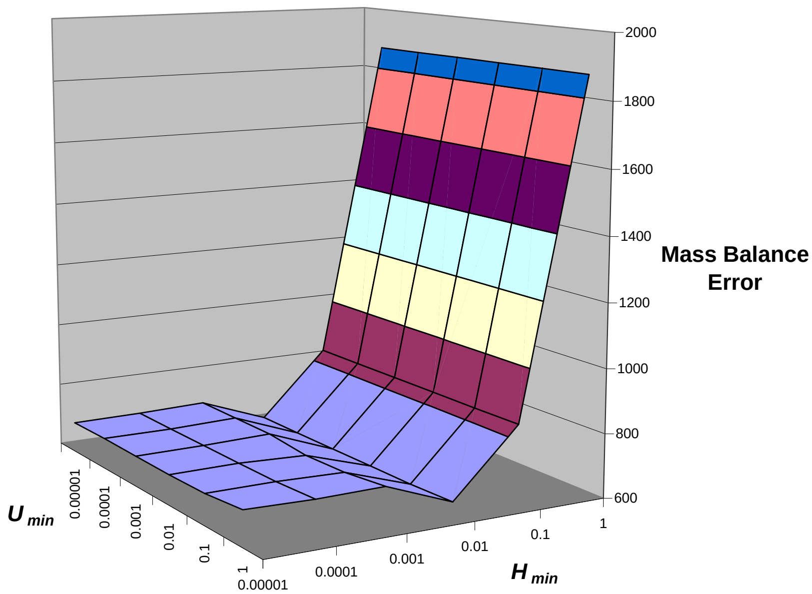

Figure 4.9. Mass balance errors over the first four tidal cycles for 36 combinations of H_{min} and U_{min}, for the improved version of the wetting and drying algorithm. Note that this version is stable for all combinations.

combination where $H_{min} = 0.01$ meters; the mass balance errors for that scenario are about 620 m^2. Thus, we will continue to use the combination of $H_{min} = 0.01$ meters and $U_{min} = 0.01$ m/sec as our "optimal" condition.

Note that, like the results from the study of the one-dimensional ADCIRC model in Chapter 3, these results again indicate that the U_{min} parameter does not affect the performance of the model. For both versions of the two-dimensional wetting and drying algorithm, and for both error measures, the act of varying the U_{min} parameter has no visible effect.

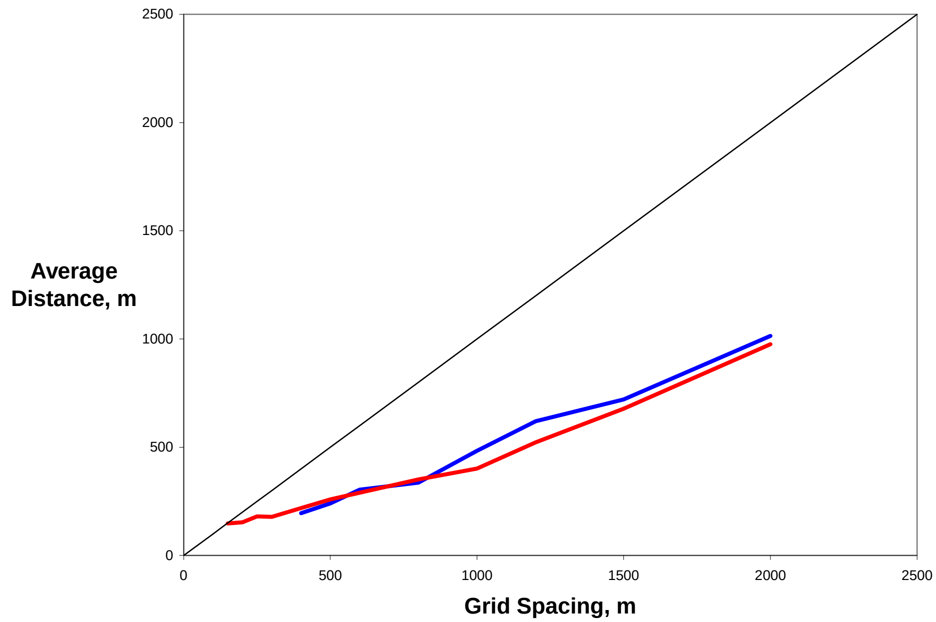

Figure 4.10. The average distance between the shorelines from the simulation results and the analytical solution, for the original (blue line) and improved (red line) versions of the wetting and drying algorithm, for varying grid spacings.

4.2.1.4. Horizontal Resolution

Figure 4.10 shows the average distance between the shorelines from the simulation results and the analytical solution, for varying horizontal resolutions. Note that the black line represents a one-to-one line; we have included it to show that the average distances are always less than or equal to the grid spacing. In fact, the simulated shoreline is always about half a grid spacing away from the analytical shoreline. For example, when the improved algorithm is run with a grid spacing of 500 meters, the average error over the fourth tidal cycle is about 260 meters. This behavior makes sense; if the analytical shoreline is more than a half grid spacing away from one node point, then it must be less than a half grid spacing away from another node point. Thus, for our "optimal"

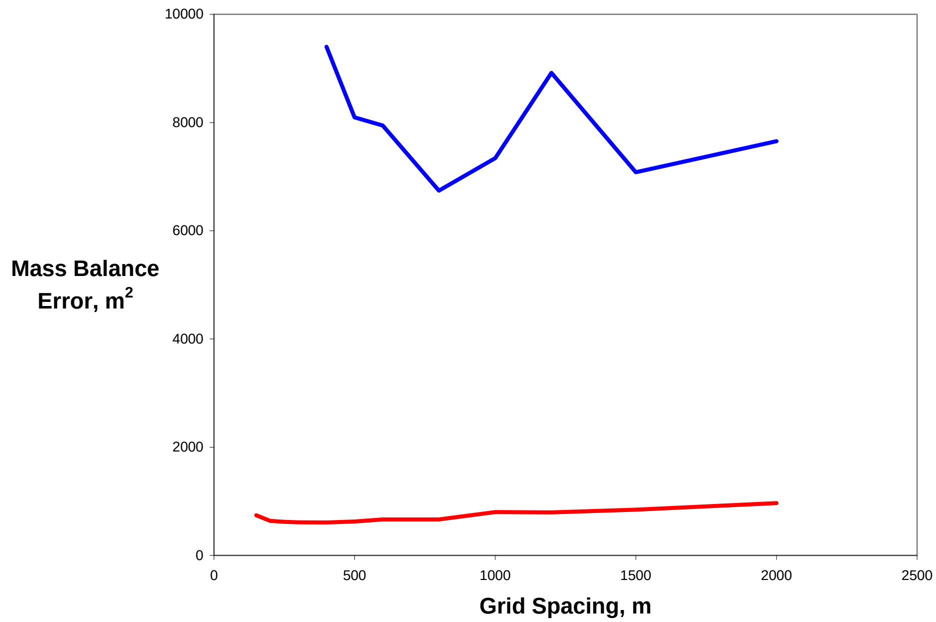

Figure 4.11. Mass balance errors over the four tidal cycles for the original (blue line) and improved (red line) wetting and drying algorithms. The improved algorithm produces mass balance errors that are about an order of magnitude smaller than those from the original algorithm.

combination of G, K_{slip}, H_{min}, and U_{min}, the wetting and drying algorithm consistently matches the analytical solution within one grid space.

Figure 4.11 shows the mass balance errors for the original and improved versions of the wetting and drying algorithm, for varying horizontal resolutions. Three observations can be made from this figure. First, neither version of the algorithm produces mass balance errors that converge as the horizontal resolution is refined. The mass balance errors from the improved version do decrease as the horizontal resolution is decreased, but they do not converge to zero. Second, the improved version is stable for much smaller grid spacings. The original version becomes unstable when the grid spacing is 300 meters or less, while the improved version does not become unstable until the grid spacing is 120 meters or less. This improvement in stability is important for wetting and

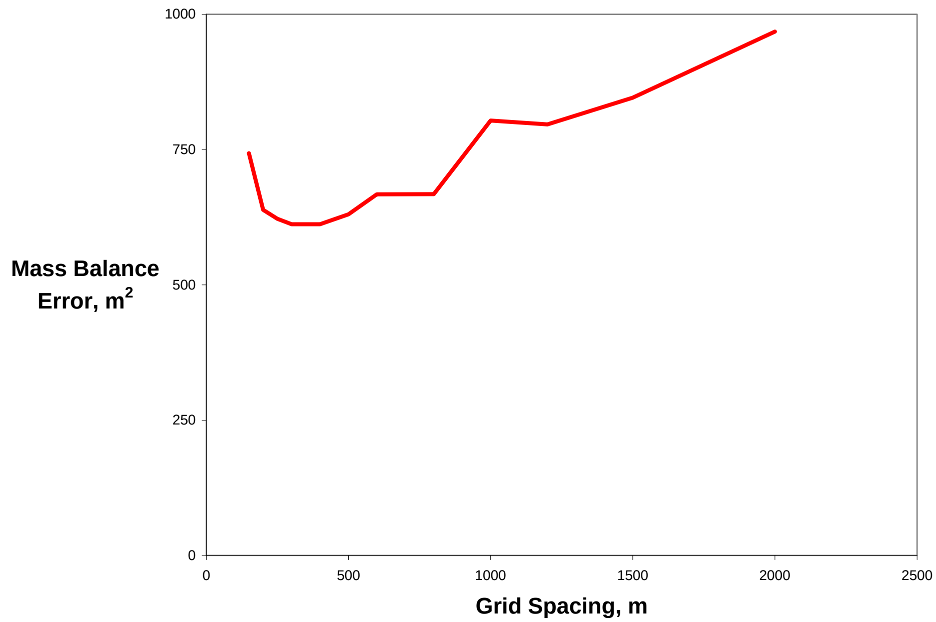

Figure 4.12. Mass balance errors over the first four tidal cycles for a range of horizontal resolutions, for the improved wetting and drying algorithm. Note that this figure is simply a close-up of part of Figure 4.11.

drying applications, which occur in near-shore areas where the grid spacing must be small in order to represent the topography. Third, the improved algorithm produces mass balance errors that are about an order of magnitude smaller than those from the original algorithm. In fact, if we decrease the vertical extents, as in Figure 4.12, then we see that the errors produced by the improved algorithm are not flat at all. In fact, with the exception of one or two fine resolutions where the model is near the point of becoming unstable, the errors converge as the grid spacing is decreased.

4.2.1.5. Vertical Resolution

To test the effect of the second (z) dimension, we varied the number of vertical layers and examined their effect on accuracy and mass balance. Basically, the number of

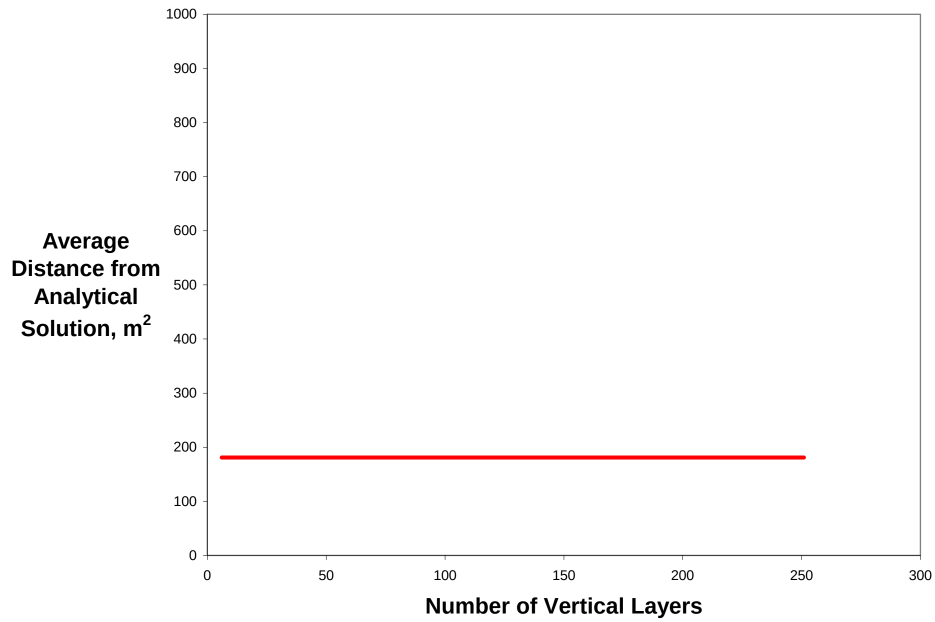

Figure 4.13. The average distance between the shorelines from the simulation results and the analytical solution, for the improved version of the wetting and drying algorithm, for varying vertical resolutions. Note that, for this set of run parameters, the original algorithm was unstable for all vertical resolutions.

layers has no effect. We varied the number of layers from 6 to 251, for a fixed horizontal spacing of 250 meters, and the error measures did not change. Note that, for this set of run parameters, the original algorithm was unstable for all vertical resolutions. The improved algorithm was stable all of the vertical resolutions we studied. For all vertical resolutions, the model shoreline is an average distance of 180 meters away from the analytical shoreline, over the fourth tidal cycle. And, again for all vertical resolutions, the mass balance error is 622 m^2, over all four tidal cycles. Figure 4.13 and Figure 4.14 depict this behavior.

It should be noted that the Linear Sloping Beach domain does not experience the type of vertical mixing that would require refinement in the vertical direction. As the tide either inundates or recedes, the velocity field is dominated by the *x*-component. Perhaps a

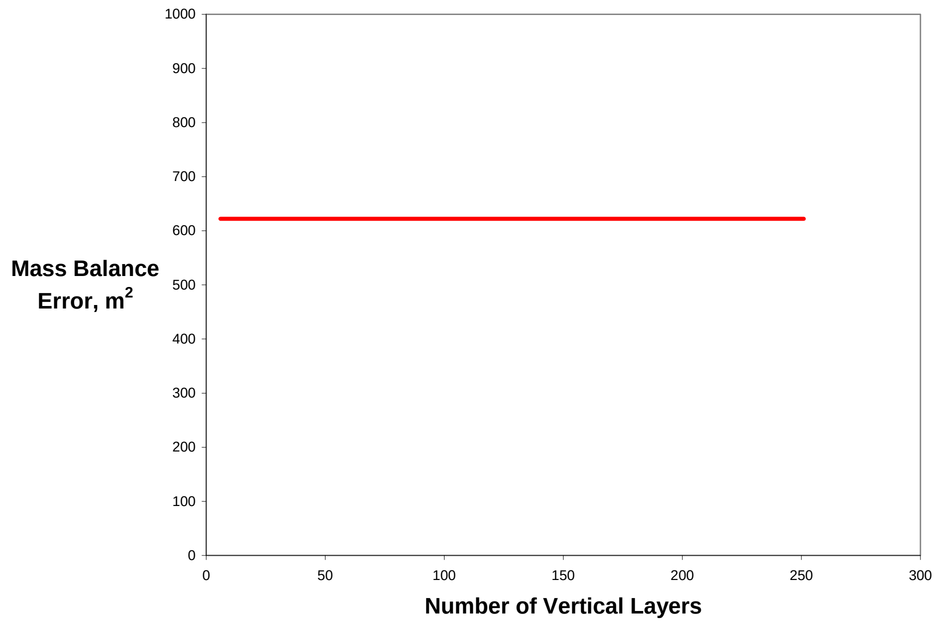

Figure 4.14. Mass balance errors over the four tidal cycles for the improved wetting and drying algorithm. Note that, for this set of run parameters, the original algorithm was unstable for all vertical resolutions.

more interesting model domain might induce vertical mixing, which in turn might depend on vertical resolution. In the next subsection, we will repeat these numerical experiments for just such a domain.

4.2.2. Plateau Domain

As discussed above in Section 4.1.3, the Plateau domain was designed to test the behavior of the improved wetting and drying algorithm. The domain features a flat region to simulate tidal waves on a flood plain, and it also features a steeper slope to simulate thin films of water draining downhill. This subsection contains the results of five numerical experiments: heuristic stability, parameter sensitivity with G and K_{slip}, parameter sensitivity with H_{min} and U_{min}, horizontal resolution, and vertical resolution.

Table 4.2: Summary of heuristic stability results for the two versions of the wetting and drying algorithm. The two versions show significant differences for the Plateau domain. Note that mass balance error is an average error over all four tidal cycles.

	Original Algorithm	Improved Algorithm
Maximum stable time step	10 sec	20 sec
Mass balance error	15881.4 m^2	20148 m^2

4.2.2.1. Heuristic Stability

Table 4.2 summarizes the heuristic stability results for the Plateau domain and the two versions of the wetting and drying algorithm. Unlike the heuristic stability results in Section 4.2.1.1 for the Linear Sloping Beach domain, these results do show a difference between the two versions of the algorithm. The improved algorithm increases the maximum stable time step by 100 percent, while increasing the mass balance error by only about 27 percent. And, as we will show with the rest of the Plateau domain results, when the time step is held steady at 1 second, the improved algorithm behaves better.

4.2.2.2. Parameter Sensitivity - K_{slip} and G

To examine the effects of the roughness parameter K_{slip} and the numerical parameter G, the two-dimensional (x-z) ADCIRC model was run using 36 combinations of the two parameters. Figure 4.15 shows the mass balance errors for the original wetting and drying algorithm, and Figure 4.16 shows a similar graph for the improved algorithm. These sensitivity results are as dramatic as the results for the Linear Sloping Beach

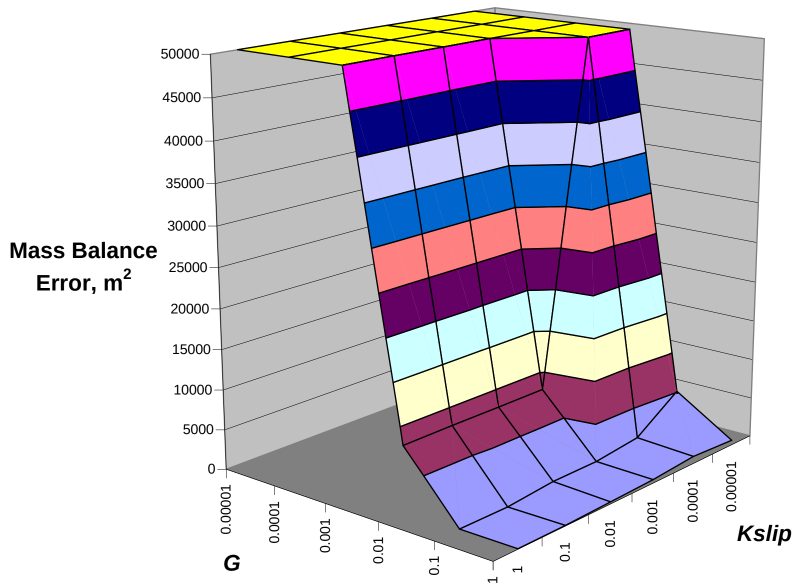

Figure 4.15. Mass balance errors for the original wetting and drying algorithm applied to the Plateau domain, for a range of G-K_{slip} combinations. Note that we have cropped the vertical scale for comparison to Figure 4.16; some combinations where G is small and K_{slip} is large are stable, but they produce undesirably large mass balance errors.

domain in Section 4.2.1.2. The improved algorithm is unstable for roughly the same combinations of G and K_{slip} as the original algorithm. However, the improved algorithm produces significantly smaller mass balance errors, which are more in line with the results from both the one-dimensional and improved two-dimensional (x-z) ADCIRC models applied to the Linear Sloping Beach domain (Figure 3.9 and Figure 4.5, respectively).

These results do not dissuade us of our belief that the optimal combination is $G = 0.01 \text{ sec}^{-1}$ and $K_{slip} = 0.0001$. The mass balance error is larger at that combination than it is when the parameters are increased, but we saw similar behavior for the Linear Sloping Beach domain, where this combination proved to be the most accurate.

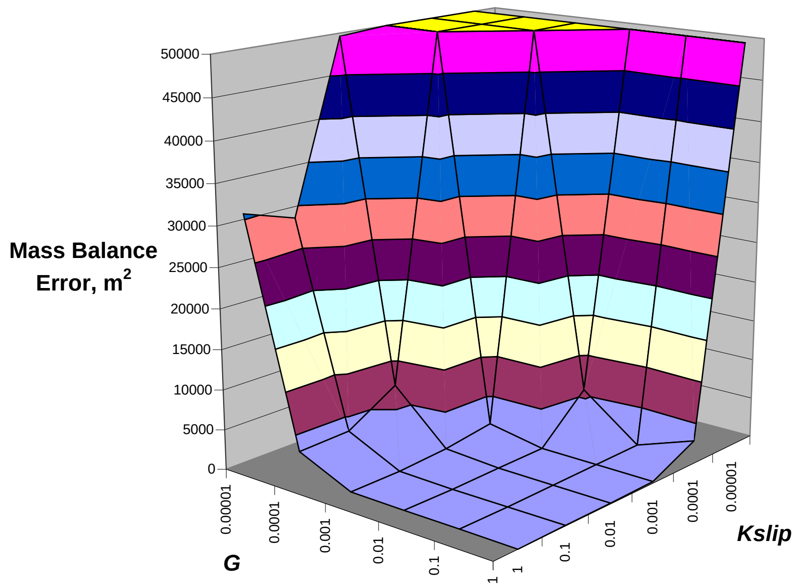

Figure 4.16. Mass balance errors for the improved wetting and drying algorithm applied to the Plateau domain, for a range of G-K_{slip} combinations.

Thus, we will continue to use these values for G and K_{slip}, even though the original wetting and drying algorithm is unstable at that combination.

4.2.2.3. Parameter Sensitivity - H_{min} and U_{min}

The effect of the wetting and drying parameters H_{min} and U_{min} was examined by varying each parameter from 0.00001 to 1.0 (meters for H_{min}; m/sec for U_{min}), creating a matrix of 36 combinations. Figure 4.17 shows the mass balance errors produced by the original wetting and drying algorithm, while Figure 4.18 shows a similar graph for the improved algorithm. Note that we are paying the price for our decision in the previous section to use the combination of G = 0.01 sec^{-1} and K_{slip} = 0.0001; the original

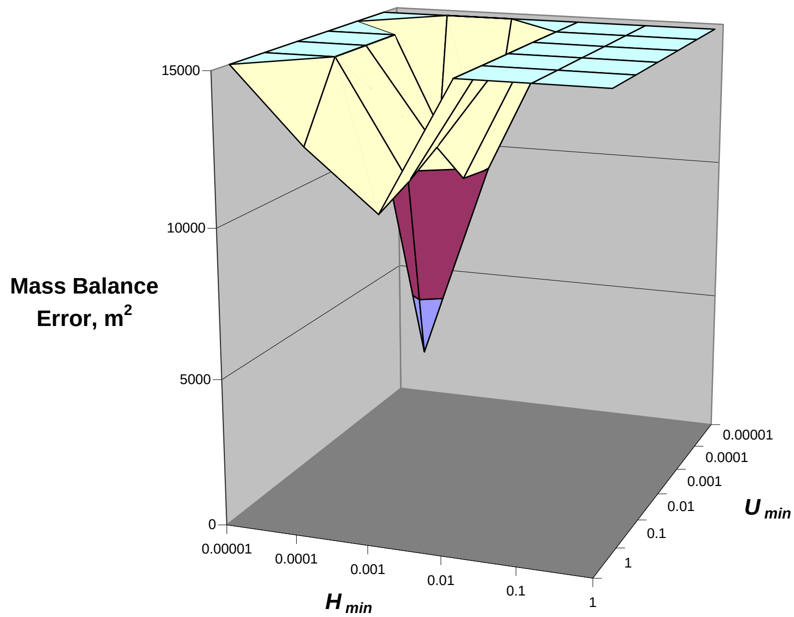

Figure 4.17. Mass balance errors for a range of H_{min}-U_{min} combinations, for the original wetting and drying algorithm. Note that most combinations cause the model to be unstable.

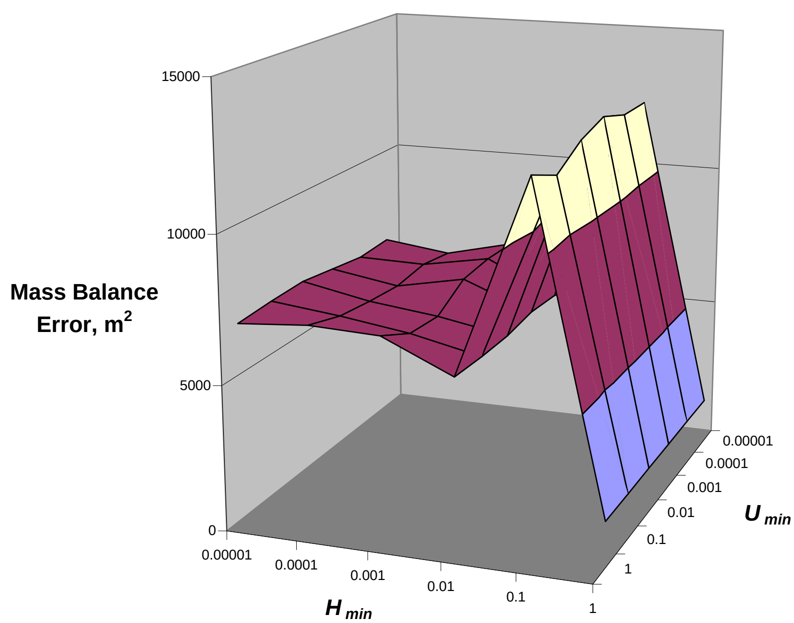

Figure 4.18. Mass balance errors for a range of H_{min}-U_{min} combinations, for the improved wetting and drying algorithm.

algorithm is unstable for most combinations of H_{min} and U_{min}, and it produces large errors when it is stable.

The improved algorithm, on the other hand, is stable and produces reasonable errors for all combinations. Note that its smallest errors occur when H_{min} is largest and thus most restrictive; at $H_{min} = 1.0$ meters, the model is prevented from wetting the flat region of the Plateau domain, and thus the mass balance errors are much better. As with previous results, the errors level off as H_{min} is decreased, meaning that model users can use any value of that parameter that is sufficiently small. And, as with previous results, the U_{min} parameter has negligible effects.

4.2.2.4. Horizontal Resolution

Figure 4.19 shows the mass balance errors for a range of horizontal resolutions. Now, the problems that existed for the horizontal resolution study with the Linear Sloping Beach domain have been exacerbated. The mass balance errors do not converge as the resolution is refined; in fact, many of the largest errors occur when the grid spacings are relatively small. This behavior is a concern, because a good algorithm should behave better as the resolution is refined. We would propose that the Plateau domain is not a good test of horizontal resolution because, at fine resolutions, more nodes are placed at the top of the steep incline, where elements oscillate between being wet and dry and thus the mass balance errors would be worst. It may not be appropriate to expect convergence under these conditions. The Linear Sloping Beach domain does not incorporate this type of bathymetry, and it shows convergence when the improved version of the wetting and drying algorithm is used (as in Figure 4.12). For the Plateau domain, the improved

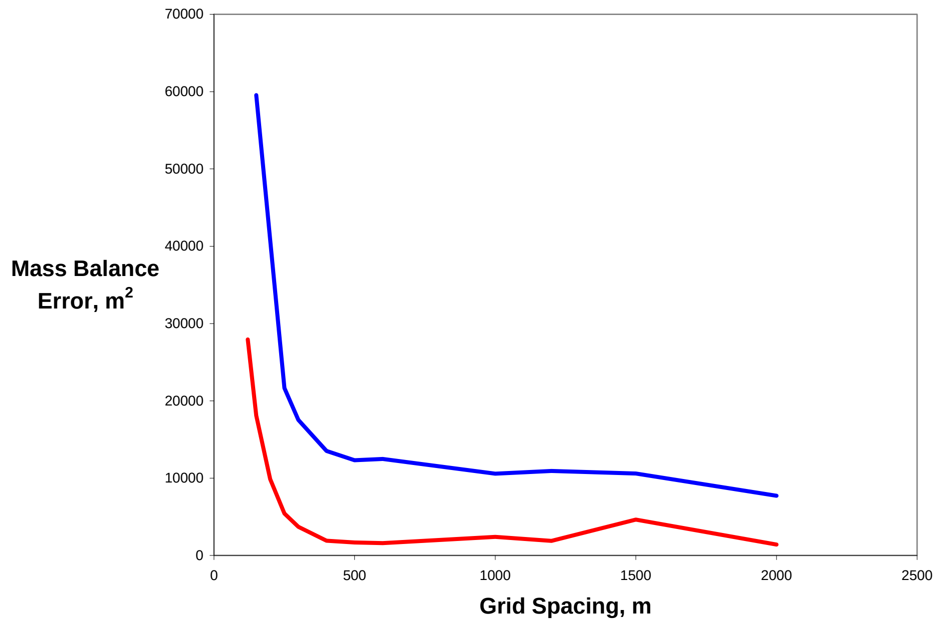

Figure 4.19. Mass balance errors over the four tidal cycles for the original (blue line) and improved (red line) wetting and drying algorithms. The improved algorithm produces mass balance errors that are considerably smaller than those from the original algorithm.

version does effect a significant reduction in the magnitude of the mass balance errors. Thus, the horizontal resolution is useful, in the sense that it confirms that the improved wetting and drying algorithm is better.

4.2.2.5. Vertical Resolution

To study the effect of vertical resolution, the number of vertical layers was varied from six layers to 201 layers for a horizontal resolution of 250 meters. Figure 4.20 shows the mass balance errors over the first four tidal cycles for that range of vertical resolutions. Note that, although the improved algorithm was stable for every vertical resolution in that range, the original algorithm was unstable at both the coarse end (six and 11 layers) and the fine end (201 layers). Also note the difference in magnitude between the mass balance

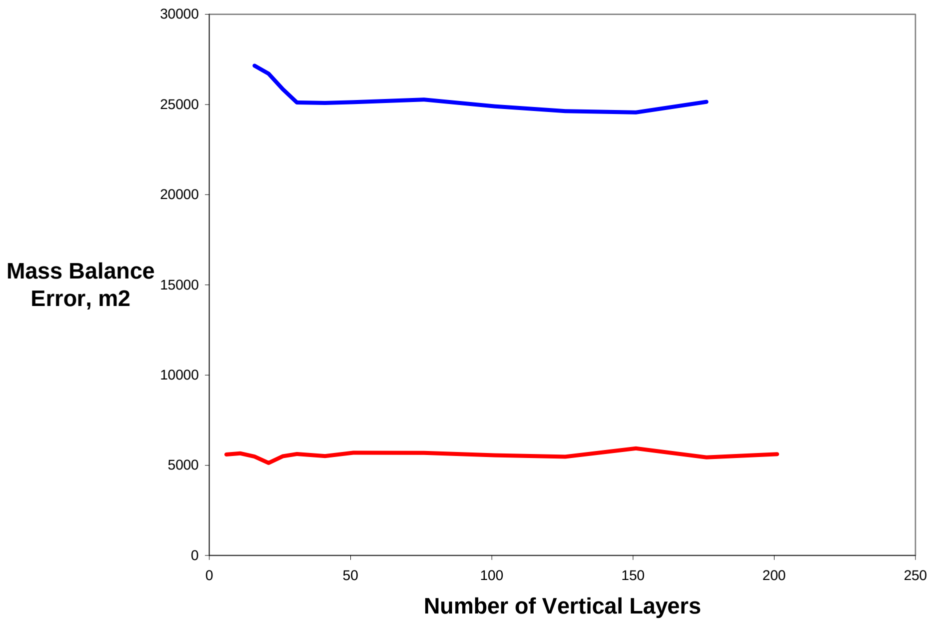

Figure 4.20. Mass balance errors over the first four tidal cycles for a range of vertical resolutions, for the original (blue line) and improved (red line) wetting and drying algorithms. The improved algorithm reduces the mass balance errors by about 80 percent.

errors from the two algorithms. The original algorithm produces errors of about 25,000 m^2, while the improved algorithm produces errors of about 5,000 m^2. That is a decrease of about 80 percent. The improved algorithm continues to behave significantly better.

Like the vertical resolution results in Section 4.2.1.5 from the Linear Sloping Beach, these results show that the mass balance errors are not sensitive to vertical resolution. As the number of layers is increased, the errors do not converge toward zero. The cause is the same; because this simulation is forced with a tide at the open ocean boundary, the flow is unidirectional throughout the water column. There is not enough mixing to require additional resolution in the vertical direction, and thus the two-dimensional (*x*-*z*) ADCIRC model is able to simulate the problem with only a few vertical layers. In the future, a vertical resolution study should be performed on a problem that is guaranteed to have vertical mixing, such as a wind-driven or density-driven problem.

4.3. Conclusions

This study of the two-dimensional (*x*-*z*) ADCIRC model attempted to answer two related questions: (1) were the recent updates to the wetting and drying algorithm beneficial?, and (2) does the two-dimensional (*x*-*z*) wetting and drying algorithm behave similarly to the one-dimensional algorithm?

The recent updates to the algorithm were beneficial. In every study in this chapter, we have shown that the improved algorithm exhibits better stability or mass balance properties, and usually both. This finding is especially true with respect to the Plateau domain, which was designed specifically to test the improved algorithm under the conditions for which it was implemented. In the Plateau domain, the improved algorithm doubled the maximum stable time step, proved stable for a wider range of parameters than did the original algorithm, and produced significantly lesser mass balance errors. The updates to the wetting and drying algorithm are worthwhile.

And, when the improved algorithm is used, the two-dimensional (*x*-*z*) ADCIRC model produces results that are qualitatively similar to the results in Chapter 3 from the one-dimensional model. The Linear Sloping Beach domain shows the best behavior at the combination of K_{slip} = 0.0001 and G = 0.01 sec^{-1}, for both models. The H_{min} parameter produces the best behavior when it is set to a relatively low value, such as $H_{min} \leq 0.01$ meters. The U_{min} parameter does not affect the performance of the models. And both versions of the ADCIRC model are sensitive to horizontal resolution. These results are encouraging, and they suggest that the wetting and drying algorithm can be implemented in three dimensions without significant problems.

In Chapter 5, we will perform that implementation and assess the behavior of the three-dimensional wetting and drying algorithm. Unless stated otherwise, we will use the improved version of the algorithm.

5. Three-Dimensional Wetting and Drying

One of the goals of this thesis is the implementation of the wetting and drying algorithm in the three-dimensional version of ADCIRC. Three-dimensional simulations have become increasingly practical as computer architectures become faster and more efficient. And, in many applications of the model, the vertical profile and mixing in near-shore regions are most important. Thus, a three-dimensional version of ADCIRC with wetting and drying would be beneficial.

In this chapter, we will discuss how the wetting and drying algorithm was implemented in the three-dimensional ADCIRC model, and we will discuss the results of a series of numerical experiments conducted on it. We will show that it is possible to simulate three-dimensional wetting and drying. We will also show that the same optimal set of model parameters applies in three dimensions, as did in lower dimensions in Chapter 3 and Chapter 4.

5.1. Methods

This subsection contains a discussion of how the wetting and drying algorithm was implemented in this form of the ADCIRC model, an introduction of the two major changes to the algorithm since the study of the one-dimensional model in Chapter 3, a description of the two model problems used in this chapter, and a review of the two error measures used in our numerical experiments.

5.1.1. Implementation in 3D ADCIRC

The wetting and drying algorithm for the three-dimensional ADCIRC model occurs in the middle of the time step, between the solution of the GWC equation (for water surface elevations) and the solution of the momentum equation (for velocities or fluxes). The two-dimensional (*x*-*y*, not to be confused with the *x*-*z* study in Chapter 4) and three-dimensional ADCIRC models exist as the same code and share many of the same features, so the wetting and drying algorithm already exists in the two-dimensional (*x*-*y*) version. To make it compatible with the three-dimensional version, we made two major changes.

First, the algorithm was removed from the time step subroutine and made into its own subroutine. This change was made primarily for ease of coding; now, instead of having several hundred lines of wetting and drying code in the middle of the time step subroutine, the code exists as its own unit. If the wetting and drying algorithm is ever modified or re-designed, then it will be easier to simply swap in the new algorithm as its own subroutine. As part of its transition to a separate subroutine, the algorithm was modified to comply with the three-dimensional aspects of the model. Specifically, the computation of the bottom stress at newly wet nodes was changed, so that either the two-dimensional (*x*-*y*) stress or the three-dimensional stress can be computed [16].

Second, the subroutine that solves the three-dimensional momentum equation was modified to allow for wet and dry regions. As noted earlier, dry regions are not technically dry; the water depth at a dry node can be larger than zero, so long as it is less than the user-specified H_{min}. Thus, a thin film of water can exist at dry nodes. This water should not contribute to the momentum computations at a neighboring wet node. If a wet node is connected to a dry node, then the contribution from the dry node is not included in the summation. This issue was addressed in the two-dimensional implementation of the algorithm, and the three-dimensional implementation follows that same logic.

5.1.2. Updates to the Wetting and Drying Algorithm

In the summer of 2004, two changes were made to the wetting and drying algorithm. First, the two parameters *NODEDRYMIN* and *NODEWETMIN* were eliminated. Second, an elemental drying check was added. These changes were discussed in Section 4.1.2, but we will review them here for completeness.

The first change relates to the propagation of waves on relatively flat flood plains. The user specified the two parameters *NODEDRYMIN* and *NODEWETMIN* in the input file, and they were used to control how long a node had to remain either dry or wet. Thus, if *NODEDRYMIN* was set to 20, then any node had to remain dry for at least 20 time steps. These parameters were included originally to control oscillations at the wetting front, but it was discovered that they also slowed the propagation of flood waves. To prevent this, the two parameters were removed from the algorithm.

The second change relates to the flow of water down a steep incline. It was discovered that the simple momentum balance used in the node-based wetting check allowed “barely wet” nodes to remain active in areas with steep topography. Thus, a thin film of water would be allowed to remain wet if it was on an incline where water was flowing from above. Mass balance problems occurred in these regions. To prevent this, a new parameter, H_{OFF}, was hardwired into the code, and it is set to 120 percent of the H_{min} parameter. If any of the nodes on an element has a water depth that is less than H_{OFF}, then the element itself is dried. This change allows water to build up on an incline before it is allowed to flow downhill.

The effects of these changes were examined with the two-dimensional (*x*-*z*) model in Chapter 4, and it was shown that they improve stability and mass balance, often dramatically. We will examine their effects for some limited test cases in this section; the model problems were designed to mirror the two-dimensional model problems on which we tested extensively previous versions. However, unless stated differently, we will use the improved version of the wetting and drying algorithm.

5.1.3. Model Problems

The first model problem is the Linear Sloping Beach domain, shown in Figure 5.1. It is similar to the Linear Sloping Beach domains used in the previous sections, except now we have extended it in the *y*-direction for 12 kilometers. This problem has the following parameters (unless stated otherwise): a linear slope of 0.03 percent, an undisturbed length of 18 kilometers, a bathymetric depth at the open ocean boundary of 6 meters, a grid spacing of 500 meters, a time step of 1 second, a forcing amplitude of 1.0 meter, a tidal period of 12 hours (43,200 sec), a duration of 4 tidal periods, a linear slip coefficient of 0.0001 and a G value of 0.01 sec^{-1}, an H_{min} value of 0.01 meters, and a U_{min} value of 0.01 meters per second. Note the increase in the horizontal resolution; we will show in Section 5.2.1.4 that the three-dimensional ADCIRC model is unstable at a grid

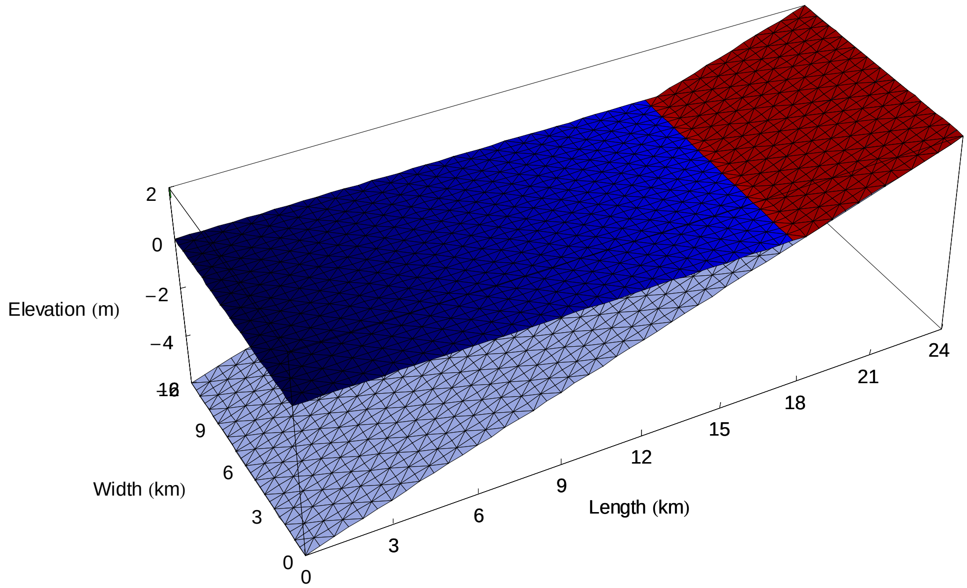

Figure 5.1. Three-dimensional view of the Linear Sloping Beach domain. Note that the bathymetry ranges from a depth of 6 meters at the ocean boundary to 2 meters above sea level at the land boundary.

spacing of 250 meters, which was used in the studies of the one- and two-dimensional models.

The second model problem was designed explicitly to test the updates in the wetting and drying algorithm. It is similar to the Plateau domain from the study of the two-dimensional (*x*-*z*) model, except it has been extended in the *y*-direction for a distance of 12 kilometers. A schematic of this domain is shown in Figure 5.2. There are three major differences from the Plateau domain in Chapter 4. First, the grid spacing has been increased from 250 meters to 500 meters, for stability reasons. Second, the flat region of the domain has been tripled in length, from 6 kilometers to 18 kilometers, to create a more robust study of the wetting and drying of floodplains. Third, the slope at the left and right edges of the domain has been doubled, to create a more robust study of drainage down a

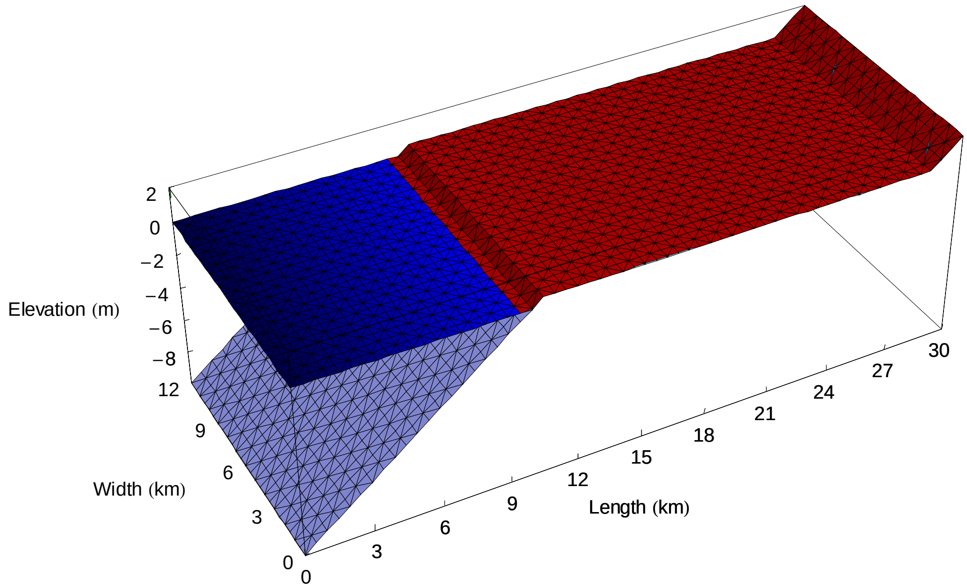

Figure 5.2. Three-dimensional view of the Plateau domain. Note that the flat range has a bathymetry of 0.5 meters above sea level, and it extends from 10.5 kilometers to 28.5 kilometers in the *x*-direction.

steep incline. Taken together, these changes make simulations on the three-dimensional Plateau domain even more difficult than those in the previous chapter, and it should be a challenging test of the three-dimensional wetting and drying algorithm. This problem has the following parameters (unless stated otherwise): an total length of 30 kilometers, an undisturbed water length of 10 kilometers, a bathymetric depth at the open ocean boundary of 10 meters, a grid spacing of 500 meters, a time step of 1 second, a forcing amplitude of 1.0 meter, a tidal period of 12 hours (43,200 sec), a duration of 4 tidal periods, a linear slip coefficient of 0.0001 and a G value of 0.01 sec^{-1}, an H_{min} value of 0.01 meters, and a U_{min} value of 0.01 meters per second.

5.1.4. Error Computations

In this chapter, we use the same error measures as for the previous wetting and drying studies. For the Linear Sloping Beach domain, we can compare our numerical results and the analytical solution described in Section 3.2.1.1. The domain is sliced at $y = 6000$ meters to obtain results that can be compared with the one-dimensional analytical solution. Then we examine the position of the wet/dry interface over the fourth tidal period (because the model is spun up from a cold start for the first three periods). After every 10-minute interval in that fourth period, we calculate the difference between the position of the interface given by the numerical results and the position of the interface given by the analytical solution. These differences are then averaged. If the numerical results successfully approximate the analytical solution, then the average difference should be zero. However, spatial discretization often prevents a perfect match between numerical and analytical, so we are satisfied if the average difference is less than the grid spacing of 250 meters. Also, it is important to remember that the analytical solution does not include bottom friction, so optimal ADCIRC results will occur at relatively low values of that parameter.

The second error measure is an examination of mass balance. Again, we use a procedure similar to that from the one-dimensional wetting and drying study. We utilize a cumulative mass balance error over the entire simulation, and it is calculated using a finite volume approach. However, instead of using a depth-averaged flux and computing the mass balance error at each horizontal element, we now compute mass balance error at all elements. We begin with the three-dimensional continuity equation:

$$\nabla \cdot \vec{v} = 0 , \tag{5.1}$$

where $\vec{v}$ is the three-dimensional velocity. If we integrate this equation over some region Ω (here taken to be an individual element), we get:

$$\int_{\Omega} (\nabla \cdot \vec{v}) d\Omega = 0 . \tag{5.2}$$

We can then apply the divergence theorem on an individual element to get:

$$\int_{\partial\Omega} (\vec{v} \cdot \vec{n}) d(\partial\Omega) A = 0 , \tag{5.3}$$

where $\vec{n}$ is the unit normal vector on each face of the element. When we compute the fluxes on an element, we first compute an average velocity on each face as an arithmetic average of the velocities at the three (or four) nodes that define the face. Then, to get the flux, we take the dot product of that average velocity and the unit normal vector. Thus, the local mass balance error for any element is simply the residual when that element's fluxes are summed. The global mass balance error is a sum of those residuals. To allow for a comparison with previous studies, we divided the global mass balance error by the width of the domain to obtain an error per unit width.

As we will show, this new method of computing mass balance errors prevents them from being truly comparable to the errors reported in the one-dimensional and two-dimensional (*x*-*z*) studies. When the three-dimensional ADCIRC model solves for vertical velocities, it uses the same equation that we are using to solve for fluxes for mass balance.

In effect, the vertical velocities are computed in a way that minimizes mass balance error. Because of the continuous finite element approximation, the vertical velocity solver couples the entire water column, so, while the "global" mass balance errors are minimized for the column, the local mass balance error at any element in the column may be non-zero. We will show that this method of computing mass balance produces much smaller errors, because it is more closely tied to the way the model solves for vertical velocities.

Recently, several papers [1, 8] have advocated computing mass balance from finite element residuals in order to be consistent with the numerical discretization. However, we have shown (Kolar et al. [13]) the finite volume approach to be a good surrogate variable for accuracy and phasing errors; that is, small mass balance errors (as computed with finite volume) correlate with small constituent errors. Additionally, in Chapter 2, we showed that the finite volume method is a good indicator of truncation errors, especially for domains that have a constant node spacing. Hence our reason for using the finite volume approach herein.

5.2. Numerical Experiments

This subsection contains the results of numerical experiments conducted using the Linear Sloping Beach domain and the Plateau domain.

5.2.1. Linear Sloping Beach Domain

This subsection contains the results of five numerical experiments: heuristic stability, parameter sensitivity with G and K_{slip}, parameter sensitivity with H_{min} and U_{min}, horizontal resolution, and vertical resolution.

Table 5.1: Summary of heuristic stability results for the two versions of the wetting and drying algorithm. The two versions do not show significant differences for the Linear Sloping Beach domain. Note that mass balance error is an average error over all four tidal cycles, while the difference between the shoreline from the numerical results and the shoreline from the analytical solution is an average over only the fourth tidal cycle.

	Original Algorithm	Improved Algorithm
Maximum stable time step	45 sec	45 sec
Mass balance error	6.073 m^2	6.099 m^2
Average difference from analytical solution	267.247 m	287.138 m

5.2.1.1. Heuristic Stability

Although most of our three-dimensional studies will use only the improved version of the wetting and drying algorithm, we did examine the effect of both versions on heuristic stability. To examine this stability, we increased the time step (in increments of 5 seconds) until the model became unstable. The results for the two versions of the wetting and drying algorithm are shown in Table 5.1. Note that there is not a significant difference between the two versions of the algorithm. Both show maximum stable time steps of 45 seconds, which is higher than the time steps from the two-dimensional study, presumably because the grid spacing is larger for the three-dimensional simulations. Because of this increased time step and increased grid size, the two versions show greater accuracy errors than was seen in Chapter 4. (Note that, for both versions, the average difference of the shoreline from the analytical solution is well below the grid spacing of 500 meters.)

However, note the magnitude of the mass balance errors, which have been divided by the width of the domain to allow for comparison with the results from the studies on the one- and two-dimensional (x-z) versions of the algorithm. As noted in Section 5.1.4, mass balance error is computed in three dimensions as a simple flux balance on each element; the local and global accumulations are not computed.

The two versions of the wetting and drying algorithm do not show significant differences, because the Linear Sloping Beach domain was not designed to test the updates in the improved version. Thus, because these initial results do not contradict the results from the study of the two-dimensional (x-z) model in Chapter 4, we will use only the improved version of the wetting and drying algorithm for the rest of the studies that use the Linear Sloping Beach domain.

5.2.1.2. Parameter Sensitivity - K_{slip} and G

As discussed in Section 3.2.1.3, two important parameters in the ADCIRC model are the bottom friction and the numerical parameter G (sometimes called τ_0). In three dimensions, bottom friction is implemented as a term in the vertical stress calculation:

$$\frac{\tau_{bx,j}}{\rho_0} = K_{slip,j} u_j , \tag{5.4}$$

and:

$$\frac{\tau_{by,j}}{\rho_0} = K_{slip,j} v_j , \tag{5.5}$$

where τ_{bx} and τ_{by} are the bottom stresses in the x- and y-directions, respectively; ρ_0 is the reference density of the fluid; u and v are the velocities in the x- and y-directions; j is the node index; and K_{slip} is the bottom boundary condition. For a "no slip" bottom boundary condition:

$$K_{slip,\,j} \rightarrow \infty\,. \tag{5.6}$$

For a "linear slip" bottom boundary condition:

$$K_{slip,\,j} = \text{constant}\,. \tag{5.7}$$

And, for a "quadratic slip" bottom boundary condition:

$$K_{slip,\,j} = C_d\sqrt{u_j^2 + v_j^2}\,, \tag{5.8}$$

where C_d is a quadratic drag coefficient. The results shown in this section utilize a linear slip bottom boundary condition, where K_{slip} is a user-specified constant. We varied both K_{slip} and G from 10^{-5} to 10^{0} (sec^{-1} for G, unitless for K_{slip}), creating a test matrix of 36 combinations of K_{slip} and G. Then we examined the effect of each combination on the model's accuracy and mass balance properties.

Figure 5.3 shows the average distance between the shoreline as computed by ADCIRC and the shoreline from the analytical solution, over the fourth tidal cycle and for 36 combinations of K_{slip} and G. Note that this figure is similar to Figure 3.7, for the one-dimensional ADCIRC model, and Figure 4.2 and Figure 4.3, for the two-dimensional (x-z) ADCIRC model. The model is unstable for a similar set of combinations, when K_{slip} and G are both small. At high values of G, the model is much more sensitive to K_{slip}; a slice at $G = 0.01\ \mathrm{sec}^{-1}$ is similar to a slice at $G = 1.0\ \mathrm{sec}^{-1}$. Most importantly, the same set of combinations produces the best match between the numerical results and the analytical solution. The region around the combination of $K_{slip} = 10^{-4}$ and $G = 10^{-2}\ \mathrm{sec}^{-1}$ shows errors that are within the grid spacing of 500 meters. In fact, the minimum error occurs at that combination and is about 242 meters, or less than half the grid spacing. The behavior

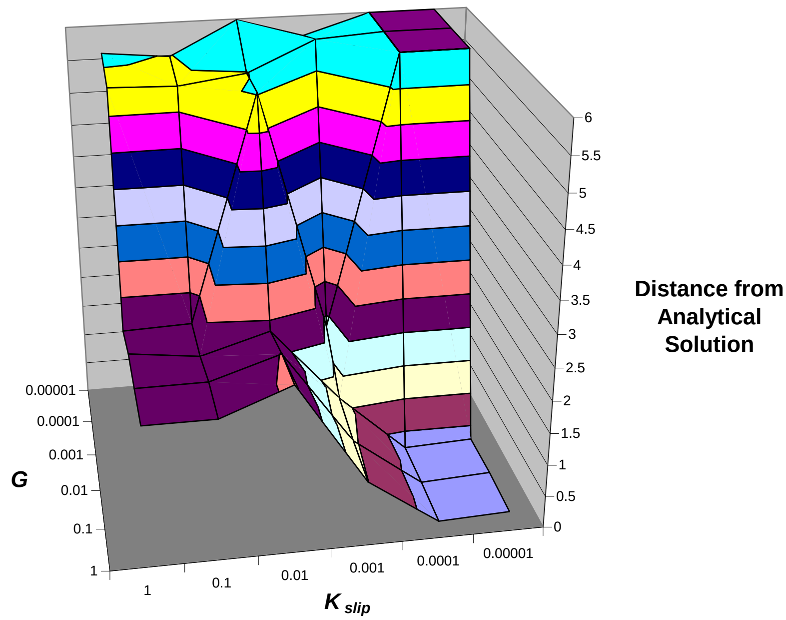

Figure 5.3. The average difference between the numerical results and the analytical solution over the fourth tidal cycle, as discussed in Section 5.1.4, for 36 combinations of K_{slip} and G. The errors are shown in intervals of 500 meters, which is the grid spacing.

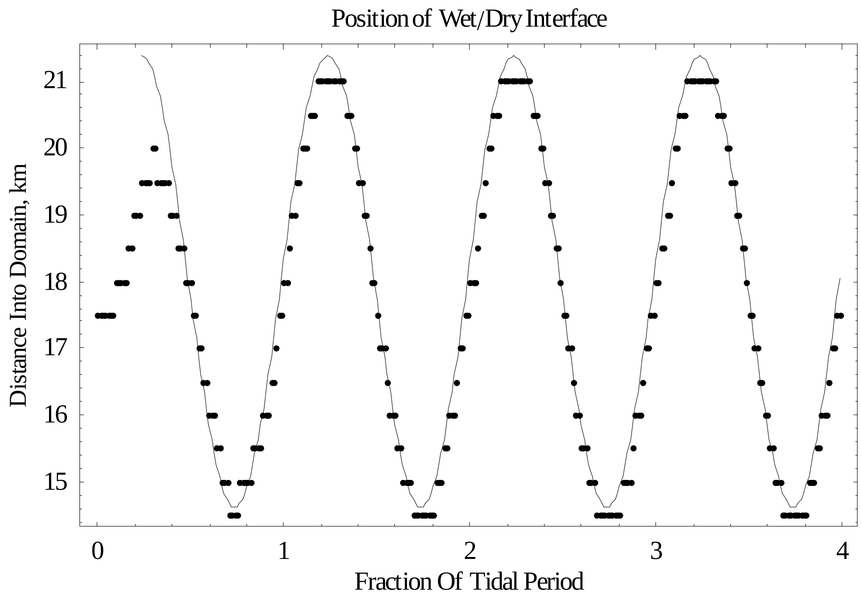

Figure 5.4. The position of the shoreline along a slice at y = 6000 meters, as given by the numerical results (black dots) and the analytical solution (solid line) for the first four tidal periods.

of the shoreline for that combination of K_{slip} and G is shown in Figure 5.4, where the numerical results match closely with the analytical solution, especially after the simulation is ramped for one tidal cycle. Thus, the wetting and drying algorithm captures accurately the physics of the problem as implemented in the three-dimensional ADCIRC model.

Figure 5.5 shows the mass balance errors per unit width of the domain for 36 combinations of K_{slip} and G. This figure is similar to Figure 3.9 from the study of the one-dimensional wetting and drying algorithm and Figure 4.4 and Figure 4.5 for the two-dimensional (x-z) wetting and drying algorithm. The minimum mass balance errors occur when both parameters are relatively large, presumably because less wetting and drying occurs at those values. Note how much smaller these mass balance errors are, compared to the errors in Figure 3.9. The “optimal” combination of $K_{slip} = 10^{-4}$ and $G = 10^{-2}$ sec^{-1} shows a mass balance error of about 0.067 square meters per unit width of the

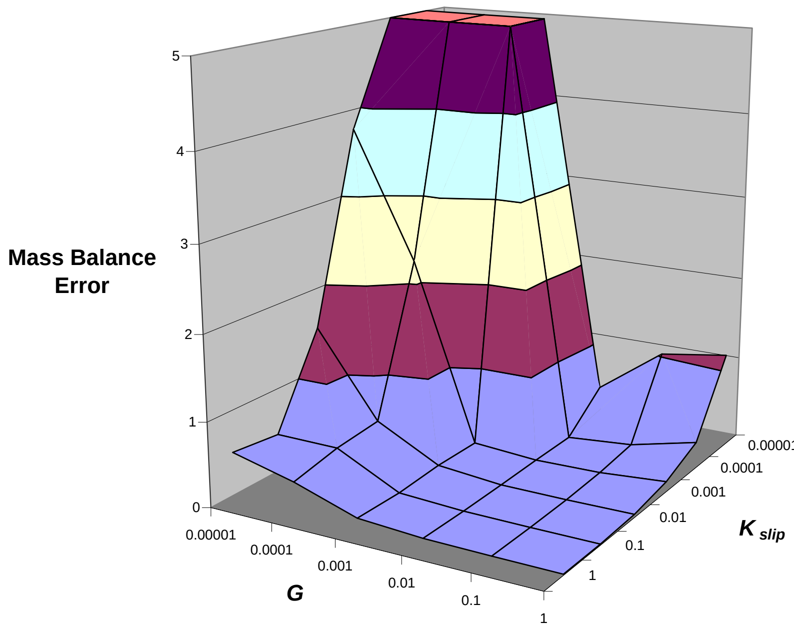

Figure 5.5. Mass balance errors for 36 combinations of K_{slip} and G. The errors are shown in intervals of 1 square meter per unit width of the domain; see Section 5.1.4 for details. The errors in the region at the front of the graph are on the order of 0.01 to 0.03 square meters.

domain, or about 10^{-4} percent of the undisturbed water area. This value is about six orders of magnitude smaller than the corresponding mass balance error from the study of the one-dimensional algorithm. As we discussed in Section 5.1.4, the different method by which we compute finite volume mass balance errors in three dimensions produces much smaller mass balance errors for the same problem.

5.2.1.3. Parameter Sensitivity - H_{min} and U_{min}

Figure 5.6 shows the average distance between the shoreline computed by ADCIRC and the shoreline predicted by the analytical solution, along a slice of the domain at y = 6000 meters. This figure is very similar to Figure 3.10 from the one-

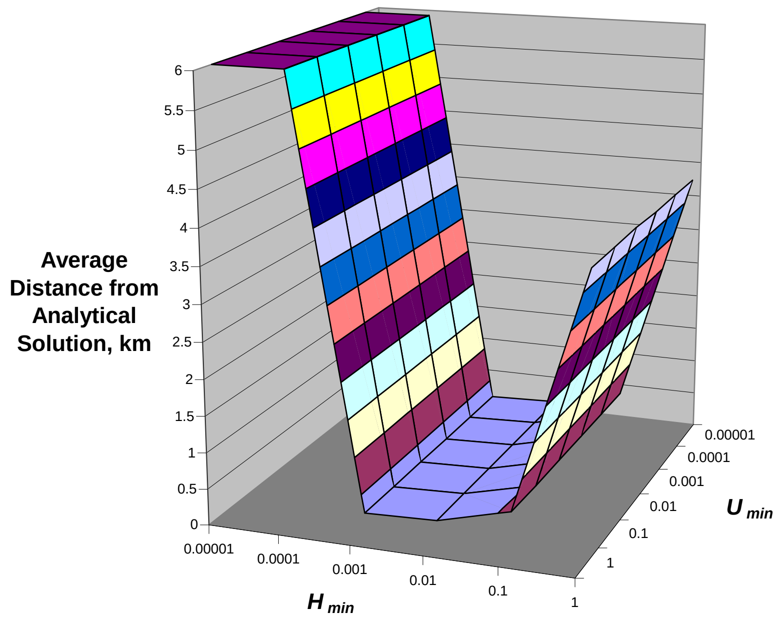

Figure 5.6. The average difference between the numerical results and the analytical solution in their calculation of the position of the shoreline over the fourth tidal cycle, along a slice at y = 6000 meters. The error is shown in intervals of 500 meters, which is the grid spacing. Note that the model is unstable when $H_{min} < 10^{-3}$ meters.

dimensional study and Figure 4.6 and Figure 4.7 from the two-dimensional (x-z) study. At relatively large values of H_{min}, the tide is not allowed to wet as far up on the beach, so the shoreline does not inundate as far as the analytical solution predicts. However, when the value of H_{min} is appropriately small, then ADCIRC is able to predict the position of the shoreline within one grid spacing. Note that, unlike the one-dimensional and two-dimensional (x-z) versions of ADCIRC, the three-dimensional version is unstable at very small values of H_{min}.

Figure 5.7 shows the mass balance errors per unit width of the domain, for 28 combinations of H_{min} and U_{min}. Note that the model is unstable for values of H_{min} smaller than 10^{-3} meters. Unlike the one-dimensional sensitivity study in Section 3.2.1.4, this

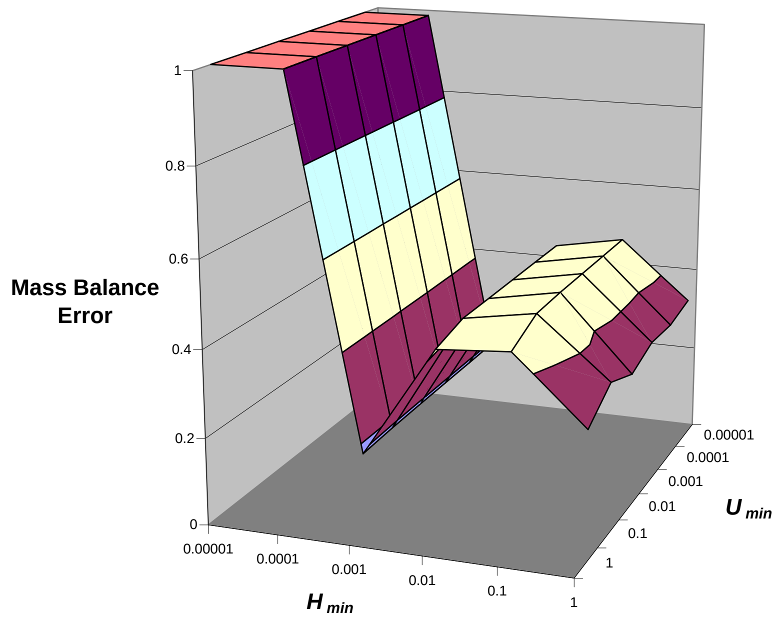

Figure 5.7. The mass balance errors for a range of H_{min} and U_{min} values. (See Section 5.1.4.) The errors are shown in intervals of 0.2 square meters. Note that the model is unstable for $H_{min} < 10^{-3}$ meters.

study shows a clear local minimum in mass balance errors at H_{min} = 0.001 meters. Thus, to obtain the optimal combination of accuracy and mass balance, H_{min} should be set to 0.001 meters.

Note that, for both the accuracy and mass balance studies, the parameter U_{min} does not affect the behavior of ADCIRC. This result is consistent with the one-dimensional study in Chapter 3 and the two-dimensional (*x*-*z*) study in Chapter 4. We have seen no evidence in any sensitivity studies that the value of U_{min} matters.

5.2.1.4. Horizontal Resolution

As we did for the one-dimensional model in Section 3.2.1.5 and the two-dimensional (*x*-*z*) model in Section 4.2.1.4, we examine here the effects of horizontal resolution on the Linear Sloping Beach domain. Note that the grid spacing was refined in

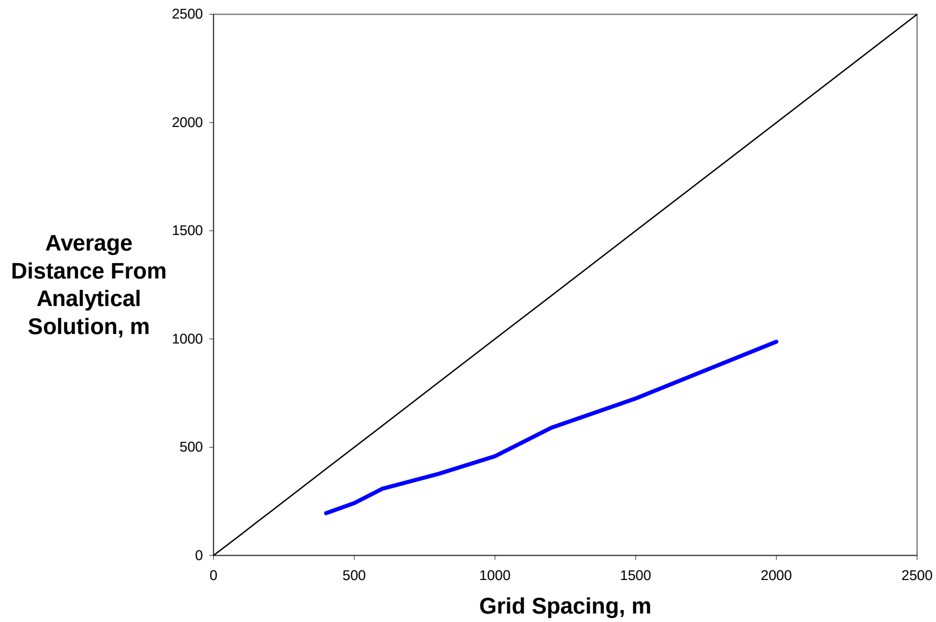

Figure 5.8. The average distance over the fourth tidal cycle between the simulated shoreline and the analytical shoreline, for a range of horizontal resolutions. In all cases, the three-dimensional ADCIRC model is able to simulate the shoreline within half a grid spacing.

both the *x*- and *y*-directions at the same time; thus, a grid spacing of 1000 meters would create triangular elements that have two 1000-meter long faces that meet at a right angle. The maximum grid spacing was 2000 meters (which creates a grid with 13 nodes in the *x*-direction and 7 nodes in the *y*-direction); and the minimum grid spacing was 400 meters (which corresponds to a 61-by-31 node grid). Note that the model was unstable (at a time step of 1 second) for grid spacings less than 400 meters.

Figure 5.8 shows the average distance between the simulated shoreline and the analytical shoreline during the fourth tidal cycle, for this range of horizontal resolutions. The thin black line is included as a reference; it shows that the model was always able to simulate the shoreline within one grid spacing. In fact, for every resolution, the average distance between the simulated shoreline and the analytical shoreline was about half a grid

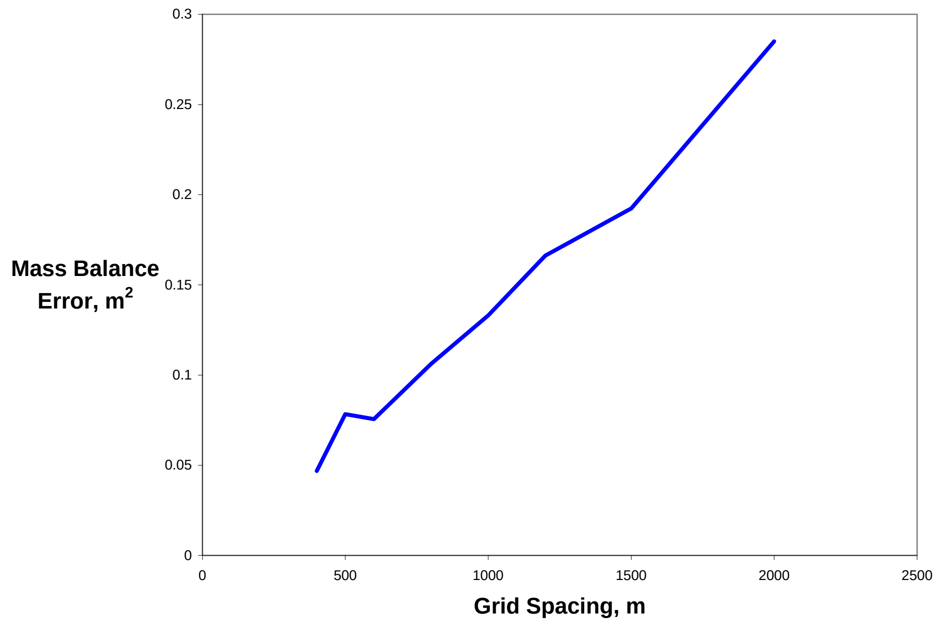

Figure 5.9. Mass balance errors over the first four tidal cycles for a range of horizontal resolutions, for the Linear Sloping Beach domain. Note that the model was unstable (at $\Delta t = 1$ second) for grid spacings less than 400 meters.

spacing. This result indicates that, although accuracy is lost when the grid spacing is increased, the model continues to be as accurate as can be expected. And, as the grid spacing is decreased, the error converges toward zero at a rate of 0.49.

Figure 5.9 shows the mass balance errors over all four tidal cycles, for the range of horizontal resolutions. Again, note how the errors converge toward zero as the horizontal resolution is refined; the convergence rate is 1.03. Although this behavior was observed using the one-dimensional model (Figure 3.12), it is a contrast to the relatively flat behavior exhibited by the two-dimensional (x-z) model (Figure 4.11). We believe this behavior is due to the better method of computing mass balance in three dimensions; here, we are conducting a flux check on each element in the vertical direction, and thus the mass balance errors are more representative of system behavior.

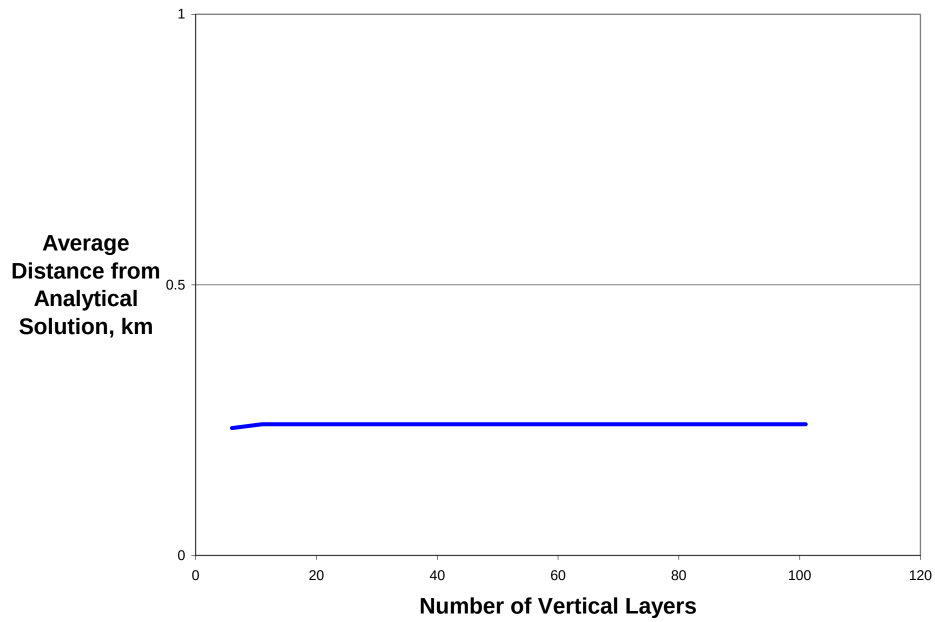

Figure 5.10. The average distance between the simulated shoreline and the analytical solution for a range of vertical resolutions, for the Linear Sloping Beach. Note that most resolutions show an error of about 242 meters, which is less than half the grid spacing of 500 meters.

5.2.1.5. Vertical Resolution

Again, as in the study of the two-dimensional (x-z) ADCIRC model in Section 4.2.1.5 and Section 4.2.2.5, we examined the effects of increased vertical resolution on the three-dimensional model. The number of vertical layers was increased from 6 layers to 101 layers until the model became unstable, at a time step of 1 second. Figure 5.10 shows the average distance over the fourth tidal cycle between the simulated shoreline and the analytical solution, for a range of vertical resolutions. Most vertical resolutions show the same accuracy error of about 242 meters, which is less than half the grid spacing of 500 meters. And, like the results from the two-dimensional (x-z) model in Section 4.2.1.5, the accuracy errors are insensitive to the vertical resolution.

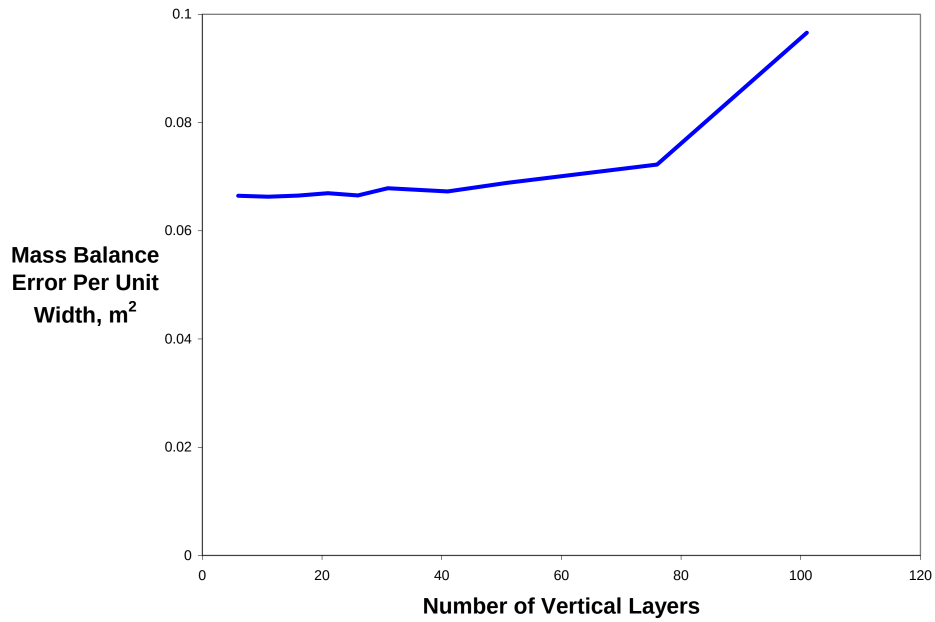

Figure 5.11. Mass balance errors per unit width for a range of vertical resolutions, for the Linear Sloping Beach domain. Note that increased resolution does not improve the mass balance properties.

Figure 5.11 shows the mass balance errors per unit width for the same range of vertical resolutions. Again, note the relative insensitivity of the errors to vertical resolution; except for the highest possible resolution of 101 vertical layers, the mass balance errors range from 0.06 m^2 to 0.075 m^2 and do not converge as the vertical resolution is refined. As we noted in the previous chapter, although the Linear Sloping Beach domain is a good test case for wetting and drying, it does not produce much variation in the vertical direction, and vertical mixing is nearly nonexistent. Thus, it is unreasonable to expect the model to perform better with increased vertical resolution, because it is can simulate the existing behavior with only a few vertical layers. In that sense, the results in this section make sense and may be optimal. Users of the three-dimensional ADCIRC model should understand the physics of their problem and select a vertical resolution that is appropriate.

5.2.2. Plateau Domain

As discussed above in Section 5.1.3, the Plateau domain was designed to test the behavior of the improved wetting and drying algorithm. The domain features a flat region to simulate wave run-up on a flood plain, and it also features a steeper slope to simulate thin films of water draining downhill. This subsection contains the results of five numerical experiments: heuristic stability, parameter sensitivity with G and K_{slip}, parameter sensitivity with H_{min} and U_{min}, horizontal resolution, and vertical resolution.

5.2.2.1. Heuristic Stability

For the Plateau domain, we determined the maximum stable time step by gradually increasing the time step in increments of 5 seconds until the model became unstable. We performed this test for both the original and improved versions of the wetting and drying algorithm, in order to examine their behavior in a three-dimensional setting. The results of these tests are summarized in Table 5.2. In contrast to the Linear Sloping Beach domain, the Plateau domain does produce different (and better) results when the improved wetting and drying algorithm is used. The time step is increased from 35 seconds to 45 seconds (or by 28 percent), and the mass balance error is roughly the same. Note the increase in the magnitude of the mass balance error; it is about 20 times larger than the mass balance errors from the Linear Sloping Beach shown in Table 5.1. This increase is

Table 5.2: Summary of heuristic stability results for the two versions of the wetting and drying algorithm. Note that mass balance error is an average error over all four tidal cycles.

	Original Algorithm	Improved Algorithm
Maximum stable time step	35 sec	45 sec
Mass balance error, with a maximum stable time step	102.519 m^2	108.794 m^2

an indicator of the Plateau domain's inherent difficulties, the effects of which will be seen in the following numerical experiments.

5.2.2.2. Parameter Sensitivity - K_{slip} and G

Here, we examine the effects of the numerical parameter G and the roughness parameter K_{slip} in a model problem. This time, it is the Plateau domain. Figure 5.12 shows the mass balance errors per unit width of the domain, for a range of 36 combinations of these parameters. The added difficulties of the Plateau domain are evident when you compare these errors with the errors from the Linear Sloping Beach domain shown in Figure 5.5. Note that the model is unstable in this domain when either $K_{slip} = 0.00001$ or when $G \leq 0.0001$. Also note that, except for the region in the front of Figure 5.12 where both parameters are large, the mass balance errors are noticeably worse in the Plateau domain. We believe this behavior is due to the flood surge in the flat region and the thin film of draining water at the edge of the plateau, both of which are problem areas that were included explicitly in the design of this domain. These parameter sensitivity results indicate that ADCIRC can obtain acceptable mass balance properties

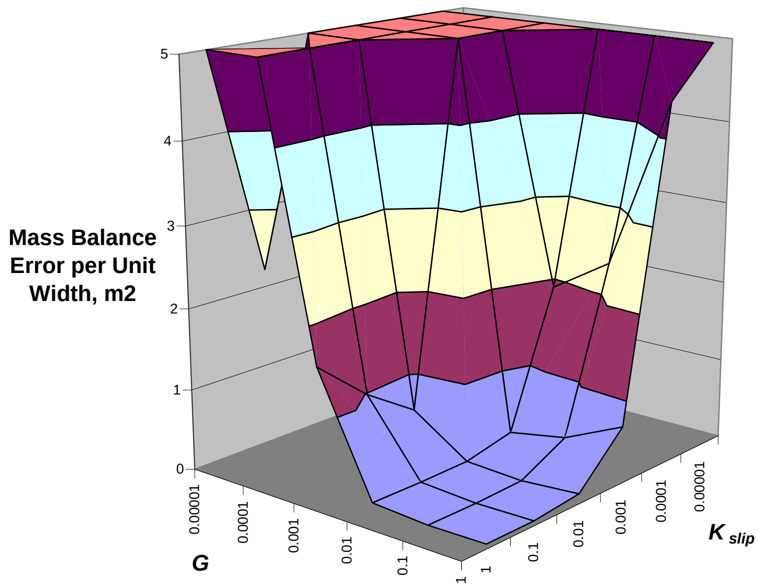

Figure 5.12. Mass balance errors per unit width of the Plateau domain, for a range of G-K_{slip} combinations. The model is unstable in this domain for combinations when $K_{slip} = 0.00001$ and/or when $G \leq 0.0001$.

even in adverse conditions, provided users select an appropriate combination of run-time parameters.

5.2.2.3. Parameter Sensitivity - H_{min} and U_{min}

The drying parameter H_{min} and the wetting parameter U_{min} were each varied from 0.00001 to 1.0 (meters for H_{min}; m/sec for U_{min}). Figure 5.13 shows the mass balance errors per unit width of the domain, for the range of H_{min}-U_{min} combinations. Note that the model is unstable in the Plateau domain when $H_{min} < 0.001$ meters. Also note that, for the first time in this thesis, we have some significant differences in the error measure when U_{min} is varied. Specifically, along the slice in the figure when $H_{min} = 0.1$ meters, the mass balance errors range from 4.3 m^2 to 5.1 m^2, and then the model becomes unstable

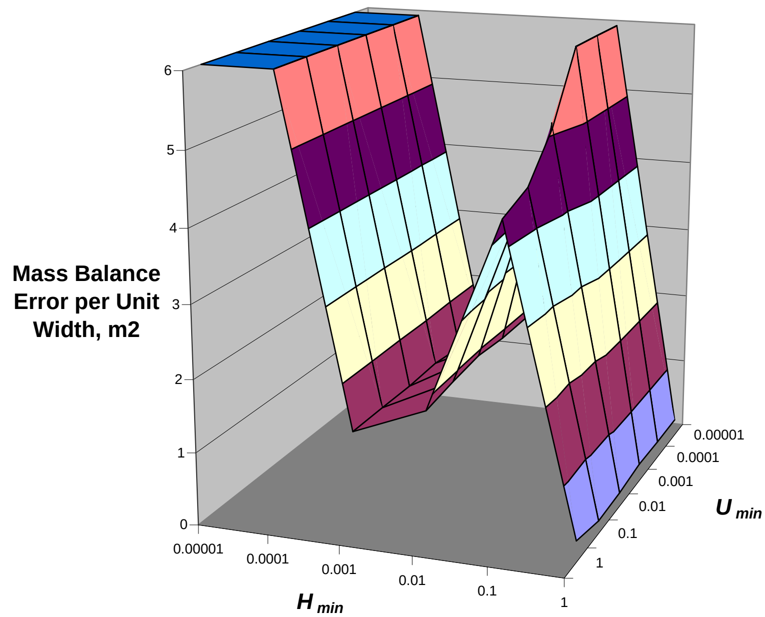

Figure 5.13. Mass balance errors per unit width of the Plateau domain, for a range of H_{min}-U_{min} combinations. Note that the model is unstable in the Plateau domain when $H_{min} < 0.001$ meters.

for combinations when $U_{min} < 0.01$ m/sec. The qualitative behavior of these results is similar to the behavior of the mass balance errors for the Linear Sloping Beach domain shown in Figure 5.7; the optimal mass balance errors occur at the extremes of the stable region, and they are larger in the center. However, for the Plateau domain, some of the mid-range values for H_{min} also cause the model to be unstable, depending on the value of U_{min}.

5.2.2.4. Horizontal Resolution

To examine the effects of horizontal resolution on the three-dimensional wetting and drying algorithm, the grid spacing was varied from 100 meters to 2000 meters, and the mass balance errors per unit width of the domain were again examined. Figure 5.14

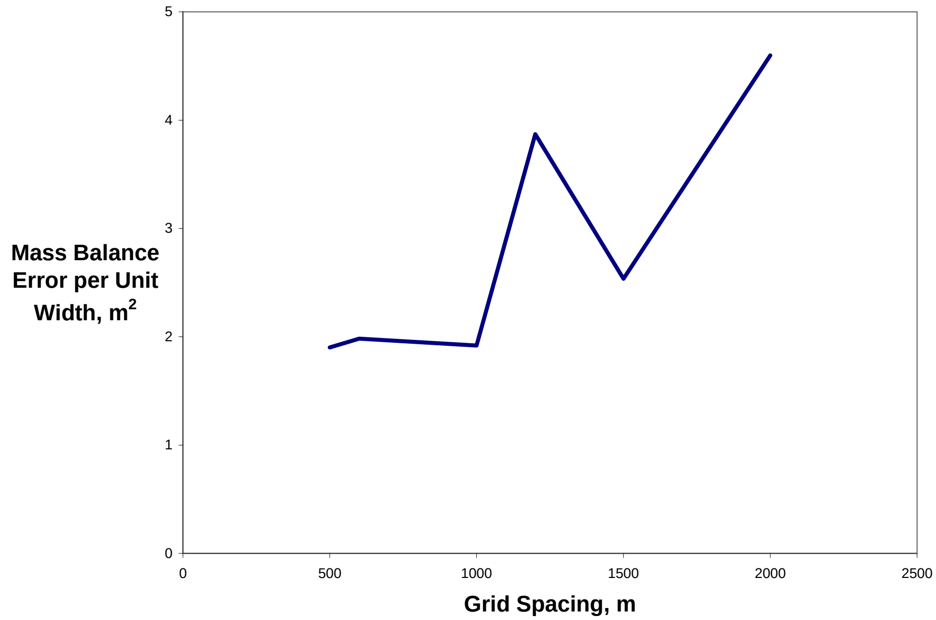

Figure 5.14. Mass balance errors per unit width of the Plateau domain, for a range of horizontal resolutions. Note that the model was unstable in this domain for grid spacings smaller than 500 meters.

shows the results of this study. Note that the model was unstable in this domain for grid spacings less than 500 meters, at a time step of 1 second. The qualitative behavior of the errors is good, because the errors converge as the grid spacing is refined. Note that, when the grid spacing is divided by four (from 2000 meters to 500 meters), the corresponding errors decrease by a factor of 2.4, which indicates sublinear convergence. Also, at the larger grid spacings, the mass balance errors oscillate. Each data point represents a slightly different domain; for example, it is possible to begin the flat region of the domain at $x = 10.5$ kilometers if the grid spacing is 1500 meters, but the flat region must begin at $x = 12$ kilometers if the grid spacing is 2000 meters. Similar differences are observed in the ability of each domain to pinpoint the location of the wetting front. These differences in the domains cause the simulations themselves to be different, but this is a phenomenon that is mirrored with more realistic domains; as more node points are added, the

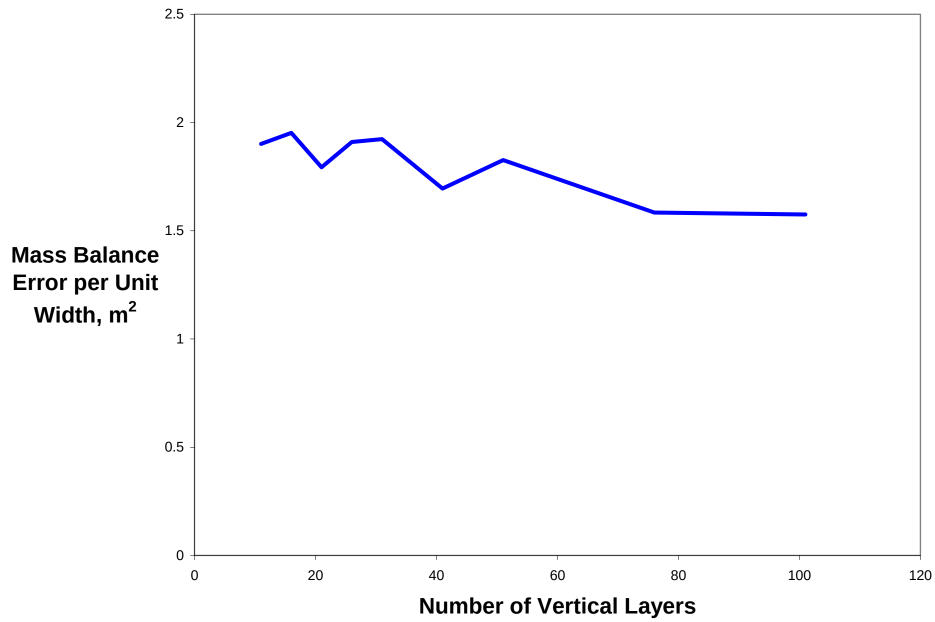

Figure 5.15. Mass balance errors per unit width of the domain for a range of vertical resolutions.

underlying bathymetry is represented better. Thus, the oscillations and sublinear convergence are most likely a consequence of the subtle differences between the domains. Overall, we believe the observed behavior is physically realistic.

5.2.2.5. Vertical Resolution

The effect of vertical resolution was examined by varying the number of vertical layers from six to 201. Figure 5.15 shows the mass balance errors per unit width of the domain for a range of vertical resolutions. Note that the model was unstable at vertical resolutions with six layers and with 126 or more vertical layers. However, the results shown in the figure indicate that simulations on the three-dimensional Plateau domain produce errors that are insensitive to vertical resolution. This finding is similar to previous studies in three dimensions (Section 5.2.1.5) and in two dimensions (Section 4.2.1.5 and Section 4.2.2.5). Like those earlier domains, the three-dimensional Plateau domain does not experience enough vertical mixing for it to be sensitive to vertical resolution. Future studies should include a wetting and drying problem where vertical mixing is guaranteed.

5.3. Conclusions and Future Work

The wetting and drying algorithm has been successfully implemented in the three-dimensional ADCIRC model. Furthermore, the algorithm produces results that are qualitatively similar to the results in Chapter 3 from the one-dimensional model and Chapter 4 from the two-dimensional (*x*-*z*) model. The Linear Sloping Beach domain continues to behave best at the combination of K_{slip} = 0.0001 and G = 0.01 sec^{-1}. The H_{min} parameter produces the best behavior when it is set to a relatively low value, such as 0.01 meters or 0.001 meters; however, for the first time, the model is unstable if H_{min} is set too low. The U_{min} parameter does not affect the performance of any of the models. And all versions of the ADCIRC model are sensitive to horizontal resolution. These results are encouraging, and they suggest that a set of optimal parameters for the wetting and drying algorithm can be recommended. We will do that as part of the formal conclusions in Chapter 6.

6. Conclusions

In this thesis, we have accomplished six objectives: (1) refuted an attack on the usefulness of the finite volume method for computing mass balance errors, (2) laid the groundwork for a future study that will automate the placement of grid points based on a minimization of local mass balance error, (3) implemented and assessed the wetting and drying algorithm in one-, two-, and three-dimensional versions of the ADCIRC model, (4) identified a set of optimal parameters for wetting and drying simulations, (5) proved that recent updates to the wetting and drying algorithm were beneficial, and (6) shown that smaller mass balance errors are obtained when they are computed for each vertical element in the water column.

First, in Chapter 2, we successfully refuted an attack on the usefulness of the finite volume method for computing mass balance errors. The finite volume method has been used traditionally to compute mass balance errors. However, recent papers have suggested that the finite element method produces fluxes that are more consistent with the model's formulation, and thus better for use in the computation of mass balance [1, 8]. We have shown that the finite element method produces mass balance errors that are trivial, even for model domains that have exhibited poor mass balance properties in the past. Furthermore, we have shown that the finite volume method produces mass balance errors that correlate well with truncation errors, especially for grids with constant node spacing. Thus, these finite volume mass balance errors can be useful as an assessment tool, because they indicate where the truncation errors are significant. Because of this result, we used finite volume mass balance errors as an assessment tool in the rest of this thesis.

Second, also in Chapter 2, we laid the groundwork for a future study that will automate the placement of grid points based on a minimization of local mass balance error. In Section 2.7, we started with a grid that has constant node spacing and used it to develop a grid that minimized both mass balance errors and truncation errors. Our process was “crude,” in that we moved nodes by hand from areas with small local mass balance errors to areas with large local mass balance errors. However, we have shown that even this simple process can produce a grid that compares favorably to more sophisticated grids. A future study will take this study one step farther and attempt to automate the placement of grid points based on local mass balance error. This automated method will be less costly than current grid generation methods that attempt to place nodes based on local truncation errors, and it will produce grids that show good mass balance properties and good truncation errors.

Third, in Chapter 5, we implemented the wetting and drying algorithm in a three-dimensional version of the ADCIRC model. Three-dimensional simulations have become increasingly practical as computer architectures become faster and more efficient. And, in many applications of the model, the vertical profile and mixing in near-shore regions are most important. We have shown that the three-dimensional algorithm can be used to simulate problems with challenging bathymetries. We have also shown that the three-dimensional algorithm behaves in a manner that is qualitatively similar to the behavior of the one- and two-dimensional algorithms in Chapter 3 and Chapter 4, respectively.

Fourth, in all three of the wetting and drying chapters, we identified a set of optimal parameters for wetting and drying simulations. We will discuss this behavior in detail:

- The maximum stable time step ranged from 10 seconds to 55 seconds, but, for both of the model problems from the study of the three-dimensional algorithm in Chapter 5, the maximum stable time step was 45 seconds. If wave celerity is assumed to be based on $H_{min} = 0.01$ meters, then the Courant number for that time step is about 0.00063. For wetting and drying applications, we recommend that ADCIRC users first try a time step that produces a similar Courant number, and then adjust it accordingly.
- The numerical parameter G and the slip coefficient K_{slip} produce the best behavior when G = 0.01 sec^{-1} and K_{slip} = 0.0001. Smaller values of G tend to cause the model to become unstable, regardless of the domain. And, larger values of K_{slip} tend to limit or prevent wetting and drying. We recommend that ADCIRC users begin with these values and adjust them to suit their problems.
- The drying parameter H_{min} produces the best behavior when it is in the range from 0.001 to 0.01 meters. Larger values tend to limit or prevent drying, and smaller values tend to cause the three-dimensional model to become unstable.
- The wetting parameter U_{min} does not affect the performance of the wetting and drying algorithm. It can be set to the same value as H_{min} and then forgotten. We recommend that it be hard-wired or removed eventually.
- The horizontal node spacing affects the ability of the model to track the shoreline or other wave fronts. The errors tend to converge when the horizontal resolution is

refined, but that is not always the case. As always with horizontal resolution, the model user should be careful to strike a balance between representation of the physical features and model efficiency.

- The vertical node spacing does not affect the behavior of the model in simulations that do not contain vertical mixing. Future work is needed to identify simulations when vertical resolution is important.

These are merely recommendations. ADCIRC users should tailor their input parameters to represent their problems of interest.

Fifth, in Chapter 4 and Chapter 5, we proved that recent updates to the wetting and drying algorithm were beneficial. The original algorithm proved to be unstable for a wide range of parameters and problems, including cases that worked well in one dimension. And, even when the original algorithm was stable, it required smaller time steps, it was less accurate, and it produced greater mass balance errors. The improved algorithm not only behaved better, but its behavior was qualitatively similar to that of the one-dimensional model. Thus, the recent updates were beneficial. This finding won't impact an improved wetting and drying algorithm that has already been implemented and adopted in the production ADCIRC code, but it does help to explain the reasoning for its adoption.

Sixth, in Chapter 5, we showed that smaller mass balance errors are obtained when they are computed for each vertical element in the water column. As discussed in Section 5.1.4, the finite volume method of computing mass balance errors is consistent with the three-dimensional continuity equation that is used to compute the vertical velocities. In effect, the vertical velocities are computed in a way that satisfies primitive continuity, at least for each vertical column of elements. The errors at an individual element in that column may be non-zero, but they are significantly less than they would be if they were computed for the entire column by using the average velocity, as is done in the studies of the one- and two-dimensional models. Thus, when possible, mass balance errors should be computed for each element, because that method follows the way in which the model is formulated and produces a metric that seems to mimic truncation errors in three dimensions.

Taken together, these six objectives represent an important and unique contribution to the field of hydrodynamic modeling in general and to the group of ADCIRC users and developers in particular.

7. References

1. R.C. Berger, S.E. Howington, “Discrete Fluxes and Mass Balance in Finite Elements,” *Journal of Hydraulic Engineering*, Vol. 128, No. 1, pp. 87-92 (2002).
2. S.F. Bradford and B.F. Sanders, “Finite-Volume Model for Shallow-Water Flooding of Arbitrary Topography,” *Journal of Hydraulic Engineering*, Vol. 128, No. 3, pp. 289-298 (2002).
3. G.F. Carrier, H.P. Greenspan, “Water waves of finite amplitude on a sloping beach,” *Journal of Fluid Mechanics*, Vol. 4, pp. 97-109 (1958).
4. K.M. Dresback, R.L. Kolar, J.C. Dietrich, “On the Form of the Momentum Equation for Shallow Water Models Based on the Generalized Wave Continuity Equation,” *Advances in Water Resources*, in press.
5. P.M. Gresho., R.L. Lee, “Don’t Suppress the Wiggles - They’re Telling You Something,” *Computers and Fluids*, Vol. 9, pp. 223-253 (1981).
6. S.C. Hagen., J.J. Westerink, R.L. Kolar, “One-dimensional finite element grids based on a localized truncation error analysis,” *International Journal for Numerical Methods in Fluids*, Vol. 32, pp. 241-261 (2000).
7. S.C. Hagen, J.J. Westerink, R.L. Kolar, and O. Horstmann, “Two-dimensional, unstructured mesh generation for tidal models,” *International Journal for Numerical Methods in Fluids*, Vol. 35, pp. 659-686 (2001).

8. T.J.R. Hughes, G. Engel, L. Mazzei, M.G. Larson, "The continuous Galerkin method is locally conservative," *Journal of Computational Physics*, Vol. 163, No. 2, pp. 467-488 (2000).

9. J.T.C. Ip, D.R. Lynch, and C.T. Friedrichs, "Simulation of Estuarine Flooding and Dewatering with Application to Great Bay, New Hampshire," *Estuarine, Coastal and Shelf Science*, Vol. 47, pp. 119-141 (1998).

10. B. Johns, "Numerical Integration of the Shallow Water Equations over a Sloping Shelf," *International Journal for Numerical Methods in Fluids*, Vol. 2, pp. 253-261 (1982).

11. I.P.E. Kinnmark, "The shallow water wave equations: formulations, analysis and application," in *Lecture Notes in Engineering*, C.A. Brebbia, S.A. Orsszag (eds), Springer-Verlag, Berlin, Vol. 15, p. 187 (1986).

12. R.L. Kolar, W.G. Gray, J.J. Westerink, and R.A. Luettich, "Shallow water modeling in spherical coordinates: equation formulation, numerical implementation and application," *Journal of Hydraulic Research*, Vol. 32, No. 1, pp. 3-24 (1994).

13. R.L. Kolar, J.J. Westerink, M.E. Cantekin, C.A. Blain, "Aspects of Nonlinear Simulations using Shallow-Water Models based on the Wave Continuity Equation," *Computers and Fluids*, Vol. 23, pp. 523-538 (1994).

14. H.C.J. Lin, H.P. Cheng, E.V. Edris, and G.T. Yeh, "Modeling surface and subsurface hydrologic interactions in a south Florida watershed near the Biscayne Bay," *Proceedings of the XV International Conference on Computational Methods in Water Resources (CMWR XV)*, Chapel Hill, NC, June 13-17, 2004, pp. 1607-1618.

15. P.L.F. Liu, P. Lynett, and C.E. Synolakis, “Analytical solutions for forced long waves on a sloping beach,” *Journal of Fluid Mechanics*, Vol. 478, pp. 101-109 (2003).

16. R.A. Luettich, J.J. Westerink, and N.W. Scheffner, “ADCIRC: an advanced three-dimensional circulation model for shelves, coasts and estuaries. Report 1: theory and methodology of ADCIRC-2DDI and ADCIRC-3DL,” Technical Report DRP-92-6, Department of the Army, USACE, Washington, DC (1992).

17. R.A. Luettich, J.J. Westerink, “An Assessment of Flooding and Drying Techniques for Use in the ADCIRC Hydrodynamic Model: Implementation and Performance in One-Dimensional Flows,” Report for the Department of the Army, Contract Number DACW39-94-M-5869 (1995).

18. R.A. Luettich, J.J. Westerink, “Implementation and Testing of Elemental Flooding and Drying in the ADCIRC Hydrodynamic Model,” Final Report for the Department of the Army, Contract Number DACW39-94-M-5869 (1995).

19. D.R. Lynch and W.G. Gray, “A wave equation model for finite element tidal computations,” *Computers and Fluids*, Vol. 7, No. 3, pp. 207-228 (1979).

20. T.C. Massey, C.A. Blain, “In search of a consistent and conservative mass flux for the GWCE,” *Computer Methods in Applied Mechanics and Engineering*, to appear.

21. A. Militello, N.C. Kraus, “Shinnecock Inlet, New York, Site Investigation Report 4, Evaluation of Flood and Ebb Shoal Sediment Source Alternatives for the West of Shinnecock Interim Project, New York,” Technical Report CHL-98-32, U.S. Army Engineer Research and Development Center, Vicksburg, Mississippi (2000).

22. A. Morang, “Shinnecock Inlet, New York, Site Investigation Report 1, Morphology and Historical Behavior,” Technical Report CHL-98-32, U.S. Army Engineer Waterways Experiment Station, Vicksburg, Mississippi (1999).

23. A. Shapiro, “Nonlinear shallow-water oscillations in a parabolic channel: exact solutions and trajectory analyses,” *Journal of Fluid Mechanics*, Vol. 318, pp. 49-76 (1996).

24. G.L.D. Siden, D.R. Lynch, “Wave Equation Hydrodynamics on Deforming Elements,” *International Journal for Numerical Methods in Fluids*, Vol. 8, pp. 1071-1093 (1988).

25. W.C. Thacker, “Some exact solutions to the nonlinear shallow-water wave equations,” *Journal of Fluid Mechanics*, Vol. 107, pp. 499-508 (1981).

26. J.J. Westerink, R.A. Luettich, C.A. Blain, and N.W. Scheffner, “ADCIRC: an advanced three-dimensional circulation model for shelves, coasts and estuaries. Report 2: Users Manual for ADCIRC-2DDI,” Department of the Army, USA (1994).

27. G.L. Williams, A. Morang, L. Lillycrop, “Shinnecock Inlet, New York, Site Investigation Report 2, Evaluation of Sand Bypass Options,” Technical Report CHL-98-32, U.S. Army Engineer Waterways Experiment Station, Vicksburg, Mississippi (1998).

A. Appendix

As stated previously, ADCIRC is based on two governing equations: the generalized wave continuity (GWC) equation, and either the nonconservative momentum (NCM) equation or the conservative momentum (CM) equation. We will present each equation and its respective truncation error terms in that order.

A.1. Truncation Error Terms for the GWC Equation

In one dimension, the generalized wave continuity equation is given by:

$$\frac{\partial^2\zeta}{\partial t^2} + G\frac{\partial\zeta}{\partial t} - q\frac{\partial G}{\partial x} - \frac{\partial}{\partial x}\left[\frac{\partial}{\partial x}(qu) + (G-\tau)q + gH\frac{\partial\zeta}{\partial x} - \varepsilon\frac{\partial^2 q}{\partial x^2}\right] = 0\,, \qquad \text{(A.1)}$$

where the variables are defined below. The truncation error terms will be presented for each term in the governing equation shown in Equation A.1, beginning with the first term, $\partial^2\zeta/\partial t^2$, which is given by:

$$-\frac{1}{12}(\Delta t)^2\left(\frac{\partial^4\zeta_{j,k}}{\partial t^4}\right) + \frac{1}{36}(\Delta x_j - \Delta x_{j+1})(\Delta t)^2\left(\frac{\partial^5\zeta_{j,k}}{\partial x\partial t^4}\right) \qquad \text{(A.2)}$$

$$-\frac{1}{72}[(\Delta x_j)^2 - (\Delta x_j)(\Delta x_{j+1}) + (\Delta x_{j+1})^2](\Delta t)^2\left(\frac{\partial^6\zeta_{j,k}}{\partial x^2\partial t^4}\right)$$

$$+\frac{1}{3}(\Delta x_j - \Delta x_{j+1})\left(\frac{\partial^3\zeta_{j,k}}{\partial x\partial t^2}\right) - \frac{1}{6}[(\Delta x_j)^2 - (\Delta x_j)(\Delta x_{j+1}) + (\Delta x_{j+1})^2]\left(\frac{\partial^4\zeta_{j,k}}{\partial x^2\partial t^2}\right),$$

where: x is distance and it is indexed with j; Δx_j is the grid spacing at element j; t is time and it is indexed with k; Δt is the time step; and ζ is the water surface elevation from the mean. The second term, $G(\partial\zeta/\partial t)$, is given by:

$$-\frac{1}{6}G(\Delta t)^2\left(\frac{\partial^3\zeta_{j,k}}{\partial t^3}\right) + \frac{1}{18}G(\Delta x_j - \Delta x_{j+1})(\Delta t)^2\left(\frac{\partial^4\zeta_{j,k}}{\partial x\partial t^3}\right) \tag{A.3}$$

$$-\frac{1}{36}G[(\Delta x_j)^2 - (\Delta x_j)(\Delta x_{j+1}) + (\Delta x_{j+1})^2](\Delta t)^2\left(\frac{\partial^5\zeta_{j,k}}{\partial x^2\partial t^3}\right)$$

$$+\frac{1}{3}G(\Delta x_j - \Delta x_{j+1})\left(\frac{\partial^2\zeta_{j,k}}{\partial x\partial t}\right) - \frac{1}{6}G[(\Delta x_j)^2 - (\Delta x_j)(\Delta x_{j+1}) + (\Delta x_{j+1})^2]\left(\frac{\partial^3\zeta_{j,k}}{\partial x^2\partial t}\right),$$

where G is the numerical parameter introduced by Kinnmark [11]. The third term, $q(\partial G/\partial x)$ is the spatially-varied G term, which was not used in any of our studies. The fourth term is:

$$\frac{\partial^2}{\partial x^2}(qu), \tag{A.4}$$

which is the advective term, and it can be formulated conservatively or non-conservatively. The conservative form of the advective term is $\partial^2(qu)/\partial x^2$, and its truncation error is given by:

$$\frac{1}{3}g(\Delta x_{j+1} - \Delta x_j)\left(\frac{\partial^3(qu)_{j,k}}{\partial x^3}\right), \tag{A.5}$$

$$+\frac{1}{12}g[(\Delta x_j)^2 - (\Delta x_j)(\Delta x_{j+1}) + (\Delta x_{j+1})^2]\left(\frac{\partial^4(qu)_{j,k}}{\partial x^4}\right)$$

where qu is the product of the flux, q, and the velocity, u. The non-conservative form of the advective term has two parts. The first part of the non-conservative form of the advective term is $\partial(u(\partial\zeta/\partial t))/\partial x$, and its truncation error is given by:

$$-\frac{1}{6}(\Delta t)^2\left(\frac{\partial^3\zeta_{j,k}}{\partial t^3}\right)\left(\frac{\partial u_{j,k}}{\partial x}\right)-\frac{1}{6}(\Delta t)^2\left(\frac{\partial^4\zeta_{j,k}}{\partial x\partial t^3}\right)(u_{j,k}) \tag{A.6}$$

$$+\frac{1}{12}(\Delta x_j-\Delta x_{j+1})(\Delta t)^2\left(\frac{\partial^4\zeta_{j,k}}{\partial x\partial t^3}\right)\left(\frac{\partial u_{j,k}}{\partial x}\right)+\frac{1}{12}(\Delta x_j-\Delta x_{j+1})(\Delta t)^2\left(\frac{\partial^3\zeta_{j,k}}{\partial t^3}\right)\left(\frac{\partial^2 u_{j,k}}{\partial x^2}\right)$$

$$-\frac{1}{24}[(\Delta x_j)^2-(\Delta x_j)(\Delta x_{j+1})+(\Delta x_{j+1})^2](\Delta t)^2\left(\frac{\partial^4\zeta_{j,k}}{\partial x\partial t^3}\right)\left(\frac{\partial^2 u_{j,k}}{\partial x^2}\right)$$

$$+\frac{1}{12}(\Delta x_j-\Delta x_{j+1})(\Delta t)^2\left(\frac{\partial^5\zeta_{j,k}}{\partial x^2\partial t^3}\right)(u_{j,k})$$

$$-\frac{1}{24}[(\Delta x_j)^2-(\Delta x_j)(\Delta x_{j+1})+(\Delta x_{j+1})^2](\Delta t)^2\left(\frac{\partial^5\zeta_{j,k}}{\partial x^2\partial t^3}\right)\left(\frac{\partial u_{j,k}}{\partial x}\right)$$

$$-\frac{1}{36}[(\Delta x_j)^2-(\Delta x_j)(\Delta x_{j+1})+(\Delta x_{j+1})^2](\Delta t)^2\left(\frac{\partial^3\zeta_{j,k}}{\partial t^3}\right)\left(\frac{\partial^3 u_{j,k}}{\partial x^3}\right)$$

$$-\frac{1}{36}[(\Delta x_j)^2-(\Delta x_j)(\Delta x_{j+1})+(\Delta x_{j+1})^2](\Delta t)^2\left(\frac{\partial^6\zeta_{j,k}}{\partial x^3\partial t^3}\right)(u_{j,k})$$

$$+\frac{1}{2}(\Delta t)\left(\frac{\partial^2\zeta_{j,k}}{\partial t^2}\right)\left(\frac{\partial u_{j,k}}{\partial x}\right)+\frac{1}{2}(\Delta t)\left(\frac{\partial^3\zeta_{j,k}}{\partial x\partial t^2}\right)(u_{j,k})$$

$$+\frac{1}{4}(\Delta x_{j+1}-\Delta x_j)(\Delta t)\left(\frac{\partial^3\zeta_{j,k}}{\partial x\partial t^2}\right)\left(\frac{\partial u_{j,k}}{\partial x}\right)+\frac{1}{4}(\Delta x_{j+1}-\Delta x_j)(\Delta t)\left(\frac{\partial^2\zeta_{j,k}}{\partial t^2}\right)\left(\frac{\partial^2 u_{j,k}}{\partial x^2}\right)$$

$$+\frac{1}{8}[(\Delta x_j)^2-(\Delta x_j)(\Delta x_{j+1})+(\Delta x_{j+1})^2](\Delta t)\left(\frac{\partial^3\zeta_{j,k}}{\partial x\partial t^2}\right)\left(\frac{\partial^2 u_{j,k}}{\partial x^2}\right)$$

$$+\frac{1}{4}(\Delta x_{j+1}-\Delta x_j)(\Delta t)\left(\frac{\partial^4\zeta_{j,k}}{\partial x^2\partial t^2}\right)(u_{j,k})$$

$$+\frac{1}{8}[(\Delta x_j)^2-(\Delta x_j)(\Delta x_{j+1})+(\Delta x_{j+1})^2](\Delta t)\left(\frac{\partial^4\zeta_{j,k}}{\partial x^2\partial t^2}\right)\left(\frac{\partial u_{j,k}}{\partial x}\right)$$

$$+\frac{1}{12}[(\Delta x_j)^2-(\Delta x_j)(\Delta x_{j+1})+(\Delta x_{j+1})^2](\Delta t)\left(\frac{\partial^2\zeta_{j,k}}{\partial t^2}\right)\left(\frac{\partial^3 u_{j,k}}{\partial x^3}\right)$$

$$+\frac{1}{12}[(\Delta x_j)^2-(\Delta x_j)(\Delta x_{j+1})+(\Delta x_{j+1})^2](\Delta t)\left(\frac{\partial^5\zeta_{j,k}}{\partial x^3\partial t^2}\right)(u_{j,k})$$

$$+\frac{1}{2}(\Delta x_j-\Delta x_{j+1})\left(\frac{\partial^2\zeta_{j,k}}{\partial x\partial t}\right)\left(\frac{\partial u_{j,k}}{\partial x}\right)+\frac{1}{2}(\Delta x_j-\Delta x_{j+1})\left(\frac{\partial\zeta_{j,k}}{\partial t}\right)\left(\frac{\partial^2 u_{j,k}}{\partial x^2}\right)$$

$$-\frac{1}{4}[(\Delta x_j)^2-(\Delta x_j)(\Delta x_{j+1})+(\Delta x_{j+1})^2]\left(\frac{\partial^2\zeta_{j,k}}{\partial x\partial t}\right)\left(\frac{\partial^2 u_{j,k}}{\partial x^2}\right)$$

$$+\frac{1}{2}(\Delta x_j-\Delta x_{j+1})\left(\frac{\partial^3\zeta_{j,k}}{\partial x^2\partial t}\right)(u_{j,k})$$

$$-\frac{1}{4}[(\Delta x_j)^2-(\Delta x_j)(\Delta x_{j+1})+(\Delta x_{j+1})^2]\left(\frac{\partial^3\zeta_{j,k}}{\partial x^2\partial t}\right)\left(\frac{\partial u_{j,k}}{\partial x}\right)$$

$$-\frac{1}{6}[(\Delta x_j)^2-(\Delta x_j)(\Delta x_{j+1})+(\Delta x_{j+1})^2]\left(\frac{\partial\zeta_{j,k}}{\partial t}\right)\left(\frac{\partial^3 u_{j,k}}{\partial x^3}\right)$$

$$-\frac{1}{6}[(\Delta x_j)^2-(\Delta x_j)(\Delta x_{j+1})+(\Delta x_{j+1})^2]\left(\frac{\partial^4\zeta_{j,k}}{\partial x^3\partial t}\right)(u_{j,k})\,.$$

The second part of the non-conservative form of the advective term is $\partial(q(\partial u/\partial x))/\partial x$, and its truncation error is given by:

$$-\frac{1}{2}(\Delta x_j-\Delta x_{j+1})\left(\frac{\partial^2 q_{j,k}}{\partial x^2}\right)\left(\frac{\partial u_{j,k}}{\partial x}\right) \tag{A.7}$$

$$+\frac{1}{4}[(\Delta x_j)^2-(\Delta x_j)(\Delta x_{j+1})+(\Delta x_{j+1})^2]\left(\frac{\partial^2 q_{j,k}}{\partial x^2}\right)\left(\frac{\partial^2 u_{j,k}}{\partial x^2}\right)$$

$$+\frac{1}{2}(\Delta x_{j+1}-\Delta x_j)\left(\frac{\partial q_{j,k}}{\partial x}\right)\left(\frac{\partial^2 u_{j,k}}{\partial x^2}\right)$$

$$+\frac{1}{6}[(\Delta x_j)^2-(\Delta x_j)(\Delta x_{j+1})+(\Delta x_{j+1})^2]\left(\frac{\partial^3 q_{j,k}}{\partial x^3}\right)\left(\frac{\partial u_{j,k}}{\partial x}\right)$$

$$+\frac{1}{3}(\Delta x_{j+1}-\Delta x_j)(q_{j,k})\left(\frac{\partial^3 u_{j,k}}{\partial x^3}\right)$$

$$+\frac{1}{6}[(\Delta x_j)^2-(\Delta x_j)(\Delta x_{j+1})+(\Delta x_{j+1})^2]\left(\frac{\partial q_{j,k}}{\partial x}\right)\left(\frac{\partial^3 u_{j,k}}{\partial x^3}\right)$$

$$+\frac{1}{12}[(\Delta x_j)^2-(\Delta x_j)(\Delta x_{j+1})+(\Delta x_{j+1})^2](q_{j,k})\left(\frac{\partial^4 u_{j,k}}{\partial x^4}\right).$$

The fifth term, $(G-\tau)(\partial q/\partial x)$, is a combination of the GWC flux term and the bottom friction flux term, and its truncation error is given by:

$$\frac{1}{2}(G-\tau)(\Delta x_j-\Delta x_{j+1})\left(\frac{\partial^2 q_{j,k}}{\partial x^2}\right) \tag{A.8}$$

$$-\frac{1}{6}(G-\tau)[(\Delta x_j)^2-(\Delta x_j)(\Delta x_{j+1})+(\Delta x_{j+1})^2]\left(\frac{\partial^3 q_{j,k}}{\partial x^3}\right),$$

where τ is bottom friction. The sixth term is:

$$g\frac{\partial}{\partial x}\left(H\frac{\partial\zeta}{\partial x}\right), \tag{A.9}$$

which is the finite amplitude term. It is broken into two parts. The first part of the finite amplitude term is $gh(\partial^2\zeta/\partial x^2)$, and its truncation error is given by:

$$\frac{1}{3}g(\Delta t)^2\left(\frac{\partial h_{j,k}}{\partial x}\right)\left(\frac{\partial^3\zeta_{j,k}}{\partial x\partial t^2}\right)+\frac{1}{6}g(\Delta x_{j+1}-\Delta x_j)(\Delta t)^2\left(\frac{\partial^2 h_{j,k}}{\partial x^2}\right)\left(\frac{\partial^3\zeta_{j,k}}{\partial x\partial t^2}\right) \tag{A.10}$$

$$+\frac{1}{3}g(\Delta t)^2(h_{j,k})\left(\frac{\partial^4\zeta_{j,k}}{\partial x^2\partial t^2}\right)+\frac{1}{6}g(\Delta x_{j+1}-\Delta x_j)(\Delta t)^2\left(\frac{\partial h_{j,k}}{\partial x}\right)\left(\frac{\partial^4\zeta_{j,k}}{\partial x^2\partial t^2}\right)$$

$$+\frac{1}{12}g[(\Delta x_j)^2-(\Delta x_j)(\Delta x_{j+1})+(\Delta x_{j+1})^2](\Delta t)^2\left(\frac{\partial^2 h_{j,k}}{\partial x^2}\right)\left(\frac{\partial^4\zeta_{j,k}}{\partial x^2\partial t^2}\right)$$

$$+\frac{1}{18}g[(\Delta x_j)^2-(\Delta x_j)(\Delta x_{j+1})+(\Delta x_{j+1})^2](\Delta t)^2\left(\frac{\partial^3 h_{j,k}}{\partial x^3}\right)\left(\frac{\partial^3 \zeta_{j,k}}{\partial x \partial t^2}\right)$$

$$+\frac{1}{9}g(\Delta x_{j+1}-\Delta x_j)(\Delta t)^2(h_{j,k})\left(\frac{\partial^5 \zeta_{j,k}}{\partial x^3 \partial t^2}\right)$$

$$+\frac{1}{18}g[(\Delta x_j)^2-(\Delta x_j)(\Delta x_{j+1})+(\Delta x_{j+1})^2](\Delta t)^2\left(\frac{\partial h_{j,k}}{\partial x}\right)\left(\frac{\partial^5 \zeta_{j,k}}{\partial x^3 \partial t^2}\right)$$

$$+\frac{1}{36}g[(\Delta x_j)^2-(\Delta x_j)(\Delta x_{j+1})+(\Delta x_{j+1})^2](\Delta t)^2(h_{j,k})\left(\frac{\partial^6 \zeta_{j,k}}{\partial x^4 \partial t^2}\right)$$

$$+\frac{1}{2}g(\Delta x_{j+1}-\Delta x_j)\left(\frac{\partial^2 h_{j,k}}{\partial x^2}\right)\left(\frac{\partial \zeta_{j,k}}{\partial x}\right)+\frac{1}{2}g(\Delta x_{j+1}-\Delta x_j)\left(\frac{\partial h_{j,k}}{\partial x}\right)\left(\frac{\partial^2 \zeta_{j,k}}{\partial x^2}\right)$$

$$+\frac{1}{4}g[(\Delta x_j)^2-(\Delta x_j)(\Delta x_{j+1})+(\Delta x_{j+1})^2]\left(\frac{\partial^2 h_{j,k}}{\partial x^2}\right)\left(\frac{\partial^2 \zeta_{j,k}}{\partial x^2}\right)$$

$$+\frac{1}{6}g[(\Delta x_j)^2-(\Delta x_j)(\Delta x_{j+1})+(\Delta x_{j+1})^2]\left(\frac{\partial^3 h_{j,k}}{\partial x^3}\right)\left(\frac{\partial \zeta_{j,k}}{\partial x}\right)$$

$$+\frac{1}{3}g(\Delta x_{j+1}-\Delta x_j)(h_{j,k})\left(\frac{\partial^3 \zeta_{j,k}}{\partial x^3}\right)$$

$$+\frac{1}{6}g[(\Delta x_j)^2-(\Delta x_j)(\Delta x_{j+1})+(\Delta x_{j+1})^2]\left(\frac{\partial h_{j,k}}{\partial x}\right)\left(\frac{\partial^3 \zeta_{j,k}}{\partial x^3}\right)$$

$$+\frac{1}{12}g[(\Delta x_j)^2-(\Delta x_j)(\Delta x_{j+1})+(\Delta x_{j+1})^2](h_{j,k})\left(\frac{\partial^4 \zeta_{j,k}}{\partial x^4}\right),$$

where h is the bathymetry, and g is the acceleration due to gravity. The second part of the finite amplitude term is $g(\partial^2\zeta^2/\partial x^2)$, and its truncation error is given by:

$$\frac{1}{6}g(\Delta x_{j+1}-\Delta x_j)\left(\frac{\partial^3 \zeta^2_{j,k}}{\partial x^3}\right), \tag{A.11}$$

$$+\frac{1}{24}g[(\Delta x_j)^2-(\Delta x_j)(\Delta x_{j+1})+(\Delta x_{j+1})^2]\left(\frac{\partial^4 \zeta^2_{j,k}}{\partial x^4}\right)$$

where ζ^2 is the square of the water surface elevation from the mean. Finally, the seventh term in Equation A.1 is:

$$\varepsilon\frac{\partial^2 q}{\partial x^2}, \tag{A.12}$$

which is the viscous term. In ADCIRC, this term is formulated as $\varepsilon(\partial^3\zeta/\partial x^2\partial t)$, and its truncation error term is given by:

$$\begin{aligned}&\frac{1}{6}\varepsilon(\Delta t)^2\left(\frac{\partial^5\zeta_{j,k}}{\partial x^2\partial t^3}\right)+\frac{1}{18}\varepsilon(\Delta x_{j+1}-\Delta x_j)(\Delta t)^2\left(\frac{\partial^6\zeta_{j,k}}{\partial x^3\partial t^3}\right)\\&+\frac{1}{72}\varepsilon[(\Delta x_j)^2-(\Delta x_j)(\Delta x_{j+1})+(\Delta x_{j+1})^2](\Delta t)^2\left(\frac{\partial^7\zeta_{j,k}}{\partial x^4\partial t^3}\right)\\&+\frac{1}{3}\varepsilon(\Delta x_{j+1}-\Delta x_j)\left(\frac{\partial^4\zeta_{j,k}}{\partial x^3\partial t}\right)+\frac{1}{12}\varepsilon[(\Delta x_j)^2-(\Delta x_j)(\Delta x_{j+1})+(\Delta x_{j+1})^2]\left(\frac{\partial^5\zeta_{j,k}}{\partial x^4\partial t}\right),\end{aligned} \tag{A.13}$$

where ε is eddy viscosity.

A.2. Truncation Error Terms for the NCM Equation

In one dimension, the non-conservative momentum equation is given by:

$$\frac{\partial u}{\partial t}+u\frac{\partial u}{\partial x}+\tau u+g\frac{\partial\zeta}{\partial x}-\frac{\varepsilon}{H}\frac{\partial^2 q}{\partial x^2} = 0. \tag{A.14}$$

Again, the truncation error terms will be presented for each term in the governing equation. The first term in Equation A.14, $\partial u/\partial t$, is the accumulation term, and it is given by:

$$-\frac{1}{6}(\Delta t)^2\left(\frac{\partial^3 u_{j,k}}{\partial t^3}\right)+\frac{1}{18}(\Delta x_j-\Delta x_{j+1})(\Delta t)^2\left(\frac{\partial^4 u_{j,k}}{\partial x\partial t^3}\right) \tag{A.15}$$

$$-\frac{1}{36}[(\Delta x_j)^2-(\Delta x_j)(\Delta x_{j+1})+(\Delta x_{j+1})^2](\Delta t)^2\left(\frac{\partial^5 u_{j,k}}{\partial x^2\partial t^3}\right)$$

$$-\frac{1}{2}(\Delta t)\left(\frac{\partial^2 u_{j,k}}{\partial t^2}\right)+\frac{1}{6}(\Delta x_j-\Delta x_{j+1})(\Delta t)\left(\frac{\partial^3 u_{j,k}}{\partial x\partial t^2}\right)$$

$$-\frac{1}{12}[(\Delta x_j)^2-(\Delta x_j)(\Delta x_{j+1})+(\Delta x_{j+1})^2](\Delta t)\left(\frac{\partial^4 u_{j,k}}{\partial x^2\partial t^2}\right)$$

$$+\frac{1}{3}(\Delta x_j-\Delta x_{j+1})\left(\frac{\partial^2 u_{j,k}}{\partial x\partial t}\right)-\frac{1}{6}[(\Delta x_j)^2-(\Delta x_j)(\Delta x_{j+1})+(\Delta x_{j+1})^2]\left(\frac{\partial^3 u_{j,k}}{\partial x^2\partial t}\right).$$

The second term in Equation A.14, $u(\partial u/\partial x)$, is the advection term, and its truncation error term is given by:

$$\frac{1}{2}(\Delta x_j-\Delta x_{j+1})\left(\frac{\partial u_{j,k}}{\partial x}\right)^2 \tag{A.16}$$

$$-\frac{1}{2}[(\Delta x_j)^2-(\Delta x_j)(\Delta x_{j+1})+(\Delta x_{j+1})^2]\left(\frac{\partial^2 u_{j,k}}{\partial x^2}\right)\left(\frac{\partial u_{j,k}}{\partial x}\right)$$

$$+\frac{1}{2}(\Delta x_j-\Delta x_{j+1})(u_{j,k})\left(\frac{\partial^2 u_{j,k}}{\partial x^2}\right)$$

$$-\frac{1}{6}[(\Delta x_j)^2-(\Delta x_j)(\Delta x_{j+1})+(\Delta x_{j+1})^2](u_{j,k})\left(\frac{\partial^3 u_{j,k}}{\partial x^3}\right).$$

The third term in Equation A.14, τu, is the bottom friction term, and its truncation error term is given by:

$$-\frac{1}{4}\tau(\Delta t)^2\left(\frac{\partial^2 u_{j,k}}{\partial t^2}\right)+\frac{1}{12}\tau(\Delta x_j-\Delta x_{j+1})(\Delta t)^2\left(\frac{\partial^3 u_{j,k}}{\partial x\partial t^2}\right) \tag{A.17}$$

$$-\frac{1}{24}\tau[(\Delta x_j)^2-(\Delta x_j)(\Delta x_{j+1})+(\Delta x_{j+1})^2](\Delta t)^2\left(\frac{\partial^4 u_{j,k}}{\partial x^2\partial t^2}\right)$$

$$-\frac{1}{2}\tau(\Delta t)\left(\frac{\partial u_{j,k}}{\partial t}\right)+\frac{1}{6}\tau(\Delta x_j-\Delta x_{j+1})(\Delta t)\left(\frac{\partial^2 u_{j,k}}{\partial x\partial t}\right)$$

$$-\frac{1}{12}\tau[(\Delta x_j)^2-(\Delta x_j)(\Delta x_{j+1})+(\Delta x_{j+1})^2](\Delta t)\left(\frac{\partial^3 u_{j,k}}{\partial x^2\partial t}\right)$$

$$+\frac{1}{3}\tau(\Delta x_j-\Delta x_{j+1})\left(\frac{\partial u_{j,k}}{\partial x}\right)-\frac{1}{6}\tau[(\Delta x_j)^2-(\Delta x_j)(\Delta x_{j+1})+(\Delta x_{j+1})^2]\left(\frac{\partial^2 u_{j,k}}{\partial x^2}\right).$$

The fourth term in Equation A.14, $g(\partial\zeta/\partial x)$, is the finite amplitude term, and its truncation error term is given by:

$$-\frac{1}{4}g(\Delta t)^2\left(\frac{\partial^3\zeta_{j,k}}{\partial x\partial t^2}\right)+\frac{1}{8}g(\Delta x_j-\Delta x_{j+1})(\Delta t)^2\left(\frac{\partial^4\zeta_{j,k}}{\partial x^2\partial t^2}\right)\tag{A.18}$$

$$-\frac{1}{24}g[(\Delta x_j)^2-(\Delta x_j)(\Delta x_{j+1})+(\Delta x_{j+1})^2](\Delta t)^2\left(\frac{\partial^5\zeta_{j,k}}{\partial x^3\partial t^2}\right)$$

$$-\frac{1}{2}g(\Delta t)\left(\frac{\partial^2\zeta_{j,k}}{\partial x\partial t}\right)+\frac{1}{4}g(\Delta x_j-\Delta x_{j+1})(\Delta t)\left(\frac{\partial^3\zeta_{j,k}}{\partial x^2\partial t}\right)$$

$$-\frac{1}{12}g[(\Delta x_j)^2-(\Delta x_j)(\Delta x_{j+1})+(\Delta x_{j+1})^2](\Delta t)\left(\frac{\partial^4\zeta_{j,k}}{\partial x^3\partial t}\right)$$

$$+\frac{1}{2}g(\Delta x_j-\Delta x_{j+1})\left(\frac{\partial^2\zeta_{j,k}}{\partial x^2}\right)-\frac{1}{6}g[(\Delta x_j)^2-(\Delta x_j)(\Delta x_{j+1})+(\Delta x_{j+1})^2]\left(\frac{\partial^3\zeta_{j,k}}{\partial x^3}\right).$$

The fifth term in Equation A.14, $(\varepsilon/H)(\partial^2 q/\partial x^2)$, is the viscous term, and its truncation error term is given by:

$$\frac{1}{4}\varepsilon(\Delta t)^2\left(\frac{\partial^4 u_{j,k}}{\partial x^2\partial t^2}\right)+\frac{1}{12}\varepsilon(\Delta x_j-\Delta x_{j+1})(\Delta t)^2\left(\frac{\partial^5 u_{j,k}}{\partial x^3\partial t^2}\right)\tag{A.19}$$

$$+\frac{1}{48}\varepsilon[(\Delta x_j)^2-(\Delta x_j)(\Delta x_{j+1})+(\Delta x_{j+1})^2](\Delta t)^2\left(\frac{\partial^6 u_{j,k}}{\partial x^4\partial t^2}\right)$$

$$+\frac{1}{2}\varepsilon(\Delta t)\left(\frac{\partial^3 u_{j,k}}{\partial x^2\partial t}\right)+\frac{1}{6}\varepsilon(\Delta x_j-\Delta x_{j+1})(\Delta t)\left(\frac{\partial^4 u_{j,k}}{\partial x^3\partial t}\right)$$

$$+\frac{1}{24}\varepsilon[(\Delta x_j)^2-(\Delta x_j)(\Delta x_{j+1})+(\Delta x_{j+1})^2](\Delta t)\left(\frac{\partial^5 u_{j,k}}{\partial x^4\partial t}\right)$$

$$+\frac{1}{3}\varepsilon(\Delta x_j-\Delta x_{j+1})\left(\frac{\partial^3 u_{j,k}}{\partial x^3}\right)+\frac{1}{12}\varepsilon[(\Delta x_j)^2-(\Delta x_j)(\Delta x_{j+1})+(\Delta x_{j+1})^2]\left(\frac{\partial^4 u_{j,k}}{\partial x^4}\right).$$

A.3. Truncation Error Terms for the CM Equation

In one dimension, the conservative momentum equation is given by:

$$\frac{\partial q}{\partial t}+\frac{\partial}{\partial x}(qu)+\tau q+gH\frac{\partial \zeta}{\partial x}-\varepsilon\frac{\partial^2 q}{\partial x^2} = 0. \tag{A.20}$$

The truncation error terms will be presented for each term in the governing equation. The first term in Equation A.20, $\partial q/\partial t$, is the accumulation term, and its truncation error term is given by:

$$-\frac{1}{6}(\Delta t)^2\left(\frac{\partial^3 q_{j,k}}{\partial t^3}\right)+\frac{1}{18}(\Delta x_j-\Delta x_{j+1})(\Delta t)^2\left(\frac{\partial^4 q_{j,k}}{\partial x\partial t^3}\right) \tag{A.21}$$

$$-\frac{1}{36}[(\Delta x_j)^2-(\Delta x_j)(\Delta x_{j+1})+(\Delta x_{j+1})^2](\Delta t)^2\left(\frac{\partial^5 q_{j,k}}{\partial x^2\partial t^3}\right)$$

$$-\frac{1}{2}(\Delta t)\left(\frac{\partial^2 q_{j,k}}{\partial t^2}\right)+\frac{1}{6}(\Delta x_j-\Delta x_{j+1})(\Delta t)\left(\frac{\partial^3 q_{j,k}}{\partial x\partial t^2}\right)$$

$$-\frac{1}{12}[(\Delta x_j)^2-(\Delta x_j)(\Delta x_{j+1})+(\Delta x_{j+1})^2](\Delta t)\left(\frac{\partial^4 q_{j,k}}{\partial x^2\partial t^2}\right)$$

$$+\frac{1}{3}(\Delta x_j - \Delta x_{j+1})\left(\frac{\partial^2 q_{j,k}}{\partial x \partial t}\right) - \frac{1}{6}[(\Delta x_j)^2 - (\Delta x_j)(\Delta x_{j+1}) + (\Delta x_{j+1})^2]\left(\frac{\partial^3 q_{j,k}}{\partial x^2 \partial t}\right).$$

The second term in Equation A.20, $\partial(qu)/\partial x$, is the advective term, and its truncation error term is given by:

$$(\Delta x_j - \Delta x_{j+1})\left(\frac{\partial q_{j,k}}{\partial x}\right)\left(\frac{\partial u_{j,k}}{\partial x}\right) \tag{A.22}$$

$$-\frac{1}{2}[(\Delta x_j)^2 - (\Delta x_j)(\Delta x_{j+1}) + (\Delta x_{j+1})^2]\left[\left(\frac{\partial^2 q_{j,k}}{\partial x^2}\right)\left(\frac{\partial u_{j,k}}{\partial x}\right) + \left(\frac{\partial q_{j,k}}{\partial x}\right)\left(\frac{\partial^2 u_{j,k}}{\partial x^2}\right)\right]$$

$$+\frac{1}{2}(\Delta x_j - \Delta x_{j+1})\left[\left(\frac{\partial^2 q_{j,k}}{\partial x^2}\right)(u_{j,k}) + (q_{j,k})\left(\frac{\partial^2 u_{j,k}}{\partial x^2}\right)\right]$$

$$-\frac{1}{6}[(\Delta x_j)^2 - (\Delta x_j)(\Delta x_{j+1}) + (\Delta x_{j+1})^2]\left[\left(\frac{\partial^3 q_{j,k}}{\partial x^3}\right)(u_{j,k}) + (q_{j,k})\left(\frac{\partial^3 u_{j,k}}{\partial x^3}\right)\right].$$

The third term in Equation A.20, τq, is the bottom friction term, and its truncation error term is given by:

$$-\frac{1}{2}\tau(\Delta t)\left(\frac{\partial q_{j,k}}{\partial t}\right) - \frac{1}{4}\tau(\Delta t)^2\left(\frac{\partial^2 q_{j,k}}{\partial t^2}\right) + \frac{1}{3}\tau(\Delta x_j - \Delta x_{j+1})\left(\frac{\partial q_{j,k}}{\partial x}\right) \tag{A.23}$$

$$+\frac{1}{6}\tau(\Delta x_j - \Delta x_{j+1})\left(\frac{\partial^2 q_{j,k}}{\partial x \partial t}\right) + \frac{1}{12}\tau(\Delta x_j - \Delta x_{j+1})(\Delta t)^2\left(\frac{\partial^3 q_{j,k}}{\partial x \partial t^2}\right)$$

$$+\frac{1}{36}\tau(\Delta x_j - \Delta x_{j+1})(\Delta t)^3\left(\frac{\partial^4 q_{j,k}}{\partial x \partial t^3}\right) - \frac{1}{6}\tau[(\Delta x_j)^2 - (\Delta x_j)(\Delta x_{j+1}) + (\Delta x_{j+1})^2]\left(\frac{\partial^2 q_{j,k}}{\partial x^2}\right)$$

$$-\frac{1}{12}\tau[(\Delta x_j)^2 - (\Delta x_j)(\Delta x_{j+1}) + (\Delta x_{j+1})^2](\Delta t)\left(\frac{\partial^3 q_{j,k}}{\partial x^2 \partial t}\right)$$

$$-\frac{1}{24}\tau[(\Delta x_j)^2 - (\Delta x_j)(\Delta x_{j+1}) + (\Delta x_{j+1})^2](\Delta t)^2\left(\frac{\partial^4 q_{j,k}}{\partial x^2 \partial t^2}\right).$$

The fourth term in Equation A.20 is:

$$gH\frac{\partial\zeta}{\partial x}, \tag{A.24}$$

which is the finite amplitude term. This term has two parts. The first part of the finite amplitude term is $gh(\partial\zeta/\partial x)$, and its truncation error term is given by:

$$-\frac{1}{4}g(\Delta t)^2(h_{j,k})\left(\frac{\partial^3\zeta_{j,k}}{\partial x\partial t^2}\right)+\frac{1}{8}g(\Delta x_j-\Delta x_{j+1})(\Delta t)^2\left(\frac{\partial h_{j,k}}{\partial x}\right)\left(\frac{\partial^3\zeta_{j,k}}{\partial x\partial t^2}\right) \tag{A.25}$$

$$-\frac{1}{16}g[(\Delta x_j)^2-(\Delta x_j)(\Delta x_{j+1})+(\Delta x_{j+1})^2](\Delta t)^2\left(\frac{\partial^2 h_{j,k}}{\partial x^2}\right)\left(\frac{\partial^3\zeta_{j,k}}{\partial x\partial t^2}\right)$$

$$+\frac{1}{8}g(\Delta x_j-\Delta x_{j+1})(\Delta t)^2(h_{j,k})\left(\frac{\partial^4\zeta_{j,k}}{\partial x^2\partial t^2}\right)$$

$$-\frac{1}{16}g[(\Delta x_j)^2-(\Delta x_j)(\Delta x_{j+1})+(\Delta x_{j+1})^2](\Delta t)^2\left(\frac{\partial h_{j,k}}{\partial x}\right)\left(\frac{\partial^4\zeta_{j,k}}{\partial x^2\partial t^2}\right)$$

$$-\frac{1}{24}g[(\Delta x_j)^2-(\Delta x_j)(\Delta x_{j+1})+(\Delta x_{j+1})^2](\Delta t)^2(h_{j,k})\left(\frac{\partial^5\zeta_{j,k}}{\partial x^3\partial t^2}\right)$$

$$-\frac{1}{2}g(\Delta t)(h_{j,k})\left(\frac{\partial^2\zeta_{j,k}}{\partial x\partial t}\right)+\frac{1}{4}g(\Delta x_j-\Delta x_{j+1})(\Delta t)\left(\frac{\partial h_{j,k}}{\partial x}\right)\left(\frac{\partial^2\zeta_{j,k}}{\partial x\partial t}\right)$$

$$-\frac{1}{8}g[(\Delta x_j)^2-(\Delta x_j)(\Delta x_{j+1})+(\Delta x_{j+1})^2](\Delta t)\left(\frac{\partial^2 h_{j,k}}{\partial x^2}\right)\left(\frac{\partial^2\zeta_{j,k}}{\partial x\partial t}\right)$$

$$+\frac{1}{4}g(\Delta x_j-\Delta x_{j+1})(\Delta t)(h_{j,k})\left(\frac{\partial^3\zeta_{j,k}}{\partial x^2\partial t}\right)$$

$$-\frac{1}{8}g[(\Delta x_j)^2-(\Delta x_j)(\Delta x_{j+1})+(\Delta x_{j+1})^2](\Delta t)\left(\frac{\partial h_{j,k}}{\partial x}\right)\left(\frac{\partial^3\zeta_{j,k}}{\partial x^2\partial t}\right)$$

$$-\frac{1}{12}g[(\Delta x_j)^2-(\Delta x_j)(\Delta x_{j+1})+(\Delta x_{j+1})^2](\Delta t)(h_{j,k})\left(\frac{\partial^4\zeta_{j,k}}{\partial x^3\partial t}\right)$$

$$+\frac{1}{2}g(\Delta x_j-\Delta x_{j+1})\left(\frac{\partial h_{j,k}}{\partial x}\right)\left(\frac{\partial\zeta_{j,k}}{\partial x}\right)$$

$$-\frac{1}{4}g[(\Delta x_j)^2-(\Delta x_j)(\Delta x_{j+1})+(\Delta x_{j+1})^2]\left(\frac{\partial^2 h_{j,k}}{\partial x^2}\right)\left(\frac{\partial \zeta_{j,k}}{\partial x}\right)$$

$$+\frac{1}{2}g(\Delta x_j-\Delta x_{j+1})(h_{j,k})\left(\frac{\partial^2 \zeta_{j,k}}{\partial x^2}\right)$$

$$-\frac{1}{4}g[(\Delta x_j)^2-(\Delta x_j)(\Delta x_{j+1})+(\Delta x_{j+1})^2]\left(\frac{\partial h_{j,k}}{\partial x}\right)\left(\frac{\partial^2 \zeta_{j,k}}{\partial x^2}\right)$$

$$-\frac{1}{6}g[(\Delta x_j)^2-(\Delta x_j)(\Delta x_{j+1})+(\Delta x_{j+1})^2](h_{j,k})\left(\frac{\partial^3 \zeta_{j,k}}{\partial x^3}\right).$$

The second part of the finite amplitude term is $(g/2)(\partial(\zeta^2)/\partial x)$, and its truncation error term is given by:

$$-\frac{1}{8}g(\Delta t)^2\left(\frac{\partial^3 \zeta_{j,k}^2}{\partial x\partial t^2}\right)+\frac{1}{16}g(\Delta x_j-\Delta x_{j+1})(\Delta t)^2\left(\frac{\partial^4 \zeta_{j,k}^2}{\partial x^2\partial t^2}\right) \quad \text{(A.26)}$$

$$-\frac{1}{48}g[(\Delta x_j)^2-(\Delta x_j)(\Delta x_{j+1})+(\Delta x_{j+1})^2](\Delta t)^2\left(\frac{\partial^5 \zeta_{j,k}^2}{\partial x^3\partial t^2}\right)$$

$$-\frac{1}{4}g(\Delta t)\left(\frac{\partial^2 \zeta_{j,k}^2}{\partial x\partial t}\right)+\frac{1}{8}g(\Delta x_j-\Delta x_{j+1})(\Delta t)\left(\frac{\partial^3 \zeta_{j,k}^2}{\partial x^2\partial t}\right)$$

$$-\frac{1}{24}g[(\Delta x_j)^2-(\Delta x_j)(\Delta x_{j+1})+(\Delta x_{j+1})^2](\Delta t)\left(\frac{\partial^4 \zeta_{j,k}^2}{\partial x^3\partial t}\right)$$

$$+\frac{1}{4}g(\Delta x_j-\Delta x_{j+1})\left(\frac{\partial^2 \zeta_{j,k}^2}{\partial x^2}\right)-\frac{1}{12}g[(\Delta x_j)^2-(\Delta x_j)(\Delta x_{j+1})+(\Delta x_{j+1})^2]\left(\frac{\partial^3 \zeta_{j,k}^2}{\partial x^3}\right).$$

The fifth term in Equation A.20, $\varepsilon(\partial^2 q/\partial x^2)$, is the viscous term, and its truncation error term is given by:

$$\frac{1}{4}\varepsilon(\Delta t)^2\left(\frac{\partial^4 q_{j,k}}{\partial x^2\partial t^2}\right)+\frac{1}{12}\varepsilon(\Delta x_{j+1}-\Delta x_j)(\Delta t)^2\left(\frac{\partial^5 q_{j,k}}{\partial x^3\partial t^2}\right) \quad \text{(A.27)}$$

$$+\frac{1}{48}\varepsilon[(\Delta x_j)^2-(\Delta x_j)(\Delta x_{j+1})+(\Delta x_{j+1})^2](\Delta t)^2\left(\frac{\partial^6 q_{j,k}}{\partial x^4\partial t^2}\right)$$

$$+\frac{1}{2}\varepsilon(\Delta t)\left(\frac{\partial^3 q_{j,k}}{\partial x^2\partial t}\right)+\frac{1}{6}\varepsilon(\Delta x_{j+1}-\Delta x_j)(\Delta t)\left(\frac{\partial^4 q_{j,k}}{\partial x^3\partial t}\right)$$

$$+\frac{1}{24}\varepsilon[(\Delta x_j)^2-(\Delta x_j)(\Delta x_{j+1})+(\Delta x_{j+1})^2](\Delta t)\left(\frac{\partial^5 q_{j,k}}{\partial x^4\partial t}\right)$$

$$+\frac{1}{3}\varepsilon(\Delta x_{j+1}-\Delta x_j)\left(\frac{\partial^3 q_{j,k}}{\partial x^3}\right)+\frac{1}{12}\varepsilon[(\Delta x_j)^2-(\Delta x_j)(\Delta x_{j+1})+(\Delta x_{j+1})^2]\left(\frac{\partial^4 q_{j,k}}{\partial x^4}\right).$$